Activity Dependent Trans-synaptic Tracing Of Neural Circuits In *Drosophila*

Smitha Jagadish

Submitted in partial fulfillment of the
requirements for the degree of
Doctor of Philosophy
in the Graduate School of Arts and Sciences

COLUMBIA UNIVERSITY

2013

ABSTRACT

Activity Dependent Trans-synaptic Tracing Of Neural Circuits In *Drosophila*

Smitha Jagadish

Drosophila exhibits a rich repertoire of simple and complex behaviors. In addition, the ability to allow genetic manipulations of specific neuronal populations makes the numerically simple fly brain an attractive model system to study the mechanisms that translate neural circuits to meaningful behavioral responses. Delineation of neural circuits requires development of approaches that trace functional synaptic connections. We have developed HA-Tango-trace, an activity-dependent trans-synaptic tracer to define neural circuits that convey information from the inner photoreceptors in the retina to the lobula complex in the *Drosophila* visual system. Elucidation of neural circuits and the mechanisms involved in translating the circuitry into a meaningful behavioral response with Tango-trace involves labeling of neurons in an activity-dependent manner based on the release of an endogenous neurotransmitter at a synapse. This strategy can be extended to any neural circuit in the brain with a known neurotransmitter in both flies and mice.

In the visual system, specific features of the visual image like motion, color, form and shape are extracted and processed in neural pathways. This information is transmitted to the brain where it must be processed to translate stimulus features into appropriate behavioral output. Here we investigate how this information is represented in higher visual centers in flies. The stochastically distributed p/yR7s and p/y R8s in the retina project to the medulla and make precise connections with four unique connectors that relay information to the

lobula complex. Thus, the p/yR7s and p/y R8s process spectral information in separate pathways and relay information to the lobula and lobula plate. The projections to the lobula plate afford the opportunity for inputs to the motion pathway. Moreover, our behavioral data show that R8s influence motion-evoked behavioral responses under bright light conditions. Gap junctions between the inner and outer photoreceptors could afford an explanation for the convergence of the two pathways. This by itself is sufficient for visual discrimination of objects during navigation or, alternatively, the postsynaptic partners of R7 and R8 may additionally provide inputs to the motion pathway. Thus, spectral and motion pathways may converge repetitively at each stage of the circuit and reorganize into pathways of behavioral significance.

Furthermore, histaminergic neurons have been implicated in temperature preference and circadian rhythms. These behaviors are likely to result from neuromodulation of central brain circuits mediated by histamine. Tango assay can be used to study this other important aspect of neural circuits by measuring the intensity of signal before and after neuromodulation. This approach was successfully used to map neuromodulation of dopamine mediated sugar sensitivity in flies using dopamine tango-map. Hunger enhances behavioral sensitivity to sugar and this is mediated by the release of dopamine onto primary gustatory sensory neurons, which enhances sugar-evoked calcium influx in a DopEcR-dependent manner. Tango-map permits the detection of increases in endogenous neuromodulator release in vivo.

In addition, histamine has been detected in mechanosensory neurons in *Drosophila*. Auditory systems are critical to the behavior of many insects. In *Drosophila melanogaster*, acoustic communication is essential for making decisions related to mate selection. The

projections of the HA-Tango labeled neurons overlap with the proposed higher order auditory neurons in the protocerebral areas. Further characterization of these circuits with HA-Tango-trace will provide insights into the representation of mechanosensory and auditory information that drive diverse behaviors in *Drosophila*.

Acetylcholine is a major neurotransmitter of the olfactory and gustatory systems in *Drosophila*. We have designed Ach-Tango to trace connections in the olfactory and gustatory systems in an activity-dependent manner. Characterization of circuits in higher brain areas may help us understand how odor and taste percepts are formed and how these sensory modalities are processed in the higher brain centers to generate diverse olfactory and gustatory behaviors.

The studies described in this thesis provide approaches to analyze circuits and understand their functional implications. Tango-Trace is a genetically encoded trans-synaptic tracer designed to identify synaptic connections in an activity-dependent manner by chronic activation of the presynaptic neuron with a genetically targeted neuronal activator, dTrpA1 and the identification of postsynaptic partners by GFP or any other reporter of choice. Tango-Map is designed to detect volume transmission of a neuromodulator by measuring the signal intensity of the reporter before and after a neuromodulatory effect. Furthermore, deciphering the circuit mechanisms that translate into complex behaviors will provide an understanding of more complex processes in the brain like emotion, cognition and consciousness. Our understanding of the nervous system can benefit greatly from these tools.

TABLE OF CONTENTS

TABLE OF FIGURES

Figures for chapter 1

Figures for chapter 2

Figures for chapter 3

ACKNOWLEDGEMENTS

My sincere and deepest thanks to my mom, dad and my brother who shared tiresome as well as joyous days of my Ph.D at Columbia. My husband and son have been the best people I could have ever asked to live with. This work would not have been possible without their undying love and support.

I thank all the members of Axel lab for their support, encouragement and friendly chats. I truly made some good friends in these seven years. My friends from New York, some from Columbia and some not, who would go to dinner or a drink with me at the drop of a hat have made this journey an unforgettable one.

Richard has been my greatest source of inspiration both in science and life in general. In these seven years in his lab, I have not only learnt a great deal about science, but every interaction with him has shaped my personality. My deepest thanks to Gary Struhl for being on my committee and advising me at many stages of my Ph.D. I would also like to thank Oliver Hobert and Wes Grueber for agreeing to be on my committee and advising me about my project.

Last, but not the least, I would like to thank Tom Clandinin who encouraged me, supported me and held my hand in the toughest days of my Ph.D. His nurturing mentorship has given me the last drop of energy I needed to finish this journey. I would also like to thank all his lab members for helpful discussions and support. I would like to particularly thank Damon Clark for collaborating with me on the behavior experiments.

DEDICATION

I dedicate this thesis to my dearest husband who has been with me through thick and thin

Chapter 1

INTRODUCTION

Sensory systems process information by extracting specific features of the stimulus to create an internal representation of the external world. This representation then translates the stimulus features into a behavioral response. For example, honeybees are exceedingly sensitive to the queen substance, an eight-component pheromone that maintains the queen's dominance in the colony, which is scentless to humans (Wanner et al., 2007). Although the insect eye has lower spatial acuity than the human eye, many flowers have patterns of ultraviolet (UV) reflection invisible to the human eye but visible to the insect eye. UV vision is used in foraging, navigation, and mate selection in both flying and terrestrial invertebrates (Salcedo et al., 2003; Tovee, 1995).

Delineation of the neural circuits encoding these stimulus features provides insights into the mechanism by which sensory information received by the sensory organs may be translated into motor output. The fruit fly *Drosophila melanogaster* is a model organism that allows sophisticated genetic manipulations than all other higher eukaryotes (Luo et al., 2008; Venken et al., 2011). Genetic tools permit the investigation of the complexity of the nervous system in great detail. The fly brain is estimated to contain 100,000 neurons, a million-fold fewer than the human brain, but with a remarkably similar complexity of anatomical and functional organization (Bellen et al., 2010). In addition, fruit flies exhibit a rich and diverse repertoire of simple as well as complex behaviors. Thus, mapping neural circuits that involve simple sensory inputs like olfactory, gustatory and visual, as well as more complex circuits that receive multisensory inputs like the courtship

circuit in *Drosophila* provides insights into neural mechanisms in other species. Furthermore, deciphering the circuit mechanisms that translate into these complex behaviors will provide an understanding of more complex processes in the brain like emotion, cognition and consciousness.

In this work, I present progress in designing new approaches that permit delineation of behaviorally meaningful neural circuits. We have developed a novel methodology, Tango-trace to identify synaptic connections in the *Drosophila* brain in an activity-dependent manner. This strategy can be extended to any neural circuit in the brain with a known neurotransmitter in both flies and mice. In chapter 2 of this thesis, the delineation of the neural circuitry using these novel approaches in the fly visual system has provided an understanding of the mechanisms of these circuits that drive diverse visual behaviors. In chapter 3 of this thesis, I discuss how these approaches could be extended to other neural circuits as well as used to study the mechanisms of neuromodulation of circuits. Appendix 1 presents a study where this approach was successfully used to map neuromodulation of dopamine mediated sugar sensitivity in starved flies.

1.1 The fly olfactory system

Many of the anatomical and functional features of the fly olfactory system are similar to the mammalian olfactory system (Ache and Young, 2005; Hildebrand and Shepherd, 1997; Strausfeld and Hildebrand, 1999). This conservation of the design of neural circuitry gives the numerically simpler insect olfactory system a great advantage as a model for studying neural circuits (Vosshall and Stocker, 2007). The discovery of odorant receptor (OR) genes in rodents (Buck and Axel, 1991) in *Caenorhabditis elegans* (Sengupta et al., 1996) and in

Drosophila melanogaster (Clyne et al., 1999; Gao and Chess, 1999; Vosshall et al., 1999) has provided a great deal of information on how chemosensory systems are organized in the peripheral layers. The mapping of peripheral olfactory circuits has provided insight into the representation of the sensory world in the brain, which translates stimulus features into a neural code that processes complex sensory information and elicits a behavioral response. The fly olfactory appendages are the third segment of the antenna and the maxillary palp, which are covered with specialized hairs called sensilla expressing around 1200 ORNs in each antenna. Extracellular activity of the ORNs in response to a panel of odorants was measured using single unit electrophysiology. Every ORN in a sensillum has a spike amplitude in response to an odor (de Bruyne et al., 2001). The odor responses of a majority of the antennal ORNs (de Bruyne et al., 2001; Hallem and Carlson, 2006) have been determined. All the 1200 ORNs fasciculate into the antennal nerve and project to the AL. Neurons expressing the same receptors project precisely to one or two spatially invariant glomeruli within the antennal lobe (Gao et al., 2000; Scott et al., 2001; Vosshall et al., 2000). A topographic map of receptor activity in the periphery is therefore represented in the antennal lobe.

The OR to glomerulus map has been completed and confirmed (Couto et al., 2005; Fishilevich and Vosshall, 2005). Genetic tracing of 44 (Couto et al. 2005) and 30 (Fishilevich & Vosshall 2005) different OR expressing populations of ORNs have resulted in 46 different ORs definitively mapped to glomeruli. In this study, Couto et al. (2005) assigned a glomerular identity for every antennal and palp ORN. Three glomeruli are innervated by *fruitless-expressing* neurons (Manoli et al. 2005, Stockinger et al. 2005) and have been implicated in sexual courtship behavior. Two large lateral glomeruli that are

sexually dimorphic (Kondoh et al., 2003) and *fruitless-positive* (Manoli et al. 2005, Stockinger et al. 2005) are innervated by trichoid sensilla and process pheromonal cues. ORNs expressing the 11-cis-vaccenyl acetate (cVA) responsive *Or67d* receptor project to one of these special glomeruli (Ha and Smith, 2006) (See 1.4 for more details on fru circuit).

The next step of olfactory transformation is exhibited in the representation of PNs in the higher centers, the MB and the lateral horn. Single cell clonal analysis has shown that PNs innervating a particular AL glomerulus exhibit overlapping but distinct stereotyped projection patterns in the lateral horn (Marin et al. 2002, Wong et al. 2002) but a rather disperse map with no spatial order in the MB. Behaviorally, the MBs seem to be involved in various functions such as olfactory learning, other forms of learning (Davis, 2005; Heisenberg, 2003), locomotor activity (Martin et al., 1998), male courtship behavior (Sakai and Kitamoto, 2006), and sleep (Joiner et al., 2006; Pitman et al., 2006). In contrast, the lateral horn seems to be involved in innate odor recognition (de Belle and Heisenberg, 1994; Heimbeck et al., 2001; Tanaka et al., 2004). The PNs send information to around 2500 intrinsic MB neurons, called Kenyon cells (Crittenden et al., 1998; Ito et al., 1997; Lee et al., 1999; Strausfeld et al., 2003; Yasuyama et al., 2002) with no spatial pattern. In the lateral horn, the terminals of the same types of PN map along the dorsoventral and anteroposterior axes (Tanaka et al. 2004). Together, these results demonstrate that a topographic map of olfactory information is retained in the two higher olfactory centers, but the character of the maps differs from the one in the AL. The projections of PNs in the lateral horn contribute to this transformation, providing an opportunity for integration of olfactory information. Thus, innate olfactory-driven behaviors are likely to derive from stereotyped, determined neural circuits in the lateral horn whereas learned behaviors may be mediated by the random

convergent input in the mushroom body (Marin et al., 2002b; Murthy et al., 2008; Wong et al., 2002) (Figure 1.1A).

The transformation of olfactory information in the brain is translated into a behavioral output. Olfactory responses in the adult can be measured with simple and robust behavioral assays. The classical olfactory t-maze is a simple assay, which was originally designed to study olfactory behavior coupled with electric shock conditioning to measure odor learning (Quinn et al., 1974). This assay has been used for measuring behavioral avoidance of CO2 (Suh et al., 2004). Another simple avoidance assay was used to identify *smell impaired* (smi) mutants in a forward genetic screen (Anholt et al., 1996). This assay involves presenting an odor either on a filter paper (Keene et al., 2004) or a cotton swab (Anholt et al. 1996) and measuring the distance between the fly and the odor source. The chemosensory jump assay measures the startle response of flies when they encounter an odor. This assay was used to isolate the *acj6* mutant, which disrupts a transcription factor necessary for the expression of a subset of the ORs (Clyne et al., 1999; McKenna et al., 1989). Trap assays are used to measure attractive responses to odors and are trapped in a trap (Larsson et al., 2004; Woodard et al., 1989). Olfactory responses to these behavioral assays in the adult have provided insights into the underlying circuitry and mechanisms of olfactory coding in *Drosophila*.

1.2 The fly gustatory system

Another chemosensory system that fruit flies use to navigate themselves around food sources and potential mates is the gustatory system. The numerically simpler fly brain has allowed the dissection of gustatory circuits that trigger these behaviors (Yarmolinsky et al.,

2009). Like mice and humans, *Drosophila* are attracted to sugars and low concentrations of salt and are averse to noxious compounds comparable to the mammalian bitters (Amrein and Thorne, 2005). Unlike mammals, fruit flies are indifferent to L-amino acids or low pH in their diet. It is likely that this represents an adaptation to their specialized diet of rotten fruits, which is typically acidic and far more enriched in simple carbohydrates than in protein or amino acids. In addition to having taste receptors on its mouth parts, the fly also has gustatory receptor neurons (GRNs) distributed on its legs and wings.

Fly GRNs express gustatory receptors (Gr), a group of 68 distantly related genes encoding putative heptahelical transmembrane proteins (Clyne et al., 2000; Dunipace et al., 2001; Scott et al., 2001). The fly gustatory organ is the proboscis, which consists of a muscular tube, the pharynx, surrounded by two labial palps of the labellum. GRNs are housed within 200–300 gustatory sensilla distributed on the proboscis, legs, and wings. Additional GRNs are located on internal taste organs lining the pharynx. The proboscis and legs contain one mechanosensory and 2-4 GRNs hat are housed in the taste bristles. Each gustatory neuron extends a dendrite to a terminal pore at the tip of the bristle shaft and an axonal process that terminates primarily in the subesophageal ganglion (SOG). The gustatory bristles of Drosophila are accessible to extracellular recordings and the responses of the gustatory neurons can be reliably discriminated from one another by their spikes. Early studies used this approach and identified several functional classes of GRNs. Moreover, different tastants that activate the same cell such as high salt, caffeine, and quinine stimulate a common behavioral response.

Similar to mammalian taste, receptor expression in flies is strictly segregated in populations of GRNs. The trehalose sweet taste receptor, Gr5a (Chyb et al., 2003), is

expressed in a population of gustatory neurons that is non-overlapping with neurons expressing the bitter receptor Gr66a (Moon et al., 2006; Thorne et al., 2004; Wang et al., 2004b). In addition, the projections of these neurons to the SOG terminate in spatially segregated domains. The function of Gr5a as a sugar receptor immediately suggests that this class of labeled cells and projections represents a labeled line for sweet tastants, whereas Gr66a expressing neurons may correspond to a labeled line for bitter stimuli. Indeed, functional imaging, cellular ablation, and activation studies show that compounds that activate Gr5a neurons are attractive to flies, and compounds that stimulate Gr66a neurons are aversive (Marella et al., 2006a; Thorne et al., 2004; Wang et al., 2004b). Thus, these two pathways function as labeled lines for sweet and bitter taste. Moreover, experiments in which odorant receptors are expressed in Gr5a and Gr66a neurons confer attraction or repulsion, respectively, to the odorant (Hiroi et al., 2004). Furthermore, a recent study shows that expression and activation of the light-activated channelrhodopsin-2 in Gr5a neurons is sufficient to induce robust initiation of feeding upon stimulation with blue light (Gordon and Scott, 2009). Thus, distinct populations of taste receptor cells are likely to be genetically determined to elicit appropriate behavioral responses (Figure 1.1B).

The fly brain is several orders of magnitude smaller than the mammalian brain and this makes the dissection of circuits controlling behavior much simpler. The proboscis is at the base of the head, but stimulation of leg or labial taste neurons with an attractive tastant such as sugar causes extension of the proboscis, opening of the labella, and initiation of feeding. In contrast, addition of bitter substances to the food source suppresses the proboscis extension reflex (PER) and triggers proboscis retraction. Proboscis extension and retraction are robust innate behaviors and are commonly used as behavioral assays for delineating taste

circuits. For instance, a recent study identified a motor neuron within the SOG (Gordon and Scott, 2009) that appears to be involved in integration of bitter and sweet tastes. This neuron is stimulated by activity in Gr5a neurons and inhibited by Gr66a activity. Thus the bitter and sweet labeled lines result in antagonistic responses in neurons that elicit distinct behavioral responses.

Flies display a robust PER to water, particularly when they are water deprived (Inoshita and Tanimura, 2006). Molecular, cellular, calcium imaging and electrophysiological approaches identified water-sensing neurons, and that loss of responses in these neurons abolishes water sensitivity (Cameron et al., 2010). An anatomical screen of enhancer trap lines for expression demonstrated CO2 sensors in flies, activated by growing yeast, beer, carbonated water, dry ice, and gaseous CO2 (Fischler et al., 2007). In addition, expression of the TrpV1 channel in these CO2 sensors results in robust taste attraction to capsaicin (Fischler et al., 2007). Together these data suggest that flies have dedicated pathways for CO2 taste detection and water sensing. Models of taste coding propose that neuronal lines for each taste converge into common targets (Roper, 2007). However, if the spatial segregation seen in the periphery is retained in higher taste centers, there may be a topographic map of taste qualities, similar to the somatosensory, visual, and auditory systems.

1.3 The fly visual system

Vision in insects is central for food and mate detection, avoidance of prey, detection of landmarks, phototaxis and a variety of other rich behaviors. Visual perception is initiated by absorption of light by rhodopsins expressed in a dense array of photoreceptors in the retina.

The insect visual system has eight peripheral photoreceptors R1-8, classified as outer (R1-6) and inner (R7/R8) photoreceptors (Clandinin and Zipursky, 2002; Sanes and Zipursky, 2010) (Figure 1.2A). Activity mapping with 2-deoxyglucose, electrophysiological and behavioral studies demonstrate that the outer photoreceptors are involved in processing motion information and the inner photoreceptors are involved in processing spectral information (Buchner et al., 1984; Heisenberg, 1977). The outer photoreceptors R1-6 express the blue-green Rh1 opsin with a UV sensitizing pigment (O'Tousa et al., 1985; Zuker et al., 1985). R1-6 neurons looking at the same point in space project with precision to a single cartridge in the lamina, and form synapses with the lamina monopolar cells (LMCs) L1-3 in the same cartridge, forming a retinotopic map (Meinertzhagen and O'Neil, 1991; Rivera-Alba et al., 2011a; Sanes and Zipursky, 2010) (Figures 1.2B, 1.3). L1-3 from a single cartridge then project their axons to a single column in the medulla terminating in different layers, retaining the retinotopic map.

Ultrastructural studies using EM reconstruction revealed synapses between LMCs and transmedullary (Tm) cells (Takemura et al., 2011). Tm cells extend their dendrites to different layers of the medulla and send their axons to the lobula (Fischbach, 1989). The lobula complex comprises of lobula and lobula plate, the last two neuropils of the optic lobe before the sensory input results in a descending motor output (Douglass and Strausfeld, 2007; Gronenberg and Strausfeld, 1992; Haag et al., 2007; Nässel and Strausfeld, 1982) (Figure 1.2C). Although the lobula plate has been implicated in motion vision, the inputs to this area remain poorly understood. Electrophysiology, behavior and optical imaging reveal that the direction-selective lobula plate tangential cells (LPTCs) are involved in motion vision (Farrow et al., 2003; Haag and Borst, 2003; Haag and Borst, 2008; Joesch et al.,

2008). The synaptic inputs to LPTCs still remain unknown. Anatomical tracings and recent electrophysiological studies imply that T cells may provide these inputs by projecting their bushy processes in the proximal medulla, lobula and lobula plate (Fischbach, 1989; Schnell et al., 2012).

The neural circuits of the inner photoreceptors, and their role in visual information processing have remained elusive. The inner photoreceptors express UV-sensitive opsins (Rh3 in pR7 and Rh4 in yR7) (Fryxell and Meyerowitz, 1987; Montell et al., 1987; Zuker et al., 1987), blue-sensitive opsin (Rh5 in pR8) and green-sensitive opsin (Rh6 in yR8) (Chou et al., 1996; Papatsenko et al., 1997). R7s and R8s looking at the same point in space project to a single column in the medulla and terminate in different layers of the medulla (Meinertzhagen and O'Neil, 1991; Takemura et al., 2008). EM reconstruction studies have implied synaptic connections of R7 and R8 cells with Tm cells that project to the lobula (Gao et al., 2008b). However, the synaptic contacts of all the four subtypes of the inner photoreceptors, p/y R7 and R8 still remain unidentified. TransmedullaryY (TmY) cells that extend their dendrites to different layers of the medulla are likely to provide these inputs to the lobula and lobula plate (Fischbach, 1989; Morante and Desplan, 2008; Raghu and Borst, 2011) (Figure 1.2C). Moreover, it is likely that each of the four subtypes of the inner photoreceptors process information in separate neural circuits by contacting different TmYs.

All the photoreceptors in the fly visual system are histaminergic. The histamine receptors that are cloned in drosophila are histamine gated chloride channels (Gengs et al., 2002a; Zheng et al., 2002). The fly photoreceptors depolarize in response to light and release histamine. The second order neurons directly postsynaptic to the photoreceptors hyperpolarize to light (Bausenwein et al., 1992; Hardie, 1987; Pantazis et al., 2008). The

histamine receptor from drosophila, known as *ort* is expressed in the histamine receptive postsynaptic cells of the photoreceptors. R1-6 send their inputs to their post-synaptic targets L1, L2 and L3 in the lamina. L1 and L2 have recently been shown to contribute to elementary motion detection as two separate pathways (Clark et al., 2011; Joesch et al., 2010; Katsov and Clandinin, 2008; Reiff et al., 2010). A recent promoter Gal4 fusion has uncovered a few potential postsynaptic targets of R7 and R8. The *ort-Gal4* line expressing HRP was used for EM reconstructions, which was shown that Tm5 is postsynaptic to R7 and Tm9 to R8 (Gao et al., 2008b) (Figure 3). There is also a wide field amacrine cell Dm8 that was discovered in this study as a postsynaptic partner of R7, which was shown to be involved in UV phototaxis.

The anatomical design of the mammalian retina is remarkably similar to the anatomy of the fly optic lobe (Sanes and Zipursky, 2010). The mammalian photoreceptors connect to bipolar cells, which are interconnected through horizontal cells. The bipolar cells send their input to ganglion cells, which are interconnected through amacrine cells. The ganglion cells send their input to the visual cortex through the LGN. The topographic map that is created at the level of the retina is maintained all the way till the V1 and V2 cortical areas. Recent studies have suggested that the spatial segregation breaks down from V1 to V2 (Nassi and Callaway, 2009a). The retinotopy that is created in the fly retina is maintained till the visual information reaches the higher protocerebral areas. Another striking similarity between the mammalian and fly visual systems is the anatomical diversity in cell types. The prevalent model is that different cell types are involved in modular parallel processing of visual information.

In insects, visual information is transmitted from the peripheral photoreceptors to specific areas of the optic lobe implicated in behavioral output (Clark et al., 2011; de Vries and Clandinin, 2012; Douglass and Strausfeld, 2003; Götz, 1973; Hausen, 1982; Heisenberg, 1984; Zhu et al., 2009). The visual system extracts specific stimulus features, processes in neural pathways and translates to different behaviors like polarization vision, color vision, depth perception and motion vision. The visually guided behaviors of insects are as diverse as their eye morphologies and provide a rich source for tracing neural circuits.

The optomotor response in flies

Drosophila exhibits a robust optomotor response to motion stimuli. Motion cues are detected by actively moving animals. Thus, the behavior of the animal is determined by the relative motion of the animal in the surrounding environment. The resulting distribution of motion vectors is called optic flow (Gibson, 1950). The LPTCs are tuned to optic flow patterns consistent with particular flight maneuvers. Furthermore, the strength of the optomotor response is modulated by the e-vector of the stimulus light, providing evidence for polarization vision in Drosophila. Earlier studies using the photoreceptor mutants *sevenlessLY3*, in which the R7 input is absent, and *outer rhabdomeres absent (ora)*, where R1–6 are absent but R7/8 is left intact, the optomotor response of *Drosophila* was shown to rely exclusively on input from photoreceptors R1–6 (Heisenberg, 1977). In another study, *Drosophila* motion vision was implied to be color-blind. In this study, while presenting moving bars of alternating colors and high color contrast, a brightness ratio of the two colors at which the optomotor response is largely missing (point of equiluminance) was identified. In these conditions, in flies lacking functional R7 and R8 the strength of the optomotor response is not altered (Yamaguchi et al., 2008a). However, more recent studies using

electrophysiological and behavioral methods have demonstrated that R7 and R8 contribute to motion vision (Wardill et al., 2012).

The discovery of the requirement of LPTCs for the optomotor response in *Drosophila* came from a behavioral screen, where Heisenberg and colleagues isolated a mutant called "optomotor blind", which lacks the LPTCs (Pflugfelder and Heisenberg, 1995). Behavioral experiments and electrophysiological recordings from tangential cells in *Drosophila* suggests that the Reichardt detector is the elementary mechanism for local motion detection (Borst, 2009). A number of approaches were taken towards identifying the columnar neurons participating in this circuitry. From a screen for altered brain structure, Fischbach and Heisenberg isolated a mutant with a reduced number of cell types per column in the optic lobes (Fischbach and Heisenberg, 1981). These flies were found to still respond like wild-type flies in the optomotor paradigm. Interestingly, certain classes of Tm and TmY cells are not seen in the mutant, while others have wild-type like appearance. These remaining cell types are sufficient to support the function of local motion detection. Interestingly, the bushy T cells are also prime candidates for providing input to the lobula plate tangential cells since T4 and T5 cells exist in four different subtypes per column, each of which arborizes in a different stratum of the lobula.

The visually guided escape circuit in flies

The escape jump response exhibited by flies is an innate behavior triggered by visual stimuli representing danger (Waldvogel and Fischbach). The key players of this neural circuit have been identified and shown to elicit distinct movements in the escape response. Giant fibers (GF) are large descending neurons, which receive visual input from the optic

lobes and connect to the tergotrochanter motor neurons (TTMn) in the thorax and the peripherally synapsing interneurons (PSI) (Tanouye and Wyman, 1980). The escape response occurs in two steps, a flight take off and then the escape jump. A light-off stimulus elicits a non-directional flight take off response in the motor neurons by stimulating an extension of the mesothoracic legs. A looming stimulus elicits a directional response roughly 200 ms before the flight take off by initiating a series of postural adjustments, which determine the direction of their escape response. Then, three pairs of wing muscles become activated, initiating the wing muscles to swing to their flight position and then flapping of the wings (Card and Dickinson, 2008). This is the escape jump response. It was shown that by activating the GF alone, the escape jump response can be elicited in flies (Lima and Miesenbˆck, 2005). Although the part of circuit that inputs to the GF is not known, the escape circuit in flies demonstrates how visual stimuli creates a representation that is translated into an innate behavioral response.

1.4 Courtship in *Drosophila*

Mapping neural circuits that involve simple sensory inputs like olfactory, gustatory and visual inputs in *Drosophila* provides insights into neural mechanisms that control simple sensory behaviors like feeding and navigation around objects. In addition, more complex social behaviors in *Drosophila* such as con-specific recognition, courtship, aggression and avoidance are required for survival and reproduction. Characterization of the underlying neural circuits that receive multisensory inputs and trigger complex social behaviors is required to understand the organizational and functional logic of the brain. During courtship, male and female *Drosophila* communicate distinct messages using visual, chemical and

acoustic stimuli to evoke very different complex behaviors. Males detect suitable courtship objects by chemical signals including both volatile pheromones detected by the olfactory system and nonvolatile pheromones detected by the gustatory system. If the male perceives pheromone signals predictive of mating success, he initiates an elaborate courtship ritual, which comprises of a courtship song produced by unilateral wing vibration.

The male pheromone cis-vaccenyl acetate (cVA), a volatile compound modulates both male and female behaviors (Dickson, 2008). In males, detection of cVA in females suppresses courtship behavior, including the courtship song (Kurtovic et al., 2007) and promotes male-male aggression. In females, cVA activates the same sensory neurons to promote receptivity to males. ORNs expressing Or67d are required for cVA detection, and ectopic expression of Or67d in other ORNs renders them sensitive to cVA (van der Goes van Naters and Carlson, 2007). Detection of cVA is facilitated by SNMP (sensory neuron membrane protein), a transmembrane protein (Benton et al., 2007), and Lush, a secreted odorant binding protein (Xu et al., 2005). Lush binds cVA, and in doing so undergoes a conformational change (Laughlin et al., 2008).

The Or67d+ ORNs extend their axons to a glomerulus called DA1 (Kurtovic et al., 2007), where they transmit the cVA signal on to the corresponding DA1 PNs. Both Or67d+ ORNs and DA1 PNs respond equally to cVA in males and females (Datta et al., 2008; Kurtovic et al., 2007). However, the DA1 PNs form sex-specific arborizations in the protocerebrum, suggesting that they may feed the cVA signal into circuits that process it differently in males and females (Datta et al., 2008). DA1 is larger in males than in females (Schlief and Wilson, 2007). In the protocerebrum, the DA1 PNs arborize in a discrete region of the lateral horn

that is spatially segregated from the region targeted by PNs that respond to fruit odors (Marin et al., 2002a).

Courtship singing is a male-specific action. Females either do not select this action or cannot execute it. Such sex differences in neural function appear to be hard-wired during development. Sex in flies is primarily determined by the sex-specific splicing of two genes, *fruitless (fru)* and *doublesex (dsx)*, both of which encode putative transcription factors (Ryner et al., 1996). The sex differences caused by fru, but not those contributed by dsx, account for male-specific singing. Males that lack the male-specific fru^M isoforms do not sing (Villella and Hall, 1996), whereas those that lack dsx^M still do. Conversely, females forced to express fru^M sing, whereas those that express dsx^M do not. There are ~2000 fru-expressing neurons in both sexes, including sensory, central, and motor neurons. If the synaptic activity of all the fru neurons is blocked, all aspects of male courtship are suppressed, including the song (Manoli et al., 2005; Stockinger et al., 2005). If a small set of ~20 fru neurons in the dorsal brain, called the fru-P1 neurons, are masculinized in an otherwise normal female, then the female sings to other females (Kimura et al., 2008).

Direct optical stimulation of the thoracic fru neurons in headless flies (flyPods) induces both males and females to sing (Clyne and Miesenbock, 2008). The song produced by female flyPods is not a perfect rendition of the normal male courtship song. It is, however, significantly improved by expressing fru^M in all the fru neurons (Clyne and Miesenbock, 2008). This implies that fru^M contributes to the sexual differentiation of the circuits that produce the song as well as those that call them in to action. Correct male-specific differentiation of these song circuits also requires dsx^M, because the song is aberrant in flies

that express fru^M but lack dsx^M, regardless of whether they are male (Villella and Hall, 1996) or female (Rideout et al., 2007).

A recent study mapped the cVA-responsive fru neural circuit from the sensory input to the descending output using photoactivatable green fluorescent protein (PA-GFP), electrophysiology, optical imaging and laser-mediated microlesioning (Ruta et al., 2010). This concise circuit consists of four neuronal clusters and three synapses that translate pheromonal signals from the periphery to the ganglia of the nerve cord. Multiple neural components within this circuit are anatomically dimorphic. The DA1 PNs reveal dimorphic axonal arborizations (Datta et al., 2008). These dimorphic arborizations contact male-specific DC1 neurons, described as P1 neurons in another study, and send axons to male-specific neuropils, the lateral triangle and SMP tract. One output of this neuropil is a male-specific descending neuron, DN1 (Figure 1.4). This circuit is likely to participate in the generation of cVA-elicited behaviours observed only in males. In addition, the third-order lateral horn neurons afford an opportunity for multisensory integration with inputs to the DC1 cluster from the SOG and from the optic lobe. The lateral triangle and SMP tract also integrate sensory inputs from DC1 and LC1 as well as inhibitory projections from the SOG (Kimura et al., 2005). DA1 PNs also synapse onto the cluster of LC1 neurons that are present in both sexes but are numerically and anatomically dimorphic. Thus, the multiple dimorphic targets of this olfactory input permit a pheromone acting through the same sensory inputs elicit different behaviors in the two sexes. This cVA-responsive circuit provides insights into the mechanism by which sensory information received by the olfactory, gustatory and visual systems may be translated into motor output. However, this circuit is just a tip of the iceberg. In addition, both simple and complex behaviors may

involve more complex circuit mechanisms like neuromodulation that reflect the context and internal state of an organism.

1.5 Neuromodulation of neural circuits

Anatomically characterized circuits in crustaceans and in *Caenorhabditis elegans* demonstrate that a wiring diagram is not sufficient to characterize neural circuits that translate into behavior. The anatomical connections represent a set of connections that are shaped by context and internal states to allow different behaviors. Context and internal states are often mediated by neuromodulators, small molecules that activate G protein-coupled receptors (GPCRs) to modify neuronal dynamics, excitability, and synaptic efficiency. These modulators effectively change the composition of a neuronal circuit, recruiting new neurons, or excluding previous partners in a circuit (Bargmann, 2012; Marder and Bucher, 2007).

The Stomatogastric Ganglion

The stomatogastric ganglion (STG) of lobsters and crabs, a motor circuit of 30 neurons that generates rhythmic output associated with feeding, provided the first compelling evidence for the importance of neuromodulation (Marder and Bucher, 2001; Marder and Bucher, 2007). Neuromodulators can alter the connections between neurons to generate diverse behavioral outputs. The (STG) of crustaceans is a composition of neural circuits comprising of 30 neurons involved in generating diverse motor output behaviors. STG is a central pattern generator that receives modulatory input from ascending fibers, peripheral sensory neurons and hormones. The two main circuits associated with feeding behavior in

the STG are the pyloric rhythm and gastric mill rhythm circuits. The pyloric rhythm involves striated muscle groups that constrict and dilate the pyloric valve of the stomach in a faster three-phase rhythm. The gastric mill rhythm controls the muscles involved in chewing in the gastric mill oscillating in a slower six-phase rhythm.

Sensory stimulation of the stomach activates modulatory inputs to the pyloric ganglia that change the firing pattern of the PY neurons of the pyloric rhythm. A neuron called VD is normally active with the pyloric rhythm, but in the presence of neuromodulatory input can switch its input to join the gastric rhythm. Conversely, a neuron called LG that takes part in the gastric rhythm will fire with the pyloric rhythm when the gastric rhythm is silent. Furthermore, the activity of either VD or LG has the ability to reset the phase of both gastric or pyloric rhythms. Thus, the VD and LG neurons exist in two alternative circuits, depending on the modulatory input (Bargmann, 2012)(Figure 1.5 A).

Neuromodulation in *Drosophila*

Studies in *Drosophila* have provided insights into behavioral states, neuronal activity, and circuit function. Genetic tools that allow a combination of anatomical, physiological, molecular, and behavioral analysis can provide insights into modulation of neural circuits. The synaptic terminals of sensory neurons are important sites of neuromodulation, and gating of sensory inputs by neuromodulators appears to be a common principle across systems. Modulation of circuits by feeding and starvation provides numerous examples of this principle, as shown in leech mechanosensory neurons (Gaudry and Kristan, 2009), and by recent work in *Drosophila* (Figure 1.5B).

A recent study demonstrated that starvation increases the sugar sensitivity of flies, an effect that depends on the endogenous modulator dopamine and the expression of a specific dopamine receptor in taste receptor neurons (Inagaki et al., 2012) (see below; Appendix 1). Dopamine enhances presynaptic calcium influx into the taste receptor neuron, gating sensory input. This mechanism was studied using a novel method called "DopR-TANGO" (see below). Another study showed that a local signal by short neuropeptide F (sNPF) and a metabolic cue by insulin are integrated at specific odorant receptor neurons (ORNs) to modulate olfactory sensitivity necessary for starvation-induced food-search behavior. This study demonstrates that starvation increases presynaptic activity via intraglomerular sNPF signaling in a sNPF receptor (sNPFR1) dependent manner (Root et al., 2011).

The representation of sensory information is distinct in the different sensory systems. For instance, the olfactory and gustatory brain maps are different, possibly reflecting the different processing needs of these senses. Smell is designed to analyze a wide array of qualities, concentrations, and blends, whereas taste deals with a limited set of categories. This could explain why taste can be represented as labeled lines in contrast to odor. Rather, olfactory information is represented as behaviorally significant pathways that translate into innate and learned behaviors. If the quality of an odor has to be imposed upon by experience, it would be more meaningful for the brain to represent olfactory information randomly rather than labeled lines. In the visual system, visual information is extracted from the stimulus and represented in a retinotopic manner, as well as processed in pathways that encode the features of a visual stimulus. This information is then integrated spatially and the features are recombined to create a coherent visual percept. Characterization of these very different

neural circuits requires approaches that can trace anatomical and functional features of these circuits.

In insects, although the nervous system is numerically simple, it is involved in complex computations that result in diverse behaviors. How is the sensory information integrated in the higher centers to drive these behaviors? Where in the higher brain is a sensory percept formed? Moreover, most behaviors involve integrating information across sensory modalities. How are these sensory modalities integrated in the higher brain centers? What are the computations involved in this integration that generate such diverse behaviors? Future advances in understanding these questions will require a systematic analysis and characterization of these circuits. The studies described in this thesis provide approaches to analyze circuits and understand their functional implications.

1.6 Tracing circuits with small molecules

Over the last three decades, progress of tracing techniques with neuroanatomical tools has allowed delineation of many neural circuits. Retrograde axonal transport allows identification of the origin of afferent nerve fibers, while anterograde axonal transport enables the visualization of projections of individual or groups of neurons. For retrograde transport, the tracer material is applied to a fiber tract or a terminal field of innervation, becomes incorporated into the cell axons by a process of endocytosis, and is then carried back to the cell body. For anterograde transport, the uptake mechanisms involve the cell soma and its dendrites, and the tracer material is transported along the axonal microtubular system to the cell's synaptic terminals.

The first attempts at retrograde labelling with fluorescent transport substances used Evans Blue dye (EB) combined with cattle albumin (Huisman et al., 1984). The number of dyes available and the fields of application have increased rapidly. The nuclear yellow marker diamidinophenylindol (DAPI), Fast Blue (FB), True Blue (TB), Nuclear Yellow (NY) and Lucifer Yellow (LY) are typical of those developed in the late 1970s. These have now been largely superseded by the use of Fluoro-Gold (FG), choleratoxin subunit b (CTB), fluorescently tagged beads and, most recently, Mini Ruby (MR) and fluorescently tagged dextran amines. Fluorescent dyes like rhodamine-isothiocyanate (RITC) and 1,1 '-dioctadecyl-3,3,3 ',3 '-tetramethyl-indocarbocyanine perchlorate, (DiI) (Thanos and Bonhoeffer, 1983, 1987) have became available for anterograde tracing. More recently, dextran amines have become the most powerful tools for anterograde tracing (Glover et al., 1986) because they are relatively simple to use, and a great variety of detection methods have been developed for them. Dextrans can be biotinylated or conjugated to various fluorescent dyes, thus allowing immediate visibility or immunocytochemical processing.

Three basic methods are used to deliver tracer material into the target tissue are pressure injection, iontophoretic injection and the mechanical insertion of dye crystals. The dissolved tracer material is usually delivered through a glass micropipette of the type used routinely in electrophysiological experiments and produced in a standard electrode puller. Injection of the tracer solution can be achieved either with gas pressure, or by means of a hydraulic system. The latter is often preferable because it enables the injection volume to be controlled accurately. Tracer molecules usually carry an electrical charge and can therefore be ejected from the pipette by an applied electrical current. Current is applied through a micropipette with appropriate electrode tips containing the tracer solution, for both intracellular and

extracellular applications. The insertion of crystalline dyes is feasible when the target tissue is normally readily accessible. As the labeling efficiency is very high and placement of the crystals can be carried out under microscopic control, this is the method of choice for focal applications of carbocyanine dyes such as DiI and 4,4-didecylaminostyryl- N-methyl-pyridinium iodide (DiAsp) (Godement et al., 1987; Hong and Thanos, 1996; Honig and Hume, 1989a, b).

Tracers can enter axons or dendrites by active uptake via nerve terminals, or through severed neurons. For instance, dextran amines are taken up more efficiently by injured axons than by nerve terminals. In contrast, propidium iodide (PI) and FB are more readily taken up via intact terminals than through disrupted axons. Substances that diffuse passively into neurons enter because of the local concentration gradient. They must therefore be present at higher concentrations at the application site.

The plant enzyme horse radish peroxidase (HRP) was the first retrograde neuroanatomical tracer to be used. It may be pressure injected, iontophoresed or applied as lyophilyzed enzyme (Carson and Mesulam, 1982; Kristensson and Olsson, 1971; LaVail and LaVail, 1972). Usually, the tracer is driven out of micropipettes that are used for simultaneous electrophysiological recordings, by gas pressure or negative currents. Uptake by nerve terminals occurs via the cytoplasm into vesicles where the enzyme resides. Detection of the tracer molecules takes advantage of its enzymatic properties. Since the brown precipitate that is produced after the reaction of HRP with hydrogen peroxide and either DAB or tetramethylbenzidine (TMB) is stable and electron-dense. Thus, HRP-labeled neurons are amenable to ultrastructural analysis. Since receptor-mediated internalization is very efficient, WGA-HRP is internalized at a much higher rate than HRP alone. However,

the major drawback is the incomplete staining usually being limited to the cell soma and primary dendrites.

Plant lectins and related bacterial toxins are characterized by their high affinity to specific sugars. After binding to glycoconjugates of the neuronal membrane, they are internalized and transported within the neurites of many neurons. Lectins and toxins conjugated to avidin, HRP or fluorescent dyes are used for both retrograde and anterograde applications. In fact, *Phaseolus vulgaris* leukoagglutinin (PHA-L) is one of the earliest and most frequently used anterograde tracer (Cabot et al., 1991; Gerfen and Sawchenko, 1984). Some of these molecules, tetanus toxin fragment C (TTC) for instance, are transported across synapses into other neurons, and are also incorporated by fibers en passage.

Biocytin and biotinamide (neurobiotin) were introduced as intracellular markers for electrophoresis through glass micropipettes. For anatomical tracing, both compounds can be injected by extracellular iontophoresis with high currents and large bore pipettes, and are applicable for both anterograde and retrograde tracing. Compared to other tracers, biocytin and neurobiotin are relatively small and intracellular transport is very effective and leads to labeling of the finest axonal and dendritic arborizations (Horikawa and Armstrong, 1988; Kita and Armstrong, 1991; Lapper and Bolam, 1991).

1.7 Tracing circuits with genetically encoded fluorescent proteins

Several genetic techniques are available to label neurons in the fly brain. In flies, the ability to manipulate specific neuronal populations is provided by several binary systems such as GAL4/UAS, LexA/LexOP, and QF/QUAS in selective neuronal populations (Brand and Perrimon, 1993; Lai and Lee, 2006; Pfeiffer et al., 2010; Potter et al., 2010; Yagi et al.,

2010). These binary systems can be used to overexpress reporters to label neuronal subpopulations. Cytoplasmic labeling with fluorescent proteins can be achieved by overexpressing using a binary system (Gohl et al., 2011; Halfon et al., 2002; Pfeiffer et al., 2010; Yeh et al., 1995). Fluorescent markers can be fused to membrane proteins to visualize the axonal and dendritic arborizations (Lee and Luo, 1999; Pfeiffer et al., 2010; Ritzenthaler et al., 2000). Synaptic vesicle protein fusions label the presynaptic partners (Estes et al., 2000; Rolls et al., 2007; Zhang et al., 2002). Moreover, synaptic active zones can be labeled with cacophony-GFP (Kawasaki et al., 2004) or bruchpilot-GFP (Wagh et al., 2006). Postsynaptic sites can be marked with Denmark (Nicolai et al., 2010) or Dscam (Wang et al., 2004a), which labels dendrites. Neurotransmitter receptor protein fusion such as UAS-Rdl-HA and UAS-Dα7-GFP can characterize postsynaptic cells and their connections (Leiss et al., 2009; Sanchez-Soriano and Prokop, 2005). Promoter fusions with horseradish peroxidase (HRP) can be used in ultrastructural studies (Larsen et al., 2003; Watts et al., 2004) to enumerate synapses.

Binary drivers usually label large neuronal populations and can be confounding for deciphering a circuit (Pfeiffer et al., 2008). Intersectional strategies can label specific neuronal subpopulation with two independent drivers that share an expression domain in the neurons of interest. Manipulating *Gal4* expression using additional binary systems by a convertible genetic platform, called the Integrase Swappable *In vivo* Targeting Element (InSITE) system make it easier to label subpopulations of neurons (Gohl et al., 2011). The strategy can be additive, where the expression pattern of two binary drivers is combined or, subtractive by restricting the function of GAL4 to those cells that do not express its inhibitor, GAL80 (Lee and Luo, 1999). A variation of this approach is an intersectional

technique that relies on split binary systems like the split-GAL4 system (Luan et al., 2006). The GAL4 transcription factor is split into two hemidrivers, each of which is driven by separate regulatory elements. Reconstitution of the expression domains causes heterodimerization via leucine zippers, and results in a functional activator. Flp-out intersectional strategies combining GAL4 with Flp recombinase (Golic and Lindquist, 1989; Wong et al., 2002), each driven by separate regulatory elements depends on recombinase activity removing an intervening stop cassette (Struhl and Basler, 1993) and subsequent expression of transactivator, or repressor. Many such combinations of the orthogonal binary expression systems and Flp recombinase can be used to label specific neuronal subpopulations.

To characterize the morphology of individual neurons, stochastic labeling techniques were developed to label single neurons or small subpopulations. This allows visualization of cellular morphology and tracing projections of neurons. These techniques are based on Flp recombinase and are referred to as Flp-on or Flp-out and MARCM. Generation of genetic mosaics in specific tissues in Drosophila was achieved by the integration of FRT sites to permit efficient mitotic recombination. This allows the creation of two differently labeled daughter cells after division of the mother cell through chromosomal exchange, using the Flp recombinase. This system is known as MARCM (mosaic analysis with a repressible cell marker) (Lee and Luo, 1999). Upon mitotic recombination, GAL80 expression is lost in the mutant cells, resulting in GAL4 activation and transcriptional activation of the reporter. A non-random labeling approach involves expression of photoactivatible GFP (PA-GFP) under the control of either a pan-neuronal Gal4 line or a more restricted promoter (Datta et al., 2008; Ruta et al., 2010). Photoactivation of a small region of a neuropil can label PA-GFP

expressing neurons driven by Gal4 intersecting that region. For example, photoactivating a region where an axon tract terminates should label the dendrites of postsynaptic partners. Diffusion of photoactivated GFP out of these dendrites then labels the somata of the candidate cells.

1.8 Mapping functional connections

However, anatomical proximity does not ensure functional connectivity. Functional connectivity between neurons can be established by direct and indirect methods. A direct method of establishing functional connectivity is by paired recordings, which establishes synaptic connectivity between two neurons. Alternatively, functional connectivity between two neurons can be established by recording calcium activity in the target neuron while activating or silencing an upstream neuron. An action potential due to a neuron firing results in a large local increase in calcium concentration that can be detected by genetically encoded calcium indicators (GECIs). Most GECIs use a calcium binding peptide resulting in either circularization of a single split fluorophore (GCaMP) (Wang et al., 2003) or energy transfer (FRET) between two fluorophores like Cameleon, Camgaroo, and TN-XXL (Fiala et al., 2002; Mank et al., 2008; Yu et al., 2003). Ratiometric imaging is advantageous in imaging preparations that undergo movement because the baseline fluorescence serves as a reference and the change in wavelength shows the change in neural activity. *UAS-GCaMP3* is being used to monitor activity in intact behaving flies (Chiappe et al., 2010; Seelig et al., 2010). However, the absence of a change in fluorescence cannot yet be interpreted to mean that neurons show no activity, since graded potential changes or single action potentials are not reliably detected.

Neurons can be activated by increasing sodium or calcium conductance or by reducing potassium conductance. The temperature activated cation channel *UAS-dTrpA1* (Hamada et al., 2008; Rosenzweig et al., 2005; Rosenzweig et al., 2008) can acutely activate neural activity and has been used to identify neurons involved in sleep and courtship behavior (Parisky et al., 2008; von Philipsborn et al., 2011). The chemical ligand capsaicin can activate mammalian TrpV1 channels expressed in flies and has been used to map gustatory inputs (Marella et al., 2006). Overexpression of a bacterial sodium channel, NaChBac, can increase neural excitability (Nitabach et al., 2006) but may have other effects in other cell types or over longer time-scales (Sheeba et al., 2008).

Silencing a neuron, either by preventing the release of neurotransmitter or by blocking changes in membrane potential is a precise way to determine its function. *Drosophila* neurons release common neurotransmitters such as glutamate, GABA, and acetylcholine from synaptic vesicles in response to calcium influx. Disruption of function of proteins such as neural synaptobrevin (nSyb) can silence neurons by preventing the release of neurotransmitter from vesicles. Expression of the light chain of tetanus toxin (*UAS-TNT or Tet or TeTxLc*) cleaves nSyb and blocks vesicle release (Sweeney et al., 1995), although some neurons seem to be less susceptible to TNT (Thum et al., 2006). Dominant-negative versions of the tetrameric potassium channels Shaker, Eag, Shaw, and Shal have been made by truncation of the wild-type channels (Broughton et al., 2004; Hodge et al., 2005; Mosca et al., 2005; Ping et al., 2011). *UAS-Shibire*^{ts1}, a temperature-sensitive dominant-negative form of dynamin, a GTPase required for vesicle recycling, blocks chemical neurotransmission (Kitamoto, 2001). The common approach to increase potassium conductance, which lowers the resting membrane potential or acts as a shunting current to

prevent depolarization is by expressing *UAS-Kir2.1*, which encodes a mammalian inward rectifying K+ channel (Baines et al., 2001; Paradis et al., 2001).

1.9 Mapping synaptic connectivity

Functional connectivity between two neurons does not ensure that they are synaptically connected. Characterization of neural circuits that may mediate behavior requires the development of approaches that trace functional synaptic connections. Fractions of neuronal circuitry driving behaviors have been delineated for simpler nervous systems and include circuits for rhythmic neuronal activity, such as those that drive the heart in *Hirudo medicinalis* (Kristan et al., 2005), swimming in *H. medicinalis* (Friesen et al., 1978), swimming in *Clione limacina* (Satterlie, 1985), and the escape swim response in *Tritonia diomedea* (Getting, 1983; Kleinfeld and Sompolinsky, 1988), among other stereotypic behaviors (Delcomyn, 1980).

Recently, huge efforts have been invested into reconstructing entire wiring diagrams of organisms by high-throughput and automated reconstruction of thin serial sections of transmission electron micrographs. By analogy with the genome, this catalog of putative synaptic connections of an organism obtained by ultrastructural enumeration of synapses has been called the connectome. The entire wiring diagram of *c.elegans* was reconstructed by pioneering serial section electron microscopy study (White et al., 1986), which contains both electrical and chemical synapses. After a hiatus of 25 years, a near-finished wiring diagram based on the original data and new micrographs have been obtained (Varshney et al., 2011). Another example where EM reconstruction was used to establish synaptic connectivity is in the peripheral visual system of the fly (Meinertzhagen and O'Neil, 1991; Meinertzhagen and

Sorra, 2001; Rivera-Alba et al., 2011b; Takemura et al., 2008). Although the wiring diagram of *C.elegans* has resulted in functional connections that mediate behaviors as in the case of mapping circuit motifs for egg-laying behavior (Zhang et al., 2008) and pheromone sensing (Macosko et al., 2009) and many other behaviors (Chalfie et al., 1985; Mori and Ohshima, 1995), a wiring diagram could be misleading resulting in an overrepresentation of connections. Mapping connectomes across a variety of animals (Bohland et al., 2009; DeFelipe, 2010; Lichtman and Sanes, 2008; Lu et al., 2009; Seung, 2009; Sporns et al., 2005; Swanson and Bota, 2010), using high-throughput automated histology still remains incomplete.

Polysynaptic tracers

Characterization of synaptic connections was pioneered by the discovery in the early 1970s that certain molecules (Grafstein, 1971; Schubert and Kreutzberg, 1974), including proteins (Evinger and Erichsen, 1986; Schwab and Thoenen, 1976) such as wheat germ agglutinin (WGA), could be transported along series of synaptically connected neurons. Genetically encoded modifications of these approaches can be targeted to particular cell types (Braz and Basbaum, 2008) and fused to GFP (Maskos et al., 2002) or Cre recombinase (Gradinaru et al., 2010) for diverse manipulations. However, these approaches lack synaptic specificity, are bidirectional (Harrison et al., 1984; Porter et al., 1985), polysynaptic and diluted at every synaptic connection. Neurotropic viruses used to cross synapses are herpes simplex virus type 1 (HSV-1) (Ugolini et al., 1989), pseudorabies virus (PRV) (Card et al., 1990; Card et al., 1991), and rabies virus (Gillet et al., 1986). These viruses appear to spread specifically between synaptically connected neurons (Card et al., 1993; Curanovic and Enquist, 2009). The mechanism of the transsynaptic spread of rabies virus still remains

poorly understood. But, its accuracy of labeling in known pathways, lack of spread across gap junctions (Tang et al., 1999) and to glia (Rancz et al., 2011), and lack of spread to fibers of passage makes it a good choice for tracing. Although some cell types are resistant to infection (Lafay et al., 1991; Viney et al., 2007), both rabies virus and the herpesviruses have been successfully used in many circuit-tracing studies. Recombinant versions can incorporate transgenes (Card et al., 2011; Rothermel et al., 2009) or permit Cre-dependent activation of PRV for tracing chains of inputs to genetically defined cell types (Braz et al., 2009; DeFalco et al., 2001). A relative of rabies virus, vesicular stomatitis virus (VSV), was recently reported to spread either retrogradely or anterogradely when its envelope protein gene is replaced with that of either rabies virus or the unrelated lymphocytic choriomeningitis virus (LCMV), respectively (Beier et al., 2011). However, all of the above tracers are polysynaptic tracers. While this allows tracing of multiple synaptic steps, it obscures delineation of neural circuits.

Monosynaptic tracing

To trace connections to specific cell types with rabies virus, a strategy was developed in which the initial viral infection is restricted to specific cells (Wickersham et al., 2007b). This was achieved by deleting the envelope protein, called rabies glycoprotein (RG) gene from the SAD-B19 rabies genome, replacing it with GFP, and then producing viral particles with a different envelope protein in their envelope (pseudotyping). The RG-deleted virus was pseudotyped with an avian virus envelope protein, called EnvA, resulting in a pseudotyped virus, EnvA-SADdG-GFP. When this virus is injected into the brain of a normal animal, it does not infect any neurons since the mammalian brain has no receptors for EnvA. But by

misexpressing the EnvA receptor, TVA, in particular cells, it is possible to selectively infect these cells. Since RG is required for packaging of new viral particles and trans-synaptic spread (Etessami et al., 2000; Wickersham et al., 2007a), and SAD-dG-GFP has no coding sequence for RG, RG expression is also required to allow viral spread from the infected neurons.

When neurons expressed both TVA and RG, the initial infection was restricted to TVA cells, and RG expression in these cells allowed trans-synaptic spread and GFP labeling of neurons that were directly presynaptic to the TVA expressing cells. Continued spread beyond the directly presynaptic neurons did not occur, because the presynaptic cells do not express RG and there is no RG coding sequence carried in the viral genome. Thus, this approach ensures that rabies spread is monosynaptically restricted, eliminating any ambiguity about numbers of synaptic steps that have been crossed. This method can be used in combination with, for example, cre-expressing or Tta-expressing mouse lines to obtain cell type specific expression of TVA and RG (Luo et al., 2008). Subsequently, the targeted cell type can be specifically infected with EnvA-SADdG-GFP and direct inputs labeled by trans-synaptic spread of the virus and GFP expression.

GRASP

GFP Reconstitution Across Synaptic Partners (GRASP) (Feinberg et al., 2008)was developed in *C. elegans* using two fragments of GFP (Cabantous et al., 2005) that fluoresce only when reconstituted. When the two GFP fragments are fused to the extracellular domains of transmembrane proteins expressed in two contacting neurons, the resulting fluorescence reports either generic membrane contact (when the carrier protein is the

ubiquitous surface molecule CD4) or synapses (if one of the fragments is tethered to the synaptically localized PTP-3A or NLG-1). GRASP labeling in multiple *C. elegans* circuits faithfully recapitulated EM findings. GFP fluorescence can be monitored in vivo, or alternatively, labeling can be amplified with GFP antibodies that are selective for reconstituted GFP. GRASP has now been successfully applied in *C. elegans* (Feinberg et al., 2008; Park et al., 2011), *Drosophila* (Gong et al., 2010; Gordon and Scott, 2009; Shang et al., 2011), and, most recently, mouse (Kim et al., 2012).

BLINC

A recent variant of the GRASP approach, Biotin Labeling of INtercellular Contacts (BLINC), involves replacing the split GFP fragments with the biotin ligase BirA and the substrate peptide (Thyagarajan and Ting, 2010). Interaction between BirA and its substrate is reported by the BLINC signal detected by addition of labeled streptavidin. The success of this approach in cultured mouse neurons, using neurexin-1b and neuroligin-1 as the carrier proteins, indicated that this two-component synaptic labeling is applicable in vertebrates. However, these approaches do not trace functional synaptic connections in which the activation of a presynaptic neuron results in a response in the postsynaptic neuron. Such approaches will require techniques that capture a biological process at a synapse such as the release of a neurotransmitter.

1.10 Trans-synaptic tracing with Tango assay

We designed an activity-dependent genetic trans-synaptic tracer that detects the endogenous release of a neurotransmitter in the *Drosophila* brain. The tracer is based on the

Tango assay (Barnea et al., 2008), in which transient receptor-ligand interactions result in a stable transcriptional readout of a reporter gene. Ligand activation of G-protein coupled receptors (GPCRs) results in the phosphorylation of specific serine and threonine residues at the cytoplasmic C terminus of the receptor by a class of GPCR kinases. The phosphorylated receptor occupied by the ligand then recruits arrestin; arrestin competes with G proteins for receptor binding, preventing further G protein activation. In the Tango assay, the ligand-dependent recruitment of Arr-TEV to the receptor fusion GPCR-Gal4 and the subsequent proteolytic cleavage, frees Gal4 to translocate to the nucleus and activate reporter genes.

Histamine (HA) is the major neurotransmitter released by all photoreceptors in the fly visual system. We designed the HA-Tango assay to monitor the activation of a GPCR by histamine and trace circuits in the visual system. This approach is described in detail in Chapter 2. *outer rhabdomeres transientless (ort; HisCl2)* and *HisCl1*, the two histamine receptors that are cloned in *Drosophila* are not GPCRs, but chloride channels (Gengs et al., 2002b; Gisselmann et al., 2002; Witte et al., 2002). The GPCR human histamine receptor 2 (HRH2) is pharmacologically similar to the *Drosophila* histamine receptor *ort* (Buchner et al., 1993; Roeder, 2003; Sarthy, 1991; Stark, 2003). We therefore generated a fusion protein (HRH2-Gal4) consisting of the GPCR, HRH2 joined at its cytoplasmic C terminus to the transcriptional activator, Gal4. We introduced a cleavage site for a highly specific protease, the N1a protease from tobacco etch virus (TEV), interposed between the receptor and Gal4 sequences. We then constructed a second fusion protein (Arr-TEV) consisting of the TEV protease linked to human β-arrestin2. These receptor and arrestin fusion genes were ubiquitously expressed under the control of α-tubulin promoter (tubp) for unbiased detection of histamine release.

To genetically control activation of histaminergic presynaptic cells, we expressed the temperature sensitive cation channel dTrpA1 (Hamada et al., 2008; Pulver et al., 2009) in specific photoreceptor subtypes in the HA-Tango background. We refer to this general technique of anterograde trans-synaptic tracing as 'Tango-trace' and the specific approach we used to trace histaminergic connections as 'HA-Tango-trace'. Our results demonstrate that the visual pathways converge repetitively at several stages of the circuit to shape the representation of visual information. The distinct projection patterns of the second order visual projection neurons provide an anatomical substrate for diverse visual behaviors.

1.11 Tango-Map

Standard methods used to measure the release of endogenous neuromodulators in vertebrates, such as fast-scan cyclic voltammetry (Phillips et al., 2003) or microdialysis (Benveniste and Huttemeier, 1990), have limited applicability in *Drosophila*. Moreover, such methods cannot identify neural circuits that undergo neuromodulation. Tango-map permits the detection of increases in endogenous neuromodulator release in vivo. This Tango system (DopR-Tango) was designed to detect dopamine (DA) release in the *Drosophila* brain. DopR-Tango system consists of the *Drosophila* DA receptor DopR1 (Gotzes et al., 1994; Sugamori et al., 1995) and *Drosophila* Arrestin1 (Appendix 1). Here, LexA is used as the tethered transcription factor. Stoichiometric coexpression of the Arrestin-TEV protease fusion was achieved using a 2A peptide (Szymczak and Vignali, 2005), which permits bicistronic expression in *Drosophila*.

This method revealed that the hunger enhances behavioral sensitivity to sugar and this is mediated by the release of dopamine onto primary gustatory sensory neurons, which

enhances sugar-evoked calcium influx in a DopEcR-dependent manner. Furthermore, this study supports a mechanistic model that starvation leads to increased DA release, which increases calcium influx into sugar-sensing GRNs via DopEcR, leading to increased neurotransmitter release. This method provides an anatomical readout of neuromodulation at the neural circuit level. The use of a pan-neuronal Gal4 driver to express the sensor permits, in principle, an unbiased survey of potential sites of neuromodulatory activity throughout the brain. Systematic and comprehensive application of this approach could, in principle, provide an overview of anatomic patterns of neuromodulation in the brain in a given behavioral setting. Although the Tango-map system can certainly benefit from improvements in its kinetics and SNR, it affords a means of identiying points-of-entry for studying circuit-level mechanisms of behaviorally relevant neuromodulation that are currently difficult to access in any other way. The extension of this methodology to other neuromodulators and model organisms should further our understanding of state-dependent control of neural activity and behavior.

1.12 Tango-trace and Tango-Map: Tools to trace circuits and map neuromodulation

Most neurotransmitters and neuromodulators bind to GPCRs and this makes tango assay a good choice for tracing in the nervous system (Figure 1.6). Tango assay can be used to trace synaptic connections in an activity-dependent manner as well as map neuromodulation, the two main components of a neural circuit. “Tango-Trace” is a genetically encoded trans-synaptic tracer designed to identify synaptic connections in an activity-dependent manner by chronic activation of the presynaptic neuron with a genetically targeted neuronal activator, dTrpA1 and the identification of postsynaptic partners by GFP or any other reporter of

choice (Figure 1.6B). “Tango-Map” is designed to detect volume transmission of a neuromodulator by measuring the signal intensity of the reporter before and after a neuromodulatory effect (Figure 1.6C). The main difference in the two versions of tango lies in the signal to noise ratio and the method of detection. Tango-Trace has a very high signal to noise ratio allowing precise identification of synaptic partners. Whereas, Tango-Map has a lower signal to noise ratio and allows the detection of change in Tango signal upon release of neuromodulatory transmitters in a brain area.

In the tango assay, the signal to noise ratio (SNR) can be further enhanced by altering the TEV cleavage site. The three TEV cleavage sites that were tested *in vitro* in the increasing order of their SNR were ENLYFQ/L, ENLYFQ/Y and ENLYFQ/S (Figure 1.7A). The SNR in GPCR tango was also enhanced by replacing the C-terminus tail of GPCRs with that of vasopressin receptor (AVPR2). AVPR2 belongs to the class of GPCRs that have a prolonged interaction with arrestin upon ligand binding which facilitates better cleavage of the transcriptional activator and hence a better SNR (Figure 1.7B). Future directions for Tango assay for tracing will be discussed in detail in Chapter 3. Most importantly, the transcriptional readout of the Tango system permits the expression not only of reporters allowing visualization of the neurons but also of effectors such as ion channels, calcium indicators and silencers in the tango labeled neurons. This brain-wide approach to tracing synaptic connections and mapping neuromodulation in a defined circuit can be readily adapted to other neurotransmitters and neuromodulators in both the fly and mouse.

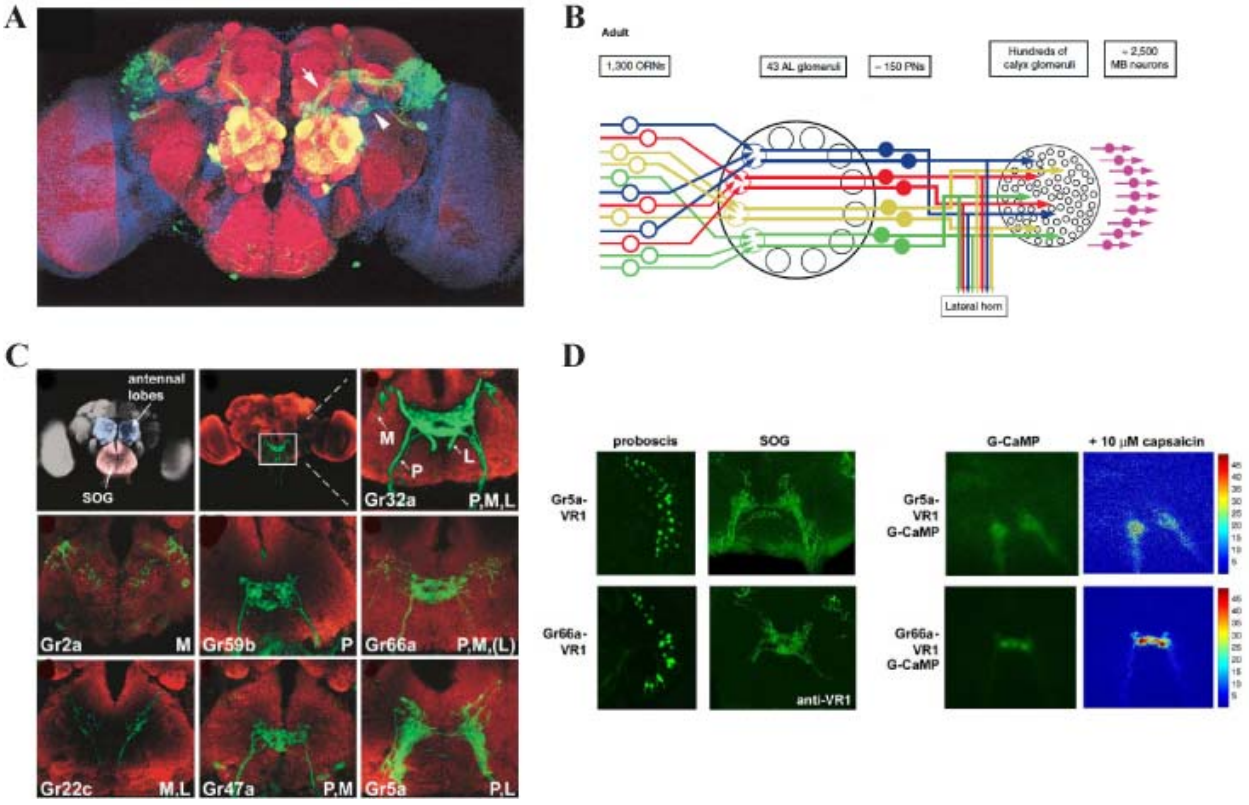
A
B
Adult
1,300 ORNs
43 AL glomeruli
~ 150 PNs
Hundreds of calyx glomeruli
~ 2,500 MB neurons
Lateral horn
C
antennal lobes
SOG
M
P
L
Gr32a
P,M,L
Gr2a
M
Gr59b
P
Gr66a
P,M,(L)
Gr22c
M,L
Gr47a
P,M
Gr5a
P,L
D
proboscis
SOG
G-CaMP
+ 10 μM capsaicin
Gr5a-VR1
Gr5a-VR1 G-CaMP
Gr66a-VR1
Gr66a-VR1 G-CaMP
anti-VR1

Figure 1.1. Olfactory and gustatory circuits in *Drosophila*

(A) Olfactory map in the antennal lobe. Visualization of the PN axons and dendrites with *GH146-Gal4* driving *UAS-CD8-GFP*. The PNs extend dendrites to glomeruli in the antennal lobe and axons to the mushroom body calyx and the lateral horn of the protocerebrum. A subset of PNs bypass the mushroom body and only innervate the protocerebrum. Arrow, inner antennocerebral tract (iACT); arrowhead, medial ante- nnocerebral tract (mACT). Adapted from (Wong et al., 2002) (B) Odorants from a stimulus activate distinct subsets of ORNs, which converge on glomeruli in the AL. From here information is relayed to higher brain centers, which have functional and neuroanatomical parallels in mammals and insects. Adapted from (Vosshall and Stocker, 2007). (C) Taste Projections in the SOG. GR expression patterns in the gustatory first relay, the subesophageal ganglia. Anti-GFP immunohistochemistry labels taste neurons (green) and anti-nc82 labels all fibers (red) reveals non-overlapping projections of gustatory neurons with different receptors. The GR promoter region is used to drive expression of GFP. Adapted from (Wang et al., 2004c). (D) A map of taste quality in the fly SOG. Changes in G-CaMP fluorescence in the central projections of sweet-responding Gr5a neurons and bitter-responding Gr66a neurons reveal spatial segregation of the two responses. Background G-CaMP fluorescence intensity increase (% $\Delta F/F$) after stimulation with 100 mM caffeine and 1 M sucrose. Adapted from (Marella et al., 2006b)

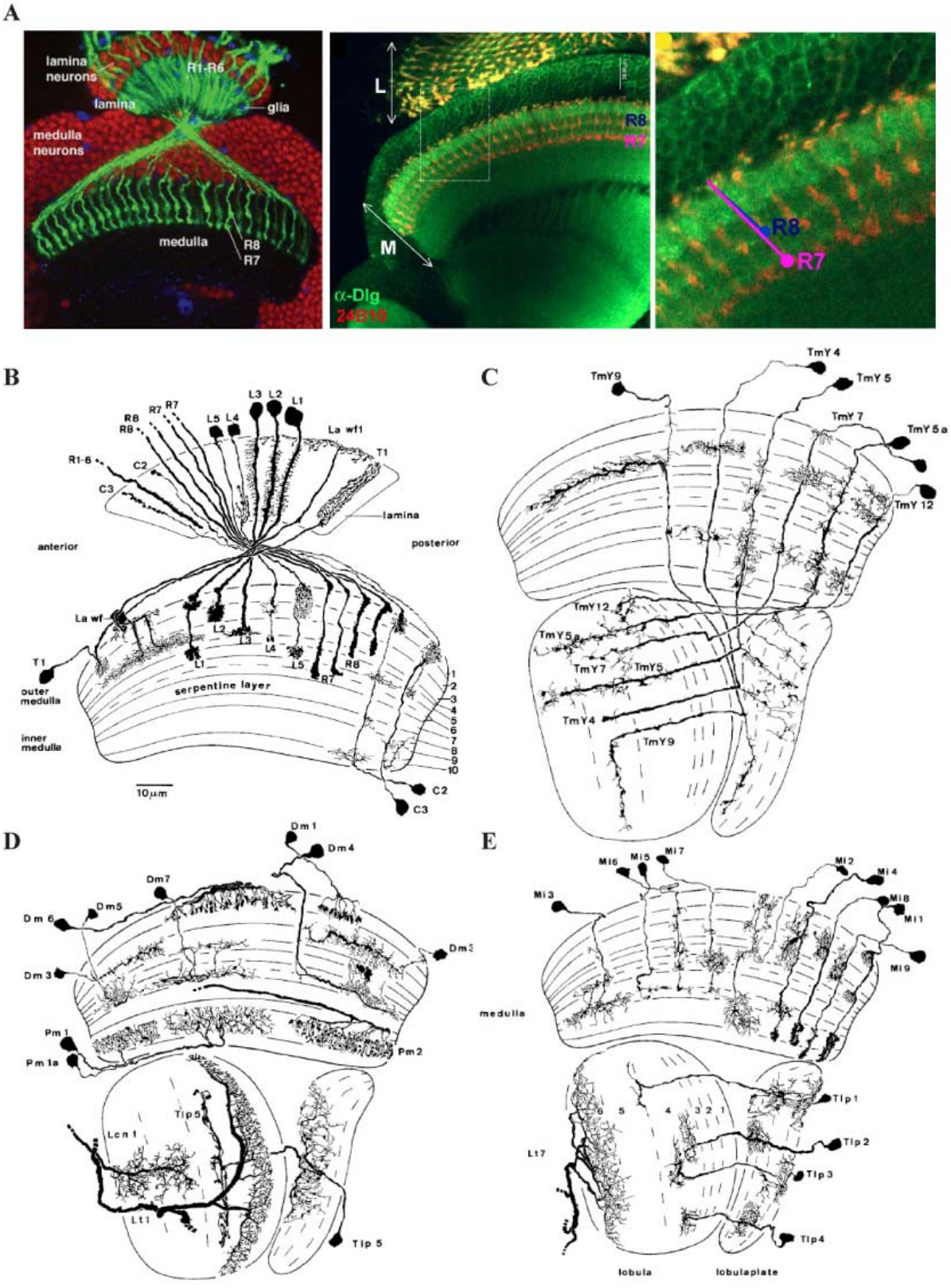
A
lamina neurons
R1-R6
lamina
glia
medulla neurons
medulla
R8
R7
L
M
R8
R7
α-Dlg
24B10
R8
R7
B
L3 L2 L1
R8 R7 R7
R8
L5 L4
La wf1
T1
R1-6
C2
C3
lamina
anterior
posterior
La wf
L2 L3 L4
T1
L1 L5 R8
R7
outer medulla
serpentine layer
inner medulla
1 2 3 4 5 6 7 8 9 10
10μm
C2
C3
C
TmY4
TmY9
TmY5
TmY7
TmY5a
TmY12
TmY12
TmY5a
TmY7
TmY5
TmY4
TmY9
D
Dm1
Dm4
Dm7
Dm5
Dm6
Dm2
Dm3
Pm1
Pm2
Pm1a
Tlp5
Lcn1
Lt1
Tlp5
E
Mi6
Mi5
Mi7
Mi2
Mi4
Mi3
Mi8
Mi1
Mi9
medulla
Tlp1
6 5 4 3 2 1
Tlp2
Lt7
Tlp3
Tlp4
lobula
lobulaplate

Figure 1.2. The *Drosophila* visual system

(A) Distribution of R7 and R8 axonal projections and synaptic contacts in the medulla. R7 and R8 projections revealed by the 24B10 antibody contact two different layers in the medulla. The synaptic marker disc large (Dlg) reveals the complexity in the number of synaptic contacts that R7 and R8 make in the medulla. High magnification of R7 and R8 axonal termini in the medulla show that the axons fasciculate at the entry of the medulla, R8 terminates in the 'M3' layer (blue line) and R7 projects deeper, to the 'M6' layer (purple line). L: lamina; M: medulla. Adapted from (Morante and Desplan, 2004). (B) Camera lucida drawings of photoreceptors and neurons connecting the lamina with the medulla. The serpentine layer (M7) separates the distal from the proximal medulla. Receptor axons of the R1-R6 terminate in the lamina, while the axons of the R7 and R8 project into the medulla. The 5 lamina monopolar neurons (L1-L5) have their cell bodies in the cell body distal to the lamina. Interneurons (T1 and lamina wide field Lawfl), C2 and C3 and Lawfl also innervate the lamina. (C) Composite of camera lucida drawings showing various types of TmY cells with retinotopically oriented terminals in the lobula and a parallel branch projecting along the different layers of the lobula plate. (D) Composite of camera lucida drawings showing amacrine cells of the distal (Dm) and proximal medulla (Pm), medulla (E) Composite of camera lucida drawings showing medulla intrinsic neurons (Mi). Medulla intrinsic neurons connect the distal with the proximal medulla. Their cell bodies are located in the medulla cortex. Mil is very frequently stained.

(B), (C), (D), (E) Adapted from (Fischbach and Dittrich, 1989).

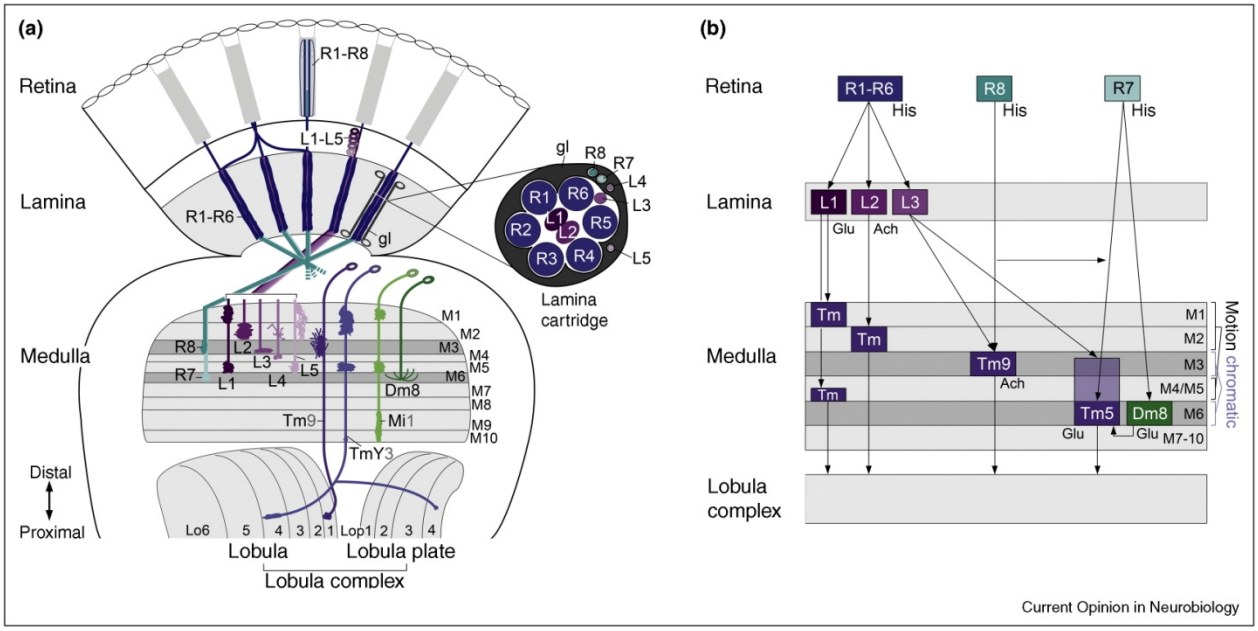
(a)
Retina
Lamina
Medulla
Distal
Proximal
R1-R8
L1-L5
R1-R6
gl
R8
R7
L4
L3
L5
R1
R6
R2
L1
L2
R5
R3
R4
Lamina cartridge
M1
M2
M3
M4
M5
M6
M7
M8
M9
M10
R8
R7
L1
L2
L3
L4
L5
Dm8
Tm9
Mi1
TmY3
Lo6
5
4
3
2
1
Lop1
2
3
4
Lobula
Lobula plate
Lobula complex
(b)
Retina
R1-R6
R8
R7
His
His
His
Lamina
L1
L2
L3
Glu
Ach
Medulla
Tm
Tm
Tm9
Ach
Tm
Tm5
Dm8
M6
Glu
Glu
M7-10
M1
M2
M3
M4/M5
Motion chromatic
Lobula complex
Current Opinion in Neurobiology

Figure 1.3 . Visual circuits in *Drosophila*

(a) Outer R-cells R1–R6 extend axons from the retina into the lamina. They form synaptic contacts with lamina neurons L1–L3. Inner Rcells R8 and R7 extend axons into the medulla and innervate M3 and M6. Lamina neurons L1–L5 form arborizations in layers M1–M5. The medulla is innervated by transmedullary neurons (Tm) connecting the medulla and the lobula, TmY neurons, whose branches connect the medulla with layers Lo1–6 in the lobula and Lop1–4 in the lobula plate, medulla intrinsic neurons (Mi) with processes solely connecting distal and proximal medulla neuropil layers, and amacrine distal medulla intrinsic neurons (Dm), branching within distal medulla neuropil layers.
(b) Motion detection involves achromatic synaptic input from R1–R6 axons to lamina neurons L1 and L2 in the lamina. These contact so far unidentified Tm and other higher order neurons in the medulla to transmit information to the lobula complex. Chromatic information processing involves synaptic input of R8 axons to R7 axons and to Tm9 neurons within the medulla. R7 axons make synaptic contacts with Tm5a–c neurons. About 13–16 R7 axons are presynaptic to wide-field amacrine Dm8 neurons, which arborize extensively within the M6 layer and provide input from a larger receptive field to Tm5 neurons. Tm5 and Tm9 neurons are postsynaptic to lamina neurons L3. R-cell axons use histamine (His) as neurotransmitter, while lamina neurons L1, Tm5c and Dm8 are glutamatergic (Glu), and L2 and Tm9 are cholinergic (Ach). Adapted from (Hadjieconomou et al., 2011)

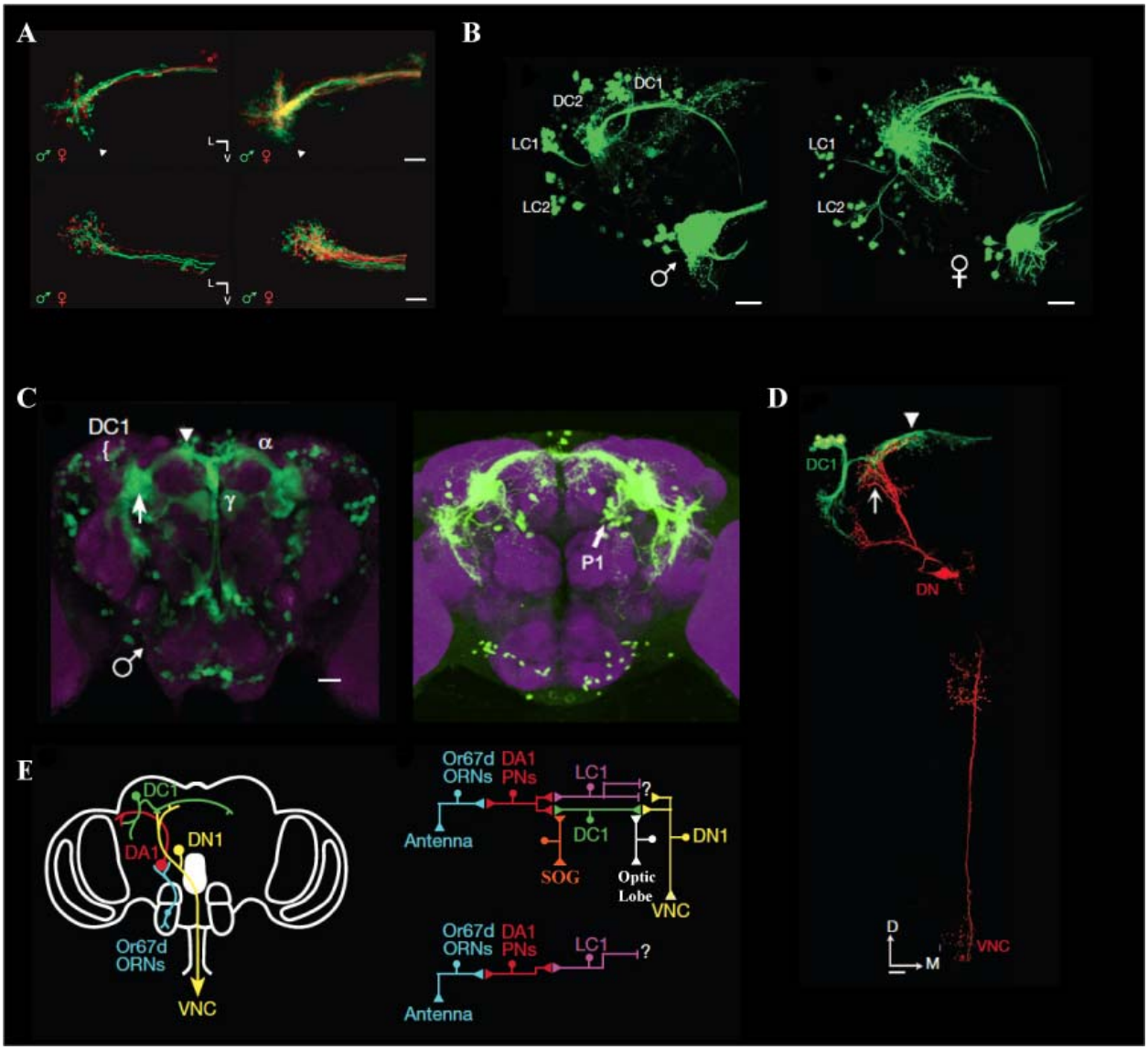
A
B
DC1
DC2
LC1
LC2
C
DC1
α
γ
P1
D
DC1
DN
VNC
D
M
E
DC1
DA1
DN1
Or67d
ORNs
VNC
Or67d ORNs
DA1 PNs
LC1
?
Antenna
DC1
DN1
SOG
Optic Lobe
VNC
Or67d ORNs
DA1 PNs
LC1
?
Antenna

Figure 1.4. cVA-responsive circuit in *Drosophila*

(A) Tracing and registration of DA1 glomerular projections reveals sexually dimorphic projections in the lateral horn. Superposition of male (green) and female (red) projections after photoconversion of all Fru1 DA1 PNs (top) in single flies reveals a ventral region of sexual dimorphism (arrowhead). Whereas, the controls with VM3 glomerulus (bottom) in single flies show no differences. Adapted from (Datta et al., 2008) (B) Photoactivation identifies dimorphic dorsal (DC1 and DC2) and lateral (LC1 and LC2) LH neuronal clusters in the male and in the female labels only lateral LH clusters. LC1 neurons are more numerous in males and DC1 and DC2 are absent in females. (C) NP2361 fruFLP UAS>stop>mCD8- GFP male labels DC1 neurons, also called P1 neurons whose activation results in song production. (D) DC1 neurons excite DN1, a cVA-responsive, male-specific descending neuron. (E) Circuit diagrams of the fly brain illustrating neurons that constitute the cVA-responsive circuit for identified dimorphic cVA pathways in the male (top) and female (bottom) and showing multimodal integration. (B), (C), (D), (E) Adapted from (Ruta et al., 2010; von Philipsborn et al., 2011)

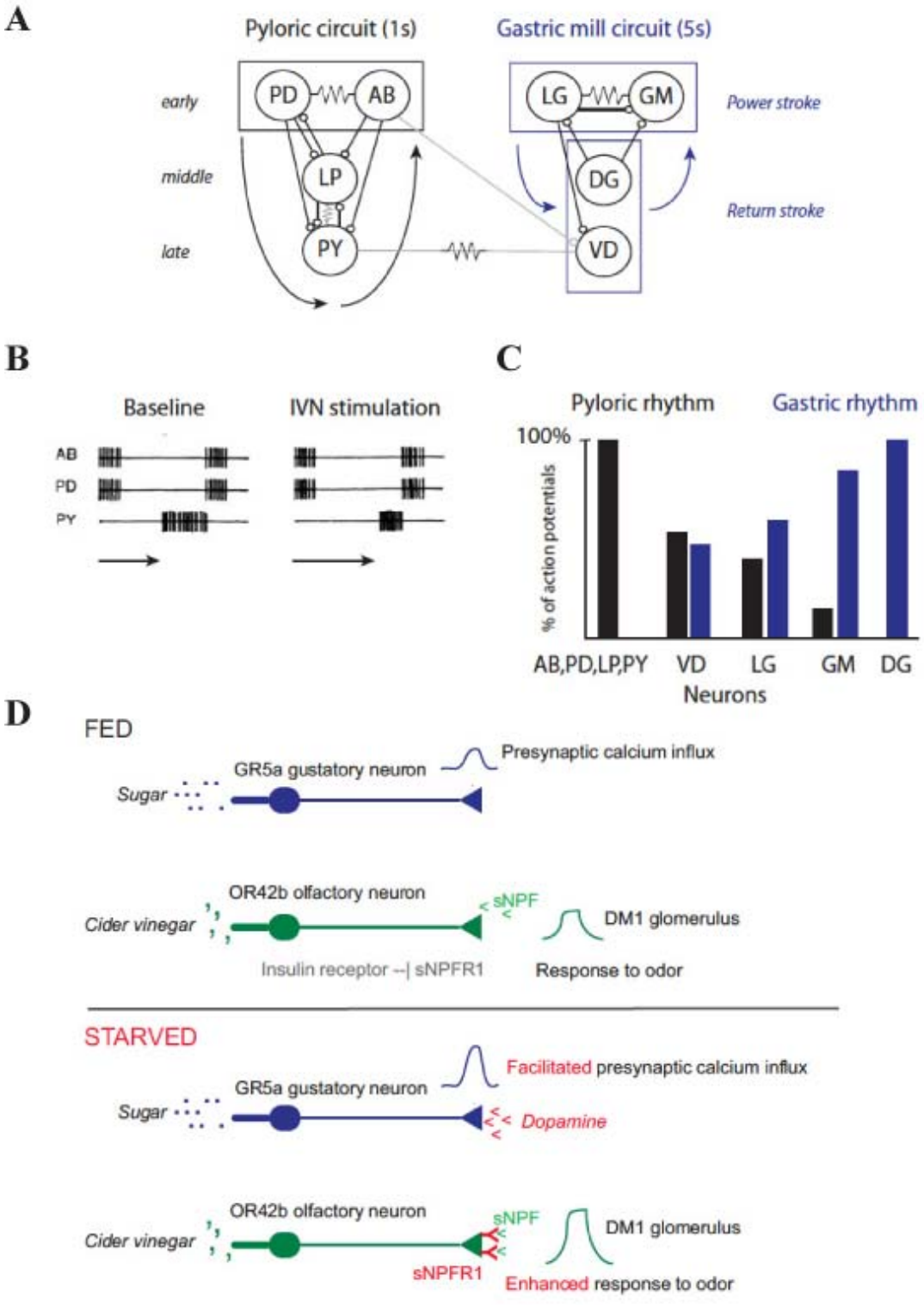
A
Pyloric circuit (1s)
Gastric mill circuit (5s)
early
middle
late
PD
AB
LP
PY
LG
GM
DG
VD
Power stroke
Return stroke
B
Baseline
IVN stimulation
AB
PD
PY
C
Pyloric rhythm
Gastric rhythm
100%
% of action potentials
AB,PD,LP,PY
VD
LG
GM
DG
Neurons
D
FED
GR5a gustatory neuron
Presynaptic calcium influx
Sugar
OR42b olfactory neuron
sNPF
Cider vinegar
DM1 glomerulus
Insulin receptor --| sNPFR1
Response to odor
STARVED
Facilitated presynaptic calcium influx
GR5a gustatory neuron
Sugar
Dopamine
OR42b olfactory neuron
sNPF
Cider vinegar
DM1 glomerulus
sNPFR1
Enhanced response to odor

Figure 1.5. Neuromodulation of circuits

(A) Two subcircuits of the STG, the pyloric and gastric circuit, showing inhibitory synapses (stopped arrows) and electrical synapses (jagged lines), arrows denote relative timing of neuronal firing during pyloric and gastric cycles. (B) The IVN nerve conveys sensory information from the stomach and its activation leads to sensory modulation of the pyloric circuit changing the phase of action potentials in component PY among the three classes of neurons in the circuit, altering circuit dynamics. (C) Quantitative analysis of individual neurons firing action potentials together with the pyloric rhythm (black) or the gastric rhythm (blue) during spontaneous activity. Modulatory inputs can change the contribution of VD and LG neurons switching between the pyloric and gastric mill subcircuits, altering circuit composition. (D) Modulation of Drosophila sensory gain by feeding state. In well-fed flies, sugar and cider vinegar stimulate gustatory (GR5a) and olfactory (OR42) neurons, respectively. The expression of the neuropeptide sNPF receptor is suppressed by insulin-like peptides that are present in fed animals. In starved flies, dopamine release onto GR5a presynaptic terminals facilitates calcium influx, and the sNPF receptor is induced on OR42 neurons, leading to presynaptic facilitation. In both gustatory and olfactory neurons, the gain of sensory input is increased by neuromodulation during starvation. Adapted from (Bargmann, 2012).

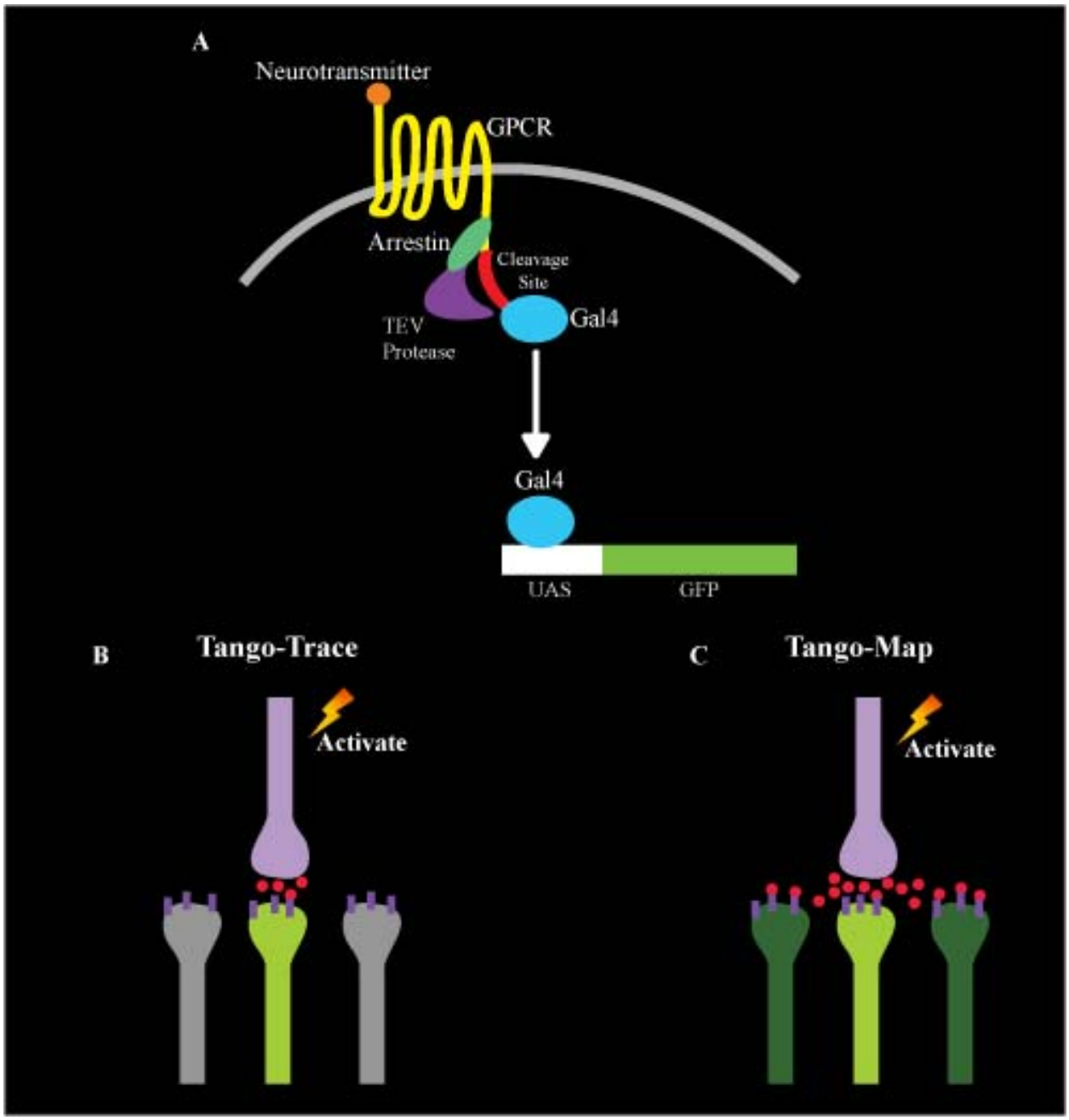
A
Neurotransmitter
GPCR
Arrestin
Cleavage Site
TEV Protease
Gal4
Gal4
UAS
GFP
B
Tango-Trace
Activate
C
Tango-Map
Activate

Figure 1.6. Tango Assay

(A) Ligand activation of GPCRs results in the phosphorylation of specific serine and threonine residues at the cytoplasmic C terminus tail of the receptor by a class of GPCR kinases (GRKs). Ligand-bound phosphorylated receptor then recruits arrestin, which competes with G protein binding to the receptor and prevents further activation of the receptor. When activated by a ligand, arrestin-TEV is recruited to the GPCR and cleaves the transcriptional activator at the cleavage site. The transcriptional activator then translocates to the nucleus to activate transcription of a reporter gene.

(B) Tango-Trace is a trans-synaptic tracer designed to detect synaptic transmission by chronic activation of the presynaptic neuron with a genetically targeted ion channel dTrpA1 and the identification of postsynaptic targets by GFP or any other reporter of choice.

(C) The design of Tango-Map allows for the detection of change in tango signal upon release of neuromodulatory transmitters in an area of the brain. Note the low signal to noise ratio due to volume transmission labels many neurons in the vicinity of the neuromodulator release.

A.

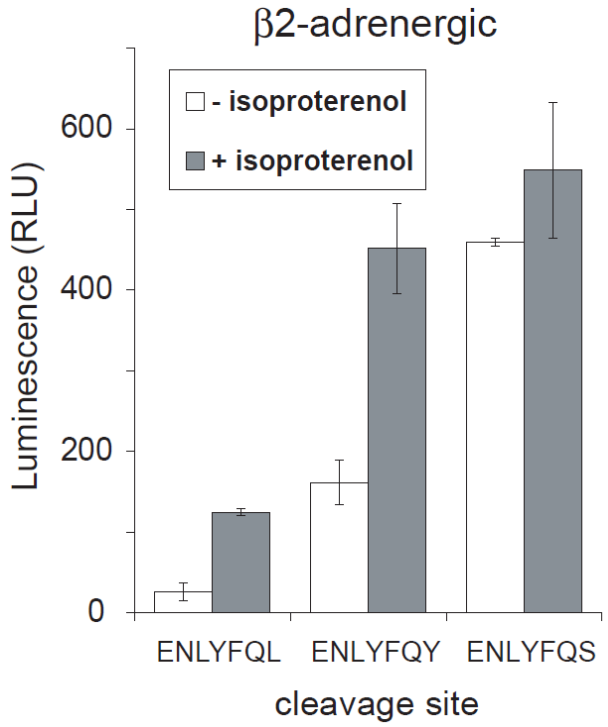
β2-adrenergic
- isoproterenol
+ isoproterenol
Luminescence (RLU)
600
400
200
0
ENLYFQL
ENLYFQY
ENLYFQS
cleavage site

B.

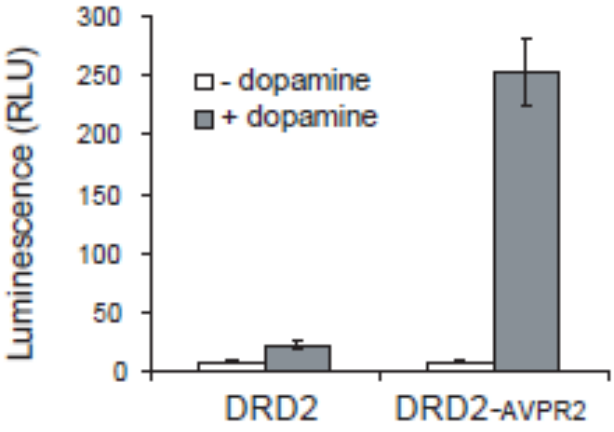
Luminescence (RLU)
300
250
200
150
100
50
0
- dopamine
+ dopamine
DRD2
DRD2-AVPR2

Figure 1.7. Enhancement of SNR in Tango assay

(A) Enhancing the signal-to-background ratio in a Tango assay by varying the TEV protease cleavage site. Quantitative reporter gene assays using b2- adrenergic receptor (b2-AR) - TCS-tTA fusions containing TEV recognition sites that are cleaved with varying efficiency. HTZ cells (an HEK293T derived cell line containing a stable integration of a tTA-dependent b-galactosidase reporter gene) were transiently transfected with b2-AR-TCS-tTA fusions containing the indicated seven amino acid TEV cleavage sites, together with a b-arrestin2-TEV protease construct.

(B) The C terminus of AVPR2 enhances the Tango assay for multiple GPCRs. Tango assay activity of the D2 dopamine receptor (DRD2) was enhanced by incorporating C-terminal tail sequences from the AVPR2. Cells were stimulated with 10 mM dopamine. Adapted from (Barnea et al., 2008).

1.13 References

Ache, B.W., and Young, J.M. (2005). Neuron *48*, 417.

Amrein, H., and Thorne, N. (2005). Curr Biol *15*, R673.

Anholt, R.R., Lyman, R.F., and Mackay, T.F. (1996). Genetics *143*, 293.

Baines, R.A., Uhler, J.P., Thompson, A., Sweeney, S.T., and Bate, M. (2001). Altered electrical properties in Drosophila neurons developing without synaptic transmission. J Neurosci *21*, 1523-1531.

Bargmann, C.I. (2012). Beyond the connectome: How neuromodulators shape neural circuits. BioEssays : news and reviews in molecular, cellular and developmental biology.

Barnea, G., Strapps, W., Herrada, G., Berman, Y., Ong, J., Kloss, B., Axel, R., and Lee, K.J. (2008). The genetic design of signaling cascades to record receptor activation. Proc Natl Acad Sci USA *105*, 64-69.

Bausenwein, B., Dittrich, A.P., and Fischbach, K.F. (1992). The optic lobe of Drosophila melanogaster. II. Sorting of retinotopic pathways in the medulla. Cell Tissue Res *267*, 17-28.

Beier, K.T., Saunders, A., Oldenburg, I.A., Miyamichi, K., Akhtar, N., Luo, L., Whelan, S.P., Sabatini, B., and Cepko, C.L. (2011). Anterograde or retrograde transsynaptic labeling of CNS neurons with vesicular stomatitis virus vectors. Proc Natl Acad Sci U S A *108*, 15414-15419.

Bellen, H.J., Tong, C., and Tsuda, H. (2010). 100 years of Drosophila research and its impact on vertebrate neuroscience: a history lesson for the future. Nat Rev Neurosci *11*, 514-522.

Benton, R., Vannice, K.S., and Vosshall, L.B. (2007). An essential role for a CD36-related receptor in pheromone detection in Drosophila. Nature *450*, 289-293.

Benveniste, H., and Huttemeier, P.C. (1990). Microdialysis--theory and application. Prog Neurobiol *35*, 195-215.

Bohland, J.W., Wu, C., Barbas, H., Bokil, H., Bota, M., Breiter, H.C., Cline, H.T., Doyle, J.C., Freed, P.J., Greenspan, R.J*., et al.* (2009). A proposal for a coordinated effort for the determination of brainwide neuroanatomical connectivity in model organisms at a mesoscopic scale. PLoS Comput Biol *5*, e1000334.

Borst, A. (2009). Drosophila's view on insect vision. Curr Biol *19*, R36-47.

Brand, A.H., and Perrimon, N. (1993). Development *118*, 401.

Braz, J.M., and Basbaum, A.I. (2008). Genetically expressed transneuronal tracer reveals direct and indirect serotonergic descending control circuits. J Comp Neurol *507*, 1990-2003.

Braz, J.M., Enquist, L.W., and Basbaum, A.I. (2009). Inputs to serotonergic neurons revealed by conditional viral transneuronal tracing. J Comp Neurol *514*, 145-160.

Broughton, S.J., Kitamoto, T., and Greenspan, R.J. (2004). Excitatory and inhibitory switches for courtship in the brain of Drosophila melanogaster. Curr Biol *14*, 538-547.

Buchner, E., Buchner, S., and Bülthoff, H. (1984). Identification of [3H]deoxyglucose-labelled interneurons in the fly from serial autoradiographs. Brain Res *305*, 384-388.

Buchner, E., Buchner, S., Burg, M.G., Hofbauer, A., Pak, W.L., and Pollack, I. (1993). Histamine is a major mechanosensory neurotransmitter candidate in Drosophila melanogaster. Cell Tissue Res *273*, 119-125.

Buck, L., and Axel, R. (1991). A novel multigene family may encode odorant receptors: a molecular basis for odor recognition. Cell *65*, 175-187.

Cabantous, S., Terwilliger, T.C., and Waldo, G.S. (2005). Protein tagging and detection with engineered self-assembling fragments of green fluorescent protein. Nature biotechnology *23*, 102-107.

Cabot, J.B., Mennone, A., Bogan, N., Carroll, J., Evinger, C., and Erichsen, J.T. (1991). Retrograde, trans-synaptic and transneuronal transport of fragment C of tetanus toxin by sympathetic preganglionic neurons. Neuroscience *40*, 805-823.

Cameron, P., Hiroi, M., Ngai, J., and Scott, K. (2010). The molecular basis for water taste in Drosophila. Nature *465*, 91-95.

Card, G., and Dickinson, M.H. (2008). Visually Mediated Motor Planning in the Escape Response of Drosophila. Current biology : CB *18*, 1300-1307.

Card, J.P., Kobiler, O., McCambridge, J., Ebdlahad, S., Shan, Z., Raizada, M.K., Sved, A.F., and Enquist, L.W. (2011). Microdissection of neural networks by conditional reporter expression from a Brainbow herpesvirus. Proc Natl Acad Sci U S A *108*, 3377-3382.

Card, J.P., Rinaman, L., Lynn, R.B., Lee, B.H., Meade, R.P., Miselis, R.R., and Enquist, L.W. (1993). Pseudorabies virus infection of the rat central nervous system: ultrastructural characterization of viral replication, transport, and pathogenesis. J Neurosci *13*, 2515-2539.

Card, J.P., Rinaman, L., Schwaber, J.S., Miselis, R.R., Whealy, M.E., Robbins, A.K., and Enquist, L.W. (1990). Neurotropic properties of pseudorabies virus: uptake and transneuronal passage in the rat central nervous system. J Neurosci *10*, 1974-1994.

Card, J.P., Whealy, M.E., Robbins, A.K., Moore, R.Y., and Enquist, L.W. (1991). Two alpha-herpesvirus strains are transported differentially in the rodent visual system. Neuron *6*, 957-969.

Carson, K.A., and Mesulam, M.M. (1982). Electron microscopic demonstration of neural connections using horseradish peroxidase: a comparison of the tetramethylbenzidine procedure with seven other histochemical methods. The journal of histochemistry and cytochemistry : official journal of the Histochemistry Society *30*, 425-435.

Chalfie, M., Sulston, J.E., White, J.G., Southgate, E., Thomson, J.N., and Brenner, S. (1985). The neural circuit for touch sensitivity in Caenorhabditis elegans. J Neurosci *5*, 956-964.

Chiappe, M.E., Seelig, J.D., Reiser, M.B., and Jayaraman, V. (2010). Walking Modulates Speed Sensitivity in Drosophila Motion Vision. Curr Biol *20*, 1470-1475.

Chou, W.H., Hall, K.J., Wilson, D.B., Wideman, C.L., Townson, S.M., Chadwell, L.V., and Britt, S.G. (1996). Identification of a novel Drosophila opsin reveals specific patterning of the R7 and R8 photoreceptor cells. Neuron *17*, 1101-1115.

Chyb, S., Dahanukar, A., Wickens, A., and Carlson, J.R. (2003). Drosophila Gr5a encodes a taste receptor tuned to trehalose. Proc Natl Acad Sci U S A *100 Suppl 2*, 14526-14530.

Clandinin, T.R., and Zipursky, S.L. (2002). Making connections in the fly visual system. Neuron *35*, 827-841.

Clark, D.A., Bursztyn, L., Horowitz, M.A., Schnitzer, M.J., and Clandinin, T.R. (2011). Defining the computational structure of the motion detector in Drosophila. Neuron *70*, 1165-1177.

Clyne, J.D., and Miesenbock, G. (2008). Sex-specific control and tuning of the pattern generator for courtship song in Drosophila. Cell *133*, 354-363.

Clyne, P.J., Warr, C.G., and Carlson, J.R. (2000). Science *287*, 1830.

Clyne, P.J., Warr, C.G., Freeman, M.R., Lessing, D., Kim, J., and Carlson, J.R. (1999). Neuron *22*, 327.

Couto, A., Alenius, M., and Dickson, B.J. (2005). Curr Biol *15*, 1535.

Crittenden, J.R., Skoulakis, E.M., Han, K.A., Kalderon, D., and Davis, R.L. (1998). Learn Mem *5*, 38.

Curanovic, D., and Enquist, L. (2009). Directional transneuronal spread of alpha-herpesvirus infection. Future virology *4*, 591.

Datta, S.R., Vasconcelos, M.L., Ruta, V., Luo, S., Wong, A., Demir, E., Flores, J., Balonze, K., Dickson, B.J., and Axel, R. (2008). The Drosophila pheromone cVA activates a sexually dimorphic neural circuit. Nature *452*, 473-477.

Davis, R.L. (2005). Annu Rev Neurosci *28*, 275.

de Belle, J.S., and Heisenberg, M. (1994). Science *263*, 692.

de Bruyne, M., Foster, K., and Carlson, J.R. (2001). Odor coding in the Drosophila antenna. Neuron *30*, 537-552.

de Vries, S.E., and Clandinin, T.R. (2012). Loom-sensitive neurons link computation to action in the Drosophila visual system. Curr Biol *22*, 353-362.

DeFalco, J., Tomishima, M., Liu, H., Zhao, C., Cai, X., Marth, J.D., Enquist, L., and Friedman, J.M. (2001). Virus-assisted mapping of neural inputs to a feeding center in the hypothalamus. Science *291*, 2608-2613.

DeFelipe, J. (2010). From the connectome to the synaptome: an epic love story. Science *330*, 1198-1201.

Delcomyn, F. (1980). Neural basis of rhythmic behavior in animals. Science *210*, 492-498.

Dickson, B.J. (2008). Wired for sex: the neurobiology of Drosophila mating decisions. Science *322*, 904-909.

Douglass, J.K., and Strausfeld, N.J. (2003). Retinotopic pathways providing motion-selective information to the lobula from peripheral elementary motion-detecting circuits. J Comp Neurol *457*, 326-344.

Douglass, J.K., and Strausfeld, N.J. (2007). Diverse speed response properties of motion sensitive neurons in the fly's optic lobe. J Comp Physiol A Neuroethol Sens Neural Behav Physiol *193*, 233-247.

Dunipace, L., Meister, S., McNealy, C., and Amrein, H. (2001). Curr Biol *11*, 822.

Estes, P.S., Ho, G.L., Narayanan, R., and Ramaswami, M. (2000). Synaptic localization and restricted diffusion of a Drosophila neuronal synaptobrevin--green fluorescent protein chimera in vivo. J Neurogenet *13*, 233-255.

Etessami, R., Conzelmann, K.K., Fadai-Ghotbi, B., Natelson, B., Tsiang, H., and Ceccaldi, P.E. (2000). Spread and pathogenic characteristics of a G-deficient rabies virus recombinant: an in vitro and in vivo study. The Journal of general virology *81*, 2147-2153.

Evinger, C., and Erichsen, J.T. (1986). Transsynaptic retrograde transport of fragment C of tetanus toxin demonstrated by immunohistochemical localization. Brain Res *380*, 383-388.

Farrow, K., Haag, J., and Borst, A. (2003). Input organization of multifunctional motion-sensitive neurons in the blowfly. J Neurosci *23*, 9805-9811.

Feinberg, E.H., Vanhoven, M.K., Bendesky, A., Wang, G., Fetter, R.D., Shen, K., and Bargmann, C.I. (2008). GFP Reconstitution Across Synaptic Partners (GRASP) defines cell contacts and synapses in living nervous systems. Neuron *57*, 353-363.

Fiala, A., Spall, T., Diegelmann, S., Eisermann, B., Sachse, S., Devaud, J.M., Buchner, E., and Galizia, C.G. (2002). Genetically expressed cameleon in Drosophila melanogaster is used to visualize olfactory information in projection neurons. Curr Biol *12*, 1877-1884.

Fischbach, K., and Dittrich, A. (1989). The optic lobe of Drosophila melanogaster. I. A Golgi analysis of wild-type structure. Cell Tissue Res.

Fischbach, K.F., Dittrich, A.P.M. (1989). The optic lobe of *Drosophila melanogaster*. I. A Golgi analysis of wild-type structure. Cell Tissue Res *258*, 441-475.

Fischbach, K.F., and Heisenberg, M. (1981). Structural brain mutant of Drosophila melanogaster with reduced cell number in the medulla cortex and with normal optomotor yaw response. Proc Natl Acad Sci U S A *78*, 1105-1109.

Fischler, W., Kong, P., Marella, S., and Scott, K. (2007). The detection of carbonation by the Drosophila gustatory system. Nature *448*, 1054-1057.

Fishilevich, E., and Vosshall, L.B. (2005). Curr Biol *15*, 1548.

Friesen, W.O., Poon, M., and Stent, G.S. (1978). Neuronal control of swimming in the medicinal leech. IV. Identification of a network of oscillatory interneurones. J Exp Biol *75*, 25-43.

Fryxell, K.J., and Meyerowitz, E.M. (1987). An opsin gene that is expressed only in the R7 photoreceptor cell of Drosophila. The EMBO journal *6*, 443-451.

Gao, Q., and Chess, A. (1999). Genomics *60*, 31.

Gao, Q., Yuan, B., and Chess, A. (2000). Nat Neurosci *3*, 780.

Gao, S., Takemura, S.Y., Ting, C.Y., Huang, S., Lu, Z., Luan, H., Rister, J., Thum, A.S., Yang, M., Hong, S.T.*, et al.* (2008). The neural substrate of spectral preference in Drosophila. Neuron *60*, 328-342.

Gaudry, Q., and Kristan, W.B., Jr. (2009). Behavioral choice by presynaptic inhibition of tactile sensory terminals. Nat Neurosci *12*, 1450-1457.

Gengs, C., Leung, H.-T., Skingsley, D.R., Iovchev, M.I., Yin, Z., Semenov, E.P., Burg, M.G., Hardie, R.C., and Pak, W.L. (2002a). The target of Drosophila photoreceptor synaptic

transmission is a histamine-gated chloride channel encoded by ort (hclA). J Biol Chem *277*, 42113-42120.

Gengs, C., Leung, H.T., Skingsley, D.R., Iovchev, M.I., Yin, Z., Semenov, E.P., Burg, M.G., Hardie, R.C., and Pak, W.L. (2002b). The target of Drosophila photoreceptor synaptic transmission is a histamine-gated chloride channel encoded by ort (hclA). J Biol Chem *277*, 42113-42120.

Gerfen, C.R., and Sawchenko, P.E. (1984). An anterograde neuroanatomical tracing method that shows the detailed morphology of neurons, their axons and terminals: immunohistochemical localization of an axonally transported plant lectin, Phaseolus vulgaris leucoagglutinin (PHA-L). Brain Res *290*, 219-238.

Getting, P.A. (1983). Mechanisms of pattern generation underlying swimming in Tritonia. II. Network reconstruction. J Neurophysiol *49*, 1017-1035.

Gibson, J.J. (1950). Perception of the Visual World.

Gillet, J.P., Derer, P., and Tsiang, H. (1986). Axonal transport of rabies virus in the central nervous system of the rat. Journal of neuropathology and experimental neurology *45*, 619-634.

Gisselmann, G., Pusch, H., Hovemann, B.T., and Hatt, H. (2002). Two cDNAs coding for histamine-gated ion channels in D. melanogaster. Nature neuroscience *5*, 11-12.

Glover, J.C., Petursdottir, G., and Jansen, J.K. (1986). Fluorescent dextran-amines used as axonal tracers in the nervous system of the chicken embryo. J Neurosci Methods *18*, 243-254.

Godement, P., Salaun, J., and Metin, C. (1987). Fate of uncrossed retinal projections following early or late prenatal monocular enucleation in the mouse. J Comp Neurol *255*, 97-109.

Gohl, D.M., Silies, M.A., Gao, X.J., Bhalerao, S., Luongo, F.J., Lin, C.C., Potter, C.J., and Clandinin, T.R. (2011). A versatile in vivo system for directed dissection of gene expression patterns. Nat Methods *8*, 231-237.

Golic, K.G., and Lindquist, S. (1989). The FLP recombinase of yeast catalyzes site-specific recombination in the Drosophila genome. Cell *59*, 499-509.

Gong, Z., Liu, J., Guo, C., Zhou, Y., Teng, Y., and Liu, L. (2010). Two pairs of neurons in the central brain control Drosophila innate light preference. Science *330*, 499-502.

Gordon, M.D., and Scott, K. (2009). Motor control in a Drosophila taste circuit. Neuron *61*, 373-384.

Götz, K.G., Wenking, H. (1973). Visual control of locomotion in the walking fruitfly Drosophila. Journal of Comparative Physiology A *85*, 235-266.

Gradinaru, V., Zhang, F., Ramakrishnan, C., Mattis, J., Prakash, R., Diester, I., Goshen, I., Thompson, K.R., and Deisseroth, K. (2010). Molecular and cellular approaches for diversifying and extending optogenetics. Cell *141*, 154-165.

Grafstein, B. (1971). Transneuronal transfer of radioactivity in the central nervous system. Science *172*, 177-179.

Gronenberg, W., and Strausfeld, N.J. (1992). Premotor descending neurons responding selectively to local visual stimuli in flies. J Comp Neurol *316*, 87-103.

Ha, T.S., and Smith, D.P. (2006). J Neurosci *26*, 8727.

Haag, J., and Borst, A. (2003). Orientation tuning of motion-sensitive neurons shaped by vertical-horizontal network interactions. J Comp Physiol A Neuroethol Sens Neural Behav Physiol *189*, 363-370.

Haag, J., and Borst, A. (2008). Electrical coupling of lobula plate tangential cells to a heterolateral motion-sensitive neuron in the fly. J Neurosci *28*, 14435-14442.

Haag, J., Wertz, A., and Borst, A. (2007). Integration of lobula plate output signals by DNOVS1, an identified premotor descending neuron. J Neurosci *27*, 1992-2000.

Hadjieconomou, D., Timofeev, K., and Salecker, I. (2011). A step-by-step guide to visual circuit assembly in Drosophila. Curr Opin Neurobiol *21*, 76-84.

Halfon, M.S., Gisselbrecht, S., Lu, J., Estrada, B., Keshishian, H., and Michelson, A.M. (2002). New fluorescent protein reporters for use with the Drosophila Gal4 expression system and for vital detection of balancer chromosomes. Genesis *34*, 135-138.

Hallem, E.A., and Carlson, J.R. (2006). Cell *125*, 143.

Hamada, F.N., Rosenzweig, M., Kang, K., Pulver, S.R., Ghezzi, A., Jegla, T.J., and Garrity, P.A. (2008). An internal thermal sensor controlling temperature preference in Drosophila. Nature *454*, 217-220.

Hardie, R.C. (1987). Is histamine a neurotransmitter in insect photoreceptors? J Comp Physiol A *161*, 201-213.

Harrison, P.J., Hultborn, H., Jankowska, E., Katz, R., Storai, B., and Zytnicki, D. (1984). Labelling of interneurones by retrograde transsynaptic transport of horseradish peroxidase from motoneurones in rats and cats. Neurosci Lett *45*, 15-19.

Hausen, K. (1982). Motion sensitive interneurons in the optomotor system of the fly. II. The horizontal cells:
receptive field organization and response characteristics. Biological Cybernetics *46*, 67-79.

Heimbeck, G., Bugnon, V., Gendre, N., Keller, A., and Stocker, R.F. (2001). Proc Natl Acad Sci USA *98*, 15336.

Heisenberg, M. (2003). Nat Rev Neurosci *4*, 266.

Heisenberg, M., Wolf, R. (1984). Vision in Drosophila: genetics of microbehavior (Berlin/Heidelberg/New York/Tokyo: Springer-Verlag).

Heisenberg, M.a.B., E. (1977). The role of retinula cell types in visual behavior of *Drosophila Melanogaster*. J Comp Physiol A *187*, 127-162.

Hildebrand, J.G., and Shepherd, G.M. (1997). Annu Rev Neurosci *20*, 595.

Hiroi, M., Meunier, N., Marion-Poll, F., and Tanimura, T. (2004). J Neurobiol *61*, 333.

Hodge, J.J., Choi, J.C., O'Kane, C.J., and Griffith, L.C. (2005). Shaw potassium channel genes in Drosophila. J Neurobiol *63*, 235-254.

Hong, Y.M., and Thanos, S. (1996). A quantitative approach to identify and isolate pure populations of fluorescently labeled adult retinal ganglion cells using a pressure-driven microaspiration technique. Neurosci Lett *214*, 111-114.

Honig, M.G., and Hume, R.I. (1989a). Carbocyanine dyes. Novel markers for labelling neurons. Trends Neurosci *12*, 336-338.

Honig, M.G., and Hume, R.I. (1989b). Dil and diO: versatile fluorescent dyes for neuronal labelling and pathway tracing. Trends Neurosci *12*, 333-335, 340-331.

Horikawa, K., and Armstrong, W.E. (1988). A versatile means of intracellular labeling: injection of biocytin and its detection with avidin conjugates. J Neurosci Methods *25*, 1-11.

Huisman, A.M., Ververs, B., Cavada, C., and Kuypers, H.G. (1984). Collateralization of brainstem pathways in the spinal ventral horn in rat as demonstrated with the retrograde fluorescent double-labeling technique. Brain Res *300*, 362-367.

Inagaki, Hidehiko K., Ben-Tabou De-Leon, S., Wong, A.M., Jagadish, S., Ishimoto, H., Barnea, G., Kitamoto, T., Axel, R., and Anderson, David J. (2012). Visualizing Neuromodulation In Vivo: TANGO-Mapping of Dopamine Signaling Reveals Appetite Control of Sugar Sensing. Cell *148*, 583-595.

Inoshita, T., and Tanimura, T. (2006). Cellular identification of water gustatory receptor neurons and their central projection pattern in Drosophila. Proc Natl Acad Sci U S A *103*, 1094-1099.

Ito, K., Awano, W., Suzuki, K., Hiromi, Y., and Yamamoto, D. (1997). Development *124*, 761.

Joesch, M., Plett, J., Borst, A., and Reiff, D.F. (2008). Response properties of motion-sensitive visual interneurons in the lobula plate of Drosophila melanogaster. Curr Biol *18*, 368-374.

Joesch, M., Schnell, B., Raghu, S.V., Reiff, D.F., and Borst, A. (2010). ON and OFF pathways in Drosophila motion vision. Nature *468*, 300-304.

Joiner, W.J., Crocker, A., White, B.H., and Sehgal, A. (2006). Nature *441*, 757.

Katsov, A.Y., and Clandinin, T.R. (2008). Motion processing streams in Drosophila are behaviorally specialized. Neuron *59*, 322-335.

Kawasaki, F., Zou, B., Xu, X., and Ordway, R.W. (2004). Active zone localization of presynaptic calcium channels encoded by the cacophony locus of Drosophila. J Neurosci *24*, 282-285.

Keene, A.C., Stratmann, M., Keller, A., Perrat, P.N., Vosshall, L.B., and Waddell, S. (2004). Neuron *44*, 521.

Kim, J., Zhao, T., Petralia, R.S., Yu, Y., Peng, H., Myers, E., and Magee, J.C. (2012). mGRASP enables mapping mammalian synaptic connectivity with light microscopy. Nat Methods *9*, 96-102.

Kimura, K., Hachiya, T., Koganezawa, M., Tazawa, T., and Yamamoto, D. (2008). Fruitless and doublesex coordinate to generate male-specific neurons that can initiate courtship. Neuron *59*, 759-769.

Kimura, K., Ote, M., Tazawa, T., and Yamamoto, D. (2005). Fruitless specifies sexually dimorphic neural circuitry in the Drosophila brain. Nature *438*, 229-233.

Kita, H., and Armstrong, W. (1991). A biotin-containing compound N-(2-aminoethyl)biotinamide for intracellular labeling and neuronal tracing studies: comparison with biocytin. J Neurosci Methods *37*, 141-150.

Kitamoto, T. (2001). Conditional modification of behavior in Drosophila by targeted expression of a temperature-sensitive shibire allele in defined neurons. J Neurobiol *47*, 81-92.

Kleinfeld, D., and Sompolinsky, H. (1988). Associative neural network model for the generation of temporal patterns. Theory and application to central pattern generators. Biophysical journal *54*, 1039-1051.

Kondoh, Y., Kaneshiro, K.Y., Kimura, K., and Yamamoto, D. (2003). Proc R Soc London B *270*, 1005.

Kristan, W.B., Jr., Calabrese, R.L., and Friesen, W.O. (2005). Neuronal control of leech behavior. Prog Neurobiol *76*, 279-327.

Kristensson, K., and Olsson, Y. (1971). Uptake and retrograde axonal transport of peroxidase in hypoglossal neurons. Electron microscopical localization in the neuronal perikaryon. Acta neuropathologica *19*, 1-9.

Kurtovic, A., Widmer, A., and Dickson, B.J. (2007). A single class of olfactory neurons mediates behavioural responses to a Drosophila sex pheromone. Nature *446*, 542-546.

Lafay, F., Coulon, P., Astic, L., Saucier, D., Riche, D., Holley, A., and Flamand, A. (1991). Spread of the CVS strain of rabies virus and of the avirulent mutant AvO1 along the olfactory pathways of the mouse after intranasal inoculation. Virology *183*, 320-330.

Lai, S.L., and Lee, T. (2006). Genetic mosaic with dual binary transcriptional systems in Drosophila. Nat Neurosci *9*, 703-709.

Lapper, S.R., and Bolam, J.P. (1991). The anterograde and retrograde transport of neurobiotin in the central nervous system of the rat: comparison with biocytin. J Neurosci Methods *39*, 163-174.

Larsen, C.W., Hirst, E., Alexandre, C., and Vincent, J.P. (2003). Segment boundary formation in Drosophila embryos. Development *130*, 5625-5635.

Larsson, M.C., Domingos, A.I., Jones, W.D., Chiappe, M.E., Amrein, H., and Vosshall, L.B. (2004). Neuron *43*, 703.

Laughlin, J.D., Ha, T.S., Jones, D.N., and Smith, D.P. (2008). Activation of pheromone-sensitive neurons is mediated by conformational activation of pheromone-binding protein. Cell *133*, 1255-1265.

LaVail, J.H., and LaVail, M.M. (1972). Retrograde axonal transport in the central nervous system. Science *176*, 1416-1417.

Lee, T., Lee, A., and Luo, L. (1999). Development *126*, 4065.

Lee, T., and Luo, L. (1999). Neuron *22*, 451.

Leiss, F., Koper, E., Hein, I., Fouquet, W., Lindner, J., Sigrist, S., and Tavosanis, G. (2009). Characterization of dendritic spines in the Drosophila central nervous system. Dev Neurobiol *69*, 221-234.

Lichtman, J.W., and Sanes, J.R. (2008). Ome sweet ome: what can the genome tell us about the connectome? Curr Opin Neurobiol *18*, 346-353.

Lima, S.Q., and Miesenbˆck, G. (2005). Remote Control of Behavior through Genetically Targeted Photostimulation of Neurons. Cell *121*, 141-152.

Lu, J., Tapia, J.C., White, O.L., and Lichtman, J.W. (2009). The interscutularis muscle connectome. PLoS Biol *7*, e32.

Luan, H., Lemon, W.C., Peabody, N.C., Pohl, J.B., Zelensky, P.K., Wang, D., Nitabach, M.N., Holmes, T.C., and White, B.H. (2006). Functional dissection of a neuronal network required for cuticle tanning and wing expansion in Drosophila. J Neurosci *26*, 573-584.

Luo, L., Callaway, E.M., and Svoboda, K. (2008). Genetic dissection of neural circuits. Neuron *57*, 634-660.

Macosko, E.Z., Pokala, N., Feinberg, E.H., Chalasani, S.H., Butcher, R.A., Clardy, J., and Bargmann, C.I. (2009). A hub-and-spoke circuit drives pheromone attraction and social behaviour in C. elegans. Nature *458*, 1171-1175.

Mank, M., Ferrão Santos, A., Direnberger, S., Mrsic-Flogel, T.D., and Hofer, S.B. (2008). Nat Methods *5*, 805.

Manoli, D.S., Foss, M., Villella, A., Taylor, B.J., Hall, J.C., and Baker, B.S. (2005). Male-specific fruitless specifies the neural substrates of Drosophila courtship behaviour. Nature *436*, 395-400.

Marder, E., and Bucher, D. (2001). Central pattern generators and the control of rhythmic movements. Curr Biol *11*, R986-996.

Marder, E., and Bucher, D. (2007). Understanding Circuit Dynamics Using the Stomatogastric Nervous System of Lobsters and Crabs. Annual Review of Physiology *69*, 291-316.

Marella, S., Fischler, W., Kong, P., Asgarian, S., Rueckert, E., and Scott, K. (2006a). Neuron *49*, 285.

Marella, S., Fischler, W., Kong, P., Asgarian, S., Rueckert, E., and Scott, K. (2006b). Imaging taste responses in the fly brain reveals a functional map of taste category and behavior. Neuron *49*, 285-295.

Marin, E.C., Jefferis, G.S., Komiyama, T., Zhu, H., and Luo, L. (2002a). Cell *109*, 243.

Marin, E.C., Jefferis, G.S., Komiyama, T., Zhu, H., and Luo, L. (2002b). Representation of the glomerular olfactory map in the Drosophila brain. Cell *109*, 243-255.

Martin, J.R., Ernst, R., and Heisenberg, M. (1998). Learn Mem *5*, 179.

Maskos, U., Kissa, K., St Cloment, C., and Brulet, P. (2002). Retrograde trans-synaptic transfer of green fluorescent protein allows the genetic mapping of neuronal circuits in transgenic mice. Proc Natl Acad Sci U S A *99*, 10120-10125.

McKenna, M., Monte, P., Helfand, S.L., Woodard, C., and Carlson, J. (1989). Proc Natl Acad Sci USA *86*, 8118.

Meinertzhagen, I.A., and O'Neil, S.D. (1991). Synaptic organization of columnar elements in the lamina of the wild type in Drosophila melanogaster. J Comp Neurol *305*, 232-263.

Meinertzhagen, I.A., and Sorra, K.E. (2001). Synaptic organization in the fly's optic lamina: few cells, many synapses and divergent microcircuits. Prog Brain Res *131*, 53-69.

Montell, C., Jones, K., Zuker, C., and Rubin, G. (1987). A second opsin gene expressed in the ultraviolet-sensitive R7 photoreceptor cells of Drosophila melanogaster. J Neurosci *7*, 1558-1566.

Moon, S.J., Kottgen, M., Jiao, Y., Xu, H., and Montell, C. (2006). A taste receptor required for the caffeine response in vivo. Curr Biol *16*, 1812-1817.

Morante, J., and Desplan, C. (2004). Building a projection map for photoreceptor neurons in the Drosophila optic lobes. Semin Cell Dev Biol *15*, 137-143.

Morante, J., and Desplan, C. (2008). The color-vision circuit in the medulla of Drosophila. Curr Biol *18*, 553-565.

Mori, I., and Ohshima, Y. (1995). Neural regulation of thermotaxis in Caenorhabditis elegans. Nature *376*, 344-348.

Mosca, T.J., Carrillo, R.A., White, B.H., and Keshishian, H. (2005). Dissection of synaptic excitability phenotypes by using a dominant-negative Shaker K+ channel subunit. Proc Natl Acad Sci U S A *102*, 3477-3482.

Murthy, M., Fiete, I., and Laurent, G. (2008). Testing odor response stereotypy in the Drosophila mushroom body. Neuron *59*, 1009-1023.

Nässel, D.R., and Strausfeld, N.J. (1982). A pair of descending neurons with dendrites in the optic lobes projecting directly to thoracic ganglia of dipterous insects. Cell Tissue Res *226*, 355-362.

Nassi, J.J., and Callaway, E.M. (2009). Parallel processing strategies of the primate visual system. Nat Rev Neurosci *10*, 360-372.

Nicolai, L.J., Ramaekers, A., Raemaekers, T., Drozdzecki, A., Mauss, A.S., Yan, J., Landgraf, M., Annaert, W., and Hassan, B.A. (2010). Genetically encoded dendritic marker sheds light on neuronal connectivity in Drosophila. Proc Natl Acad Sci U S A *107*, 20553-20558.

Nitabach, M.N., Wu, Y., Sheeba, V., Lemon, W.C., Strumbos, J., Zelensky, P.K., White, B.H., and Holmes, T.C. (2006). Electrical hyperexcitation of lateral ventral pacemaker neurons desynchronizes downstream circadian oscillators in the fly circadian circuit and induces multiple behavioral periods. J Neurosci *26*, 479-489.

O'Tousa, J.E., Baehr, W., Martin, R.L., Hirsh, J., Pak, W.L., and Applebury, M.L. (1985). The Drosophila ninaE gene encodes an opsin. Cell *40*, 839-850.

Pantazis, A., Segaran, A., Liu, C.-H., Nikolaev, A., Rister, J., Thum, A.S., Roeder, T., Semenov, E., Juusola, M., and Hardie, R.C. (2008). Distinct roles for two histamine receptors (hclA and hclB) at the Drosophila photoreceptor synapse. J Neurosci *28*, 7250-7259.

Papatsenko, D., Sheng, G., and Desplan, C. (1997). A new rhodopsin in R8 photoreceptors of Drosophila: evidence for coordinate expression with Rh3 in R7 cells. Development *124*, 1665-1673.

Paradis, S., Sweeney, S.T., and Davis, G.W. (2001). Homeostatic control of presynaptic release is triggered by postsynaptic membrane depolarization. Neuron *30*, 737-749.

Parisky, K.M., Agosto, J., Pulver, S.R., Shang, Y., Kuklin, E., Hodge, J.J.L., Kang, K., Kang, K., Liu, X., Garrity, P.A.*, et al.* (2008). PDF cells are a GABA-responsive wake-promoting component of the Drosophila sleep circuit. Neuron *60*, 672-682.

Park, J., Knezevich, P.L., Wung, W., O'Hanlon, S.N., Goyal, A., Benedetti, K.L., Barsi-Rhyne, B.J., Raman, M., Mock, N., Bremer, M.*, et al.* (2011). A conserved juxtacrine signal regulates synaptic partner recognition in Caenorhabditis elegans. Neural Dev *6*, 28.

Pfeiffer, B.D., Jenett, A., Hammonds, A.S., Ngo, T.B., and Misra, S. (2008). Proc Natl Acad Sci USA *105*, 9715.

Pfeiffer, B.D., Ngo, T.T., Hibbard, K.L., Murphy, C., Jenett, A., Truman, J.W., and Rubin, G.M. (2010). Refinement of tools for targeted gene expression in Drosophila. Genetics *186*, 735-755.

Pflugfelder, G.O., and Heisenberg, M. (1995). Optomotor-blind of Drosophila melanogaster: a neurogenetic approach to optic lobe development and optomotor behaviour. Comparative biochemistry and physiology Part A, Physiology *110*, 185-202.

Phillips, P.E., Robinson, D.L., Stuber, G.D., Carelli, R.M., and Wightman, R.M. (2003). Real-time measurements of phasic changes in extracellular dopamine concentration in freely moving rats by fast-scan cyclic voltammetry. Methods in molecular medicine *79*, 443-464.

Ping, Y., Waro, G., Licursi, A., Smith, S., Vo-Ba, D.A., and Tsunoda, S. (2011). Shal/K(v)4 channels are required for maintaining excitability during repetitive firing and normal locomotion in Drosophila. PLoS ONE *6*, e16043.

Pitman, J.L., McGill, J.J., Keegan, K.P., and Allada, R. (2006). Nature *441*, 753.

Porter, J.D., Guthrie, B.L., and Sparks, D.L. (1985). Selective retrograde transneuronal transport of wheat germ agglutinin-conjugated horseradish peroxidase in the oculomotor system. Experimental brain research Experimentelle Hirnforschung Experimentation cerebrale *57*, 411-416.

Potter, C.J., Tasic, B., Russler, E.V., Liang, L., and Luo, L. (2010). The Q system: a repressible binary system for transgene expression, lineage tracing, and mosaic analysis. Cell *141*, 536-548.

Pulver, S.R., Pashkovski, S.L., Hornstein, N.J., Garrity, P.A., and Griffith, L.C. (2009). Temporal dynamics of neuronal activation by Channelrhodopsin-2 and TRPA1 determine behavioral output in Drosophila larvae. J Neurophysiol *101*, 3075-3088.

Quinn, W.G., Harris, W.A., and Benzer, S. (1974). Proc Natl Acad Sci USA *71*, 708.

Raghu, S., and Borst, A. (2011). Candidate Glutamatergic Neurons in the Visual System of Drosophila. PLoS ONE *6*, e19472.

Rancz, E.A., Franks, K.M., Schwarz, M.K., Pichler, B., Schaefer, A.T., and Margrie, T.W. (2011). Transfection via whole-cell recording in vivo: bridging single-cell physiology, genetics and connectomics. Nat Neurosci *14*, 527-532.

Reiff, D.F., Plett, J., Mank, M., Griesbeck, O., and Borst, A. (2010). Visualizing retinotopic half-wave rectified input to the motion detection circuitry of Drosophila. Nature neuroscience *13*, 973-978.

Rideout, E.J., Billeter, J.C., and Goodwin, S.F. (2007). The sex-determination genes fruitless and doublesex specify a neural substrate required for courtship song. Curr Biol *17*, 1473-1478.

Ritzenthaler, S., Suzuki, E., and Chiba, A. (2000). Postsynaptic filopodia in muscle cells interact with innervating motoneuron axons. Nat Neurosci *3*, 1012-1017.

Rivera-Alba, M., Vitaladevuni, S.N., Mischenko, Y., Lu, Z., Takemura, S.Y., Scheffer, L., Meinertzhagen, I.A., Chklovskii, D.B., and de Polavieja, G.G. (2011a). Wiring economy and volume exclusion determine neuronal placement in the Drosophila brain. Curr Biol *21*, 2000-2005.

Rivera-Alba, M., Vitaladevuni, S.N., Mishchenko, Y., Lu, Z., Takemura, S.Y., Scheffer, L., Meinertzhagen, I.A., Chklovskii, D.B., and de Polavieja, G.G. (2011b). Wiring economy and volume exclusion determine neuronal placement in the Drosophila brain. Curr Biol *21*, 2000-2005.

Roeder, T. (2003). Metabotropic histamine receptors--nothing for invertebrates? Eur J Pharmacol *466*, 85-90.

Rolls, M.M., Satoh, D., Clyne, P.J., Henner, A.L., Uemura, T., and Doe, C.Q. (2007). Polarity and intracellular compartmentalization of Drosophila neurons. Neural Dev *2*, 7.

Root, C.M., Ko, K.I., Jafari, A., and Wang, J.W. (2011). Presynaptic facilitation by neuropeptide signaling mediates odor-driven food search. Cell *145*, 133-144.

Roper, S.D. (2007). Signal transduction and information processing in mammalian taste buds. Pflugers Archiv : European journal of physiology *454*, 759-776.

Rosenzweig, M., Brennan, K.M., Tayler, T.D., Phelps, P.O., Patapoutian, A., and Garrity, P.A. (2005). The Drosophila ortholog of vertebrate TRPA1 regulates thermotaxis. Genes Dev *19*, 419-424.

Rosenzweig, M., Kang, K., and Garrity, P.A. (2008). Distinct TRP channels are required for warm and cool avoidance in Drosophila melanogaster. Proc Natl Acad Sci U S A *105*, 14668-14673.

Rothermel, M., Brunert, D., Klupp, B.G., Luebbert, M., Mettenleiter, T.C., and Hatt, H. (2009). Advanced tracing tools: functional neuronal expression of virally encoded fluorescent calcium indicator proteins. Journal of neurovirology *15*, 458-464.

Ruta, V., Datta, S.R., Vasconcelos, M.L., Freeland, J., Looger, L.L., and Axel, R. (2010). A dimorphic pheromone circuit in Drosophila from sensory input to descending output. Nature *468*, 686-690.

Ryner, L.C., Goodwin, S.F., Castrillon, D.H., Anand, A., Villella, A., Baker, B.S., Hall, J.C., Taylor, B.J., and Wasserman, S.A. (1996). Control of male sexual behavior and sexual orientation in Drosophila by the fruitless gene. Cell *87*, 1079-1089.

Sakai, T., and Kitamoto, T. (2006). J Neurobiol *66*, 821.

Salcedo, E., Zheng, L., Phistry, M., Bagg, E.E., and Britt, S.G. (2003). Molecular basis for ultraviolet vision in invertebrates. J Neurosci *23*, 10873-10878.

Sanchez-Soriano, N., and Prokop, A. (2005). The influence of pioneer neurons on a growing motor nerve in Drosophila requires the neural cell adhesion molecule homolog FasciclinII. J Neurosci *25*, 78-87.

Sanes, J.R., and Zipursky, S.L. (2010). Design principles of insect and vertebrate visual systems. Neuron *66*, 15-36.

Sarthy, P.V. (1991). Histamine: a neurotransmitter candidate for Drosophila photoreceptors. J Neurochem *57*, 1757-1768.

Satterlie, R.A. (1985). Reciprocal inhibition and postinhibitory rebound produce reverberation in a locomotor pattern generator. Science *229*, 402-404.

Schlief, M.L., and Wilson, R.I. (2007). Olfactory processing and behavior downstream from highly selective receptor neurons. Nature neuroscience *10*, 623-630.

Schnell, B., Raghu, S.V., Nern, A., and Borst, A. (2012). Columnar cells necessary for motion responses of wide-field visual interneurons in Drosophila. J Comp Physiol A, 1-7.

Schubert, P., and Kreutzberg, G.W. (1974). Axonal transport of adenosine and uridine derivatives and transfer to postsynaptic neurons. Brain Res *76*, 526-530.

Schwab, M.E., and Thoenen, H. (1976). Electron microscopic evidence for a transsynaptic migration of tetanus toxin in spinal cord motoneurons: an autoradiographic and morphometric study. Brain Res *105*, 213-227.

Scott, K., Brady, R., Cravchik, A., Morozov, P., and Rzhetsky, A. (2001). Cell *104*, 661.

Seelig, J.D., Chiappe, M.E., Lott, G.K., Dutta, A., Osborne, J.E., Reiser, M.B., and Jayaraman, V. (2010). Two-photon calcium imaging from head-fixed Drosophila during optomotor walking behavior. Nat Methods *7*, 535-540.

Sengupta, P., Chou, J.H., and Bargmann, C.I. (1996). Cell *84*, 899.

Seung, H.S. (2009). Reading the book of memory: sparse sampling versus dense mapping of connectomes. Neuron *62*, 17-29.

Shang, Y., Haynes, P., Pirez, N., Harrington, K.I., Guo, F., Pollack, J., Hong, P., Griffith, L.C., and Rosbash, M. (2011). Imaging analysis of clock neurons reveals light buffers the wake-promoting effect of dopamine. Nat Neurosci *14*, 889-895.

Sheeba, V., Gu, H., Sharma, V.K., O'Dowd, D.K., and Holmes, T.C. (2008). Circadian- and light-dependent regulation of resting membrane potential and spontaneous action potential firing of Drosophila circadian pacemaker neurons. J Neurophysiol *99*, 976-988.

Sporns, O., Tononi, G., and Kotter, R. (2005). The human connectome: A structural description of the human brain. PLoS Comput Biol *1*, e42.

Stark, H. (2003). [News on the old histamine. II. Ion channels in Drosophila]. Pharm Unserer Zeit *32*, 93.

Stockinger, P., Kvitsiani, D., Rotkopf, S., Tirian, L., and Dickson, B.J. (2005). Neural circuitry that governs Drosophila male courtship behavior. Cell *121*, 795-807.

Strausfeld, N.J., and Hildebrand, J.G. (1999). Curr Opin Neurobiol *9*, 634.

Strausfeld, N.J., Sinakevitch, I., and Vilinsky, I. (2003). Microsc Res Tech *62*, 151.

Struhl, G., and Basler, K. (1993). Organizing activity of wingless protein in Drosophila. Cell *72*, 527-540.

Suh, G.S., Wong, A.M., Hergarden, A.C., Wang, J.W., and Simon, A.F. (2004). Nature *431*, 854.

Swanson, L.W., and Bota, M. (2010). Foundational model of structural connectivity in the nervous system with a schema for wiring diagrams, connectome, and basic plan architecture. Proc Natl Acad Sci U S A *107*, 20610-20617.

Sweeney, S.T., Broadie, K., Keane, J., Niemann, H., and O'Kane, C.J. (1995). Targeted expression of tetanus toxin light chain in Drosophila specifically eliminates synaptic transmission and causes behavioral defects. Neuron *14*, 341-351.

Takemura, S.-Y., Karuppudurai, T., Ting, C.-Y., Lu, Z., Lee, C.-H., and Meinertzhagen, Ian A. (2011). Cholinergic Circuits Integrate Neighboring Visual Signals in a Drosophila Motion Detection Pathway. Curr Biol *21*, 2077-2084.

Takemura, S.Y., Lu, Z., and Meinertzhagen, I.A. (2008). Synaptic circuits of the Drosophila optic lobe: the input terminals to the medulla. J Comp Neurol *509*, 493-513.

Tanaka, N.K., Awasaki, T., Shimada, T., and Ito, K. (2004). Curr Biol *14*, 449.

Tang, Y., Rampin, O., Giuliano, F., and Ugolini, G. (1999). Spinal and brain circuits to motoneurons of the bulbospongiosus muscle: retrograde transneuronal tracing with rabies virus. J Comp Neurol *414*, 167-192.

Tanouye, M.A., and Wyman, R.J. (1980). Motor outputs of giant nerve fiber in Drosophila. J Neurophysiol *44*, 405-421.

Thanos, S., and Bonhoeffer, F. (1983). Investigations on the development and topographic order of retinotectal axons: anterograde and retrograde staining of axons and perikarya with rhodamine in vivo. J Comp Neurol *219*, 420-430.

Thanos, S., and Bonhoeffer, F. (1987). Axonal arborization in the developing chick retinotectal system. J Comp Neurol *261*, 155-164.

Thorne, N., Chromey, C., Bray, S., and Amrein, H. (2004). Curr Biol *14*, 1065.

Thum, A.S., Knapek, S., Rister, J., Dierichs-Schmitt, E., Heisenberg, M., and Tanimoto, H. (2006). Differential potencies of effector genes in adult Drosophila. J Comp Neurol *498*, 194-203.

Thyagarajan, A., and Ting, A.Y. (2010). Imaging activity-dependent regulation of neurexin-neuroligin interactions using trans-synaptic enzymatic biotinylation. Cell *143*, 456-469.

Tovee, M.J. (1995). Ultra-violet photoreceptors in the animal kingdom: their distribution and function. Trends in ecology & evolution *10*, 455-460.

Ugolini, G., Kuypers, H.G., and Strick, P.L. (1989). Transneuronal transfer of herpes virus from peripheral nerves to cortex and brainstem. Science *243*, 89-91.

van der Goes van Naters, W., and Carlson, J.R. (2007). Receptors and neurons for fly odors in Drosophila. Curr Biol *17*, 606-612.

Varshney, L.R., Chen, B.L., Paniagua, E., Hall, D.H., and Chklovskii, D.B. (2011). Structural properties of the Caenorhabditis elegans neuronal network. PLoS Comput Biol *7*, e1001066.

Venken, Koen J.T., Simpson, Julie H., and Bellen, Hugo J. (2011). Genetic Manipulation of Genes and Cells in the Nervous System of the Fruit Fly. Neuron *72*, 202-230.

Villella, A., and Hall, J.C. (1996). Courtship anomalies caused by doublesex mutations in Drosophila melanogaster. Genetics *143*, 331-344.

Viney, T.J., Balint, K., Hillier, D., Siegert, S., Boldogkoi, Z., Enquist, L.W., Meister, M., Cepko, C.L., and Roska, B. (2007). Local retinal circuits of melanopsin-containing ganglion cells identified by transsynaptic viral tracing. Curr Biol *17*, 981-988.

von Philipsborn, A.C., Liu, T., Yu, J.Y., Masser, C., Bidaye, S.S., and Dickson, B.J. (2011). Neuronal control of Drosophila courtship song. Neuron *69*, 509-522.

Vosshall, L.B., Amrein, H., Morozov, P.S., Rzhetsky, A., and Axel, R. (1999). A spatial map of olfactory receptor expression in the Drosophila antenna. Cell *96*, 725-736.

Vosshall, L.B., and Stocker, R.F. (2007). Molecular architecture of smell and taste in Drosophila. Annu Rev Neurosci *30*, 505-533.

Vosshall, L.B., Wong, A.M., and Axel, R. (2000). Cell *102*, 147.

Wagh, D.A., Rasse, T.M., Asan, E., Hofbauer, A., Schwenkert, I., Durrbeck, H., Buchner, S., Dabauvalle, M.C., Schmidt, M., Qin, G.*, et al.* (2006). Bruchpilot, a protein with homology to ELKS/CAST, is required for structural integrity and function of synaptic active zones in Drosophila. Neuron *49*, 833-844.

Waldvogel, F.-M., and Fischbach, K.-F. - Plasticity of the landing response of <i>Drosophila melanogaster</i>. - *169*.

Wang, J., Ma, X., Yang, J.S., Zheng, X., Zugates, C.T., Lee, C.H., and Lee, T. (2004a). Transmembrane/juxtamembrane domain-dependent Dscam distribution and function during mushroom body neuronal morphogenesis. Neuron *43*, 663-672.

Wang, J.W., Wong, A.M., Flores, J., Vosshall, L.B., and Axel, R. (2003). Cell *112*, 271.

Wang, Z., Singhvi, A., Kong, P., and Scott, K. (2004b). Cell *117*, 981.

Wang, Z., Singhvi, A., Kong, P., and Scott, K. (2004c). Taste representations in the Drosophila brain. Cell *117*, 981-991.

Wanner, K.W., Nichols, A.S., Walden, K.K., Brockmann, A., Luetje, C.W., and Robertson, H.M. (2007). A honey bee odorant receptor for the queen substance 9-oxo-2-decenoic acid. Proc Natl Acad Sci U S A *104*, 14383-14388.

Wardill, T.J., List, O., Li, X., Dongre, S., McCulloch, M., Ting, C.Y., O'Kane, C.J., Tang, S., Lee, C.H., Hardie, R.C.*, et al.* (2012). Multiple spectral inputs improve motion discrimination in the Drosophila visual system. Science *336*, 925-931.

Watts, R.J., Schuldiner, O., Perrino, J., Larsen, C., and Luo, L. (2004). Glia engulf degenerating axons during developmental axon pruning. Curr Biol *14*, 678-684.

White, J.G., Southgate, E., Thomson, J.N., and Brenner, S. (1986). The structure of the nervous system of the nematode Caenorhabditis elegans. Philosophical transactions of the Royal Society of London Series B, Biological sciences *314*, 1-340.

Wickersham, I.R., Finke, S., Conzelmann, K.K., and Callaway, E.M. (2007a). Retrograde neuronal tracing with a deletion-mutant rabies virus. Nat Methods *4*, 47-49.

Wickersham, I.R., Lyon, D.C., Barnard, R.J., Mori, T., Finke, S., Conzelmann, K.K., Young, J.A., and Callaway, E.M. (2007b). Monosynaptic restriction of transsynaptic tracing from single, genetically targeted neurons. Neuron *53*, 639-647.

Witte, I., Kreienkamp, H.-J., Gewecke, M., and Roeder, T. (2002). Putative histamine-gated chloride channel subunits of the insect visual system and thoracic ganglion. J Neurochem *83*, 504-514.

Wong, A.M., Wang, J.W., and Axel, R. (2002). Spatial representation of the glomerular map in the Drosophila protocerebrum. Cell *109*, 229-241.

Woodard, C., Huang, T., Sun, H., Helfand, S.L., and Carlson, J. (1989). Genetics *123*, 315.

Xu, P., Atkinson, R., Jones, D.N., and Smith, D.P. (2005). Drosophila OBP LUSH is required for activity of pheromone-sensitive neurons. Neuron *45*, 193-200.

Yagi, R., Mayer, F., and Basler, K. (2010). Refined LexA transactivators and their use in combination with the Drosophila Gal4 system. Proc Natl Acad Sci U S A *107*, 16166-16171.

Yamaguchi, S., Wolf, R., Desplan, C., and Heisenberg, M. (2008). Motion vision is independent of color in Drosophila. Proc Natl Acad Sci U S A *105*, 4910-4915.

Yarmolinsky, D.A., Zuker, C.S., and Ryba, N.J. (2009). Common sense about taste: from mammals to insects. Cell *139*, 234-244.

Yasuyama, K., Meinertzhagen, I.A., and Schürmann, F.W. (2002). J Comp Neurol *445*, 211.

Yeh, E., Gustafson, K., and Boulianne, G.L. (1995). Green fluorescent protein as a vital marker and reporter of gene expression in Drosophila. Proc Natl Acad Sci U S A *92*, 7036-7040.

Yu, D., Baird, G.S., Tsien, R.Y., and Davis, R.L. (2003). Detection of calcium transients in Drosophila mushroom body neurons with camgaroo reporters. J Neurosci *23*, 64-72.

Zhang, M., Chung, S.H., Fang-Yen, C., Craig, C., Kerr, R.A., Suzuki, H., Samuel, A.D., Mazur, E., and Schafer, W.R. (2008). A self-regulating feed-forward circuit controlling C. elegans egg-laying behavior. Curr Biol *18*, 1445-1455.

Zhang, Y.Q., Rodesch, C.K., and Broadie, K. (2002). Living synaptic vesicle marker: synaptotagmin-GFP. Genesis *34*, 142-145.

Zheng, Y., Hirschberg, B., Yuan, J., Wang, A.P., Hunt, D.C., Ludmerer, S.W., Schmatz, D.M., and Cully, D.F. (2002). Identification of two novel Drosophila melanogaster histamine-gated chloride channel subunits expressed in the eye. J Biol Chem *277*, 2000-2005.

Zhu, Y., Nern, A., Zipursky, S.L., and Frye, M.A. (2009). Peripheral visual circuits functionally segregate motion and phototaxis behaviors in the fly. Curr Biol *19*, 613-619.

Zuker, C.S., Cowman, A.F., and Rubin, G.M. (1985). Isolation and structure of a rhodopsin gene from D. melanogaster. Cell *40*, 851-858.

Zuker, C.S., Montell, C., Jones, K., Laverty, T., and Rubin, G.M. (1987). A rhodopsin gene expressed in photoreceptor cell R7 of the Drosophila eye: homologies with other signal-transducing molecules. J Neurosci *7*, 1550-1557.

Chapter 2

Representations of visual information in *Drosophila* revealed by the trans-synaptic tracer Tango-trace

Statement of relative contributions:

In this chapter, all the data result from my research and experiments with the exception of data presented in the following figures, which were performed in collaboration with Damon Clark from Tom Clandinin's lab at Stanford University.

Figure 2.27

Figure 2.26

2.1 Introduction

Sensory information from the environment is transmitted from the periphery to the brain where it is processed to create an internal representation of the external world that can be used to guide a behavioral response. Characterization of neural circuits that may mediate behavior requires the development of tracing approaches that trace functional synaptic connections. Synapses can be enumerated by ultrastructural methods using serial electron microscope (EM) reconstruction and combined with functional imaging. However, such methods can currently achieve tracing microcircuitry within relatively small volumes of brain tissue (Briggman et al., 2011; Kleinfeld et al., 2011). Genetic targeting of trans-synaptic tracers like neurotropic viruses (Callaway, 2008; Wickersham et al., 2007c) has no practical applicability in *Drosophila*. We have therefore developed an activity dependent, genetic, anterograde trans-synaptic tracer that permits us to trace synaptic connections and ask how visual information is represented in the *Drosophila* brain.

The visual system processes information by extracting specific features of the visual stimulus like motion, color, form and shape (Bishop, 1933; Callaway, 2005; Goodale and Milner, 1992; Livingstone and Hubel, 1988; Strausfeld and Lee, 1991; Wassle, 2004). The neural pathways encoding these stimulus features are not strictly segregated (Gao et al., 2008b; Nassi and Callaway, 2009b; Wardill et al., 2012). Rather, the pathways must converge at several stages of the circuit and recombine to create a meaningful representation that translates into behavioral responses. In insects, visual information is transmitted from the peripheral photoreceptors to specific areas of the optic lobe implicated in behavioral output (Clark et al., 2011; de Vries and Clandinin, 2012; Douglass and Strausfeld, 2003;

Götz, 1973; Hausen, 1982; Heisenberg, 1984; Katsov and Clandinin, 2008; Rister et al., 2007; Zhu et al., 2009). Despite the numerical simplicity of the *Drosophila* brain, the delineation of circuits driving these visual behaviors has remained an arduous task. Visual perception is initiated by absorption of light by rhodopsins expressed in a dense array of photoreceptors in the retina. The insect visual system has eight peripheral photoreceptors R1-8, classified as outer (R1-6) and inner (R7/R8) photoreceptors (Clandinin and Zipursky, 2002; Sanes and Zipursky, 2010). Activity mapping with 2-deoxyglucose, electrophysiological and behavioral studies demonstrate that the outer photoreceptors are involved in processing motion information and the inner photoreceptors are involved in processing spectral information (Buchner et al., 1984; Heisenberg, 1977) (see chapter 1 for anatomy).

Electrophysiology, behavior and optical imaging reveal that the direction-selective lobula plate tangential cells (LPTCs) are involved in motion vision (Farrow et al., 2003; Haag and Borst, 2003; Haag and Borst, 2008; Joesch et al., 2008). Although the lobula complex has been implicated in motion vision, the inputs to this area remain poorly understood. Characterization of neural circuits that may mediate visual behaviors requires tracing synaptic connectivity of neurons that provide input to the lobula complex. The neural circuits of the inner photoreceptors, and their role in visual information processing have remained elusive. In the medulla, EM reconstruction studies have implied synaptic connections of R7s with the amacrine cell Dm8 and behavioral studies have demonstrated that Dm8 is required for UV phototaxis (Gao et al., 2008b). However, the neural circuits of the inner photoreceptors that transmit information from the medulla to the lobula complex remain poorly understood. TransmedullaryY (TmY) cells that extend their dendrites to

different layers of the medulla are likely to provide these inputs to the lobula and lobula plate (Fischbach, 1989). Moreover, it is likely that each of the four subtypes of the inner photoreceptors process information in separate neural circuits, but the post-synaptic partners of the p/y R7 and R8 circuits still remain unidentified.

In this study, we have identified a class of TmY cells that project to the lobula and lobula plate (Fischbach and Dittrich, 1989; Raghu and Borst, 2011), as the postsynaptic partners of p/y R7 and R8 with the activity-dependent trans-synaptic tracer. Each photoreceptor subtype contacts a unique TmY cell as a postsynaptic partner and might provide input to the motion pathway through the lobula plate projections of the TmY cells. The stochastically distributed p/yR7s and p/y R8s in the retina make precise connections with these four unique connectors that relay information to the lobula complex. Thus, the p/yR7s and p/y R8s process spectral information in separate pathways and relay information to the lobula and lobula plate. Spectral information of a visual scene is important for discrimination of objects during navigation in the external world (Gibson, 1950; Rodieck, 1979; Ungerleider and Mishkin, 1982). Behavioral and electrophysiological studies reveal that spectral information from the inner photoreceptors contributes to the motion pathway (Gao et al., 2008b; Wardill et al., 2012). Therefore, there is no strict segregation of motion and spectral information into separate visual pathways. Gap junctions between the inner and outer photoreceptors (Shaw et al., 1989; Wardill et al., 2012) could afford an explanation for an association of the inner and outer photoreceptors at the first stage of the circuit. This by itself is sufficient for visual discrimination of objects during navigation or, alternatively, the postsynaptic partners of R7 and R8 may additionally provide inputs to the motion pathway. Thus, spectral and motion pathways may converge repetitively at each stage of the circuit. The lobula projections of

the TmY cells we have identified afford the opportunity for color vision by comparing inputs from R7 and R8 in the innermost layer of the lobula. The lobula is also innervated by cells that are tuned to other visual features that may elicit innate behaviors (de Vries and Clandinin, 2012; Egelhaaf et al., 2002; Krapp et al., 1998). The TmY projections in the lobula may provide an anatomical substrate for these visual behaviors.

In addition, we label two postsynaptic partners that contact all the subtypes of R7 and R8, a wide-field amacrine cell Dm8 and an intrinsic medullary cell Mia. These cells afford an opportunity for horizontal integration of visual information at different layers of the medulla. In the TmY cells, we observe that the projections vary along the retinal coordinates and are non-stereotyped among individuals in the lobula plate. In the lobula, the projections of these neurons are stereotyped and similar among all the cell types. However, these four TmY cell types have unique projections in the medulla. Therefore, we could distinguish these cell types based on their morphology in the inner medulla.

We have developed an activity dependent, anterograde trans-synaptic tracer that has allowed us to define neural circuits in the *Drosophila* visual system and examine how visual information is represented in the insect brain. Our results demonstrate that the visual pathways converge repetitively at several stages of the circuit to shape the representation of visual information. These pathways reorganize into pathways that are likely to drive diverse visual behaviors.

2.2 Results

Histamine Tango Assay Detects Histamine Release in the Visual System

Insect photoreceptors utilize histamine (HA) as a neurotransmitter. We designed a genetically encoded trans-synaptic tracer that detects the endogenous release of histamine in the *Drosophila* brain. The tracer is based on the Tango assay (Barnea et al., 2008), a method by which transient receptor-ligand interactions produce a stable transcriptional readout. Ligand activation of G-protein coupled receptors (GPCRs) results in activation of GPCR kinases that phosphorylate specific serine and threonine residues in the C-terminal cytoplasmic domain of the receptor. Phosphorylated receptors then recruit arrestin, a cytosolic protein that competes with G proteins for receptor binding. In Drosophila, the known histamine receptors, *outer rhabdomeres transientless (ort; HisCl2)* and *HisCl1*, are chloride channels, not GPCRs (Gengs et al., 2002b; Gisselmann et al., 2002; Witte et al., 2002). We reasoned that since the human histamine receptor 2 (HRH2), a GPCR, is pharmacologically similar to the *Drosophila* histamine receptor *ort* (Buchner et al., 1993; Roeder, 2003; Sarthy, 1991; Stark, 2003), heterologous expression of HRH2 could be employed to detect endogenous histamine release in flies. We therefore generated a fusion protein (HRH2-TCS-Gal4), consisting of HRH2 joined at its C terminus to the transcriptional activator, Gal4. Interposed between these sequences, we introduced the wild-type cleavage site for a specific protease, N1a, from tobacco etch virus (TEV Cleavage Site). We then generated a second fusion protein consisting of the TEV protease linked to human β-arrestin2 (Arr-TEV). Ligand-dependent recruitment of Arr-TEV to the receptor fusion HRH2-TCS-Gal4 leads to proteolytic cleavage of the receptor, freeing Gal4 to translocate to the nucleus where it can induce expression of UAS transgenes (Figure 2.1A). These two fusion genes were expressed under the control of α-tubulin promoter (tubp) (Figure 2.1B). Next, we co-expressed *tubp-HRH2-TCS-Gal4*, *tubp-Arr-TEV* and *UAS mCD8-GFP* in

Drosophila S2 cells. Treatment of these cells with histamine resulted in HA-Tango labeling of cells with GFP expression (Figure 2.1C).

We next introduced the histamine tango system into flies and generated animals expressing *HRH2-TCS-Gal4* and *Arr-TEV* under the control of the tubulin promoter, as well as *UAS mCD8-GFP*. We refer to these flies as "HA-Tango" flies. In these flies, the Tango system should label cells that are exposed to histamine with CD8-GFP, allowing visualization of both axonal and dendritic projections. Next, in the HA-Tango flies, we tested TEV protease cleavage sites that were previously shown to maximize the signal-to-background ratio in cell culture (Barnea et al., 2008). We observed that the wild-type cleavage site provided the best signal for tracing in flies by decorating both axonal and dendritic projections, whereas the weaker TEV site that exhibited the best signal-to-background ratio in cell culture only labeled the cell bodies of histamine receptive neurons in flies (Figure 2.2). We therefore identified the wild-type site as the cleavage site that provided the best signal for HA-Tango tracing in flies. As light should activate the release of endogenous histamine from the photoreceptors, HA-Tango flies should display light-dependent labeling in the visual system. We therefore exposed the HA-Tango flies to 10s light flashes and examined the brains for HA-Tango labeling. We observed GFP expression in the lamina, medulla, lobula and lobula plate (Figure 2.1E) (n=12). In addition, GFP was also observed in glia surrounding the neuropils. Consistent with this expression reflecting light-dependent cleavage of HRH2-Gal4, GFP expression was not detected in control flies that expressed HRH2-Gal4 without the Arr-TEV fusion protein (Figure 2.1D) (n=9). To further test the requirement for histamine production, we next introduced the HRH2-Gal4 and Arr-Tev transgenes into flies homozygous for a hypomorphic mutation in histidine

decarboxylase (hdc). These flies display reduced histamine levels (Melzig et al., 1996) and in this background HA-Tango induced reporter expression is reduced (Figure 2.1F) (n=8), showing GFP expression mostly in the glia. These data demonstrate that GFP expression in HA-Tango flies is dependent on both Arrestin-TEV and histamine.

Histamine Tango Detects Histamine Release in Many Brain Regions

We next examined the extent of HA-Tango labeling in *Drosophila* brain. Histaminergic neurons have been implicated in temperature preference and circadian rhythms (Hamasaka and Nässel, 2006; Hong et al., 2006), and histamine has been detected in mechanosensory neurons (Buchner et al., 1993; Melzig et al., 1996). Consistent with these previous results, immunohistochemistry revealed histamine staining in the lamina, medulla and lobula of the optic lobe and strong staining in several areas of the central brain like the central complex, suboesophageal ganglion (SOG), antennal mechanosensory and motor center (AMMC), protocerebral regions, mushroom bodies (MB) and antennal lobes (AL) (Figure 2.3). In accord with these data, we observed HA-Tango labeling in the optic lobes, several areas of the central brain like the central complex, SOG, AMMC, protocerebral regions, MB and AL as well as theVNC of light-activated flies (Figures 2.4A-H and 2.5). Immunohistochemistry reveals long-range projections of these histaminergic neurons in the central brain. Modulatory neurons often exhibit widespread projections throughout the brain (Mao and Davis, 2009; Monastirioti, 1999). Therefore, behaviors like temperature preference and circadian rhythms are likely to result from neuromodulation of central brain circuits mediated by histamine. To determine the number of cells labeled by the Tango system, we used UAS nuclacZ, a transgene that encodes a β-Galactosidase variant bearing a nuclear

localization signal. We observed lacZ expression in 190 nuclei in the optic lobe (±63, n=16) (Figures 2.4A-C, 2.4I), 646 nuclei in the central brain (±86, n=27) (Figs 2.4D-F, 2.4I) and 605 nuclei in the VNC (±3, n=4) (Figures 2.4G-H, 2.4I). The projections of these cells were visualized with UAS mCD8-GFP (Figure 2.5, n=4) and we observed that these projections are in accord with the immunohistochemistry of histaminergic neurons in the brain (Figure 2.3). In control flies that were fed with the HRH2 antagonist cimetidine, HA-Tango labeling in the central brain was reduced (Figure 2.6, n=6). The number of cells labeled by the Tango system in the different brain areas suggests that the histamine is likely to be released as a neuromodulator in higher concentrations in the central brain and therefore labeling higher number of cells and as a fast neurotransmitter in the optic lobes.

Histamine Tango assay is Activity Dependent in the Visual System

We next determined the experimental conditions required to induce Tango labeling in the visual system. In initial experiments, HA-Tango flies were reared in different light conditions and then stained for GFP. The experimental light conditions we employed were: dark (Figure 2.7B) (n=8), ambient light (Figure 2.7A) (n=12), and dark followed by sudden exposure to 10s light flashes (Figure 2.7C) (n=12). We examined the brains by immunostaining 16 hours after light exposure to allow transcription of the reporter. To keep conditions consistent, immunohistochemistry and imaging for all the samples were performed on the same day. Quantitative analysis of the normalized fluorescence revealed that in the optic lobe, both dark reared and flies reared in ambient light exhibited low levels of GFP labeling. However, when flies were reared in the dark and exposed to sudden light flashes, GFP fluorescence increased 300-fold in the lamina (Figure 2.7D). We observed

strong GFP expression in the histamine receptive LMCs, which receive synaptic inputs from R1-6. In the medulla, we observed that GFP fluorescence increased by 60-fold (Figure 2.7E). The cell bodies of the HA-Tango labeled neurons were outside the distal medulla and their projections extended to several layers of the medulla and the lobula complex. In addition, there was a 20-fold increase in GFP expression in the lobula and lobula plate (Figure 2.7F-G). These results demonstrate that GFP expression in HA-Tango flies is dependent on light-dependent histamine release in optic lobe by photoreceptors and other histaminergic neurons.

To genetically control activation of histaminergic presynaptic cells, we next expressed the temperature sensitive cation channel dTrpA1 (Hamada et al., 2008; Pulver et al., 2009) in specific photoreceptor subtypes in the HA-Tango background. In these flies, heat should activate dTrpa1expressing neurons, independent of light. We used Rh promoter-Gal4 lines to drive *UAS dTrpA1* in p/y R7 and R8. In this approach, flies were reared in ambient light to keep any light-induced activity at low-levels and then exposed to heat to activate each photoreceptor subtype individually. We observed strong GFP expression in the medulla, where the postsynaptic cells receive inputs from R7 driven by *Rh4-Gal4* (Figure 2.8A, n=5) and R8 driven by *Rh6Gal4* (2.8B, n=4). In addition, GFP expression was observed in lobula and lobula plate where the postsynaptic partners of R7 and R8 are likely to project (Figure 2.8A-B). The pattern of arborization in the medulla and the lobula complex was strikingly similar for both the *Rh-Gal4* lines. In the medulla, there was richer arborization in layers 7-10 of the proximal medulla than the distal medulla. In the lobula complex, it appeared that the projections arborized more in the lobula plate than in the lobula. Expression of GFP was not detected in control flies that expressed HA-Tango

transgenes and dTrpA1, but not exposed to heat (Figure 2.8C, n=7), as well as control flies that expressed HA-Tango transgenes without dTrpA1 and exposed to heat (Figure 2.8D, n=10). These results demonstrate that this HA-Tango approach allows labeling of postsynaptic partners by activating genetically controlled presynaptic cells. We refer to this general technique of anterograde trans-synaptic tracing as 'Tango-trace' and the specific approach we used to trace histaminergic connections as 'HA-Tango-trace'.

Visualizing the Projections of Individual Post-synaptic Partners of R7 and R8

We next examined the projections of individual post-synaptic partners of specific inner photoreceptors. To do this, we combined HA-Tango-trace with Mosaic Analysis with a Repressible Cell Marker (MARCM), to allow expression of the transmembrane reporter mCD8-GFP in sparse populations of post-synaptic neurons. We generated flies that carry both the HA-Tango-trace transgenes, as well as the transgenes for MARCM. The loss of the transcriptional repressor Gal80 is achieved by FLP/FRT-mediated inter-chromosomal recombination in the visual neurons, induced by heat shock during development. Activation of the photoreceptors expressing dTrpA1 was then achieved by gradually warming these flies to 37^0C for two hours (see experimental procedures). In flies treated in this manner, mCD8-GFP is expressed in a sparse population of neurons that are labeled by HA-Tango-trace, and allows the visualization of the dendritic and axonal arbors of sparsely labeled post-synaptic neurons. This strategy also labels the presynaptic photoreceptors with *Rh-Gal4* driving the *UAS mCD8-GFP* reporter. Examination of over 3,000 fly brains has allowed us to trace the patterns of projections of 1697 individual post-synaptic targets of the inner photoreceptors from their dendritic arbor in the medulla to their axonal target. Since HA-

Tango-trace is activity dependent, some flies that got exposed to changes in light conditions exhibited HA-Tango labeling in L2 cells and we therefore excluded L2 from our analysis.

Analysis of the dendritic projections of the individual post-synaptic targets of R7 and R8 in the medulla reveals several features of visual representation. First, the inner photoreceptors, p/y R7 and R8 contact TmY cells that primarily send rich arbors in the proximal medulla, all the four layers of the lobula plate and the innermost layer of the lobula. The morphology of this cell type closely resembles a recently characterized cell type TmY^{new1}, which was identified using a Gal4 line that labels glutamatergic cells (Raghu and Borst, 2011). Each photoreceptor subtype contacts a unique variant of this cell type as a postsynaptic target. We refer to these variants as Rh3TmY, Rh4TmY, Rh5TmY and Rh6TmY (Figures 2.9 and 2.10) corresponding to their presynaptic partner. These variants extend their projections to the medulla and exhibit a morphological variation in their projection patterns in the proximal medulla. Rh3TmY and Rh6 TmYs have richer arbors than Rh4TmY and Rh5TmY (Figure 2.11). In the proximal medulla, Rh5TmY and Rh6 TmY have very distinct projection patterns in three dimensions with their arbors projecting in the antero-posterior (AP) axis and appear to contact two other photoreceptors (Figures 2.10- 2.11). The TmY cells then project to the lobula and lobula plate in a columnar manner maintaining the retinotopy (Figure 2.12). These projection patterns of all the TmY cell variants were conserved across animals (Figure 2.17). Second, an amacrine cell Dm8 was identified to be postsynaptic to all the inner photoreceptor subtypes (Figures 2.13A1-D1 and 2.14). Dm8 was shown to be a post-synaptic target of R7 using the histamine receptor ort promoter fusion, *ort-Gal4* line (Gao et al., 2008b). Dm8 is a wide field amacrine cell contacting 14-15 columns in the both the AP and dorso-ventral (DV) axes in layer 6 of the

distal medulla and was shown to be involved in UV phototaxis. Third, p/y R7s and R8s contact another post-synaptic target, an intrinsic medullary cell, which we refer to as Mia (Figures 2.13A2-D2 and 2.14). This cell type resembles a cell type Mi^{new2} that was identified using the *dvGluT-Gal4* line (Raghu and Borst, 2011), and innervates 4-5 columns in the DV axis in layers 7-9 of the proximal medulla as well innervates broadly in layer 1 of the distal medulla contacting 14-15 columns in both the AP and DV axes. Occasionally, we labeled Mi1 (n=3) and Tm20 (n=2) as the postsynaptic partners of yR8s (Figure 2.15).

On average, the sparse labeling strategy we employed with HA-Tango-trace resulted in TmY cells (346±58, n=45, Figure 2.16A, Table 1) being labeled an order of magnitude more frequently than Dm8 (33±10, n=24, Figure 2.16A, Table1) and Mia (46±23, n=24, Figure 2.16A, Table1) for every *Rh-Gal4* line. We also observe that the ratio of presynaptic and post-synaptic cells labeled by HA-Tango-trace in the case of TmY cells (0.35±0.05, n=45, Figure 2.16B, Table 2) was an order of magnitude higher than Dm8 (0.05±0.01, n=24, Figure 2.16B, Table 2) and Mia (0.03±0.02, n=24, Figure 2.16B, Table 2) for every *Rh-Gal4* line. If the MARCM technique randomly labels the post-synaptic targets of R7 and R8 with equal frequency, our data would imply that more TmY cells are likely to receive input from the inner photoreceptors and project to lobula and lobula plate maintaining the retinotopy. Fewer medulla local neurons project to different layers in the medulla. Dm8 projects to the distal medulla, Mia projects to the proximal medulla, and innervate multiple columns. Alternatively, the MARCM labeling approach may be nonrandom, such that some visual neurons may be more susceptible to MARCM. If true, there may be more post-synaptic targets that we may not detect with our approach. In order to distinguish among these alternatives, we adopted a MARCM-independent strategy that involves FLP mediated

excision of a cassette carrying Gal80 independent of cell division. In this approach, the HA-Tango-trace flies also carry the *hs-Flp* and *tubP>Gal80>* transgenes. Although we did not perform a detailed analysis as in the case of the data set with MARCM, we examined over 200 fly brains and 125 individual post-synaptic targets of the inner photoreceptors for any additional cell types. This approach did not result in identification of any additional post-synaptic targets of R7 and R8 (data not shown). However, this does not exclude the possibility that HA-Tango-trace can only selectively label strong synaptic connections and miss weaker connections.

Projections of the Individual TmY cells in the Lobula Plate

We next asked how visual information is represented in higher visual centers in the fly brain. We therefore analyzed the patterns of axonal projections of individual TmY neurons in the lobula and lobula plate (Figures 2.10, 2.18 and 2.19). In the sparse labeling strategy we employed with HA-Tango-trace in concert with MARCM, we were able to label 10-20 TmY neurons in the same brain (Figure 2.12). It is therefore possible to examine the axonal patterns from multiple, different TmYs that innervate the lobula and lobula plate of the same fly and compare this pattern across flies. For example, we have visualized the pattern of lobula plate axonal projections of three Rh3TmY neurons in one fly and two Rh3TmY neurons in another independent fly (Figure 2.19). TmY axons send a main branch to the lobula plate and extend into all the four layers exhibiting a coarse stereotypy (Figure 2.9-2.12 and 2.19). However, in some cases the main branch splits into two branches and has rich arborizations in the different layers of the lobula plate (Figure 2.19B). The finer

projections from this main branch vary and exhibit no stereotypy that we could discern. This projection pattern was observed in all the TmY variants and was conserved across animals.

Projections in the Lobula

In contrast to the lobula plate projections, the projections of the all the TmY variants extend to the innermost layer in the lobula and have a strikingly similar projection pattern and this pattern is conserved across animals. The axonal projections in lobula appear far simpler than the rich arborizations in the lobula plate (Figure 2.18). There could have been minor differences in this main pattern that we may not have been able to detect in our analysis.

Quantitative Analysis of TmY Projections.

Although visual inspection and semi-automated neuron tracing (Figure 6; see Methods) revealed that the projections of TmY cells in the proximal medulla, lobula and lobula plate differ in their complexity and stereotypy, we further analyzed these traced neurites quantitatively for anatomical differences. Sholl analysis is a widely used method to analyze morphological characteristics of an imaged neuron. The sholl intersections of branching topology of the semi-automated traced neurites (Figures 2.20-2.22) were further subjected to hierarchical cluster analysis (Figure 2.23). The proximal medulla projections clusters the TmY cells into four clusters corresponding to the four presynaptic partners they contact (Figures 2.17, 2.20 and 2.23, n=10). The lobula (Figures 2.18, 2.21 and 2.23, n=10) and lobula plate (Figures 2.19, 2.22 and 2.23, n=16) projections fall into two separate clusters. However, there was no cell-type specific clustering observed in either of the two projections.

Since the projections looked non-stereotyped in the lobula plate and not in the proximal medulla or lobula, more tracings from lobula plate were subjected to cluster analysis than proximal medulla and lobula to look for any hidden similarity and none was observed from the analysis.

Behavioral Responses to Motion Stimuli by Pale and Yellow R8s

We next wanted to examine whether the postsynaptic cells we label might be behaviorally significant. Do the TmY projections that extend to all the layers in the lobula plate, have a role in motion vision? We used a fly on the ball behavioral set up and monitored the turning response of a fly that has been presented with motion stimuli (Clark et al., 2011; Hassenstein, 1956). In this system, a walking fly is fixed in place by a pin glued to its thorax; as it walks, it counter-rotates a nearly frictionless, air-suspended ball. Three projection screens surround the fly where the motion stimuli are presented. When the fly attempts to rotate in response to a stimulus, the ball rotates and two optical mice record the motion of the ball as a read-out of the animal's behavioral response to the stimulus (Figure 2.24). We used norpA mutant flies that were blind and rescued in pale and yellow R8 cells with UAS norpA. We presented motion stimuli under bright light conditions to 2-3 day old flies and recorded their responses to motion stimuli with R8 being the only functional photoreceptor. First, we presented virtual cylinders consisting of sine wave contrast patterns rotating at varying speeds (Figure 2.25). In the control flies with just UAS norpA, this stimulus, as expected, did not elicit any motion response for these blind flies (Figures 2.26A-C, n=8). However, when we rescued norpA in R8 photoreceptors and presented the

stimuli, we saw a significant behavioral response to the motion stimulus (Figures 2.26D-F, n=6).

The elementary motion detectors in flies are thought to be Reichardt detectors, which work by correlating light intensities between neighboring points in space at different temporal delays. In a second experiment, we presented the fly with stimuli that swept contrast frequency, which provide an indirect measure of the delay filter in the Reichardt detector. The R8 rescue flies respond to these stimuli (Fig 2.27A-D) similar to Rh1 rescue flies (Fig 2.27E-H) and wild type flies (Fig 2.27I-L). The magnitude of raw response traces was slightly higher in Rh1 rescue flies (Fig 2.27F) and even higher in wild type flies (Fig 2.27J) than R8 rescue flies, which is what we would expect, given the efficiency with which the different rescued receptors collect light. Rescuing in norpA flies with rescued R1-R6 and R8 photoreceptors roughly sum up the mean responses of WT flies (Figure 2.27 B, F and J). These data imply that R8 photoreceptors additionally contribute to motion detection. Although these data do not directly demonstrate that the TmY cells we labeled are involved in motion detection, they demonstrate that the output of R8 photoreceptors can influence motion-evoked behavioral responses.

2.3 Discussion

We have devised an activity-dependent, genetic, anterograde, trans-synaptic tracing technique that permits us to ask how visual information is represented in the *Drosophila* brain. A “structural connectome” cannot predict functional connections that can lead to a behavioral output. Here we describe a genetically based method to trace synaptic connections based on the release of an endogenous neurotransmitter in an activity-dependent

manner. This is an unbiased, brain-wide approach that allows us to map connections in the *Drosophila* brain in an activity-dependent manner.

In this study, we ask how visual information from the inner photoreceptors is represented in the *Drosophila* optic lobe. We demonstrate that the spectral and motion pathways converge repetitively at two stages of the circuit. The neural circuits of the inner photoreceptors, and their role in visual information processing have remained elusive. EM reconstruction studies have implied synaptic connections of R7 and R8 cells with Tm5 and Tm9 cells that project to the lobula (Gao et al., 2008b). However, the synaptic contacts of all the four subtypes of the inner photoreceptors, p/y R7 and R8 still remain unidentified. The identification of the postsynaptic partners of all the subtypes of the inner photoreceptors is important for understanding how visual information is represented in the insect brain. Moreover, although the lobula plate has been implicated in motion vision, and anatomical tracings and recent electrophysiological studies imply that T cells may provide these inputs by projecting their bushy processes in the proximal medulla, lobula and lobula plate (Fischbach, 1989; Schnell et al., 2012), the inputs to this area still remain poorly understood.

We have traced synaptic connections of the inner photoreceptors with the trans-synaptic tracer HA-Tango-trace in an activity-dependent manner. In concert with MARCM, we achieved a sparse labeling of TmY cells, the synaptic partners we identified with the trans-synaptic tracer, and visualized the projections of these neurons. The second-order visual projection neurons receive information from the inner photoreceptors, arborize in the proximal medulla, split into two branches and then project to all the four layers of the lobula plate and the innermost layer of the lobula. The lobula plate is innervated by tangential cells that show direction-selective responses to motion stimuli. However, the inputs to these

tangential cells still remain unidentified. Therefore, the lobula plate projections of the synaptic partners of R7 and R8 we have identified may input to these neurons and deliver spectral information to the motion pathway at the second stage of the circuit. Furthermore, we used a fly on the ball behavioral set-up and presented motion stimuli under bright light conditions. When we selectively rescue norpA mutants in R8 cells, we see optomotor responses that differ from the responses we see with R1-6 rescue flies and wild-type flies. These data show that R8s influence motion-evoked behavioral responses under bright light conditions. Recent studies imply that the gap junctional connections between the inner and outer photoreceptors afford an opportunity for the spectral and motion vision pathways to converge at the first stage of the circuit (Wardill et al., 2012). Thus, these pathways converge repetitively at two stages of the circuit (Figure 2.29).

Interestingly, we observe that the innervations in the lobula plate reveal very different patterns of projections, whereas they exhibit strikingly similar axonal topography in the lobula. Thus, these neurons reveal non-stereotyped patterns of axon arborization in the lobula plate and strikingly stereotyped patterns of axon arborization in the lobula that are apparent upon visual inspection and are confirmed by more quantitative cluster analysis. This finding is in accord with anatomical tracing studies that demonstrate that lobula plate tangential cells exhibit non-stereotyped finer dendritic projections (Cuntz et al., 2008; Scott et al., 2002) in the lobula plate. However, these four TmY cell types have unique projections in the medulla. Therefore, we could distinguish these cell types based on their morphology in the inner medulla.

Moreover, activity mapping by 2-deoxyglucose labeling demonstrates activity in the proximal medulla to flicker stimulus and not motion stimuli (Buchner et al., 1984).

However, the innermost layer of the lobula and all the four layers of the lobula plate shows responses to motion stimuli in these activity mapping studies. Consistent with these results, the proximal medulla, lobula and lobula plate projections of the TmY cells we have identified are likely to provide a neural substrate for visual behaviors evoked by these stimuli. In addition, we label two postsynaptic partners of p/y R7 and R8, a wide-field amacrine cell Dm8 and an intrinsic medullary cell Mia that innervate multiple columns in the medulla. These cells afford an opportunity for horizontal integration of visual information at different layers of the medulla (Figures 2.28 and 2.29). Although behavioral studies show color discrimination in *Drosophila,* color vision has not been clearly demonstrated at the level of a neural circuit (Morante and Desplan, 2008; Pichaud et al., 1999). Color vision requires a comparator of information from two inputs. Electrophysiological studies in honeybees suggest color opponent neurons in the lobula (Yang et al., 2004). In *Drosophila*, a similar comparison of inputs from R7/R8 may occur in the lobula. The lobula projections of the TmY cells we have identified afford the opportunity for this comparison. The lobula is also innervated by cells that are tuned to other visual features that may elicit innate behaviors (de Vries and Clandinin, 2012; Egelhaaf et al., 2002; Krapp et al., 1998). The TmY projections in the lobula may provide an anatomical substrate for these visual behaviors.

Earlier studies have led to models in which stimulus features of the visual world are processed in parallel pathways before creating a unified and coherent visual percept (Callaway, 2005; Livingstone and Hubel, 1988). There is evidence in more recent studies in the vertebrate visual system, that the early parallel pathways converge significantly in the first few synapses rather than maintain strict segregation (Lachica et al., 1992; Nassi and

Callaway, 2009b; Sincich and Horton, 2004; Yabuta and Callaway, 1998). In this model, the pathways are recombined such that they form new output channels that project to specific areas of the brain resulting in specific visual behaviors. Thus, the stimulus features are actively recombined into a meaningful representation of the sensory world. This model is supported by experiments in this study demonstrating that the motion and spectral pathways converge at several stages of the circuit and reorganize into pathways in the lobula and lobula plate that are likely to drive diverse visual behaviors.

Despite the six hundred million years of evolution separating insects from mammals, the organizational logic of the visual pathways appears remarkably similar in fruit flies and vertebrates. Rods and cones relay visual information to bipolar cells in the retina. The bipolar cells synapse on retinal ganglion cells (RGCs). In the vertebrate visual system, midget, parasol and bistratified ganglion cells relay most information to the lateral geniculate nucleus (LGN) of the thalamus and is processed in parvocellular, magnocellular and koniocellular pathways respectively (Nassi and Callaway, 2009b; Sanes and Zipursky, 2010). The magnocellular pathway is specialized for motion detection, the parvocellular pathway appears to subserve form and high-acuity vision and the koniocellular pathway carries information about color. Cone bipolars input information to both magnocellular and koniocellular pathways through parasol and bistratified ganglion cells (Nassi and Callaway, 2009b). Thus, cones provide information to both motion and color pathways in the retina.

This information from the LGN is conveyed to the primary visual cortex (V1) before reaching the extrastriate visual cortex. Early models have proposed that magnocellular and parvocellular pathways remain segregated in V1 as they pass through layers 4B and 2/3 respectively (Fitzpatrick et al., 1985; Livingstone and Hubel, 1988). But, more recent

evidence shows that the blobs and interblobs of layer 2/3 receive convergent input from magnocellular and parvocellular pathways, with the blobs receiving additional direct input from the koniocellular layers of the LGN (Hendry and Yoshioka, 1994; Yabuta and Callaway, 1998; Yoshioka et al., 1994). These parallel input channels are thus recombined in V1 to create a meaningful visual representation in higher visual areas.

Sensitivity of Tango-Trace:

Tango-trace allows the detection of release of endogenous neurotransmitters in vivo in an activity-dependent manner. A similar approach Tango-map, was demonstrated to detect the release of endogenous neuromodulators in vivo and identify the circuits on which they act (Inagaki et al., 2012). The distinction between genetically targeted trans-neuronal tracers that trace anatomical connections, and Tango-trace is the ability to activate a genetically targeted presynaptic partner and detect the release of an endogenous neurotransmitter that activates a receptor on the postsynaptic partner. Thus, Tango-trace can identify postsynaptic partners of genetically defined subpopulations of neurons and trace synaptic connections in an activity-dependent and an unbiased manner. This approach allows the visualization of projection patterns of a population of synaptically connected partners in several areas of the brain as we describe here with the TmY projections in the lobula and lobula plate. Moreover, the transcriptional readout of the Tango system permits the expression not only of reporters allowing visualization of the neurons but also of effectors such as ion channels, calcium indicators and silencers in the synaptically connected neurons.

However, the sensitivity of Tango-trace to efficiently label all the postsynaptic partners of a given presynaptic partner is dependent on several factors. First, the overall expression

of the components of the tango assay, the GPCR-TCS-Gal4 fusion and the Arr-TEV fusion determines the extent of the tango assay reporter expression. Second, the random labeling strategies, both MARCM and MARCM-independent methods, employed in this study may have still missed a few postsynaptic partners. Third, cells lacking the GPCR kinases required for the phosphorylation of the receptor so that arrestin gets recruited to the receptor may not be labeled by the Tango-trace approach. Future versions of the assay can address these possibilities to look for any additional partners. Alternatively, if the strategy we employed with HA-Tango-trace labels the post-synaptic targets of R7 and R8 with equal frequency, our data would imply that the remaining Tm, Dm, Mi and TmYcells of the medulla do not receive direct input from the photoreceptors, but may be involved indirectly in visual information processing. Therefore, we describe a genetically based method to trace synaptic connections based on the release of an endogenous neurotransmitter in an activity-dependent manner. This brain-wide approach to tracing synaptic connections in a defined circuit can be readily adapted to other neurotransmitters in both the fly and mouse.

2.4 Experimental Procedures

Fly stocks

The *UAS dTrpA1* lines were generously provided by Paul Garrity (Hamada et al., 2008); *hs-Flp; tubp>Gal80,y*$^{+}$*>* transgenic flies were provided by Gary Struhl (Columbia University). *Rh3-Gal4* on II, *Rh4-Gal4* on II, *Rh5-Gal4* on II and *Rh6-Gal4* on III, *P(neoFRT)19A, P(tubP-GAL80)LL1, P(hsFLP)1, w[*]; P(UAS-mCD8::GFP)LL5;* (Bloomington Stock Center, Indiana)*, y[1]w[1118] P(neoFRT)19A;;* (Bloomington Stock Center, Indiana), *w[*]; noc[Sco]/CyO; P(tubP-GAL80*^{ts}*)7* (Bloomington Stock Center, Indiana).

Genotypes

Genotypes are listed by figures.

2.1D. *w; UAS CD8-GFP; tubP Arr-TEV*

2.1E. *w; UAS CD8-GFP; tubP HRH2-TCS-Gal4, tubP Arr-TEV/Tm6B*

2.1F. *w; dhdcp217 UAS CD8-GFP; tubP HRH2-TCS-Gal4, tubP Arr-TEV/Tm6B*

2.2A. *tubP Arr-TEV; UAS CD8-GFP; tubP HRH2-TCS-Gal4*

2.2B. *tubP Arr-TEV; UAS CD8-GFP; tubP HRH2-TCS(weak site)-Gal4*

2.4(A-H). *w; UAS nuc lacZ; tubP HRH2-TCS-Gal4, tubP Arr-TEV/Tm6B*

2.5. *w; UAS CD8-GFP; tubP HRH2-TCS-Gal4, tubP Arr-TEV/Tm6B*

2.6. *w; UAS CD8-GFP; tubP HRH2-TCS-Gal4, tubP Arr-TEV/Tm6B*

2.7(A-C). *w; UAS CD8-GFP; tubP HRH2-TCS-Gal4, tubP Arr-TEV/tubP Gal80^{ts}*

2.8A. *w; UAS CD8-GFP/Rh4Gal4; tubP HRH2-TCS-Gal4, tubP Arr-TEV/UAS dTrpA1*

2.8B. *w; UAS CD8-GFP/UASdTrpA1; tubP HRH2-TCS-Gal4, tubP Arr-TEV/Rh6Gal4*

2.8C. *w; UAS CD8-GFP; tubP HRH2-TCS-Gal4, tubP Arr-TEV/UAS dTrpA1*

2.8D. *w; UAS CD8-GFP; tubP HRH2-TCS-Gal4, tubP Arr-TEV/Tm6B*

2.9A. *w, hsFlp, neoFRT19A tubPGal80/neoFRT19A; UAS CD8-GFP/Rh3Gal4; tubP HRH2-TCS-Gal4, tubP Arr-TEV/UAS dTrpA1*

2.9B. *w, hsFlp, neoFRT19A tubPGal80/neoFRT19A; UAS CD8-GFP/Rh4Gal4; tubP HRH2-TCS-Gal4, tubP Arr-TEV/UAS dTrpA1*

2.9C. *w, hsFlp, neoFRT19A tubPGal80/neoFRT19A; UAS CD8-GFP/Rh5Gal4; tubP HRH2-TCS-Gal4, tubP Arr-TEV/UAS dTrpA1*

2.9D. *w, hsFlp, neoFRT19A tubPGal80/neoFRT19A; UAS CD8-GFP/UAS dTrpA1; tubP*

HRH2-TCS-Gal4, tubP Arr-TEV/Rh6Gal4

2.12A. *w, hsFlp, neoFRT19A tubPGal80/neoFRT19A; UAS CD8-GFP/Rh3Gal4; tubP HRH2-TCS-Gal4, tubP Arr-TEV/UAS dTrpA1*

2.12B. *w, hsFlp, neoFRT19A tubPGal80/neoFRT19A; UAS CD8-GFP/Rh4Gal4; tubP HRH2-TCS-Gal4, tubP Arr-TEV/UAS dTrpA1*

2.12C. *w, hsFlp, neoFRT19A tubPGal80/neoFRT19A; UAS CD8-GFP/Rh5Gal4; tubP HRH2-TCS-Gal4, tubP Arr-TEV/UAS dTrpA1*

2.12D. *w, hsFlp, neoFRT19A tubPGal80/neoFRT19A; UAS CD8-GFP/UAS dTrpA1; tubP HRH2-TCS-Gal4, tubP Arr-TEV/Rh6Gal4*

2.13(A1-A2). *w, hsFlp, neoFRT19A tubPGal80/neoFRT19A; UAS CD8-GFP/Rh3Gal4; tubP HRH2-TCS-Gal4, tubP Arr-TEV/UAS dTrpA1*

2.13(B1-B2). *w, hsFlp, neoFRT19A tubPGal80/neoFRT19A; UAS CD8-GFP/Rh4Gal4; tubP HRH2-TCS-Gal4, tubP Arr-TEV/UAS dTrpA1*

2.13(C1-C2). *w, hsFlp, neoFRT19A tubPGal80/neoFRT19A; UAS CD8-GFP/Rh5Gal4; tubP HRH2-TCS-Gal4, tubP Arr-TEV/UAS dTrpA1*

2.13(D1-D2). *w, hsFlp, neoFRT19A tubPGal80/neoFRT19A; UAS CD8-GFP/UAS dTrpA1; tubP HRH2-TCS-Gal4, tubP Arr-TEV/Rh6Gal4*

2.15A. *w, hsFlp, neoFRT19A tubPGal80/neoFRT19A; UAS CD8-GFP/UAS dTrpA1; tubP HRH2-TCS-Gal4, tubP Arr-TEV/Rh6Gal4*

2.15B. *w, hsFlp, neoFRT19A tubPGal80/neoFRT19A; UAS CD8-GFP/UAS dTrpA1; tubP HRH2-TCS-Gal4, tubP Arr-TEV/Rh6Gal4*

2.26(A-C). *deltanorpA36;; UAS norpA/+*

2.26(D-F). *deltanorpA36; R8Gal4/+; UAS norpA/+*

2.27(A-D). *deltanorpA36; R8Gal4/+; UAS norpA/+*

2.27(E-H). *deltanorpA36, Rh1Gal4; UAS norpA/+;*

2.27 (I-L) *IsoD1/Oregon-R*

Fly Husbandry

Drosophila stocks were reared on standard cornmeal-agar-dextrose medium at 25°C. *W1118* or *yw* strains were used for transgene injections. P-element mediated germline transformations and genetic manipulations were performed using standard techniques. Transgene injections were performed by BestGene, Inc. (BestGene Inc. 2918 Rustic Bridge, Chino Hills, CA 91709). Fly stocks for behavior experiments were reared and maintained as described in (Clark et al., 2011).

HA-Tango-Trace labeling

Sparse clones were generated by a 30 min heat shock everyday from early larval to late pupal stage during development to maximize the number of labeled cell types. Activation of the photoreceptors expressing dTrpA1 was then achieved by gradually warming these flies from 25^0C to 37^0C for 15 min followed by 5 min cooling. This was repeated for 2 hours.

Tubulin-Gal80^{ts} inactivation

Flies carrying the HA-Tango transgenes and the Tubulin-Gal80^{ts} transgene were first shifted to 30°C for at least 8 hours to inactivate the Gal80 protein and then stimulated with light, incubated overnight at 25°C and immunostained.

Transgenes

Tubp-HRH2-TCS-Gal4

The Tubulin promoter-HRH2-TCS-Gal4 transgene was constructed by standard PCR and cloning methods. The gene encoding HRH2 was PCR amplified from cDNA obtained from Missouri S&T cDNA resource center. The forward primer was designed with a NotI restriction site and Kozak sequence at the 5' end. The reverse primer had the wild type TEV cleavage site (ENLYFQS) with an XbaI restriction site at the 3' end. PCR products were ligated to a plasmid containing the sequence for Gal4 and subsequently ligated to the P-element transformation vector pW8, containing the *Drosophila* α-Tubulin promoter and SV40 polyadenylation sequences. The plasmids were completely sequenced and subsequently used to transfect Schneider S2 cells to confirm expression prior to germline transformation.

Tubp-βArrestin-TEV

Plasmid encoding the βArrestin-TEV protease fusion proteins were provided by Gilad Barnea (Barnea et al, 2008) and were ligated as NotI fragments to a P-element transformation vector pW8, containing the *Drosophila* α-Tubulin promoter and SV40 polyadenylation sequences.

Schneider2 (S2) cell transfection and antibody staining

Schneider2 (S2) cells **(**obtained from Nanami Senoo Matsuda, Columbia University) were seeded on 4-well chamber slides (Nunc) at a density of 100,000 cells/ml**,** and allowed to adhere overnight at 25°C. Transfection of plasmid DNA was performed using a Cellfectin transfection kit (Invitrogen) according to the manufacturer's instructions. Two days after

transfection, cells were fixed with 2% paraformaldehyde for 7 minutes, then washed several times in PBST, blocked in 5% horse serum, diluted in PBST, and incubated in primary antibody for two hours at room temperature. After several washes in PBST, the cells were then incubated in secondary antibody (diluted 1:200); cell nuclei were counterstained with TOTO-3 (Molecular Probes, diluted 1:1000). After several washes in PBST, slides were mounted in Vectashield (Vector Labs) and imaged.

Immunocytochemistry and Confocal Microscopy

Fly heads were fixed in 2% formaldehyde in phosphate buffered lysine (PBL) for 2hr RT, and washed 3x15min in PBS + 0.3% TX-100. Microdissection was performed in PBST to remove the cuticle and connective tissues. Samples were blocked for 30m in 10% normal goat serum. Primary and secondary incubations were performed overnight at 4C, with shaking. Samples were incubated in 30 min 10% normal goat serum, then in a cocktail of primary antibodies including a mouse anti-nc82 (1:20, DSHB), mouse mAb24B10 (1:50, DSHB), Abcam chicken anti-GFP (1:1000) overnight. Samples were washed three times for 10 min with PBST before incubation for 3hr with a cocktail of secondary antibodies, which include goat anti-mouse conjugated with Alexa Fluor 568 (1:1000), goat anti-chicken conjugated with Alexa Fluor 488 (1:1000), and a 1:1000 dilution of TOTO-3 (Molecular Probes). After three 10 min rinses with PBST, brains were mounted in Vectashield (Vector Labs) and imaged. Image stacks were taken either with Zeiss 510 Meta laser scanning confocal microscope or Leica TCS SP2 AOBS confocal microscope using a 40x (NA = 1.25) lens.

Image Analysis

Image analysis was carried out in ImarisXT (Bitplane, Inc.) and ImageJ (rsb.info.nih.gov/ij/). These images provide a qualitative but not a quantitative sense of the differences between the cell types, as the intensity of labeling unavoidably varied from sample to sample. To quantitate differences between individual axonal and dendritic projection patterns, tracing of sparsely labeled TmYs was done using the semi-automated tracing module in Amira (Mercury Computer Systems, Berlin).

Anatomical tracing

Images were first processed by gaussian deblur to eliminate any pixels that lie outside the labeled neurons. In initial experiments, we used the automated filament tracer in Amira (Mercury Computer Systems, Berlin). This tracing method was completely manual. We then used the module that allows semi-automated tracing (Evers et al., 2005; Schmitt et al., 2004) of neuronal structures in Amira. In this second approach, branch points and segment end points are manually defined and an automated algorithm based on local intensity gradients fits the center line and diameter of the intervening neurite at regular intervals; we used a 0.1 micron step size with this module. The algorithms are described in detail in a theoretical paper (Schmitt et al. 2004). The tracing parameters were set by the user. Then the neurites were automatically reconstructed as cylinders. The precision of the skeleton was determined by the smoothness of traced skeleton, devoid of wiggles, which are due to imaging noise. The criteria for smoothness of the reconstruction were dependent on the local staining distribution rather than on the absolute value of staining intensity. The tracing was

iteratively optimized adjusting the distance values of every voxel to maximize reconstruction quality.

Sholl Analysis

Sholl analysis was done using an imageJ plugin available at: www.biology.ucsd.edu/labs/ghosh/software/index.html. The sholl analysis parameters were set in the dialog box. The starting radius, which is the radius of the smallest analysis circle, along which the number of intersections were measured were set to 1 micron. The ending radius, which is the maximum value for the radii of the analysis circles, was set between 200-300 microns. The radius step size is a measure of the interval between radii of consecutive analysis circles was set to 1 micron. The radius span, which is the margin around each radius value in which continuous intersection measurements are made. These measurements are then combined to calculate a single value for the number of intersections at that radius. This value was set to 1 micron. The span type, a statistical function used to combine the intersection measurements within a span to produce a single value was set to the median value.

Cluster Analysis of Projection Patterns

Hierarchical cluster analysis of the traced axonal and dendritic projections was performed in Matlab (Mathworks). The linkage was measured in Euclidian distance specified by

$$d_{st}^2 = (x_s - x_t)(x_s - x_t)'$$

The cluster analysis was performed using ward's method. Ward's linkage uses the incremental sum of squares; that is, the increase in the total within-cluster sum of squares as

a result of joining two clusters. The within-cluster sum of squares is defined as the sum of the squares of the distances between all objects in the cluster and the centroid of the cluster. The sum of squares measure is equivalent to the following distance measure d(r,s), which is the formula linkage uses:

$$d(r,s) = \sqrt{2n_r n_s / (n_r + n_s)}\ \|\bar{x}_r - \bar{x}_s\|_2 ,$$

where,

$\|\bar{x}_r - \bar{x}_s\|_2$ is the Euclidean distance

$\bar{x}_r$ and $\bar{x}_s$ are the centroids of clusters r and s

$n_r$and n_s are the number of elements in clusters r and s

Behavioral Measurements

All behavioral experiments were performed on the fly-on-a-ball set-up as described in (Clark et al., 2011) .Two day old female flies were collected over CO_2 and and cold-anaesthetized after two more days. A fine gauge syringe needle was affixed to the middle of their dorsal thorax using UV-cured epoxy and a mounting stage. These flies were then positioned over an air-cushioned ball. Visual stimuli were projected on to the screens surrounding the fly-on-a-ball set-up as described in (Clark et al., 2011). But, the screens were placed further away from the fly so that the projected stimuli represented virtual cylinders. The movement of the ball was recorded by two optical mice as a readout of the behavioral assay.

Behavioral Experiments

The behavioral experiments in which we used sine wave gratings and contrast frequency sweep stimuli lasted 20 minutes each. All stimulus subtypes in the experiment were presented for 250 ms.

Virtual Cylinders

We presented virtual cylinders consisting of sine wave contrast patterns rotating at varying speeds. A 40° period sine wave was rotated around the fly at different speeds (40, 80 and 160 degrees/s) for 250 ms each, following the protocol described above.

Contrast frequency sweep

We also devised experiments in which we presented the fly with stimuli that swept different contrast frequencies ranging from 0Hz-32Hz, which provide an indirect measure of the delay filter in the Reichardt detector. The turning response of a single fly to different contrast frequencies with the same period sine waves (40 degrees) was then recorded as a behavioral readout.

Figure 2.1.

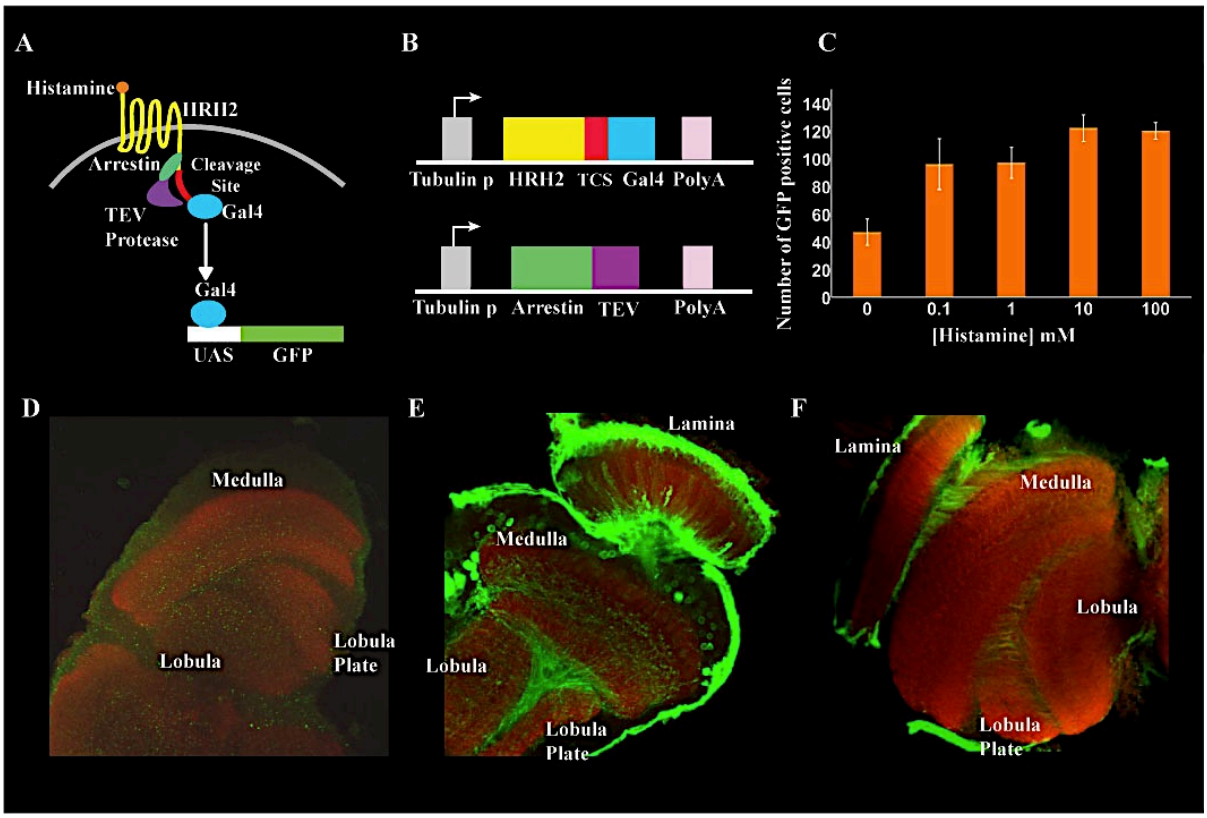
A
Histamine
HRH2
Arrestin
Cleavage Site
TEV Protease
Gal4
Gal4
UAS
GFP
B
Tubulin p HRH2 TCS Gal4 PolyA
Tubulin p Arrestin TEV PolyA
C
Number of GFP positive cells
140
120
100
80
60
40
20
0
0
0.1
1
10
100
[Histamine] mM
D
Medulla
Lobula
Lobula Plate
E
Lamina
Medulla
Lobula
Lobula Plate
F
Lamina
Medulla
Lobula
Lobula Plate

Figure 2.1. Histamine Tango is Ligand and Component Dependent.

(A) Design of Histamine tango assay with a human histamine receptor (HRH2) fused to Gal4 and human β-arrestin2 fused to TEV protease. (B) The histamine tango constructs that were used in this study were expressed ubiquitously under the control of α-tubulin promoter at the 5'end and, a polyA tail in the 3' end. In C-E, whole mount brains were immunostained for the neuropils with mouse nc82 in red and with rabbit anti-GFP in green. (C) HA-Tango labeling in S2 cells treated with histamine. (D) No GFP labeling was seen when arrestin-TEV transgene was not present in the HA-Tango fly indicating no cleavage of Gal4 from the receptor in the absence of arrestin-GPCR interaction (n=9).(E) HA-Tango assay detects histamine receptive neurons in the fly optic lobe. Histamine-receptive cells in the lamina (LMCs), few cells in the medulla, lobula complex and glia surrounding the neuropils are labeled by HA-Tango (n=12).

(F) When reduced amounts of histamine are present as in the case of an hdc hypomorph, HA-Tango labeling is reduced (n=8).

Figure 2.2.

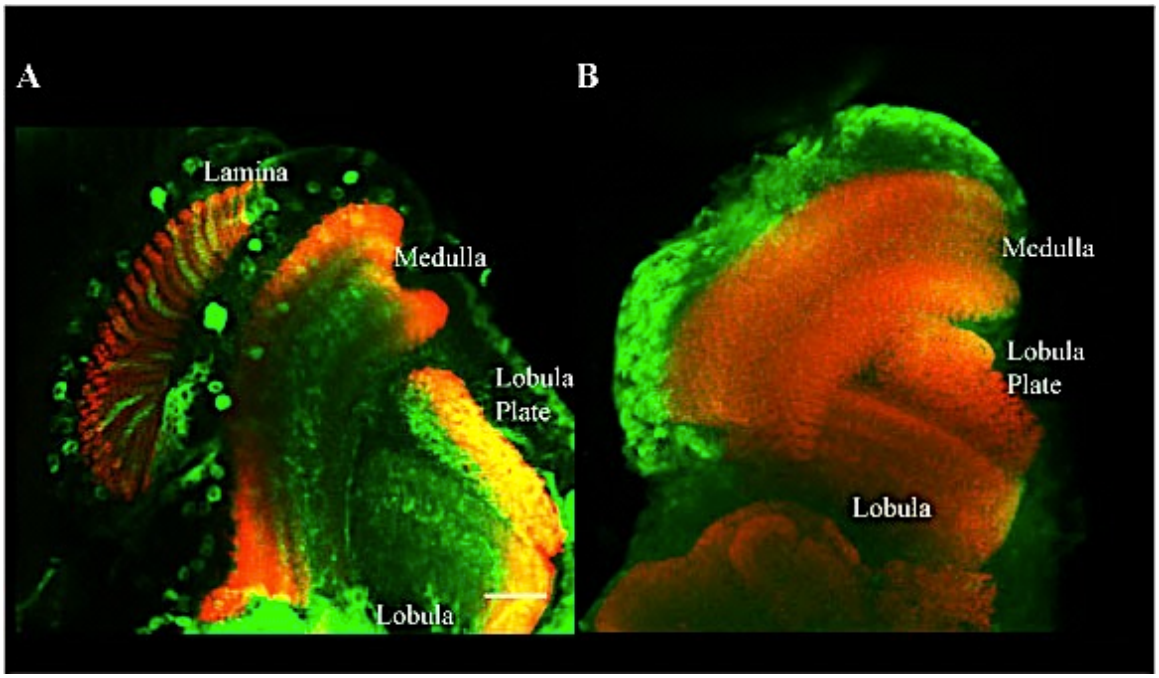
A
Lamina
Medulla
Lobula
Plate
Lobula
B
Medulla
Lobula
Plate
Lobula

Figure 2.2 Optimization of TEV Cleavage Site for HA-Tango Labeling

Light-dependent labeling of histamine-receptive cells in the medulla by HA-Tango. In (A) flies were reared in ambient light (n=6). In (B), flies were reared in the dark and suddenly exposed to bright light (n=5). Flies were then incubated at 25^0C overnight and stained. Note that the weaker TEV site that exhibited the best signal-to-background ratio in cell culture only labeled the cell bodies of histamine receptive neurons in flies. Scale bar represents 20μm.

Figure 2.3.

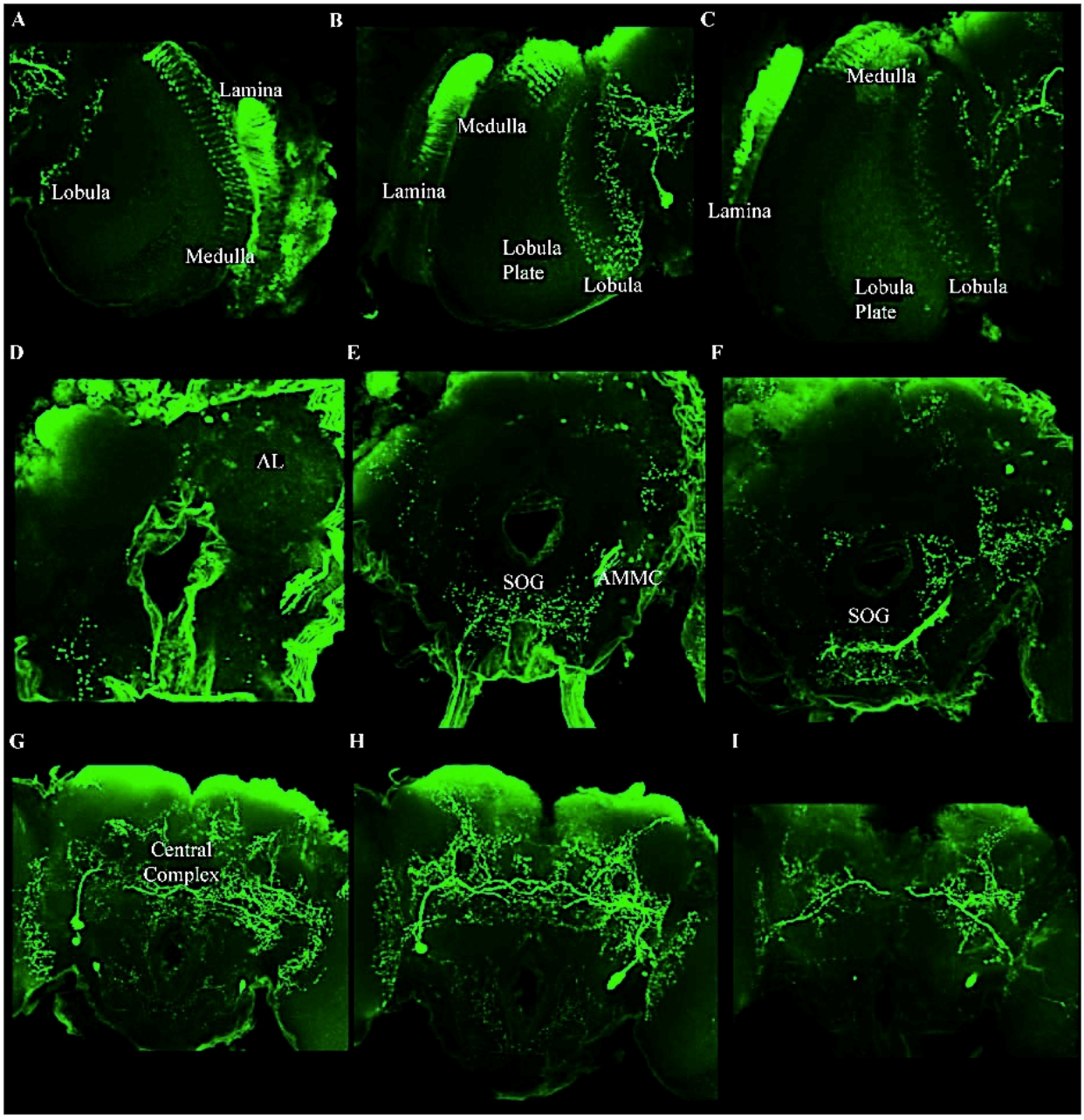
A
Lamina
Lobula
Medulla
B
Medulla
Lamina
Lobula
Plate
Lobula
C
Medulla
Lamina
Lobula
Plate
Lobula
D
AL
E
SOG
AMMC
F
SOG
G
Central
Complex
H
I

Figure 2.3. Immunohistochemical Analysis of Histamine in the *Drosophila* Brain

Immunohistochemistry reveals staining in the lamina, medulla and lobula in the optic lobe (A)-(C). Long-range projections of these histaminergic neurons were observed in several areas of the central brain like the central complex, suboesophageal ganglion (SOG), antennal mechanosensory and motor center (AMMC), protocerebral regions, mushroom bodies (MB) and antennal lobes (AL) (D)-(I).

Figure 2.4.

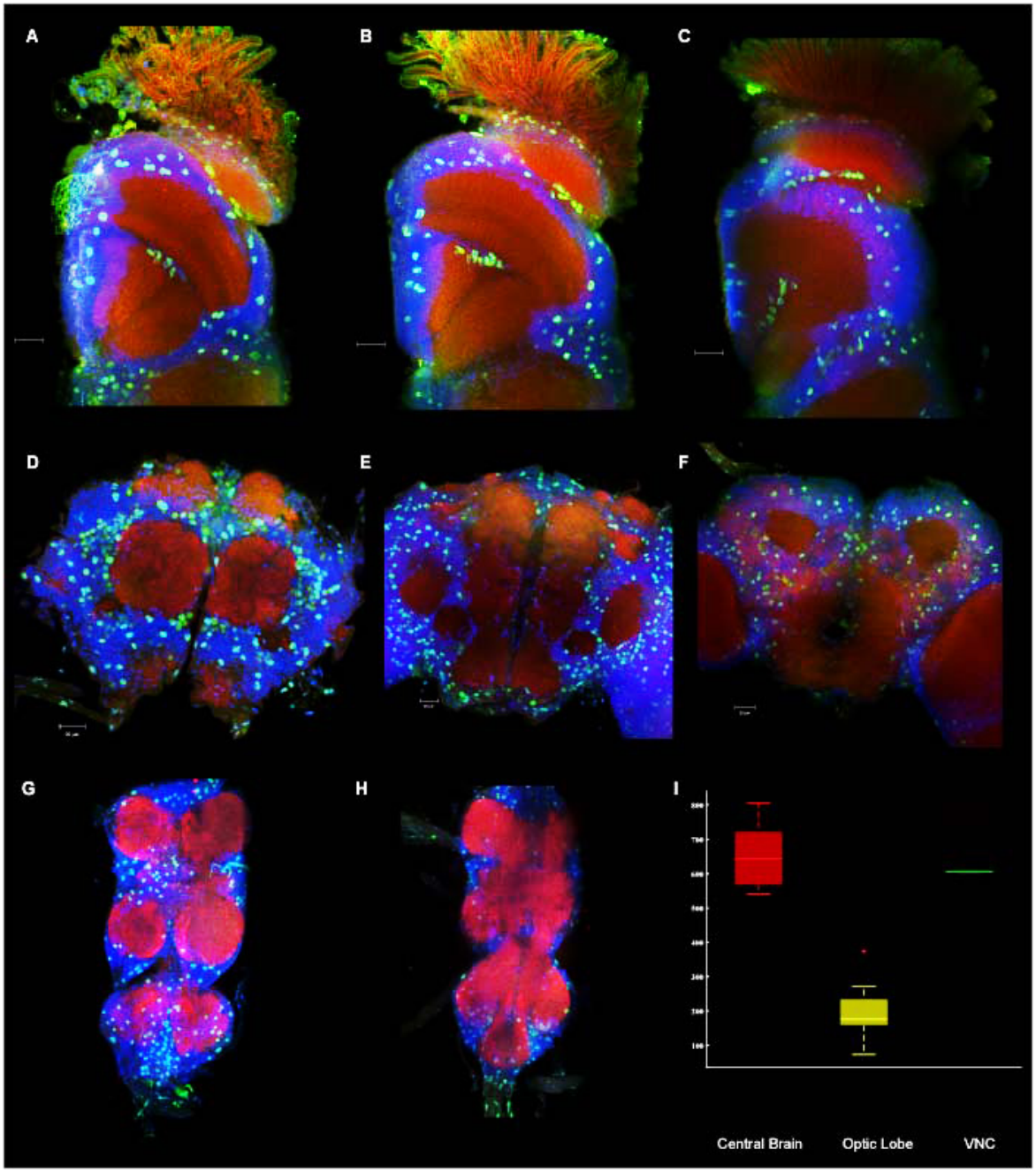

Figure 2.4. HA-Tango Detects Histamine Release in the Optic Lobes and the CNS

Flies were raised in the dark and exposed to 10s flashes of light to estimate the number of cells labeled by histamine tango due to light activation.

(A)-(C) Anterior to posterior sections of the optic lobe labeled with histamine tango driving nuclear lacz. The brains were immunostained for GFP (green) for tango labeling, nc82 (red) for marking neuropils and Toto-3 (blue) for nuclear staining. There is labeling seen in lamina, medulla and lobula complex of the optic lobe (n=20).

(D)-(F) Anterior to posterior sections of the central brain showing tango labeled cells in the central brain. Histamine tango labels cells near the antennal lobes, SOG, mushroom body calyces and the central complex (n=11).

(G)-(H) Anterior to posterior sections of the ventral nerve cord (VNC) (n=4).

(I) Box plot of the cell counts of histamine tango labeled neurons in the optic lobe, central brain and the VNC. The top and bottom boxes of each plots are the 25^{th} and 75^{th} percentiles of the samples. The middle bar denotes the median, the upper and lower whiskers extend to 1.5 times the interquartile range and points exceeding that are marked as outliers (red + sign). Scale bar represents 20μm.

Figure 2.5.

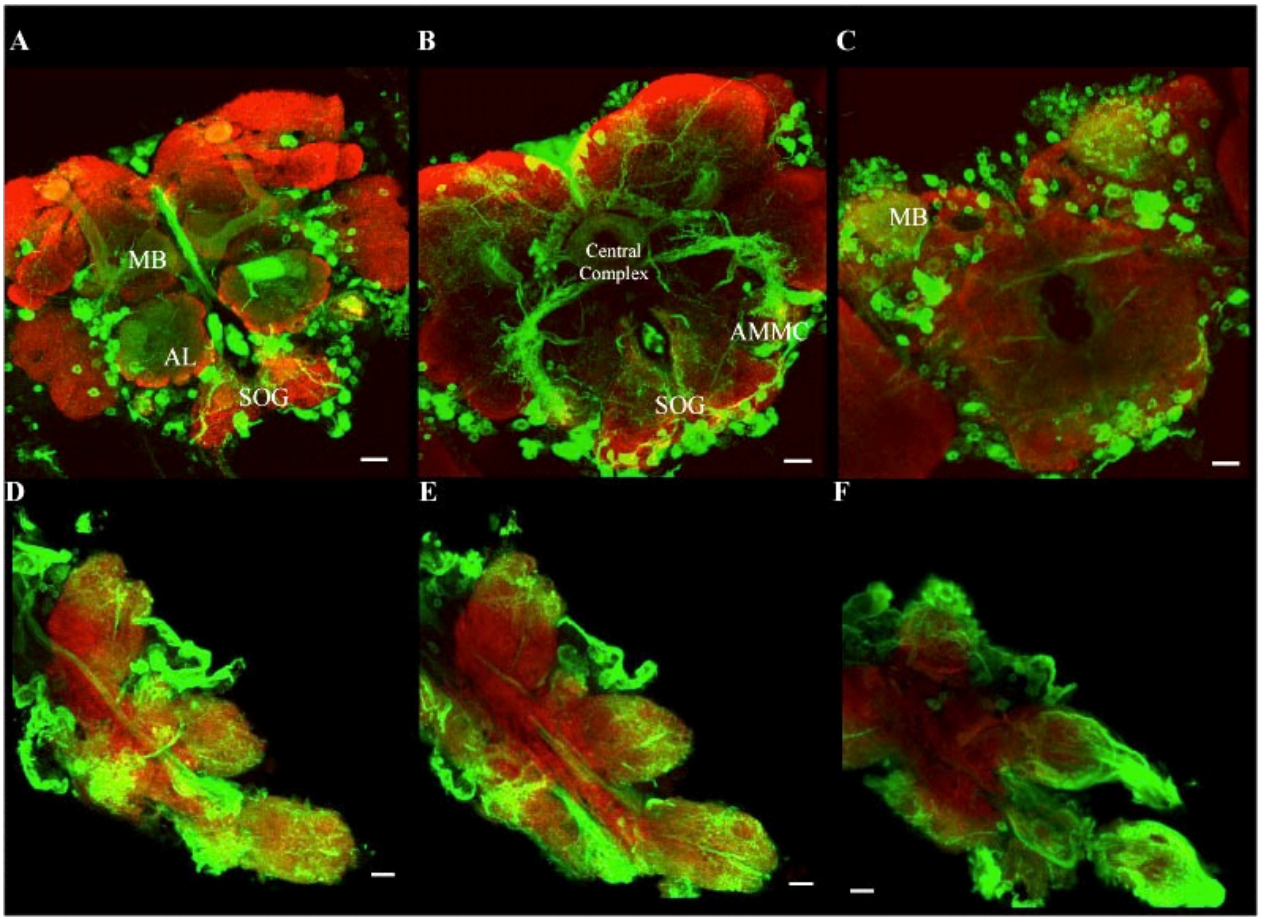

Figure 2.5. Visualizing Projections of HA-Tango Labeled Neurons in the Central Brain and VNC

HA-Tango labeling was detected in several areas of the central brain like the ellipsoid body (EB), fan shaped body (FSB), suboesophageal ganglion (SOG), antennal mechanosensory and motor center (AMMC), protocerebral regions, mushroom bodies (MB) and antennal lobes (AL) (A)-(C). Tango labeling was also observed in the VNC with the processes projecting into the AMMC and SOG (D)-(F). Scale bar represents 20μm.

Figure 2.6.

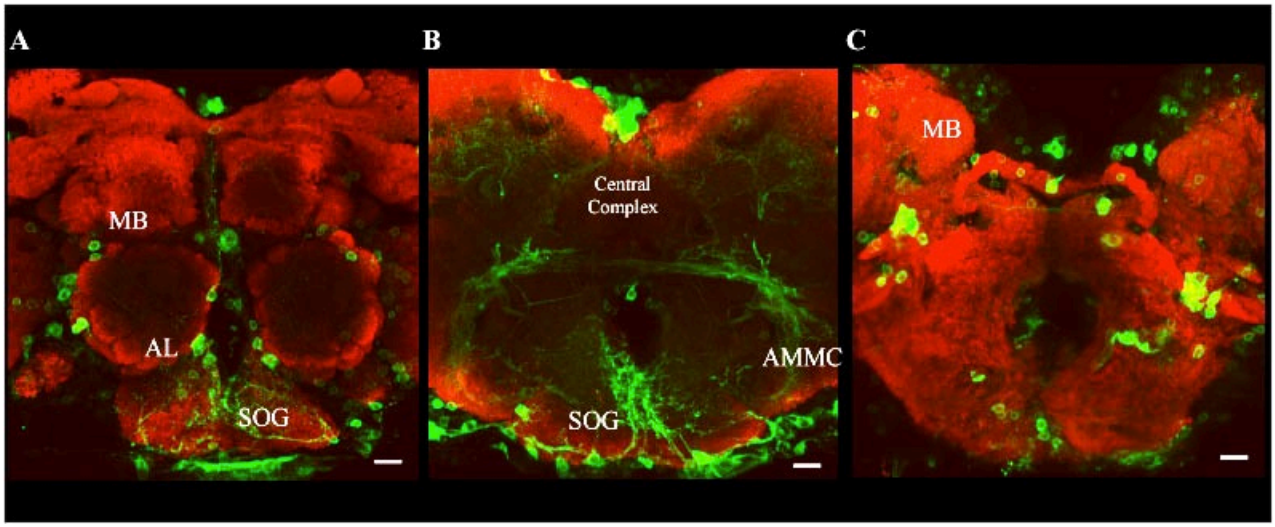

Figure 2.6. HA-Tango Labeling is Reduced in Flies Fed With a Receptor Antagonist

In flies fed with cimetidine, an HRH2 antagonist, HA-Tango labeling was reduced in the central brain. The flies were wet starved overnight and fed with cimetidine in a yeast paste (Hong et al., 2006) and the brains were stained and visualized after 18h. The brains were immunostained with nc82 (red) and GFP (green) antibodies. Scale bar represents 20μm.

Figure 2.7.

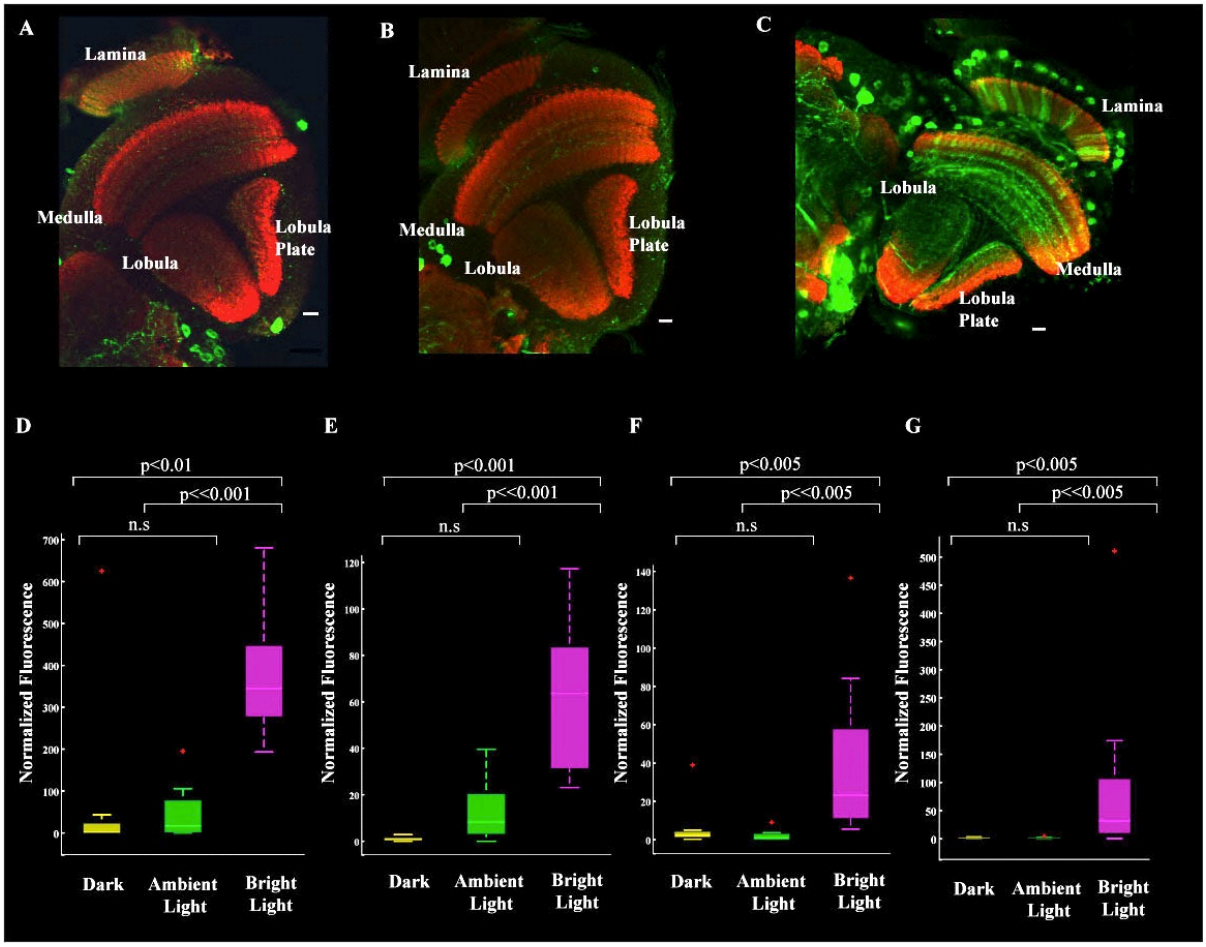
A
Lamina
Medulla
Lobula Plate
Lobula
B
Lamina
Medulla
Lobula Plate
Lobula
C
Lamina
Lobula
Medulla
Lobula Plate
D
p<0.01
p<<0.001
n.s
Normalized Fluorescence
Dark
Ambient Light
Bright Light
E
p<0.001
p<<0.001
n.s
Normalized Fluorescence
Dark
Ambient Light
Bright Light
F
p<0.005
p<<0.005
n.s
Normalized Fluorescence
Dark
Ambient Light
Bright Light
G
p<0.005
p<<0.005
n.s
Normalized Fluorescence
Dark
Ambient Light
Bright Light

Figure 2.7. Histamine Tango is Activity Dependent in the Fly Visual System

The tango components were expressed in the background of tubulin promoter driven $Gal80^{ts}$. The brains were immunostained with nc82 (red) and GFP (green) antibodies. Flies were reared in ambient light (n=12) (A), or in the dark (n=8) (B) and shifted to 30 degrees for 18h and immediately fixed and stained. In (C), flies were reared in the dark, shifted to 30 degrees for 18h and suddenly exposed to bright light. They were then shifted to 25 degrees overnight and stained (n=12). (D)-(G) Box plots of the quantification of the fluorescence in the green channel shows more than 20-fold difference between A, B and C. The top and bottom boxes of each plots are the 25th and 75th percentiles of the samples. The middle bar denotes the median, the upper and lower whiskers extend upto 1.5 times the interquartile range. The p values represent wilcoxon rank sum test. Scale bar represents 15μm.

Figure 2.8.

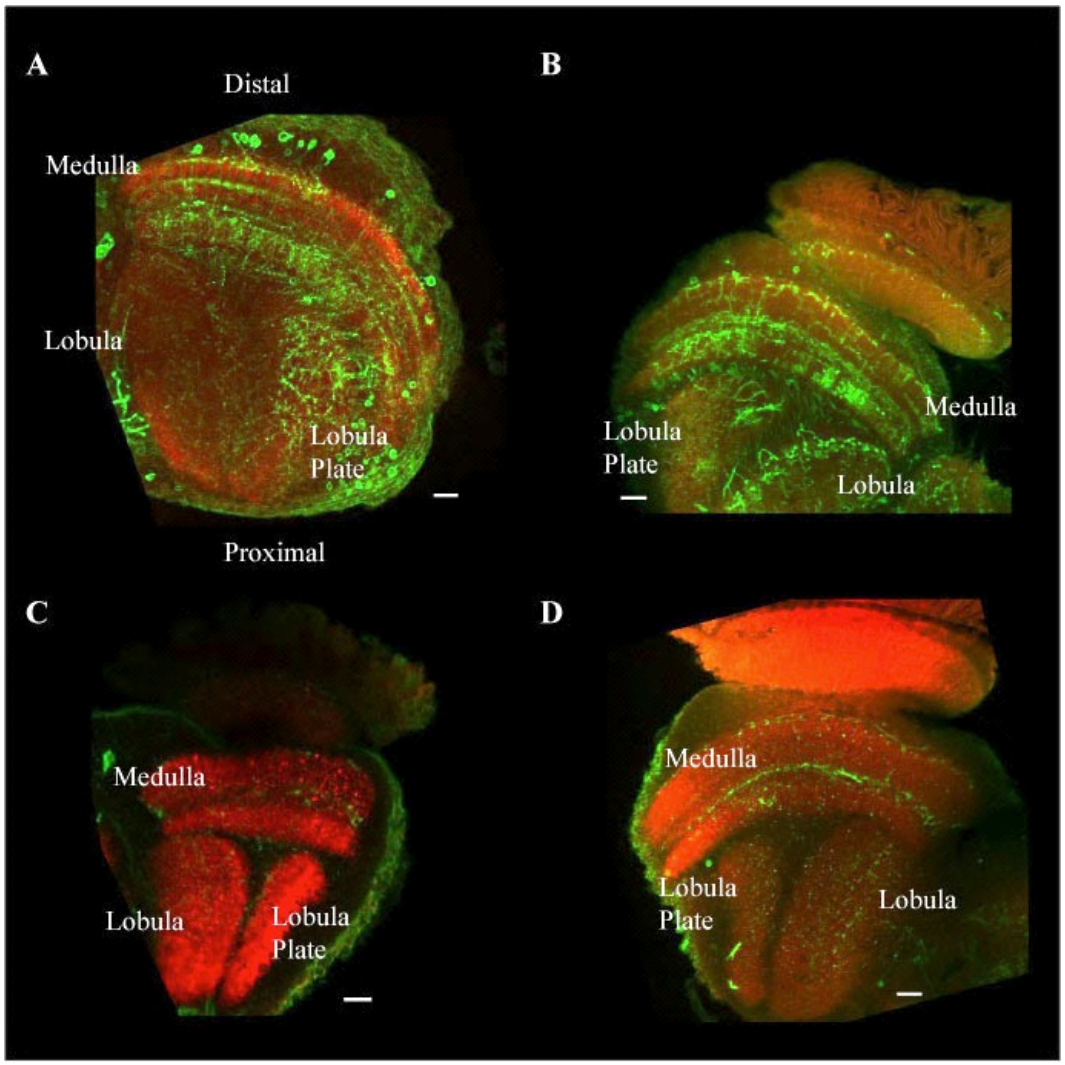
A
Distal
Medulla
Lobula
Lobula
Plate
Proximal
B
Medulla
Lobula
Plate
Lobula
C
Medulla
Lobula
Lobula
Plate
D
Medulla
Lobula
Plate
Lobula

Figure 2.8. HA-Tango-Trace Labels Postsynaptic Targets of the Inner Photoreceptors

HA-Tango-trace flies expressing HA-Tango transgenes as well as *Rh-Gal4* drivers driving dTrpA1 were reared in ambient light to keep any light-induced activity at low-levels and then exposed to heat to activate each photoreceptor subtype individually. (A) *Rh4-Gal4* (n=5), and (B) *Rh6Gal4* (n=4). The pattern of arborization in the medulla and the lobula complex was strikingly similar for both R7 and R8. (C) HA-Tango flies with dTrpA1, but not exposed to heat (n=7). (D) HA-Tango flies without dTrpA1 and exposed to heat (n=10). Scale bar represents 20μm.

Figure 2.9.

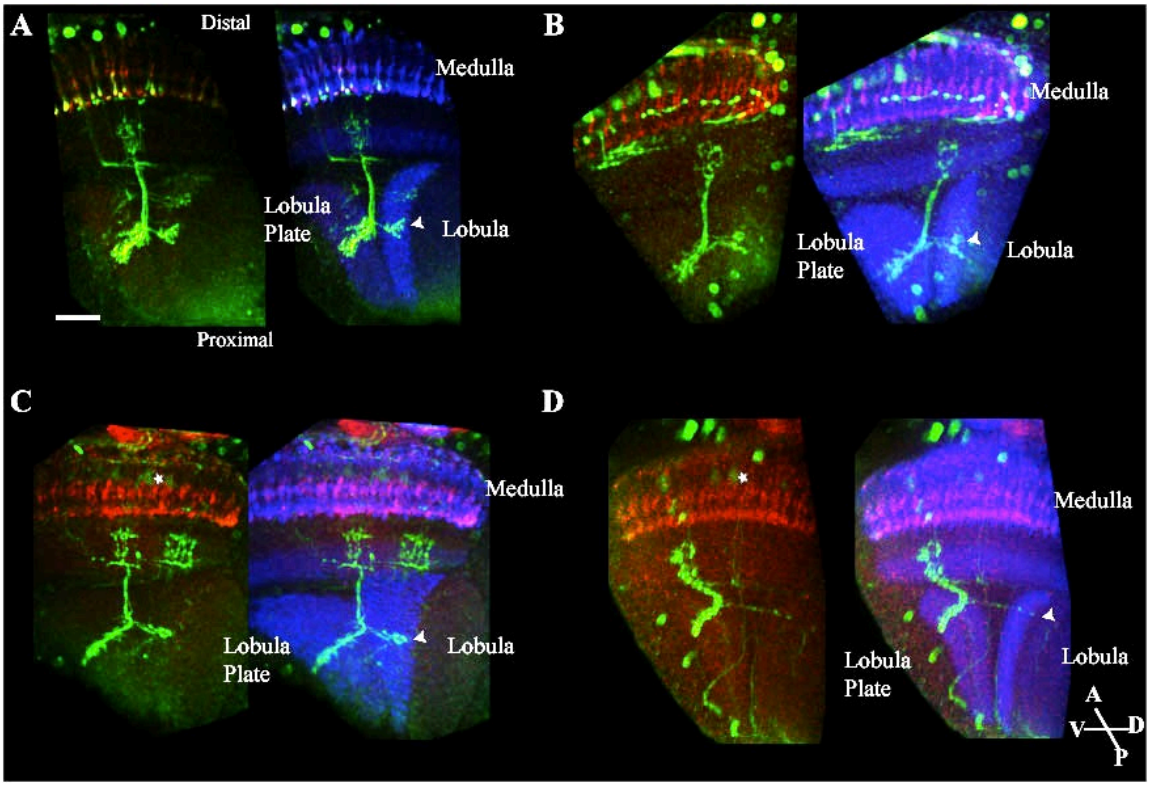
A
Distal
Medulla
Lobula
Plate
Lobula
Proximal
B
Medulla
Lobula
Plate
Lobula
C
Medulla
Lobula
Plate
Lobula
D
Medulla
Lobula
Plate
Lobula
A
V
D
P

Figure 2.9. Visualizing the Projections of Individual Post-synaptic Partners of R7 and R8 in the Medulla- TmY Cells

Sparse labeling of histamine tango-trace labeled postsynaptic targets of p/y R7s and p/y R8s with hsFlp-MARCM. Spatially separated cells were projected from confocal stacks in 3D and rendered in Imaris for visualization of the TmY cell morphology. (A) Rh3TmY (B) Rh4TmY (C) Rh5TmY (D) Rh6TmY. Tango-trace labeling was done by driving dTrpA1 using Rh-Gal4 lines and activating the photoreceptors by heat (See Experimental procedures). The arrowheads indicate the innermost lobula layer where the axons project which is also labeled by the Csp3 antibody. The LMC L2 is readily labeled by histamine tango-trace although light fluctuations were kept to a minimum (asterisk). Since we saw this labeling in control brains too, L2 was excluded from our analysis. The brains were immunostained with antibodies to visualize tango labeling with GFP (green), neuropil marker Csp3 (blue) and photoreceptors with mAb24B10 (red). Scale bar represents 20μm.

Figure 2.10.

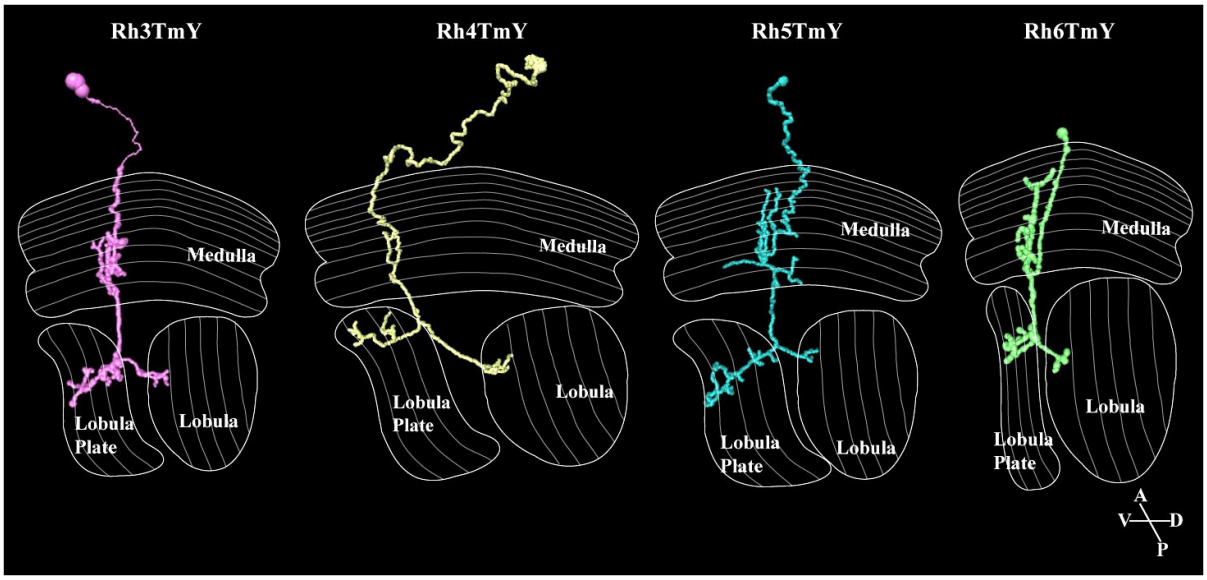
Rh3TmY
Rh4TmY
Rh5TmY
Rh6TmY
Medulla
Medulla
Medulla
Medulla
Lobula Plate
Lobula
Lobula Plate
Lobula
Lobula Plate
Lobula
Lobula Plate
Lobula
A
V
D
P

Figure 2.10. Semi-automated Neurite Tracings of TmY Cells

The inner photoreceptors, p/y R7 and R8 contact TmY cells that primarily send rich arbors in the proximal medulla, all the four layers of the lobula plate and the innermost layer of the lobula. Each photoreceptor subtype contacts a unique variant of this cell type Rh3TmY, Rh4TmY, Rh5TmY and Rh6TmY as a postsynaptic target corresponding to their presynaptic partner. These variants extend their projections to the medulla and exhibit a morphological variation in their projection patterns in the proximal medulla. The tracings were done in the skeleton tree module in Amira (see experimental methods).

Figure 2.11.

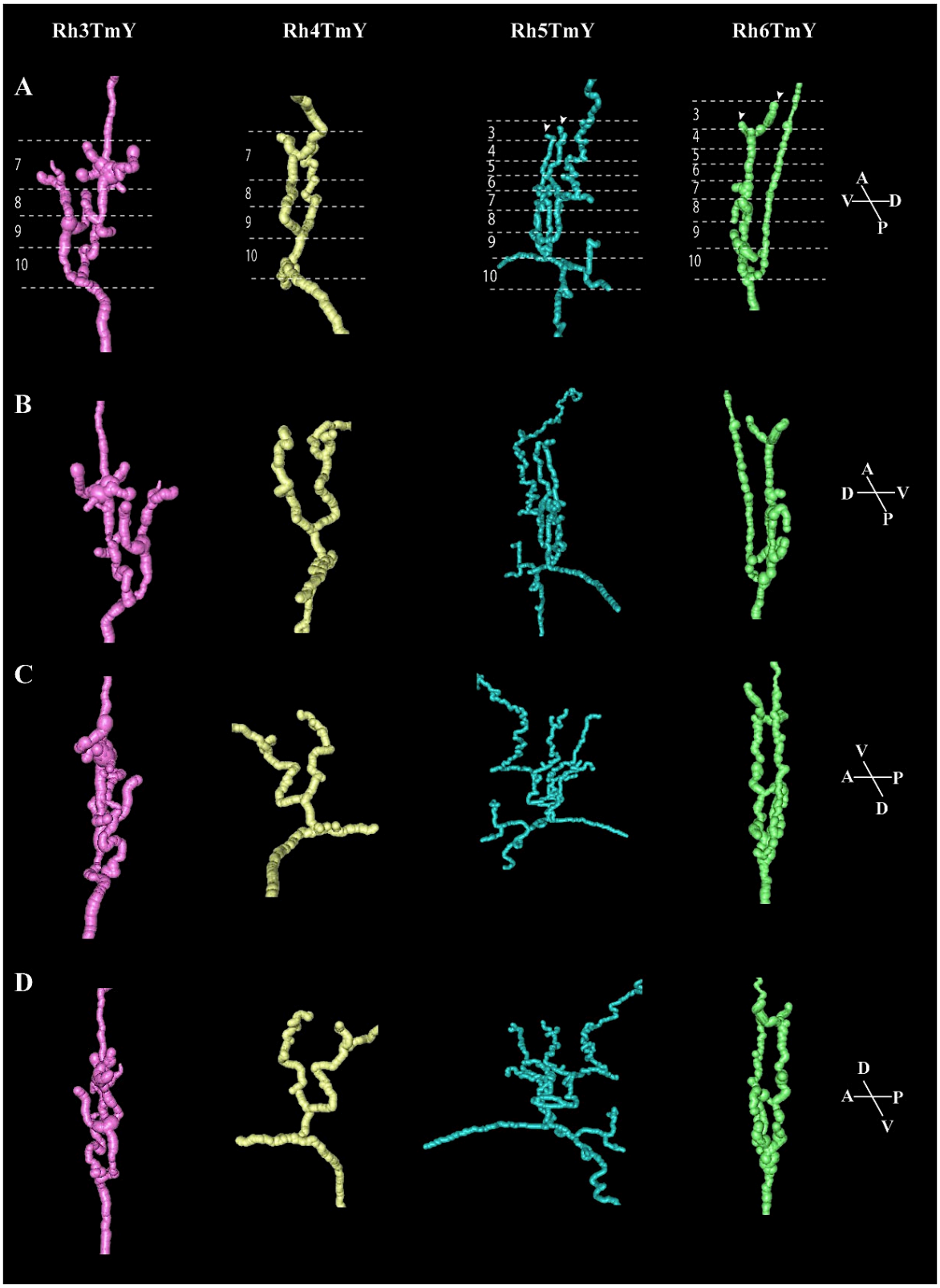

Figure 2.11. Three Dimensional Projections of TmY Cells in the Proximal Medulla

Rh3TmY and Rh6 TmYs have richer arbors than Rh4TmY and Rh5TmY. In the proximal medulla, Rh5TmY and Rh6 TmY have very distinct projection patterns in three dimensions with their arbors projecting in the antero-posterior (AP) axis and appear to contact two other photoreceptors. The arrowheads indicate that the TmY cells appear to contact two other photoreceptors. (A-D) represent different three-dimensional axes of the proximal medulla projections of the TmY variants.

Figure 2.12.

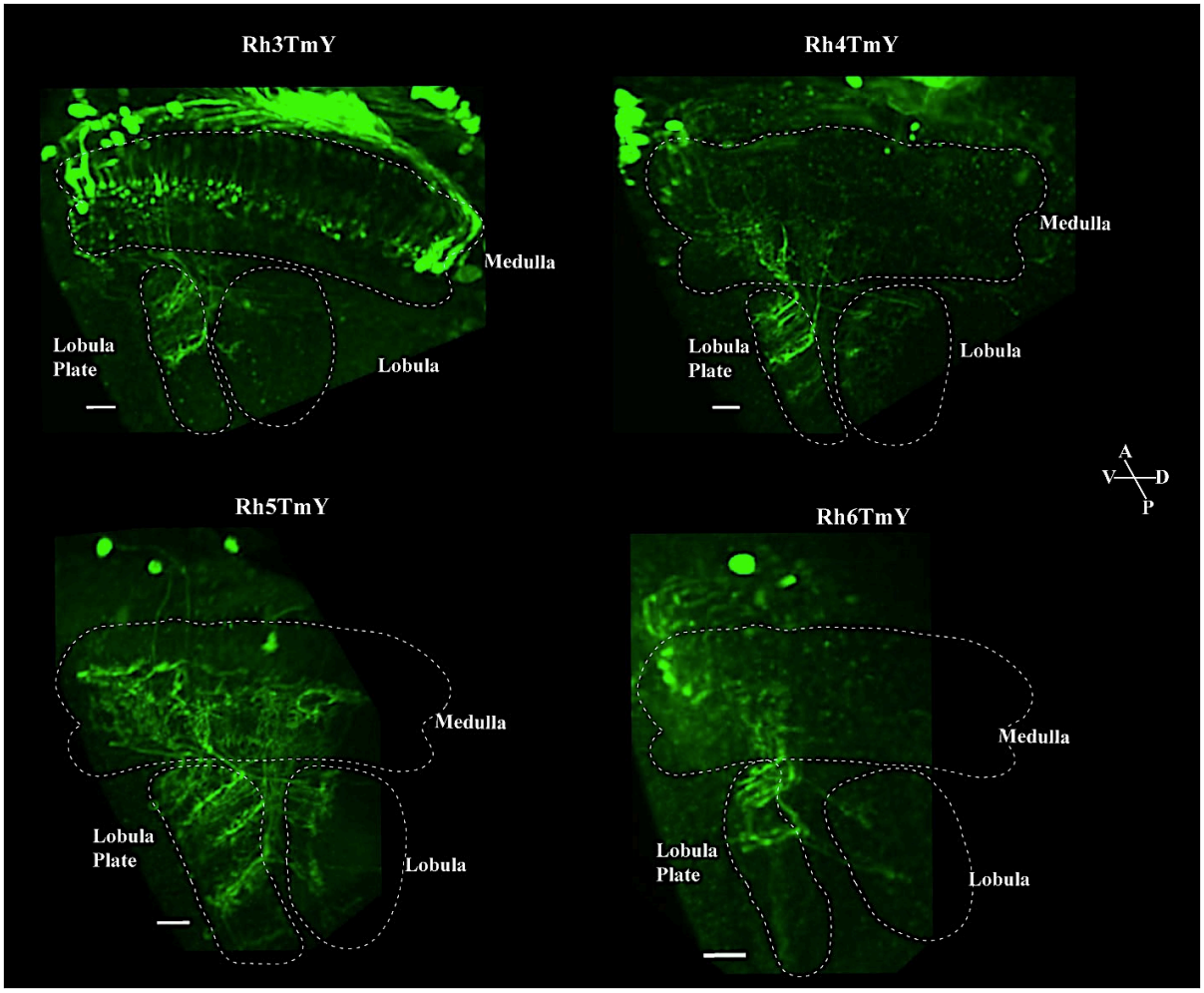
Rh3TmY
Medulla
Lobula Plate
Lobula
Rh4TmY
Medulla
Lobula Plate
Lobula
A
V
D
P
Rh5TmY
Medulla
Lobula Plate
Lobula
Rh6TmY
Medulla
Lobula Plate
Lobula

Figure 2.12. Retinotopic Columnar Organization of the Projections of TmY Cells in the Lobula and Lobula Plate.

The TmY cells project to the lobula and lobula plate in a columnar manner maintaining the retinotopy. Immunostaining of whole mount brains with GFP (green) and the images were rendered as a volume of a brain in Amira. Scale bar represents 20μm.

Figure 2.13.

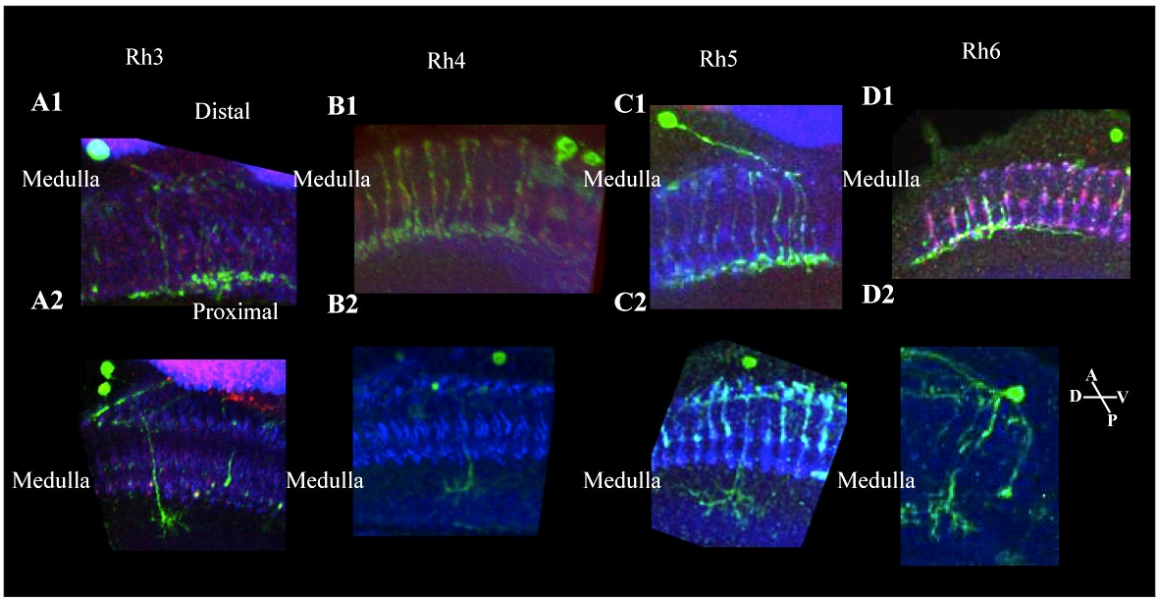
Rh3
Rh4
Rh5
Rh6
A1
Distal
B1
C1
D1
Medulla
Medulla
Medulla
Medulla
A2
Proximal
B2
C2
D2
Medulla
Medulla
Medulla
Medulla
A
D
V
P

Figure 2.13. Visualizing the Projections of Individual Post-synaptic Partners of R7 and R8 in the Medulla – Amacrine Cells

(A1)-(D1) Dm8 labeled by histamine tango-trace, a wide-field amacrine cell contacting 13-15 columns in layer 6 of the medulla is a postsynaptic target of both R7 and R8.

(A2)-(D2) Mia labeled by histamine tango-trace, a narrow-field amacrine cell contacting 4-5 columns in layer 8 of proximal medulla where the TmY cells send their arbors is postsynaptic to both R7 and R8. Immunostaining of whole mount brains with GFP (green), neuropil marker Csp3 (blue) and photoreceptors with mAb24B10 (red).

Figure 2.14.

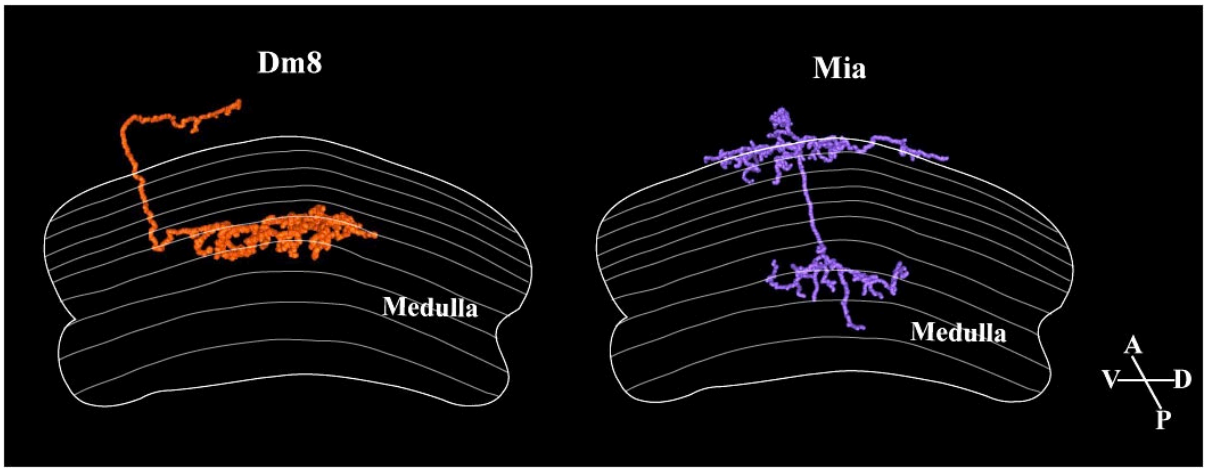

Figure 2.14. Semi-automated Neurite Tracings of Dm8 and Mia

R7 and R8 contact an amacrine cell Dm8. Dm8 is a wide field amacrine cell contacting 14-15 columns in the both the antero-posterior (AP) and dorso-ventral (DV) axes in layer 6 of the distal medulla. A third post-synaptic target of R7 and R8 is an intrinsic medullary cell, which we refer to as Mia. This cell type innervates 4-5 columns in the DV axis in layers 7-9 of the proximal medulla as well innervates broadly in layer 1 of the distal medulla contacting 14-15 columns in both the AP and DV axes.

Figure 2.15.

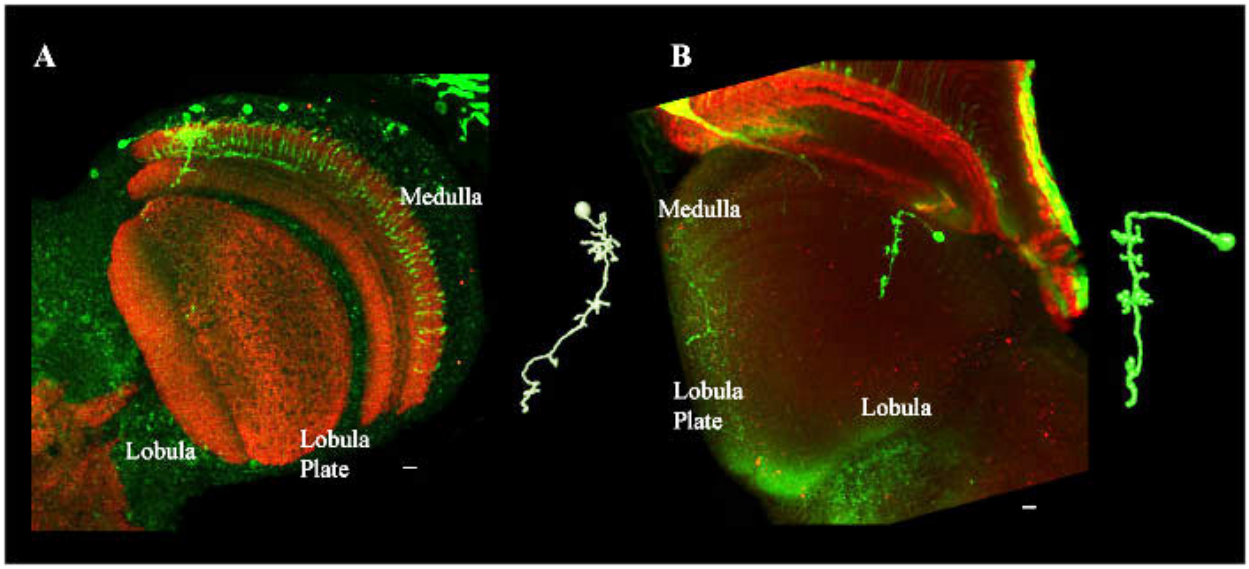
A
Medulla
Lobula
Lobula
Plate
B
Medulla
Lobula
Plate
Lobula

Figure 2.15. Rare Cells Labeled by HA-Tango-Trace

HA-Tango-trace labels two rare cells (A) Tm20 (n=2) and (B) Mi1 (n=3)) as postsynaptic partners of yR8s using *Rh6-Gal4* driving *UAS dTrpA1.* The brains were immunostained with nc82 (red) and GFP (green) antibodies. Scale bar represents 10μm.

Figure 2.16.

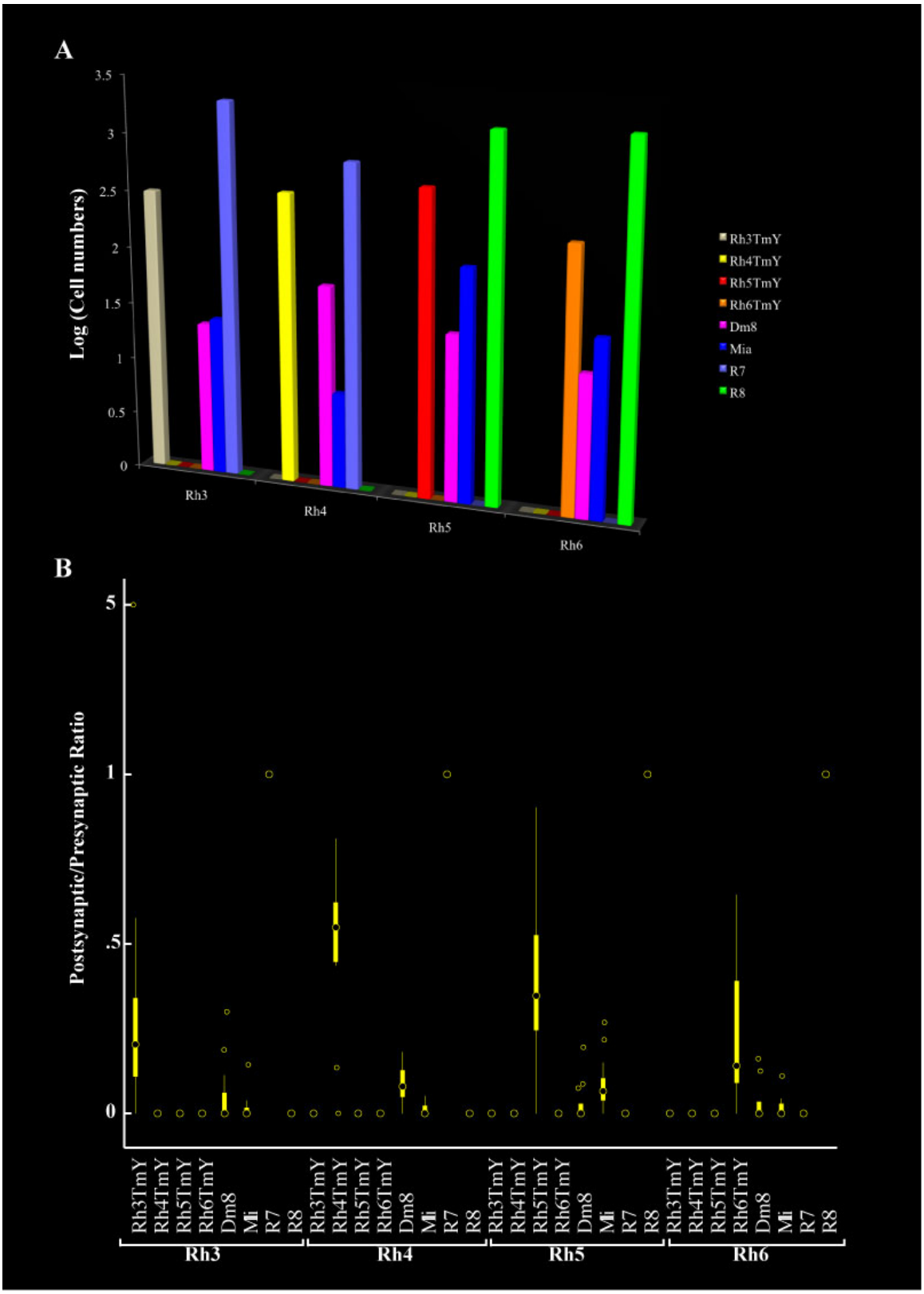
A
Log (Cell numbers)
3.5
3
2.5
2
1.5
1
0.5
0
Rh3
Rh4
Rh5
Rh6
Rh3TmY
Rh4TmY
Rh5TmY
Rh6TmY
Dm8
Mia
R7
R8
B
Postsynaptic/Presynaptic Ratio
5
1
.5
0
Rh3TmY
Rh4TmY
Rh5TmY
Rh6TmY
Dm8
Mi
R7
R8
Rh3
Rh4
Rh5
Rh6

Figure 2.16. Quantitative Analysis of Trans-Synaptic Labeling by HA-Tango-Trace

(A) Cells were visualized in a volume of a brain and counted manually and plotted on a log scale. TmY cells are labeled an order of a magnitude more frequently than the amacrine cells Dm8 and Mia. The X-axis indicates the presynaptic cell expressing a specific rhodopsin. (B) Postsynaptic/Presynaptic ratios plotted as a compact box plot for each cell type identified using histamine tango-trace. The ratio of TmY cells to their presynaptic partners were higher than those of the amacrine cells indicating the presence of more TmY cells than the amacrine cells. None of the ratios reached 100% indicating the low efficiency of HA-Tango-trace.

Table 1. Distribution of Cell numbers labeled by Tango-trace and MARCM

	Rh3	Rh4	Rh5	Rh6
Rh3TmY	311	0	0	0
Rh4TmY	0	364	0	0
Rh5TmY	0	0	494	0
Rh6TmY	0	0	0	214
Dm8	22	61	30	18
Mia	25	7	114	37
R7	2042	725	0	0
R8	0	0	1604	1712

Table 2. Presynaptic/Postsynaptic ratios labeled by Tango-trace

	Rh3	Rh4	Rh5	Rh6
Rh3TmY	0.3	0	0	0
Rh4TmY	0	0.5	0	0
Rh5TmY	0	0	0.37	0
Rh6TmY	0	0	0	0.23
Dm8	0.05	0.09	0.03	0.03
Mia	0.02	0.01	0.08	0.02
R7	1	1	0	0
R8	0	0	1	1

Figure 2.17.

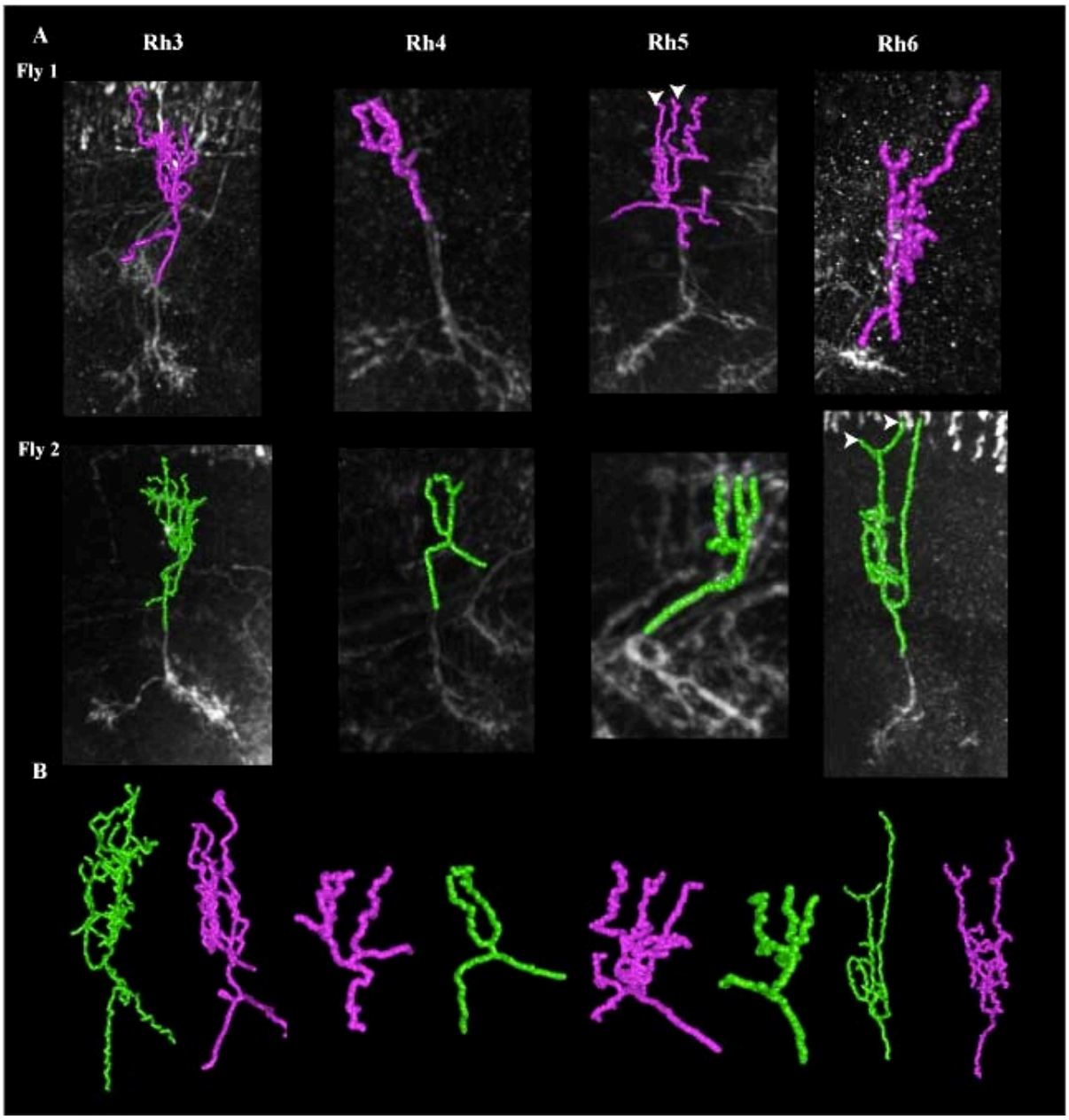

Figure 2.17. Semi-automated neurite tracings of TmY cells in the proximal medulla

The brains were visualized in a volume and projections traced using the skeleton tree algorithm (see Experimental procedures). Tracings were done within an animal and across animals. The process entering the lobula complex was chosen as the reference point for alignment. Tracings were both aligned along principal axes in 3D using rigid transformation and manually aligned along the axes of the process entering the lobula complex. The different cell types have unique projection patterns in the proximal medulla. The arrowheads indicate that the TmY cells appear to contact two other photoreceptors.

Figure 2.18.

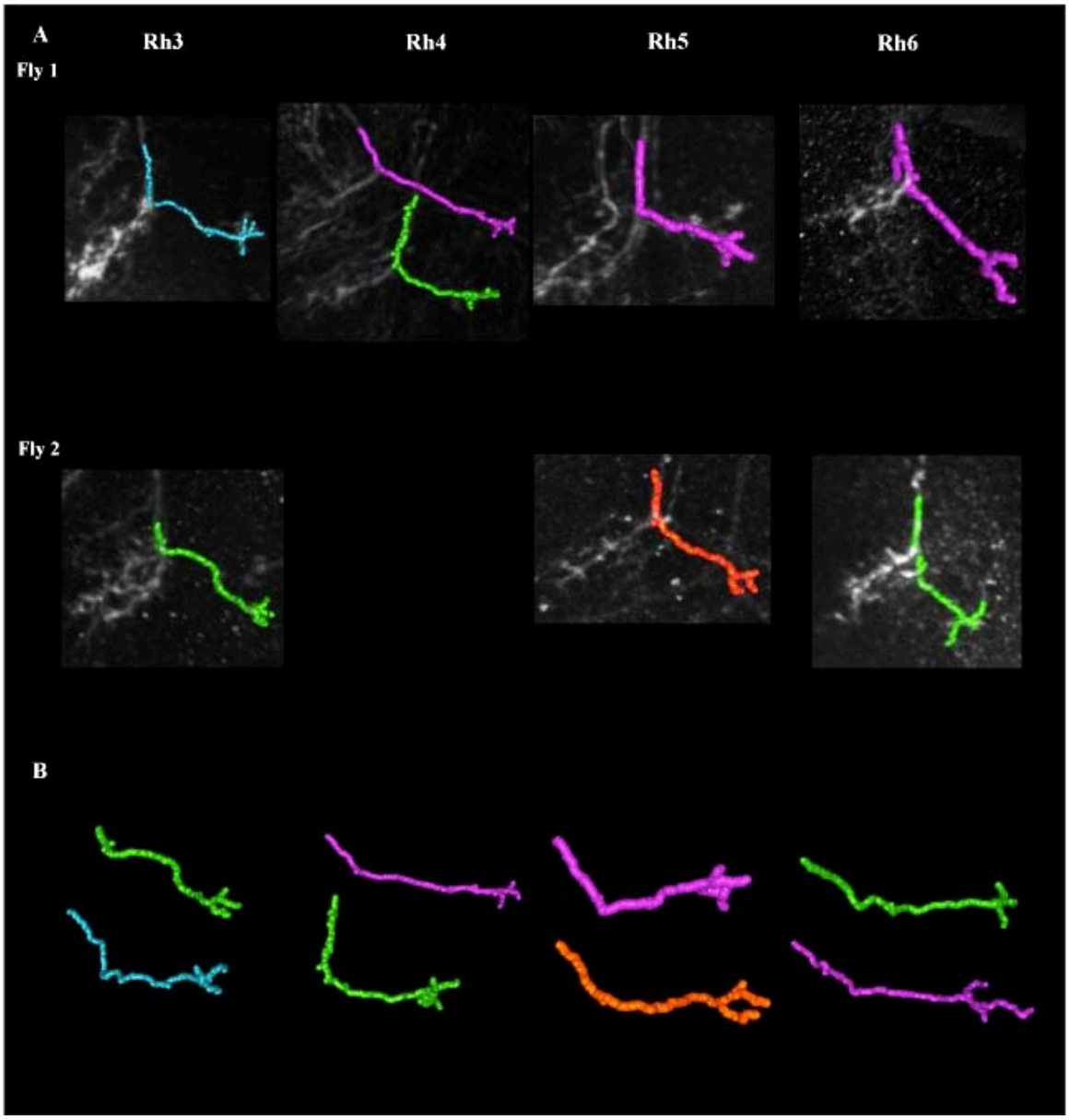

Figure 2.18. Semi-automated neurite tracings of TmY cells in the lobula

The brains were visualized in a volume and projections traced using the skeleton tree algorithm (see Experimental procedures). Tracings were done within an animal and across animals. The process entering the lobula complex was chosen as the reference point for alignment. Tracings were both aligned along principal axes in 3D using rigid transformation and manually aligned along the axes of the process entering the lobula complex. The different cell types have strikingly similar projections in the lobula. This pattern is conserved across cell types and across animals.

Figure 2.19.

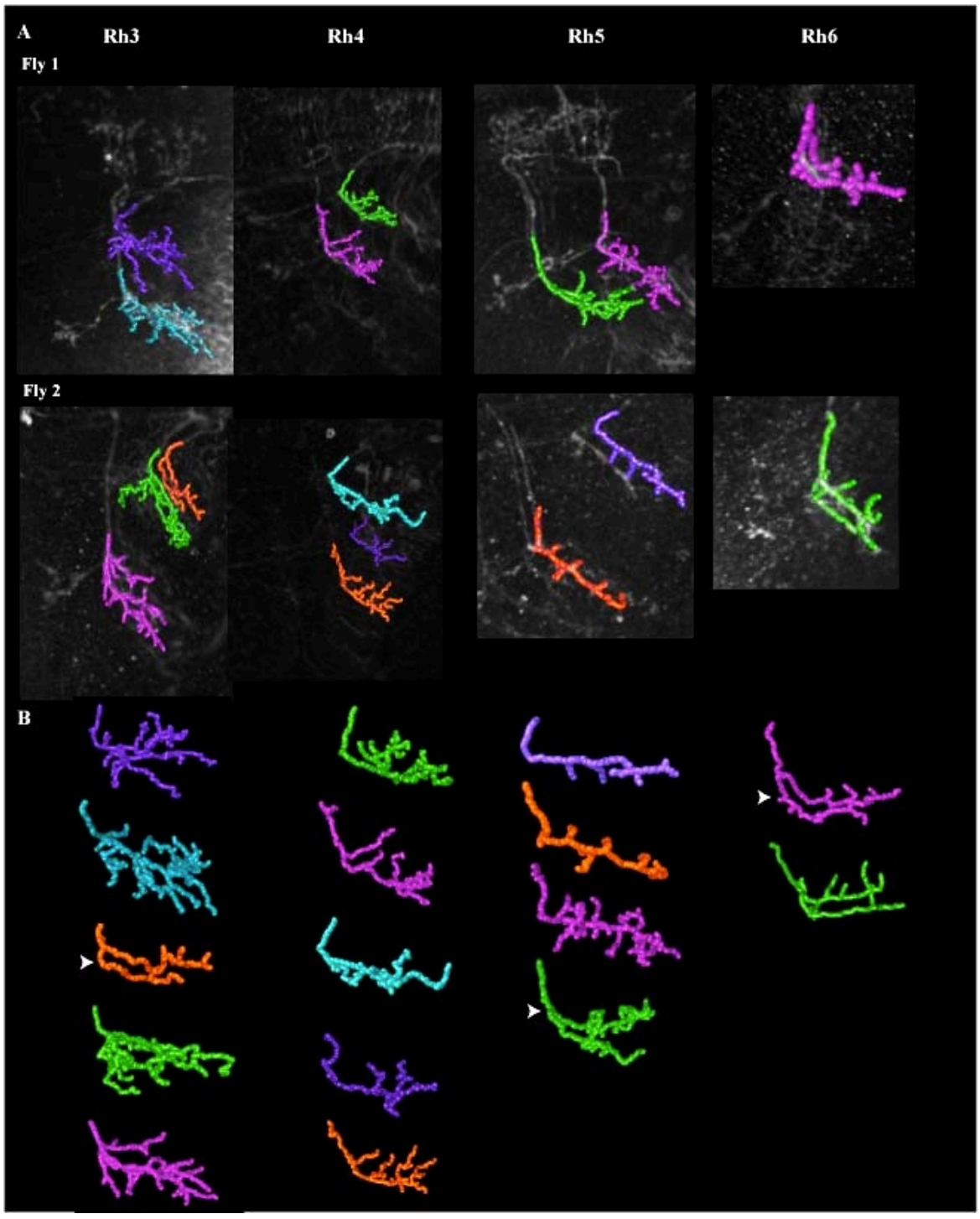

Figure 2.19. Semi-automated neurite tracings of TmY cells in the lobula plate

The brains were visualized in a volume and projections traced using the skeleton tree algorithm (see Experimental procedures). Tracings were done within an animal and across animals. The process entering the lobula complex was chosen as the reference point for alignment. Tracings were both aligned along principal axes in 3D using rigid transformation and manually aligned along the axes of the process entering the lobula complex. The different cell types reveal non-stereotyped patterns of axon arborization in the lobula plate. this pattern is conserved across cell types and across animals.

Figure 2.20.

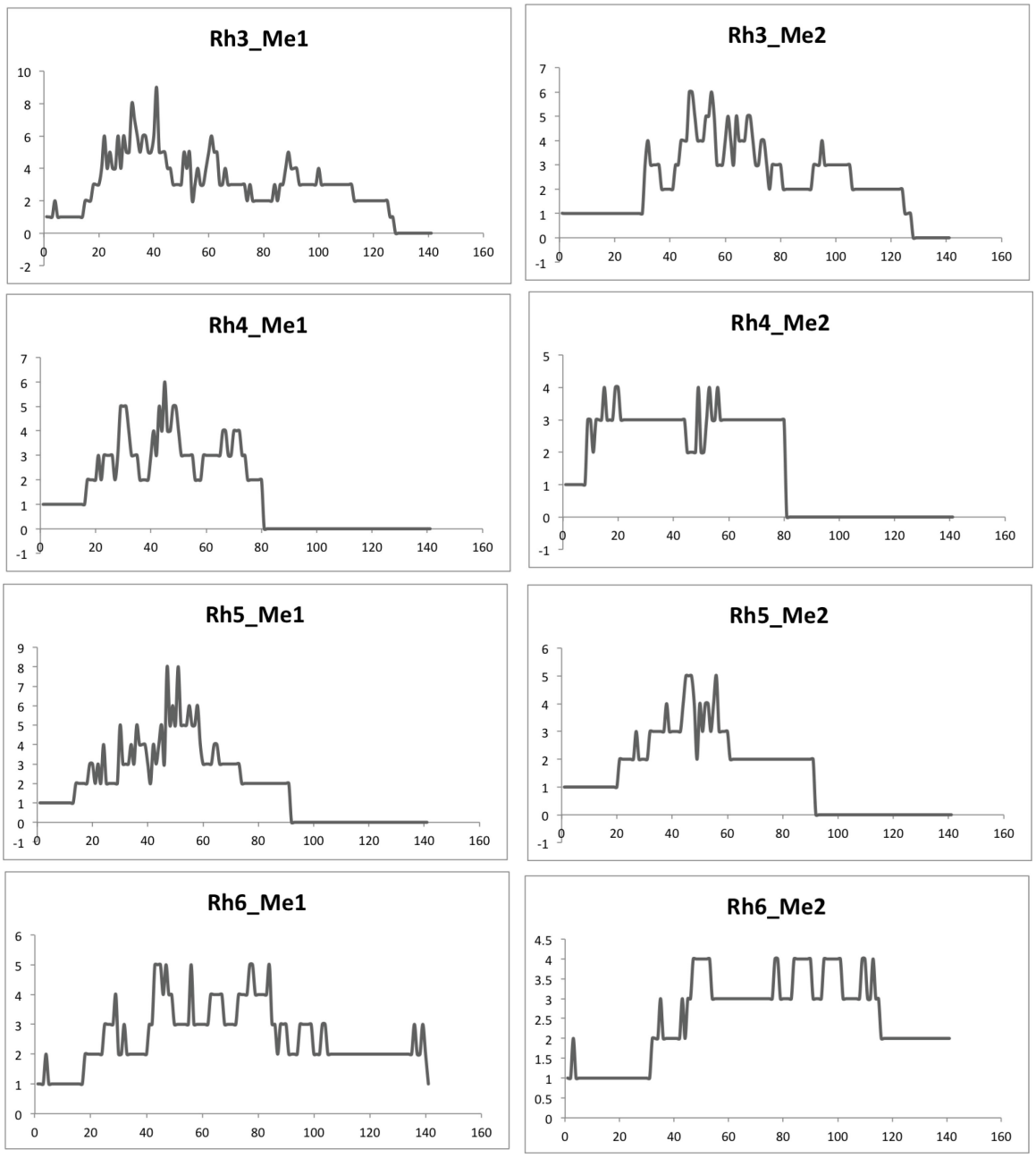

Figure 2.20. Sholl Analysis Plots of TmY Cell Projections in the Inner Medulla

Sholl plots of aligned Amira tracings of the inner medulla projections of TmY cells. The x-axis denotes the radii of the circles and the y-axis denotes the number of sholl intersections

Figure 2.21.

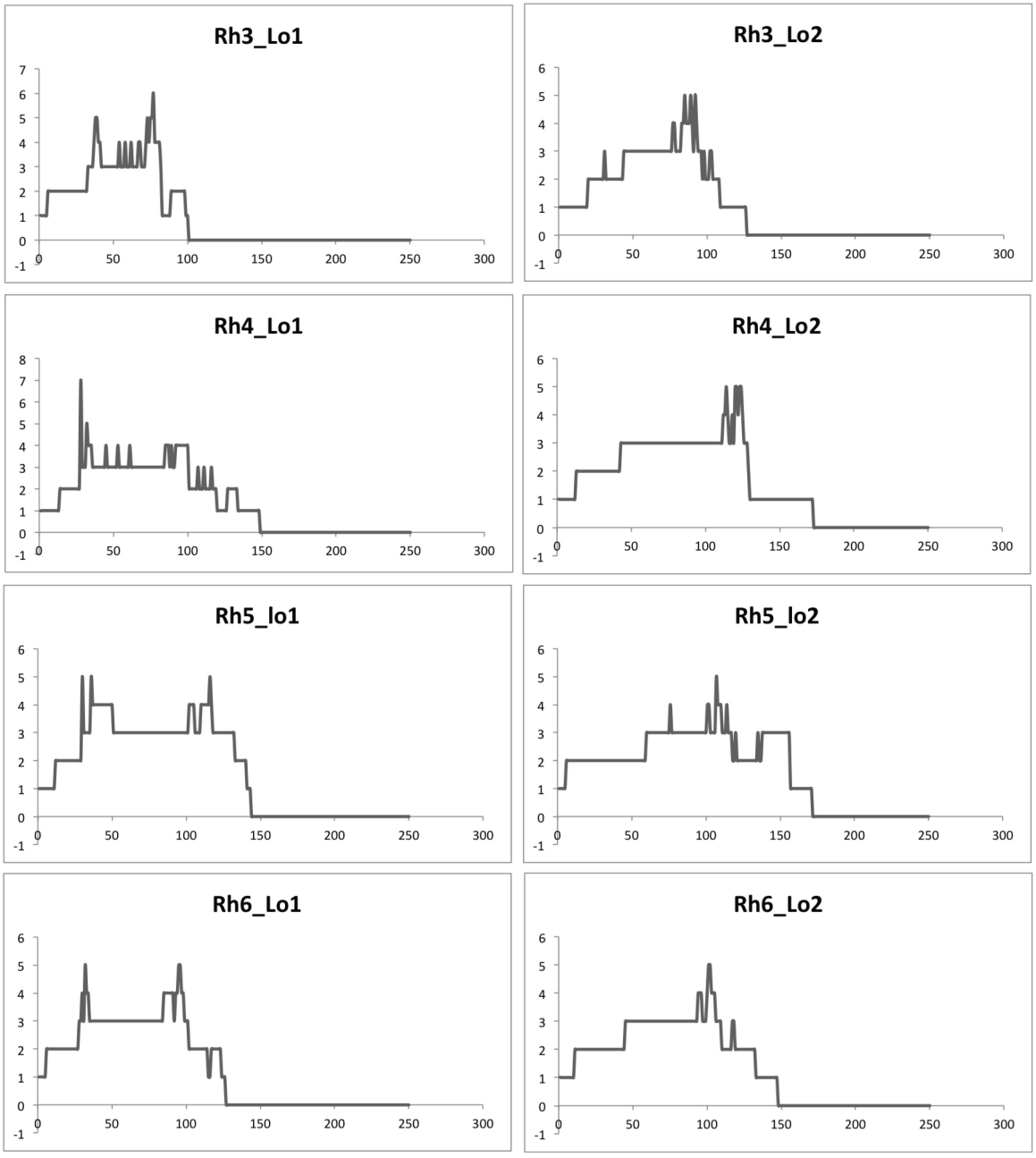

Figure 2.21. Sholl Analysis Plots of TmY Cell Projections in the Lobula

Sholl plots of aligned Amira tracings of the lobula projections of TmY cells. The x-axis denotes the radii of the circles and the y-axis denotes the number of sholl intersections

Figure 2.22.

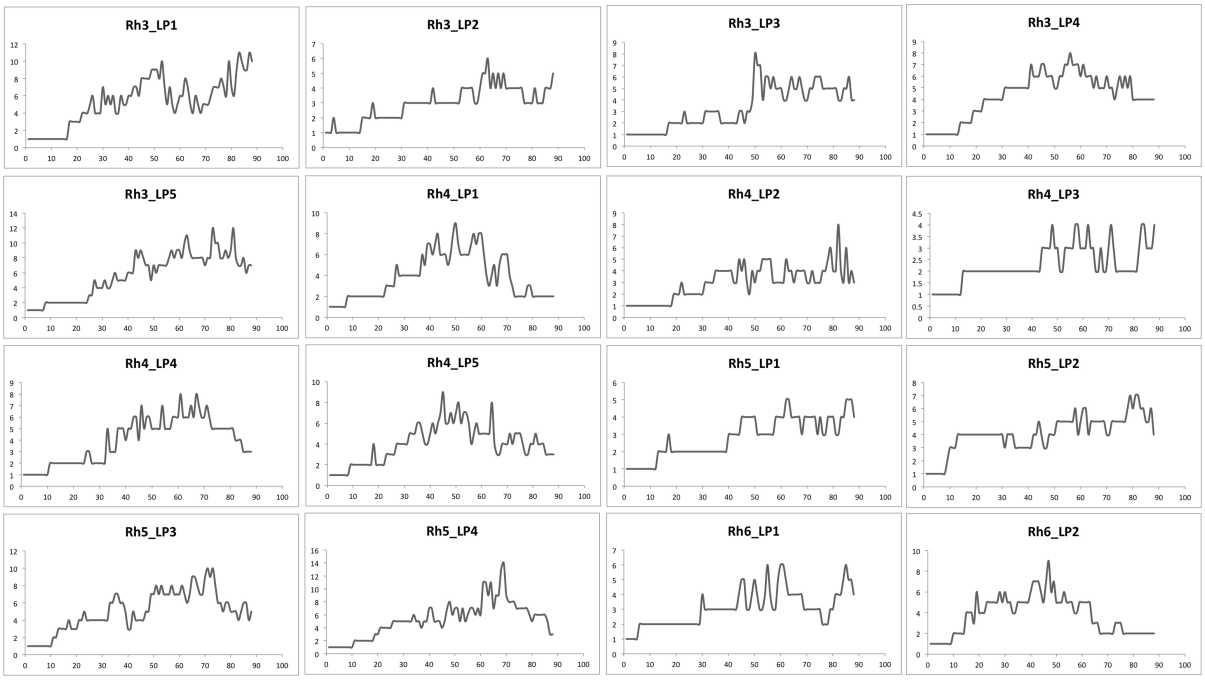
Rh3_LP1
Rh3_LP2
Rh3_LP3
Rh3_LP4
Rh3_LP5
Rh4_LP1
Rh4_LP2
Rh4_LP3
Rh4_LP4
Rh4_LP5
Rh5_LP1
Rh5_LP2
Rh5_LP3
Rh5_LP4
Rh6_LP1
Rh6_LP2

Figure 2.22. Sholl Analysis Plots of TmY Cell Projections in the Lobula Plate

Sholl plots of aligned Amira tracings of the lobula plate projections of TmY cells. The x-axis denotes the radii of the circles and the y-axis denotes the number of sholl intersections

Figure 2.23.

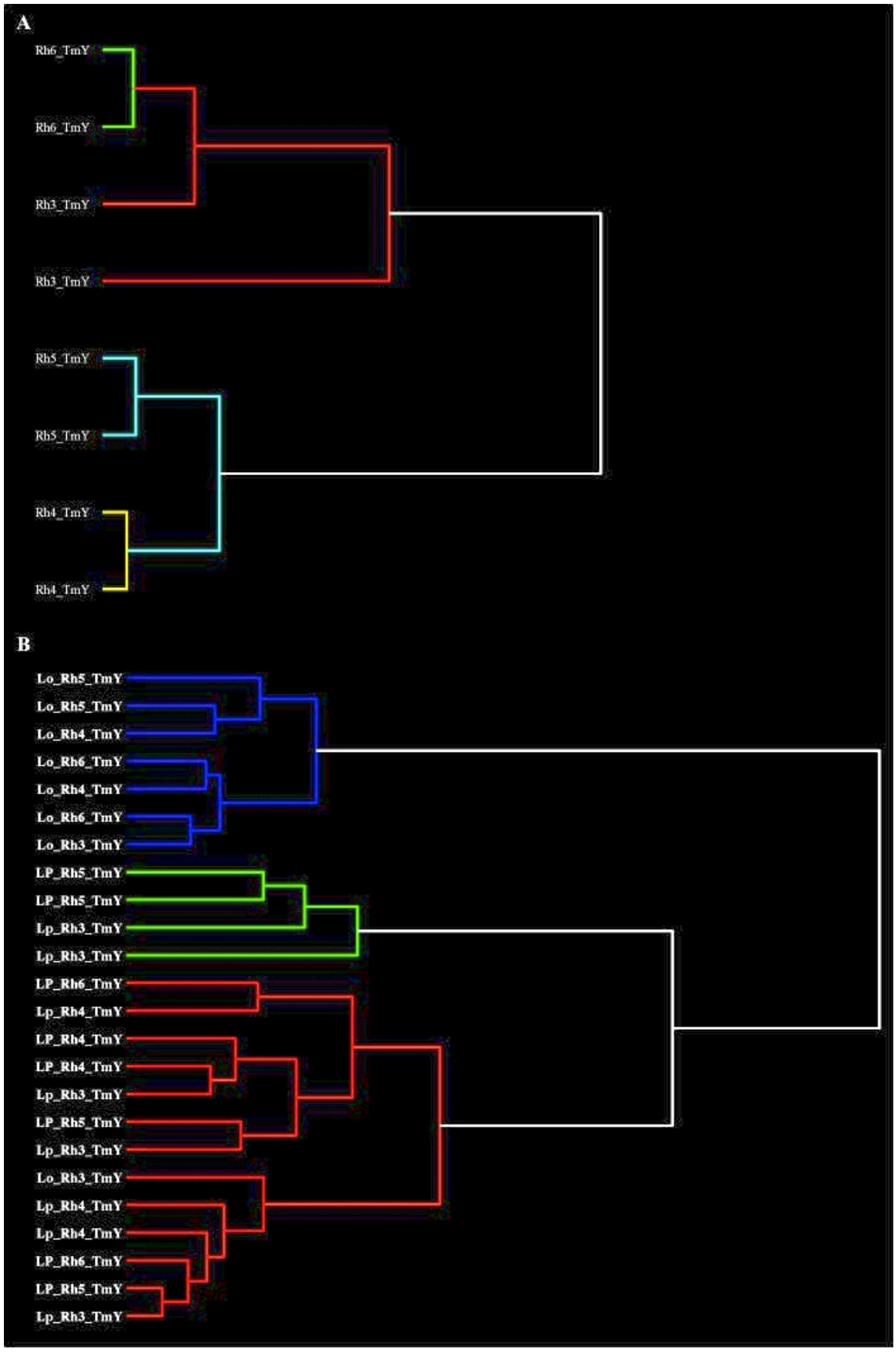
A
Rh6_TmY
Rh6_TmY
Rh3_TmY
Rh3_TmY
Rh5_TmY
Rh5_TmY
Rh4_TmY
Rh4_TmY
B
Lo_Rh5_TmY
Lo_Rh5_TmY
Lo_Rh4_TmY
Lo_Rh6_TmY
Lo_Rh4_TmY
Lo_Rh6_TmY
Lo_Rh3_TmY
LP_Rh5_TmY
LP_Rh5_TmY
Lp_Rh3_TmY
Lp_Rh3_TmY
LP_Rh6_TmY
Lp_Rh4_TmY
LP_Rh4_TmY
LP_Rh4_TmY
Lp_Rh3_TmY
LP_Rh5_TmY
Lp_Rh3_TmY
Lo_Rh3_TmY
Lp_Rh4_TmY
Lp_Rh4_TmY
LP_Rh6_TmY
LP_Rh5_TmY
Lp_Rh3_TmY

Figure 2.23. Cluster Analysis of the Projections of TmY Cells in the Optic Lobe

Hierarchical cluster analysis of sholl intersections of the aligned traces of TmY cells. (A) Projections of TmY cells in the proximal medulla indicate clustering into four different cell types. The projections of Rh3TmY and Rh6 TmY are closely related in terms of their complexity in 3D space. (B) Projections in the lobula and lobula plate projections cluster into two separate clusters but show no cell type specificity.

Figure 2.24.

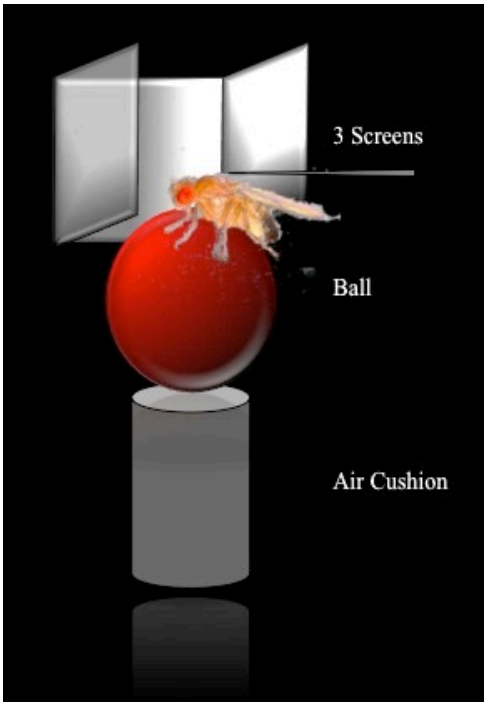

Figure 2.24. Fly-on-a-ball Behavioral Set-up

A walking fly is fixed in place by a pin glued to its thorax; as it walks, it counter-rotates a nearly frictionless, air-suspended ball. Three projection screens surround the fly where the motion stimuli are presented. When the fly attempts to rotate in response to a stimulus, the ball rotates and two optical mice record the motion of the ball as a read-out of the animal's behavioral response to the stimulus.

Figure 2.25.

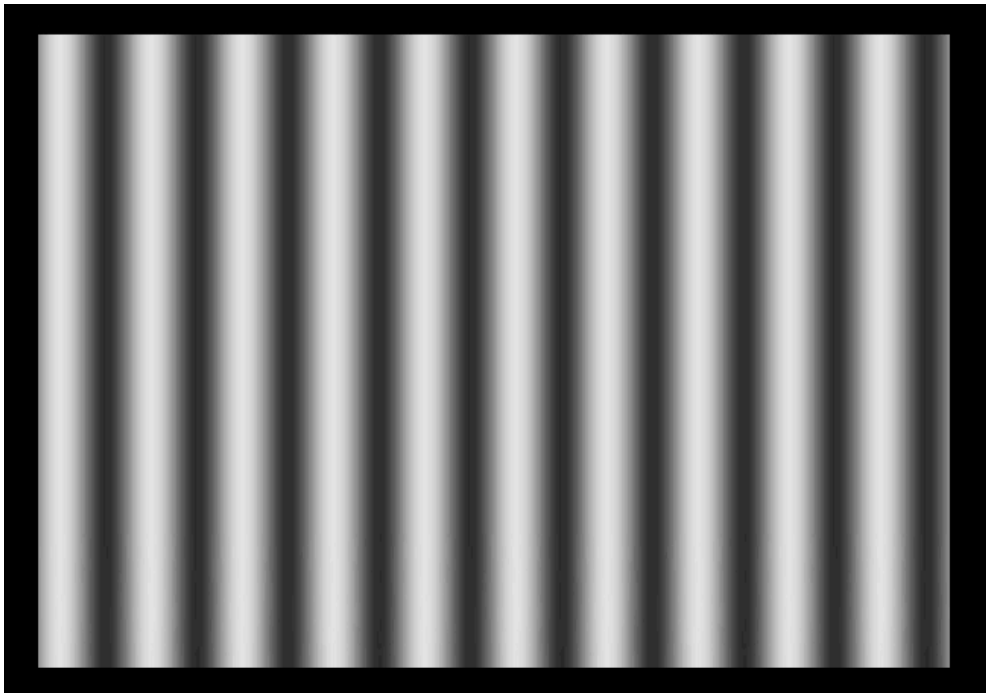

Figure 2.25. Sine Wave Grating Visual Stimulus

All experiments lasted 20 minutes. The motion stimulus itself was presented for 250 ms. First, we presented virtual cylinders consisting of sine wave contrast patterns rotating at varying speeds (40, 80 and 160 degrees/s) lasting for 250ms each. In a second experiment, we presented the fly with stimuli that swept contrast frequency, which provide an indirect measure of the delay filter in the Reichardt detector. We measured the turning response of a single fly to different contrast frequencies (0, 1, 2, 4, 8, 16 and 32 Hz) with the same period sine waves (40 degrees).

Figure 2.26.

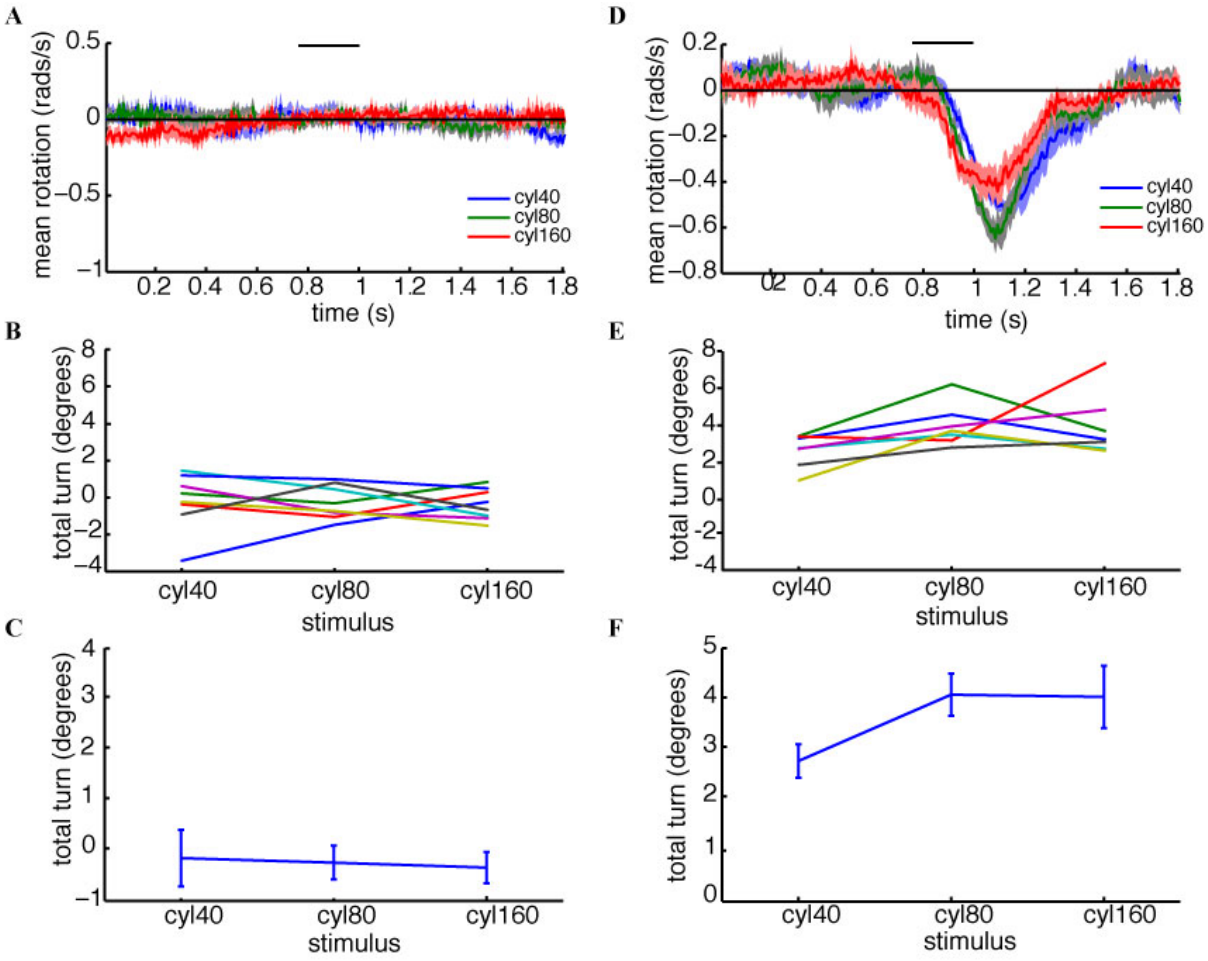
A
mean rotation (rads/s)
time (s)
cyl40
cyl80
cyl160
B
total turn (degrees)
cyl40
cyl80
cyl160
stimulus
C
total turn (degrees)
cyl40
cyl80
cyl160
stimulus
D
mean rotation (rads/s)
time (s)
cyl40
cyl80
cyl160
E
total turn (degrees)
cyl40
cyl80
cyl160
stimulus
F
total turn (degrees)
cyl40
cyl80
cyl160
stimulus

Figure 2.26. Behavioral Responses of R8s to Moving Cylinders

Plots of turning responses to motion stimuli as a function of time. Virtual cylinders consisting of sine wave contrast patterns rotating at varying speeds were presented to the fly. (A)-(C) UAS norpA control, (D)-(F) R8 Gal4, UAS norpA rescue. The thick black bar denotes the stimulus period. The stimulus was presented in the 0.75s -1s time period. (A), (D) Raw traces of the turning response of a single fly to moving cylinders of varying speeds (40, 80 and 160 degrees/s) lasting for 250ms each. (B), (E) Integrals of the responses over time for several flies (n=8), each color representing one fly. The stimulus is indicated on the X-axis and the total turn in degrees on the Y-axis. (C), (F) Average turning responses of all the flies from (B) and (E). Error bars represent ± 1 SEM.

Figure 2.27.

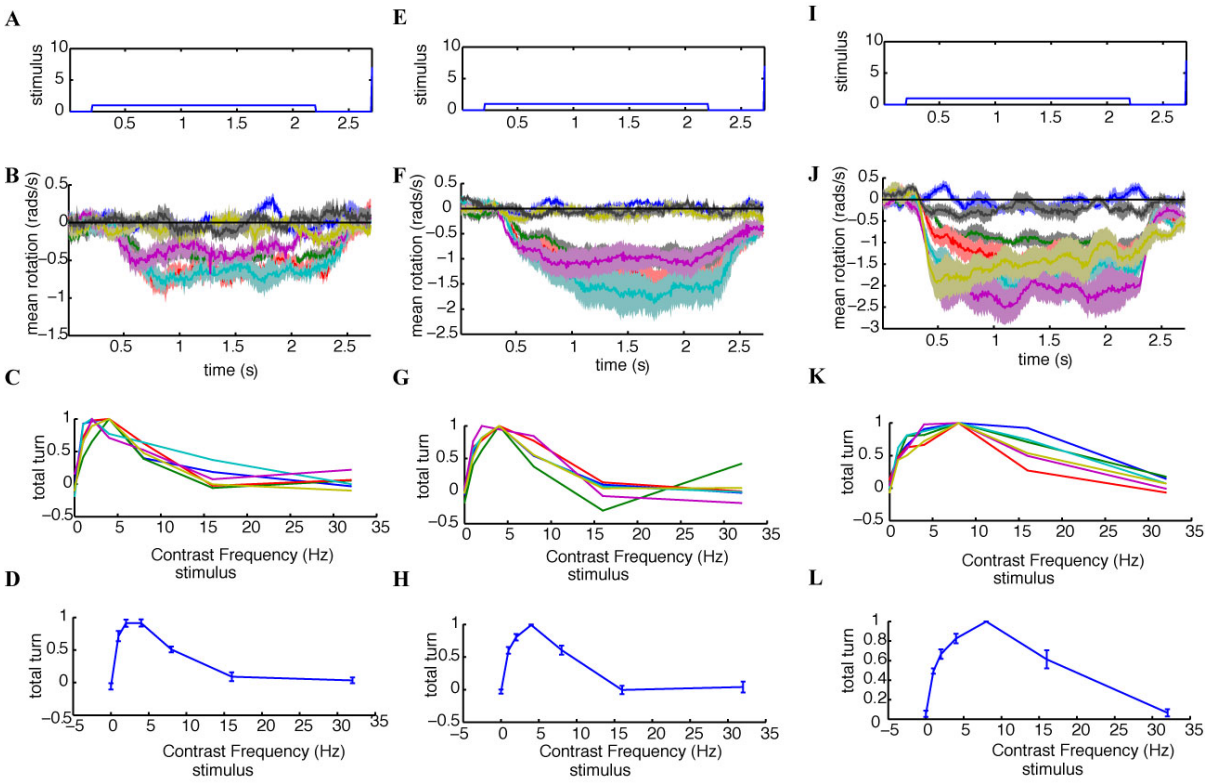
A
E
I
stimulus
B
F
J
mean rotation (rads/s)
time (s)
C
G
K
total turn
Contrast Frequency (Hz)
stimulus
D
H
L

Figure 2.27. Behavioral Responses to Contrast Frequency Sweep Stimuli

Plots of turning responses to contrast frequency motion stimuli as a function of time. (A)-(D) R8 Gal4, UAS norpA rescue motion responses (E)-(H) R1-6 Gal4, UAS norpA rescue motion responses (I)-(L) Wild type motion responses. (A), (E), (I) stimuli that swept contrast frequency presented to the fly in the time period of 0.2-2.2s. (B), (F), (J) Raw traces of the turning response of a single fly to different contrast frequencies with the same period sine waves (40 degrees). Each trace color represents the contrast frequencies used: 0, 1, 2, 4, 8, 16 and 32 Hz. The magnitudes of the responses vary in the order of WT > R1-6 rescue > R8 rescue. (C), (G), (K) Normalized Integrals of the responses over time for several flies (n=6), each color representing one fly. The stimulus is indicated on the X-axis as contrast frequency in Hz and the normalized total turn on the Y-axis. (D), (H), (L) Average responses of the normalized integrals from (C), (G), (K). Error bars represent ± 1 SEM.

Figure 2.28.

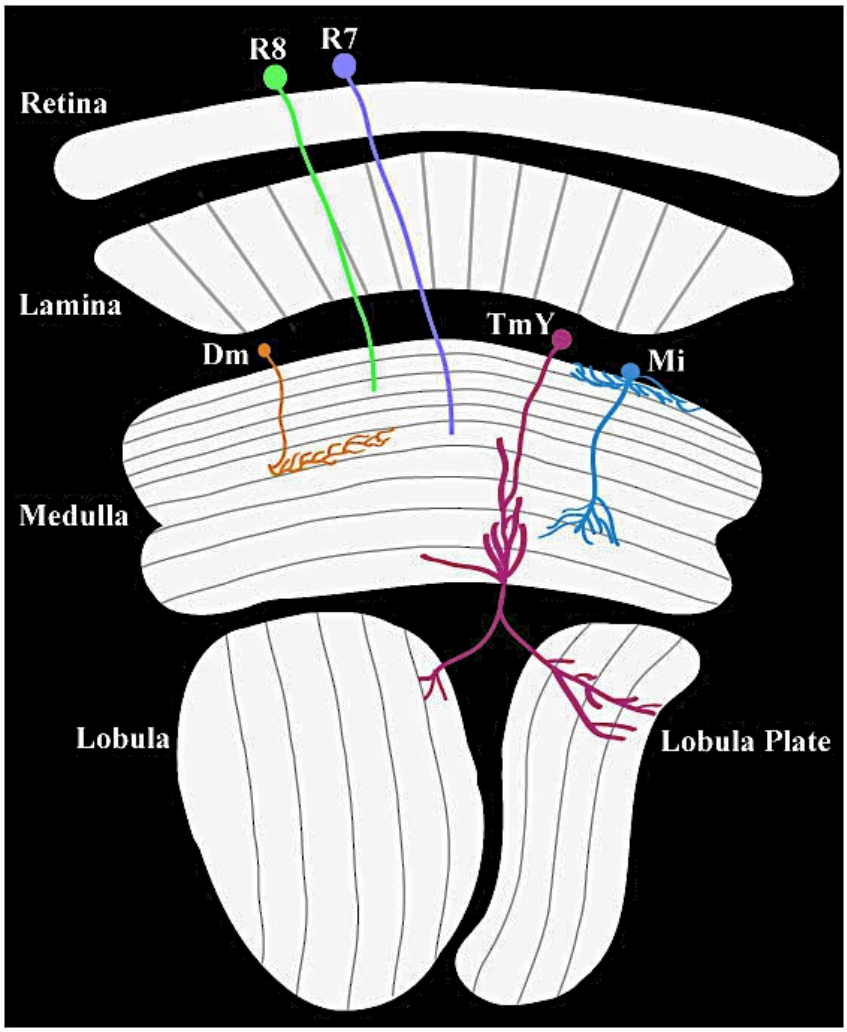

Figure 2.28 Representations of Visual Information Revealed by Tango-Trace

The inner photoreceptors, p/y R7 and R8 contact TmY cells, the second-order visual projection neurons, that arborize in the proximal medulla, split into two branches and then project to all the four layers of the lobula plate and the innermost layer of the lobula. Each photoreceptor subtype contacts a unique variant of this cell type as a postsynaptic target. We refer to these variants as Rh3TmY, Rh4TmY, Rh5TmY and Rh6TmY corresponding to their presynaptic partner. R7 and R8 contact an amacrine cell Dm8. Dm8 is a wide field amacrine cell contacting 14-15 columns in the both the antero-posterior (AP) and dorso-ventral (DV) axes in layer 6 of the distal medulla. A third post-synaptic target of R7 and R8 is an intrinsic medullary cell, which we refer to as Mia. This cell type innervates 4-5 columns in the DV axis in layers 7-9 of the proximal medulla as well innervates broadly in layer 1 of the distal medulla contacting 14-15 columns in both the AP and DV axes.

Figure 2.29.

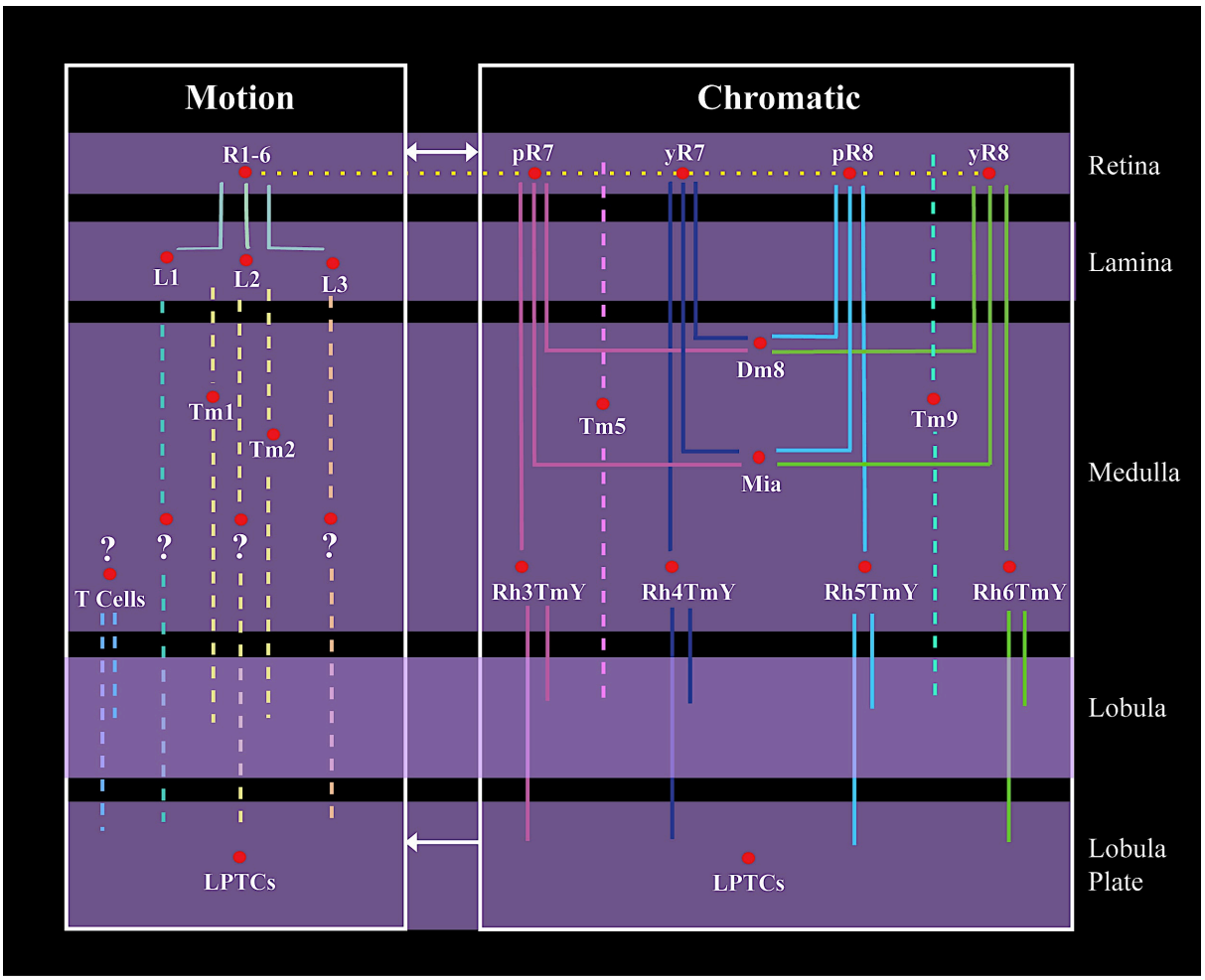
Motion
Chromatic
R1-6
pR7
yR7
pR8
yR8
Retina
Lamina
L1
L2
L3
Dm8
Tm1
Tm5
Tm9
Tm2
Mia
Medulla
?
?
?
?
T Cells
Rh3TmY
Rh4TmY
Rh5TmY
Rh6TmY
Lobula
LPTCs
LPTCs
Lobula Plate

Figure 2.29. Parallel Processing Pathways of The Fly Visual System

The visual pathways in flies are broadly classified as the motion and chromatic pathways. R1-6 encode motion information and the R7/8 encode spectral information. R1-6 form synapses with the lamina monopolar cells (LMCs) L1-3 in the lamina. Motion channels are further subdivided by LMCs. EM reconstruction studies have implied synaptic connections of L2 with Tm1 and Tm2 that project to the lobula. The inputs to the lobula plate still remain unknown. T cells may provide these inputs by projecting their bushy processes in the proximal medulla, lobula and lobula plate.

EM reconstruction studies have implied synaptic connections of R7 and R8 cells with Tm5 and Tm9 cells that project to the lobula. In this study, we have identified the second-order visual projection neurons Rh3TmY, Rh4TmY, Rh5TmY and Rh6TmY that receive information from the inner photoreceptors, arborize in the proximal medulla, and project to lobula plate and lobula. In addition, p/y R7 and R8 contact a wide-field amacrine cell Dm8 and an intrinsic medullary cell Mia that innervate multiple columns in the medulla. Recent studies imply gap junctional connections between the inner and outer photoreceptors. The lobula plate projections of the TmY cells may deliver spectral information to the motion pathway. Thus, these pathways converge repetitively at two stages of the circuit. Dashed lines represent connections implied by EM reconstruction. Yellow dotted line between R1-6 and R7/8 denotes gap junctions. The arrows indicate convergence of the motion and chromatic pathways.

2.5 References

Ache, B.W., and Young, J.M. (2005). Neuron *48*, 417.

Amrein, H., and Thorne, N. (2005). Curr Biol *15*, R673.

Anholt, R.R., Lyman, R.F., and Mackay, T.F. (1996). Genetics *143*, 293.

Baines, R.A., Uhler, J.P., Thompson, A., Sweeney, S.T., and Bate, M. (2001). Altered electrical properties in Drosophila neurons developing without synaptic transmission. J Neurosci *21*, 1523-1531.

Bargmann, C.I. (2012). Beyond the connectome: How neuromodulators shape neural circuits. BioEssays : news and reviews in molecular, cellular and developmental biology.

Barnea, G., Strapps, W., Herrada, G., Berman, Y., Ong, J., Kloss, B., Axel, R., and Lee, K.J. (2008). The genetic design of signaling cascades to record receptor activation. Proc Natl Acad Sci USA *105*, 64-69.

Bausenwein, B., Dittrich, A.P., and Fischbach, K.F. (1992). The optic lobe of Drosophila melanogaster. II. Sorting of retinotopic pathways in the medulla. Cell Tissue Res *267*, 17-28.

Beier, K.T., Saunders, A., Oldenburg, I.A., Miyamichi, K., Akhtar, N., Luo, L., Whelan, S.P., Sabatini, B., and Cepko, C.L. (2011). Anterograde or retrograde transsynaptic labeling of CNS neurons with vesicular stomatitis virus vectors. Proc Natl Acad Sci U S A *108*, 15414-15419.

Bellen, H.J., Tong, C., and Tsuda, H. (2010). 100 years of Drosophila research and its impact on vertebrate neuroscience: a history lesson for the future. Nat Rev Neurosci *11*, 514-522.

Benton, R., Vannice, K.S., and Vosshall, L.B. (2007). An essential role for a CD36-related receptor in pheromone detection in Drosophila. Nature *450*, 289-293.

Benveniste, H., and Huttemeier, P.C. (1990). Microdialysis--theory and application. Prog Neurobiol *35*, 195-215.

Bishop, G.H. (1933). Fiber groups in the optic nerves. Am J Physiol *106*, 460-470.

Blau, J., and Young, M.W. (1999). Cycling vrille expression is required for a functional Drosophila clock. Cell *99*, 661-671.

Bohland, J.W., Wu, C., Barbas, H., Bokil, H., Bota, M., Breiter, H.C., Cline, H.T., Doyle, J.C., Freed, P.J., Greenspan, R.J.*, et al.* (2009). A proposal for a coordinated effort for the determination of brainwide neuroanatomical connectivity in model organisms at a mesoscopic scale. PLoS Comput Biol *5*, e1000334.

Borst, A. (2009). Drosophila's view on insect vision. Curr Biol *19*, R36-47.

Boulant, J.A. (2000). Role of the preoptic-anterior hypothalamus in thermoregulation and fever. Clinical infectious diseases : an official publication of the Infectious Diseases Society of America *31 Suppl 5*, S157-161.

Brand, A.H., and Perrimon, N. (1993). Development *118*, 401.

Braz, J.M., and Basbaum, A.I. (2008). Genetically expressed transneuronal tracer reveals direct and indirect serotonergic descending control circuits. J Comp Neurol *507*, 1990-2003.

Braz, J.M., Enquist, L.W., and Basbaum, A.I. (2009). Inputs to serotonergic neurons revealed by conditional viral transneuronal tracing. J Comp Neurol *514*, 145-160.

Briggman, K.L., Helmstaedter, M., and Denk, W. (2011). Wiring specificity in the direction-selectivity circuit of the retina. Nature *471*, 183-188.

Brotz, T.M., Gundelfinger, E.D., and Borst, A. (2001). Cholinergic and GABAergic pathways in fly motion vision. BMC Neurosci *2*, 1.

Broughton, S.J., Kitamoto, T., and Greenspan, R.J. (2004). Excitatory and inhibitory switches for courtship in the brain of Drosophila melanogaster. Curr Biol *14*, 538-547.

Buchner, E., Buchner, S., and Bülthoff, H. (1984). Identification of [3H]deoxyglucose-labelled interneurons in the fly from serial autoradiographs. Brain Res *305*, 384-388.

Buchner, E., Buchner, S., Burg, M.G., Hofbauer, A., Pak, W.L., and Pollack, I. (1993). Histamine is a major mechanosensory neurotransmitter candidate in Drosophila melanogaster. Cell Tissue Res *273*, 119-125.

Buck, L., and Axel, R. (1991). A novel multigene family may encode odorant receptors: a molecular basis for odor recognition. Cell *65*, 175-187.

Cabantous, S., Terwilliger, T.C., and Waldo, G.S. (2005). Protein tagging and detection with engineered self-assembling fragments of green fluorescent protein. Nature biotechnology *23*, 102-107.

Cabot, J.B., Mennone, A., Bogan, N., Carroll, J., Evinger, C., and Erichsen, J.T. (1991). Retrograde, trans-synaptic and transneuronal transport of fragment C of tetanus toxin by sympathetic preganglionic neurons. Neuroscience *40*, 805-823.

Callaway, E.M. (2005). Structure and function of parallel pathways in the primate early visual system. J Physiol *566*, 13-19.

Callaway, E.M. (2008). Transneuronal circuit tracing with neurotropic viruses. Curr Opin Neurobiol *18*, 617-623.

Cameron, P., Hiroi, M., Ngai, J., and Scott, K. (2010). The molecular basis for water taste in Drosophila. Nature *465*, 91-95.

Card, G., and Dickinson, M.H. (2008). Visually Mediated Motor Planning in the Escape Response of Drosophila. Current biology : CB *18*, 1300-1307.

Card, J.P., Kobiler, O., McCambridge, J., Ebdlahad, S., Shan, Z., Raizada, M.K., Sved, A.F., and Enquist, L.W. (2011). Microdissection of neural networks by conditional reporter expression from a Brainbow herpesvirus. Proc Natl Acad Sci U S A *108*, 3377-3382.

Card, J.P., Rinaman, L., Lynn, R.B., Lee, B.H., Meade, R.P., Miselis, R.R., and Enquist, L.W. (1993). Pseudorabies virus infection of the rat central nervous system: ultrastructural characterization of viral replication, transport, and pathogenesis. J Neurosci *13*, 2515-2539.

Card, J.P., Rinaman, L., Schwaber, J.S., Miselis, R.R., Whealy, M.E., Robbins, A.K., and Enquist, L.W. (1990). Neurotropic properties of pseudorabies virus: uptake and transneuronal passage in the rat central nervous system. J Neurosci *10*, 1974-1994.

Card, J.P., Whealy, M.E., Robbins, A.K., Moore, R.Y., and Enquist, L.W. (1991). Two alpha-herpesvirus strains are transported differentially in the rodent visual system. Neuron *6*, 957-969.

Carson, K.A., and Mesulam, M.M. (1982). Electron microscopic demonstration of neural connections using horseradish peroxidase: a comparison of the tetramethylbenzidine procedure with seven other histochemical methods. The journal of histochemistry and cytochemistry : official journal of the Histochemistry Society *30*, 425-435.

Chalfie, M., Sulston, J.E., White, J.G., Southgate, E., Thomson, J.N., and Brenner, S. (1985). The neural circuit for touch sensitivity in Caenorhabditis elegans. J Neurosci *5*, 956-964.

Cheng, L.E., Song, W., Looger, L.L., Jan, L.Y., and Jan, Y.N. (2010). The role of the TRP channel NompC in Drosophila larval and adult locomotion. Neuron *67*, 373-380.

Chiang, A.S., Lin, C.Y., Chuang, C.C., Chang, H.M., Hsieh, C.H., Yeh, C.W., Shih, C.T., Wu, J.J., Wang, G.T., Chen, Y.C.*, et al.* (2011). Three-dimensional reconstruction of brain-wide wiring networks in Drosophila at single-cell resolution. Curr Biol *21*, 1-11.

Chiappe, M.E., Seelig, J.D., Reiser, M.B., and Jayaraman, V. (2010). Walking Modulates Speed Sensitivity in Drosophila Motion Vision. Curr Biol *20*, 1470-1475.

Chou, W.H., Hall, K.J., Wilson, D.B., Wideman, C.L., Townson, S.M., Chadwell, L.V., and Britt, S.G. (1996). Identification of a novel Drosophila opsin reveals specific patterning of the R7 and R8 photoreceptor cells. Neuron *17*, 1101-1115.

Chyb, S., Dahanukar, A., Wickens, A., and Carlson, J.R. (2003). Drosophila Gr5a encodes a taste receptor tuned to trehalose. Proc Natl Acad Sci U S A *100 Suppl 2*, 14526-14530.

Clandinin, T.R., and Zipursky, S.L. (2002). Making connections in the fly visual system. Neuron *35*, 827-841.

Clark, D.A., Bursztyn, L., Horowitz, M.A., Schnitzer, M.J., and Clandinin, T.R. (2011). Defining the computational structure of the motion detector in Drosophila. Neuron *70*, 1165-1177.

Clyne, J.D., and Miesenbock, G. (2008). Sex-specific control and tuning of the pattern generator for courtship song in Drosophila. Cell *133*, 354-363.

Clyne, P.J., Warr, C.G., and Carlson, J.R. (2000). Science *287*, 1830.

Clyne, P.J., Warr, C.G., Freeman, M.R., Lessing, D., Kim, J., and Carlson, J.R. (1999). Neuron *22*, 327.

Couto, A., Alenius, M., and Dickson, B.J. (2005). Curr Biol *15*, 1535.

Crittenden, J.R., Skoulakis, E.M., Han, K.A., Kalderon, D., and Davis, R.L. (1998). Learn Mem *5*, 38.

Cuntz, H., Forstner, F., Haag, J., and Borst, A. (2008). The morphological identity of insect dendrites. PLoS Comput Biol *4*, e1000251.

Curanovic, D., and Enquist, L. (2009). Directional transneuronal spread of alpha-herpesvirus infection. Future virology *4*, 591.

Datta, S.R., Vasconcelos, M.L., Ruta, V., Luo, S., Wong, A., Demir, E., Flores, J., Balonze, K., Dickson, B.J., and Axel, R. (2008). The Drosophila pheromone cVA activates a sexually dimorphic neural circuit. Nature *452*, 473-477.

Davis, R.L. (2005). Annu Rev Neurosci *28*, 275.

de Belle, J.S., and Heisenberg, M. (1994). Science *263*, 692.

de Bruyne, M., Foster, K., and Carlson, J.R. (2001). Odor coding in the Drosophila antenna. Neuron *30*, 537-552.

de Vries, S.E., and Clandinin, T.R. (2012). Loom-sensitive neurons link computation to action in the Drosophila visual system. Curr Biol *22*, 353-362.

DeFalco, J., Tomishima, M., Liu, H., Zhao, C., Cai, X., Marth, J.D., Enquist, L., and Friedman, J.M. (2001). Virus-assisted mapping of neural inputs to a feeding center in the hypothalamus. Science *291*, 2608-2613.

DeFelipe, J. (2010). From the connectome to the synaptome: an epic love story. Science *330*, 1198-1201.

Delcomyn, F. (1980). Neural basis of rhythmic behavior in animals. Science *210*, 492-498.

Dickson, B.J. (2008). Wired for sex: the neurobiology of Drosophila mating decisions. Science *322*, 904-909.

Douglass, J.K., and Strausfeld, N.J. (2003). Retinotopic pathways providing motion-selective information to the lobula from peripheral elementary motion-detecting circuits. J Comp Neurol *457*, 326-344.

Douglass, J.K., and Strausfeld, N.J. (2007). Diverse speed response properties of motion sensitive neurons in the fly's optic lobe. J Comp Physiol A Neuroethol Sens Neural Behav Physiol *193*, 233-247.

Dunipace, L., Meister, S., McNealy, C., and Amrein, H. (2001). Curr Biol *11*, 822.

Eberl, D.F., Duyk, G.M., and Perrimon, N. (1997). A genetic screen for mutations that disrupt an auditory response in Drosophila melanogaster. Proc Natl Acad Sci U S A *94*, 14837-14842.

Egelhaaf, M., Borst, A., and Reichardt, W. (1989). Computational structure of a biological motion-detection system as revealed by local detector analysis in the fly's nervous system. J Opt Soc Am A *6*, 1070-1087.

Egelhaaf, M., Kern, R., Krapp, H.G., Kretzberg, J., Kurtz, R., and Warzecha, A.K. (2002). Neural encoding of behaviourally relevant visual-motion information in the fly. Trends Neurosci *25*, 96-102.

Ejima, A., and Griffith, L.C. (2008). Courtship initiation is stimulated by acoustic signals in Drosophila melanogaster. PLoS ONE *3*, e3246.

Estes, P.S., Ho, G.L., Narayanan, R., and Ramaswami, M. (2000). Synaptic localization and restricted diffusion of a Drosophila neuronal synaptobrevin--green fluorescent protein chimera in vivo. J Neurogenet *13*, 233-255.

Etessami, R., Conzelmann, K.K., Fadai-Ghotbi, B., Natelson, B., Tsiang, H., and Ceccaldi, P.E. (2000). Spread and pathogenic characteristics of a G-deficient rabies virus recombinant: an in vitro and in vivo study. The Journal of general virology *81*, 2147-2153.

Evers, J.F., Schmitt, S., Sibila, M., and Duch, C. (2005). Progress in functional neuroanatomy: precise automatic geometric reconstruction of neuronal morphology from confocal image stacks. J Neurophysiol *93*, 2331-2342.

Evinger, C., and Erichsen, J.T. (1986). Transsynaptic retrograde transport of fragment C of tetanus toxin demonstrated by immunohistochemical localization. Brain Res *380*, 383-388.

Farrow, K., Haag, J., and Borst, A. (2003). Input organization of multifunctional motion-sensitive neurons in the blowfly. J Neurosci *23*, 9805-9811.

Feinberg, E.H., Vanhoven, M.K., Bendesky, A., Wang, G., Fetter, R.D., Shen, K., and Bargmann, C.I. (2008). GFP Reconstitution Across Synaptic Partners (GRASP) defines cell contacts and synapses in living nervous systems. Neuron *57*, 353-363.

Fiala, A., Spall, T., Diegelmann, S., Eisermann, B., Sachse, S., Devaud, J.M., Buchner, E., and Galizia, C.G. (2002). Genetically expressed cameleon in Drosophila melanogaster is used to visualize olfactory information in projection neurons. Curr Biol *12*, 1877-1884.

Fischbach, K., and Dittrich, A. (1989). The optic lobe of Drosophila melanogaster. I. A Golgi analysis of wild-type structure. Cell Tissue Res.

Fischbach, K.F., Dittrich, A.P.M. (1989). The optic lobe of *Drosophila melanogaster*. I. A Golgi analysis of wild-type structure. Cell Tissue Res *258*, 441-475.

Fischbach, K.F., and Heisenberg, M. (1981). Structural brain mutant of Drosophila melanogaster with reduced cell number in the medulla cortex and with normal optomotor yaw response. Proc Natl Acad Sci U S A *78*, 1105-1109.

Fischler, W., Kong, P., Marella, S., and Scott, K. (2007). The detection of carbonation by the Drosophila gustatory system. Nature *448*, 1054-1057.

Fishilevich, E., and Vosshall, L.B. (2005). Curr Biol *15*, 1548.

Fitzpatrick, D., Lund, J.S., and Blasdel, G.G. (1985). Intrinsic connections of macaque striate cortex: afferent and efferent connections of lamina 4C. J Neurosci *5*, 3329-3349.

Friesen, W.O., Poon, M., and Stent, G.S. (1978). Neuronal control of swimming in the medicinal leech. IV. Identification of a network of oscillatory interneurones. J Exp Biol *75*, 25-43.

Fryxell, K.J., and Meyerowitz, E.M. (1987). An opsin gene that is expressed only in the R7 photoreceptor cell of Drosophila. The EMBO journal *6*, 443-451.

Gao, Q., and Chess, A. (1999). Genomics *60*, 31.

Gao, Q., Yuan, B., and Chess, A. (2000). Nat Neurosci *3*, 780.

Gao, S., Takemura, S.-Y., Ting, C.-Y., Huang, S., Lu, Z., Luan, H., Rister, J., Thum, A.S., Yang, M., Hong, S.-T.*, et al.* (2008a). The neural substrate of spectral preference in Drosophila. Neuron *60*, 328-342.

Gao, S., Takemura, S.Y., Ting, C.Y., Huang, S., Lu, Z., Luan, H., Rister, J., Thum, A.S., Yang, M., Hong, S.T.*, et al.* (2008b). The neural substrate of spectral preference in Drosophila. Neuron *60*, 328-342.

Gaudry, Q., and Kristan, W.B., Jr. (2009). Behavioral choice by presynaptic inhibition of tactile sensory terminals. Nat Neurosci *12*, 1450-1457.

Gengs, C., Leung, H.-T., Skingsley, D.R., Iovchev, M.I., Yin, Z., Semenov, E.P., Burg, M.G., Hardie, R.C., and Pak, W.L. (2002a). The target of Drosophila photoreceptor synaptic transmission is a histamine-gated chloride channel encoded by ort (hclA). J Biol Chem *277*, 42113-42120.

Gengs, C., Leung, H.T., Skingsley, D.R., Iovchev, M.I., Yin, Z., Semenov, E.P., Burg, M.G., Hardie, R.C., and Pak, W.L. (2002b). The target of Drosophila photoreceptor synaptic transmission is a histamine-gated chloride channel encoded by ort (hclA). J Biol Chem *277*, 42113-42120.

Gerfen, C.R., and Sawchenko, P.E. (1984). An anterograde neuroanatomical tracing method that shows the detailed morphology of neurons, their axons and terminals: immunohistochemical localization of an axonally transported plant lectin, Phaseolus vulgaris leucoagglutinin (PHA-L). Brain Res *290*, 219-238.

Getting, P.A. (1983). Mechanisms of pattern generation underlying swimming in Tritonia. II. Network reconstruction. J Neurophysiol *49*, 1017-1035.

Gibson, J.J. (1950). Perception of the Visual World.

Gillet, J.P., Derer, P., and Tsiang, H. (1986). Axonal transport of rabies virus in the central nervous system of the rat. Journal of neuropathology and experimental neurology *45*, 619-634.

Gisselmann, G., Pusch, H., Hovemann, B.T., and Hatt, H. (2002). Two cDNAs coding for histamine-gated ion channels in D. melanogaster. Nature neuroscience *5*, 11-12.

Glover, J.C., Petursdottir, G., and Jansen, J.K. (1986). Fluorescent dextran-amines used as axonal tracers in the nervous system of the chicken embryo. J Neurosci Methods *18*, 243-254.

Godement, P., Salaun, J., and Metin, C. (1987). Fate of uncrossed retinal projections following early or late prenatal monocular enucleation in the mouse. J Comp Neurol *255*, 97-109.

Gohl, D.M., Silies, M.A., Gao, X.J., Bhalerao, S., Luongo, F.J., Lin, C.C., Potter, C.J., and Clandinin, T.R. (2011). A versatile in vivo system for directed dissection of gene expression patterns. Nat Methods *8*, 231-237.

Golic, K.G., and Lindquist, S. (1989). The FLP recombinase of yeast catalyzes site-specific recombination in the Drosophila genome. Cell *59*, 499-509.

Gong, Z., Liu, J., Guo, C., Zhou, Y., Teng, Y., and Liu, L. (2010). Two pairs of neurons in the central brain control Drosophila innate light preference. Science *330*, 499-502.

Gong, Z., Son, W., Chung, Y.D., Kim, J., Shin, D.W., McClung, C.A., Lee, Y., Lee, H.W., Chang, D.J., Kaang, B.K.*, et al.* (2004). Two interdependent TRPV channel subunits, inactive and Nanchung, mediate hearing in Drosophila. J Neurosci *24*, 9059-9066.

Goodale, M.A., and Milner, A.D. (1992). Separate visual pathways for perception and action. Trends Neurosci *15*, 20-25.

Gopfert, M.C., and Robert, D. (2001). Biomechanics. Turning the key on Drosophila audition. Nature *411*, 908.

Gordon, M.D., and Scott, K. (2009). Motor control in a Drosophila taste circuit. Neuron *61*, 373-384.

Goto, S.G., and Kimura, M.T. (1998). Heat- and cold-shock responses and temperature adaptations in subtropical and temperate species of Drosophila. J Insect Physiol *44*, 1233-1239.

Götz, K.G., Wenking, H. (1973). Visual control of locomotion in the walking fruitfly Drosophila. Journal of Comparative Physiology A *85*, 235-266.

Gradinaru, V., Zhang, F., Ramakrishnan, C., Mattis, J., Prakash, R., Diester, I., Goshen, I., Thompson, K.R., and Deisseroth, K. (2010). Molecular and cellular approaches for diversifying and extending optogenetics. Cell *141*, 154-165.

Grafstein, B. (1971). Transneuronal transfer of radioactivity in the central nervous system. Science *172*, 177-179.

Granzin, J., Wilden, U., Choe, H.W., Labahn, J., Krafft, B., and Buldt, G. (1998). X-ray crystal structure of arrestin from bovine rod outer segments. Nature *391*, 918-921.

Gronenberg, W., and Strausfeld, N.J. (1992). Premotor descending neurons responding selectively to local visual stimuli in flies. J Comp Neurol *316*, 87-103.

Ha, T.S., and Smith, D.P. (2006). J Neurosci *26*, 8727.

Haag, J., and Borst, A. (2003). Orientation tuning of motion-sensitive neurons shaped by vertical-horizontal network interactions. J Comp Physiol A Neuroethol Sens Neural Behav Physiol *189*, 363-370.

Haag, J., and Borst, A. (2008). Electrical coupling of lobula plate tangential cells to a heterolateral motion-sensitive neuron in the fly. J Neurosci *28*, 14435-14442.

Haag, J., Denk, W., and Borst, A. (2004). Fly motion vision is based on Reichardt detectors regardless of the signal-to-noise ratio. Proc Natl Acad Sci USA *101*, 16333-16338.

Haag, J., Wertz, A., and Borst, A. (2007). Integration of lobula plate output signals by DNOVS1, an identified premotor descending neuron. J Neurosci *27*, 1992-2000.

Hadjieconomou, D., Timofeev, K., and Salecker, I. (2011). A step-by-step guide to visual circuit assembly in Drosophila. Curr Opin Neurobiol *21*, 76-84.

Halfon, M.S., Gisselbrecht, S., Lu, J., Estrada, B., Keshishian, H., and Michelson, A.M. (2002). New fluorescent protein reporters for use with the Drosophila Gal4 expression system and for vital detection of balancer chromosomes. Genesis *34*, 135-138.

Hall, J.C. (2003). Genetics and molecular biology of rhythms in Drosophila and other insects. Advances in genetics *48*, 1-280.

Hallem, E.A., and Carlson, J.R. (2006). Cell *125*, 143.

Hamada, F.N., Rosenzweig, M., Kang, K., Pulver, S.R., Ghezzi, A., Jegla, T.J., and Garrity, P.A. (2008). An internal thermal sensor controlling temperature preference in Drosophila. Nature *454*, 217-220.

Hamasaka, Y., and Nässel, D.R. (2006). Mapping of serotonin, dopamine, and histamine in relation to different clock neurons in the brain of Drosophila. J Comp Neurol *494*, 314-330.

Han, M., Gurevich, V.V., Vishnivetskiy, S.A., Sigler, P.B., and Schubert, C. (2001). Crystal structure of beta-arrestin at 1.9 A: possible mechanism of receptor binding and membrane Translocation. Structure *9*, 869-880.

Hardie, R.C. (1987). Is histamine a neurotransmitter in insect photoreceptors? J Comp Physiol A *161*, 201-213.

Harrison, P.J., Hultborn, H., Jankowska, E., Katz, R., Storai, B., and Zytnicki, D. (1984). Labelling of interneurones by retrograde transsynaptic transport of horseradish peroxidase from motoneurones in rats and cats. Neurosci Lett *45*, 15-19.

Hassenstein, B., and Reichardt, W. (1956). Systemtheoretische analyse der zeit-, reihenfolgen- und vorzeichenauswertung bei der bewegungsperzeption des ru¨sselka¨ fers chlorophanus. Zeitschrift fu¨ r Naturforschung *11*, 513–524.

Hausen, K. (1982). Motion sensitive interneurons in the optomotor system of the fly. II. The horizontal cells:
receptive field organization and response characteristics. Biological Cybernetics *46*, 67-79.

Heimbeck, G., Bugnon, V., Gendre, N., Keller, A., and Stocker, R.F. (2001). Proc Natl Acad Sci USA *98*, 15336.

Heisenberg, M. (2003). Nat Rev Neurosci *4*, 266.

Heisenberg, M., Wolf, R. (1984). Vision in Drosophila: genetics of microbehavior (Berlin/Heidelberg/New York/Tokyo: Springer-Verlag).

Heisenberg, M.a.B., E. (1977). The role of retinula cell types in visual behavior of *Drosophila Melanogaster*. J Comp Physiol A *187*, 127-162.

Helfrich-Forster, C. (1995). The period clock gene is expressed in central nervous system neurons which also produce a neuropeptide that reveals the projections of circadian pacemaker cells within the brain of Drosophila melanogaster. Proc Natl Acad Sci U S A *92*, 612-616.

Helfrich-Forster, C. (2002). The circadian system of Drosophila melanogaster and its light input pathways. Zoology (Jena) *105*, 297-312.

Helfrich-Forster, C. (2003). The neuroarchitecture of the circadian clock in the brain of Drosophila melanogaster. Microsc Res Tech *62*, 94-102.

Helfrich-Forster, C. (2005). Neurobiology of the fruit fly's circadian clock. Genes, brain, and behavior *4*, 65-76.

Helfrich-Forster, C., Winter, C., Hofbauer, A., Hall, J.C., and Stanewsky, R. (2001). The circadian clock of fruit flies is blind after elimination of all known photoreceptors. Neuron *30*, 249-261.

Hendry, S.H., and Yoshioka, T. (1994). A neurochemically distinct third channel in the macaque dorsal lateral geniculate nucleus. Science *264*, 575-577.

Hildebrand, J.G., and Shepherd, G.M. (1997). Annu Rev Neurosci *20*, 595.

Hiroi, M., Meunier, N., Marion-Poll, F., and Tanimura, T. (2004). J Neurobiol *61*, 333.

Hirsch, J.A., Schubert, C., Gurevich, V.V., and Sigler, P.B. (1999). The 2.8 A crystal structure of visual arrestin: a model for arrestin's regulation. Cell *97*, 257-269.

Hodge, J.J., Choi, J.C., O'Kane, C.J., and Griffith, L.C. (2005). Shaw potassium channel genes in Drosophila. J Neurobiol *63*, 235-254.

Hong, S.-T., Bang, S., Paik, D., Kang, J., Hwang, S., Jeon, K., Chun, B., Hyun, S., Lee, Y., and Kim, J. (2006). Histamine and its receptors modulate temperature-preference behaviors in Drosophila. J Neurosci *26*, 7245-7256.

Hong, Y.M., and Thanos, S. (1996). A quantitative approach to identify and isolate pure populations of fluorescently labeled adult retinal ganglion cells using a pressure-driven microaspiration technique. Neurosci Lett *214*, 111-114.

Honig, M.G., and Hume, R.I. (1989a). Carbocyanine dyes. Novel markers for labelling neurons. Trends Neurosci *12*, 336-338.

Honig, M.G., and Hume, R.I. (1989b). Dil and diO: versatile fluorescent dyes for neuronal labelling and pathway tracing. Trends Neurosci *12*, 333-335, 340-331.

Horikawa, K., and Armstrong, W.E. (1988). A versatile means of intracellular labeling: injection of biocytin and its detection with avidin conjugates. J Neurosci Methods *25*, 1-11.

Huisman, A.M., Ververs, B., Cavada, C., and Kuypers, H.G. (1984). Collateralization of brainstem pathways in the spinal ventral horn in rat as demonstrated with the retrograde fluorescent double-labeling technique. Brain Res *300*, 362-367.

Inagaki, Hidehiko K., Ben-Tabou De-Leon, S., Wong, A.M., Jagadish, S., Ishimoto, H., Barnea, G., Kitamoto, T., Axel, R., and Anderson, David J. (2012). Visualizing Neuromodulation In Vivo: TANGO-Mapping of Dopamine Signaling Reveals Appetite Control of Sugar Sensing. Cell *148*, 583-595.

Inoshita, T., and Tanimura, T. (2006). Cellular identification of water gustatory receptor neurons and their central projection pattern in Drosophila. Proc Natl Acad Sci U S A *103*, 1094-1099.

Ito, K., Awano, W., Suzuki, K., Hiromi, Y., and Yamamoto, D. (1997). Development *124*, 761.

Jefferis, G.S.X.E., Potter, C.J., Chan, A.M., Marin, E.C., Rohlfing, T., Maurer, C.R., and Luo, L. (2007). Comprehensive maps of Drosophila higher olfactory centers: spatially segregated fruit and pheromone representation. Cell *128*, 1187-1203.

Joesch, M., Plett, J., Borst, A., and Reiff, D.F. (2008). Response properties of motion-sensitive visual interneurons in the lobula plate of Drosophila melanogaster. Curr Biol *18*, 368-374.

Joesch, M., Schnell, B., Raghu, S.V., Reiff, D.F., and Borst, A. (2010). ON and OFF pathways in Drosophila motion vision. Nature *468*, 300-304.

Johnsson, N., and Varshavsky, A. (1994). Split ubiquitin as a sensor of protein interactions in vivo. Proc Natl Acad Sci U S A *91*, 10340-10344.

Joiner, W.J., Crocker, A., White, B.H., and Sehgal, A. (2006). Nature *441*, 757.

Kamikouchi, A., Inagaki, H.K., Effertz, T., Hendrich, O., Fiala, A., Gopfert, M.C., and Ito, K. (2009). The neural basis of Drosophila gravity-sensing and hearing. Nature *458*, 165-171.

Kamikouchi, A., Shimada, T., and Ito, K. (2006). Comprehensive classification of the auditory sensory projections in the brain of the fruit fly Drosophila melanogaster. J Comp Neurol *499*, 317-356.

Kaneko, M. (1998). Neural substrates of Drosophila rhythms revealed by mutants and molecular manipulations. Curr Opin Neurobiol *8*, 652-658.

Kaneko, M., and Hall, J.C. (2000). Neuroanatomy of cells expressing clock genes in Drosophila: transgenic manipulation of the period and timeless genes to mark the perikarya of circadian pacemaker neurons and their projections. J Comp Neurol *422*, 66-94.

Kaneko, M., Helfrich-Forster, C., and Hall, J.C. (1997). Spatial and temporal expression of the period and timeless genes in the developing nervous system of Drosophila: newly identified pacemaker candidates and novel features of clock gene product cycling. J Neurosci *17*, 6745-6760.

Katsov, A.Y., and Clandinin, T.R. (2008). Motion processing streams in Drosophila are behaviorally specialized. Neuron *59*, 322-335.

Kawasaki, F., Zou, B., Xu, X., and Ordway, R.W. (2004). Active zone localization of presynaptic calcium channels encoded by the cacophony locus of Drosophila. J Neurosci *24*, 282-285.

Keene, A.C., Stratmann, M., Keller, A., Perrat, P.N., Vosshall, L.B., and Waddell, S. (2004). Neuron *44*, 521.

Kim, J., Zhao, T., Petralia, R.S., Yu, Y., Peng, H., Myers, E., and Magee, J.C. (2012). mGRASP enables mapping mammalian synaptic connectivity with light microscopy. Nat Methods *9*, 96-102.

Kimura, K., Hachiya, T., Koganezawa, M., Tazawa, T., and Yamamoto, D. (2008). Fruitless and doublesex coordinate to generate male-specific neurons that can initiate courtship. Neuron *59*, 759-769.

Kimura, K., Ote, M., Tazawa, T., and Yamamoto, D. (2005). Fruitless specifies sexually dimorphic neural circuitry in the Drosophila brain. Nature *438*, 229-233.

Kimura, K.D., Miyawaki, A., Matsumoto, K., and Mori, I. (2004). The C. elegans thermosensory neuron AFD responds to warming. Curr Biol *14*, 1291-1295.

Kita, H., and Armstrong, W. (1991). A biotin-containing compound N-(2-aminoethyl)biotinamide for intracellular labeling and neuronal tracing studies: comparison with biocytin. J Neurosci Methods *37*, 141-150.

Kitamoto, T. (2001). Conditional modification of behavior in Drosophila by targeted expression of a temperature-sensitive shibire allele in defined neurons. J Neurobiol *47*, 81-92.

Kleinfeld, D., Bharioke, A., Blinder, P., Bock, D.D., Briggman, K.L., Chklovskii, D.B., Denk, W., Helmstaedter, M., Kaufhold, J.P., Lee, W.-C.A.*, et al.* (2011). Large-Scale Automated Histology in the Pursuit of Connectomes. Journal of Neuroscience *31*, 16125-16138.

Kleinfeld, D., and Sompolinsky, H. (1988). Associative neural network model for the generation of temporal patterns. Theory and application to central pattern generators. Biophysical journal *54*, 1039-1051.

Kondoh, Y., Kaneshiro, K.Y., Kimura, K., and Yamamoto, D. (2003). Proc R Soc London B *270*, 1005.

Krapp, H.G., Hengstenberg, B., and Hengstenberg, R. (1998). J Neurophysiol *79*, 1902.

Krashes, M.J., DasGupta, S., Vreede, A., White, B., Armstrong, J.D., and Waddell, S. (2009). A neural circuit mechanism integrating motivational state with memory expression in Drosophila. Cell *139*, 416-427.

Kristan, W.B., Jr., Calabrese, R.L., and Friesen, W.O. (2005). Neuronal control of leech behavior. Prog Neurobiol *76*, 279-327.

Kristensson, K., and Olsson, Y. (1971). Uptake and retrograde axonal transport of peroxidase in hypoglossal neurons. Electron microscopical localization in the neuronal perikaryon. Acta neuropathologica *19*, 1-9.

Kurtovic, A., Widmer, A., and Dickson, B.J. (2007). A single class of olfactory neurons mediates behavioural responses to a Drosophila sex pheromone. Nature *446*, 542-546.

Lachica, E.A., Beck, P.D., and Casagrande, V.A. (1992). Parallel pathways in macaque monkey striate cortex: anatomically defined columns in layer III. Proc Natl Acad Sci USA *89*, 3566-3570.

Lafay, F., Coulon, P., Astic, L., Saucier, D., Riche, D., Holley, A., and Flamand, A. (1991). Spread of the CVS strain of rabies virus and of the avirulent mutant AvO1 along the olfactory pathways of the mouse after intranasal inoculation. Virology *183*, 320-330.

Lai, J.S., Lo, S.J., Dickson, B.J., and Chiang, A.S. (2012). Auditory circuit in the Drosophila brain. Proc Natl Acad Sci U S A *109*, 2607-2612.

Lai, S.L., and Lee, T. (2006). Genetic mosaic with dual binary transcriptional systems in Drosophila. Nat Neurosci *9*, 703-709.

Lapper, S.R., and Bolam, J.P. (1991). The anterograde and retrograde transport of neurobiotin in the central nervous system of the rat: comparison with biocytin. J Neurosci Methods *39*, 163-174.

Larsen, C.W., Hirst, E., Alexandre, C., and Vincent, J.P. (2003). Segment boundary formation in Drosophila embryos. Development *130*, 5625-5635.

Larsson, M.C., Domingos, A.I., Jones, W.D., Chiappe, M.E., Amrein, H., and Vosshall, L.B. (2004). Neuron *43*, 703.

Laughlin, J.D., Ha, T.S., Jones, D.N., and Smith, D.P. (2008). Activation of pheromone-sensitive neurons is mediated by conformational activation of pheromone-binding protein. Cell *133*, 1255-1265.

LaVail, J.H., and LaVail, M.M. (1972). Retrograde axonal transport in the central nervous system. Science *176*, 1416-1417.

Lee, T., Lee, A., and Luo, L. (1999). Development *126*, 4065.

Lee, T., and Luo, L. (1999). Neuron *22*, 451.

Lee, Y., Lee, Y., Lee, J., Bang, S., Hyun, S., Kang, J., Hong, S.T., Bae, E., Kaang, B.K., and Kim, J. (2005). Pyrexia is a new thermal transient receptor potential channel endowing tolerance to high temperatures in Drosophila melanogaster. Nature genetics *37*, 305-310.

Leiss, F., Koper, E., Hein, I., Fouquet, W., Lindner, J., Sigrist, S., and Tavosanis, G. (2009). Characterization of dendritic spines in the Drosophila central nervous system. Dev Neurobiol *69*, 221-234.

Lichtman, J.W., and Sanes, J.R. (2008). Ome sweet ome: what can the genome tell us about the connectome? Curr Opin Neurobiol *18*, 346-353.

Lima, S.Q., and Miesenbˆck, G. (2005). Remote Control of Behavior through Genetically Targeted Photostimulation of Neurons. Cell *121*, 141-152.

Lin, Y., Stormo, G.D., and Taghert, P.H. (2004). The neuropeptide pigment-dispersing factor coordinates pacemaker interactions in the Drosophila circadian system. J Neurosci *24*, 7951-7957.

Livingstone, M., and Hubel, D. (1988). Segregation of form, color, movement, and depth: anatomy, physiology, and perception. Science *240*, 740-749.

Lu, J., Tapia, J.C., White, O.L., and Lichtman, J.W. (2009). The interscutularis muscle connectome. PLoS Biol *7*, e32.

Luan, H., Lemon, W.C., Peabody, N.C., Pohl, J.B., Zelensky, P.K., Wang, D., Nitabach, M.N., Holmes, T.C., and White, B.H. (2006). Functional dissection of a neuronal network required for cuticle tanning and wing expansion in Drosophila. J Neurosci *26*, 573-584.

Luo, L., Callaway, E.M., and Svoboda, K. (2008). Genetic dissection of neural circuits. Neuron *57*, 634-660.

Macosko, E.Z., Pokala, N., Feinberg, E.H., Chalasani, S.H., Butcher, R.A., Clardy, J., and Bargmann, C.I. (2009). A hub-and-spoke circuit drives pheromone attraction and social behaviour in C. elegans. Nature *458*, 1171-1175.

Maimon, G., Straw, A.D., and Dickinson, M.H. (2010). Active flight increases the gain of visual motion processing in Drosophila. Nature neuroscience *13*, 393-399.

Mank, M., Ferrão Santos, A., Direnberger, S., Mrsic-Flogel, T.D., and Hofer, S.B. (2008). Nat Methods *5*, 805.

Manoli, D.S., Foss, M., Villella, A., Taylor, B.J., Hall, J.C., and Baker, B.S. (2005). Male-specific fruitless specifies the neural substrates of Drosophila courtship behaviour. Nature *436*, 395-400.

Manoli, D.S., Meissner, G.W., and Baker, B.S. (2006). Blueprints for behavior: genetic specification of neural circuitry for innate behaviors. Trends Neurosci *29*, 444-451.

Mao, Z., and Davis, R.L. (2009). Eight different types of dopaminergic neurons innervate the Drosophila mushroom body neuropil: anatomical and physiological heterogeneity. Front Neural Circuits *3*, 5.

Marder, E., and Bucher, D. (2001). Central pattern generators and the control of rhythmic movements. Curr Biol *11*, R986-996.

Marder, E., and Bucher, D. (2007). Understanding Circuit Dynamics Using the Stomatogastric Nervous System of Lobsters and Crabs. Annual Review of Physiology *69*, 291-316.

Marella, S., Fischler, W., Kong, P., Asgarian, S., Rueckert, E., and Scott, K. (2006a). Neuron *49*, 285.

Marella, S., Fischler, W., Kong, P., Asgarian, S., Rueckert, E., and Scott, K. (2006b). Imaging taste responses in the fly brain reveals a functional map of taste category and behavior. Neuron *49*, 285-295.

Marin, E.C., Jefferis, G.S., Komiyama, T., Zhu, H., and Luo, L. (2002a). Cell *109*, 243.

Marin, E.C., Jefferis, G.S., Komiyama, T., Zhu, H., and Luo, L. (2002b). Representation of the glomerular olfactory map in the Drosophila brain. Cell *109*, 243-255.

Martin, J.R., Ernst, R., and Heisenberg, M. (1998). Learn Mem *5*, 179.

Maskos, U., Kissa, K., St Cloment, C., and Brulet, P. (2002). Retrograde trans-synaptic transfer of green fluorescent protein allows the genetic mapping of neuronal circuits in transgenic mice. Proc Natl Acad Sci U S A *99*, 10120-10125.

McKenna, M., Monte, P., Helfand, S.L., Woodard, C., and Carlson, J. (1989). Proc Natl Acad Sci USA *86*, 8118.

Meinertzhagen, I.A., and O'Neil, S.D. (1991). Synaptic organization of columnar elements in the lamina of the wild type in Drosophila melanogaster. J Comp Neurol *305*, 232-263.

Meinertzhagen, I.A., and Sorra, K.E. (2001). Synaptic organization in the fly's optic lamina: few cells, many synapses and divergent microcircuits. Prog Brain Res *131*, 53-69.

Melzig, J., Buchner, S., Wiebel, F., Wolf, R., Burg, M., Pak, W.L., and Buchner, E. (1996). Genetic depletion of histamine from the nervous system of Drosophila eliminates specific visual and mechanosensory behavior. J Comp Physiol A *179*, 763-773.

Michnick, S.W., Remy, I., Campbell-Valois, F.X., Vallee-Belisle, A., and Pelletier, J.N. (2000). Detection of protein-protein interactions by protein fragment complementation strategies. Methods in enzymology *328*, 208-230.

Milano, S.K., Pace, H.C., Kim, Y.M., Brenner, C., and Benovic, J.L. (2002). Scaffolding functions of arrestin-2 revealed by crystal structure and mutagenesis. Biochemistry *41*, 3321-3328.

Monastirioti, M. (1999). Biogenic amine systems in the fruit fly Drosophila melanogaster. Microsc Res Tech *45*, 106-121.

Montell, C., Jones, K., Zuker, C., and Rubin, G. (1987). A second opsin gene expressed in the ultraviolet-sensitive R7 photoreceptor cells of Drosophila melanogaster. J Neurosci *7*, 1558-1566.

Moon, S.J., Kottgen, M., Jiao, Y., Xu, H., and Montell, C. (2006). A taste receptor required for the caffeine response in vivo. Curr Biol *16*, 1812-1817.

Morante, J., and Desplan, C. (2004). Building a projection map for photoreceptor neurons in the Drosophila optic lobes. Semin Cell Dev Biol *15*, 137-143.

Morante, J., and Desplan, C. (2008). The color-vision circuit in the medulla of Drosophila. Curr Biol *18*, 553-565.

Mori, I., and Ohshima, Y. (1995). Neural regulation of thermotaxis in Caenorhabditis elegans. Nature *376*, 344-348.

Mori, T., Oda, F., Umeno, D., Murata, M., and Maeda, M. (1999). Affinity separation of messenger RNA by thermo-responsive polymer carrying oligo(dT). Nucleic acids symposium series, 55-56.

Mosca, T.J., Carrillo, R.A., White, B.H., and Keshishian, H. (2005). Dissection of synaptic excitability phenotypes by using a dominant-negative Shaker K+ channel subunit. Proc Natl Acad Sci U S A *102*, 3477-3482.

Murthy, M. (2010). Unraveling the auditory system of Drosophila. Curr Opin Neurobiol *20*, 281-287.

Murthy, M., Fiete, I., and Laurent, G. (2008). Testing odor response stereotypy in the Drosophila mushroom body. Neuron *59*, 1009-1023.

Nässel, D.R., and Strausfeld, N.J. (1982). A pair of descending neurons with dendrites in the optic lobes projecting directly to thoracic ganglia of dipterous insects. Cell Tissue Res *226*, 355-362.

Nassi, J.J., and Callaway, E.M. (2009a). Parallel processing strategies of the primate visual system. Nat Rev Neurosci *10*, 360-372.

Nassi, J.J., and Callaway, E.M. (2009b). Parallel processing strategies of the primate visual system. Nat Rev Neurosci *10*, 360-372.

Nicolai, L.J., Ramaekers, A., Raemaekers, T., Drozdzecki, A., Mauss, A.S., Yan, J., Landgraf, M., Annaert, W., and Hassan, B.A. (2010). Genetically encoded dendritic marker sheds light on neuronal connectivity in Drosophila. Proc Natl Acad Sci U S A *107*, 20553-20558.

Nitabach, M.N., Wu, Y., Sheeba, V., Lemon, W.C., Strumbos, J., Zelensky, P.K., White, B.H., and Holmes, T.C. (2006). Electrical hyperexcitation of lateral ventral pacemaker neurons desynchronizes downstream circadian oscillators in the fly circadian circuit and induces multiple behavioral periods. J Neurosci *26*, 479-489.

O'Tousa, J.E., Baehr, W., Martin, R.L., Hirsh, J., Pak, W.L., and Applebury, M.L. (1985). The Drosophila ninaE gene encodes an opsin. Cell *40*, 839-850.

Oakley, R.H., Laporte, S.A., Holt, J.A., Caron, M.G., and Barak, L.S. (2000). Differential affinities of visual arrestin, beta arrestin1, and beta arrestin2 for G protein-coupled receptors delineate two major classes of receptors. J Biol Chem *275*, 17201-17210.

Obrdlik, P., El-Bakkoury, M., Hamacher, T., Cappellaro, C., Vilarino, C., Fleischer, C., Ellerbrok, H., Kamuzinzi, R., Ledent, V., Blaudez, D.*, et al.* (2004). K+ channel interactions

detected by a genetic system optimized for systematic studies of membrane protein interactions. Proc Natl Acad Sci U S A *101*, 12242-12247.

Overgaard, J., Sorensen, J.G., Petersen, S.O., Loeschcke, V., and Holmstrup, M. (2005). Changes in membrane lipid composition following rapid cold hardening in Drosophila melanogaster. J Insect Physiol *51*, 1173-1182.

Pantazis, A., Segaran, A., Liu, C.-H., Nikolaev, A., Rister, J., Thum, A.S., Roeder, T., Semenov, E., Juusola, M., and Hardie, R.C. (2008). Distinct roles for two histamine receptors (hclA and hclB) at the Drosophila photoreceptor synapse. J Neurosci *28*, 7250-7259.

Papatsenko, D., Sheng, G., and Desplan, C. (1997). A new rhodopsin in R8 photoreceptors of Drosophila: evidence for coordinate expression with Rh3 in R7 cells. Development *124*, 1665-1673.

Paradis, S., Sweeney, S.T., and Davis, G.W. (2001). Homeostatic control of presynaptic release is triggered by postsynaptic membrane depolarization. Neuron *30*, 737-749.

Parisky, K.M., Agosto, J., Pulver, S.R., Shang, Y., Kuklin, E., Hodge, J.J.L., Kang, K., Kang, K., Liu, X., Garrity, P.A.*, et al.* (2008). PDF cells are a GABA-responsive wake-promoting component of the Drosophila sleep circuit. Neuron *60*, 672-682.

Park, J., Knezevich, P.L., Wung, W., O'Hanlon, S.N., Goyal, A., Benedetti, K.L., Barsi-Rhyne, B.J., Raman, M., Mock, N., Bremer, M.*, et al.* (2011). A conserved juxtacrine signal regulates synaptic partner recognition in Caenorhabditis elegans. Neural Dev *6*, 28.

Park, J.H., Helfrich-Forster, C., Lee, G., Liu, L., Rosbash, M., and Hall, J.C. (2000). Differential regulation of circadian pacemaker output by separate clock genes in Drosophila. Proc Natl Acad Sci U S A *97*, 3608-3613.

Pfeiffer, B.D., Jenett, A., Hammonds, A.S., Ngo, T.B., and Misra, S. (2008). Proc Natl Acad Sci USA *105*, 9715.

Pfeiffer, B.D., Ngo, T.T., Hibbard, K.L., Murphy, C., Jenett, A., Truman, J.W., and Rubin, G.M. (2010). Refinement of tools for targeted gene expression in Drosophila. Genetics *186*, 735-755.

Pflugfelder, G.O., and Heisenberg, M. (1995). Optomotor-blind of Drosophila melanogaster: a neurogenetic approach to optic lobe development and optomotor behaviour. Comparative biochemistry and physiology Part A, Physiology *110*, 185-202.

Phillips, P.E., Robinson, D.L., Stuber, G.D., Carelli, R.M., and Wightman, R.M. (2003). Real-time measurements of phasic changes in extracellular dopamine concentration in freely moving rats by fast-scan cyclic voltammetry. Methods in molecular medicine *79*, 443-464.

Pichaud, F., Briscoe, A., and Desplan, C. (1999). Evolution of color vision. Curr Opin Neurobiol *9*, 622-627.

Ping, Y., Waro, G., Licursi, A., Smith, S., Vo-Ba, D.A., and Tsunoda, S. (2011). Shal/K(v)4 channels are required for maintaining excitability during repetitive firing and normal locomotion in Drosophila. PLoS ONE *6*, e16043.

Pitman, J.L., McGill, J.J., Keegan, K.P., and Allada, R. (2006). Nature *441*, 753.

Porter, J.D., Guthrie, B.L., and Sparks, D.L. (1985). Selective retrograde transneuronal transport of wheat germ agglutinin-conjugated horseradish peroxidase in the oculomotor system. Experimental brain research Experimentelle Hirnforschung Experimentation cerebrale *57*, 411-416.

Potter, C.J., Tasic, B., Russler, E.V., Liang, L., and Luo, L. (2010). The Q system: a repressible binary system for transgene expression, lineage tracing, and mosaic analysis. Cell *141*, 536-548.

Pulver, S.R., Pashkovski, S.L., Hornstein, N.J., Garrity, P.A., and Griffith, L.C. (2009). Temporal dynamics of neuronal activation by Channelrhodopsin-2 and TRPA1 determine behavioral output in Drosophila larvae. J Neurophysiol *101*, 3075-3088.

Quinn, W.G., Harris, W.A., and Benzer, S. (1974). Proc Natl Acad Sci USA *71*, 708.

Raghu, S., and Borst, A. (2011). Candidate Glutamatergic Neurons in the Visual System of Drosophila. PLoS ONE *6*, e19472.

Raghu, S., Joesch, M., and Borst…, A. (2007). Synaptic organization of lobula plate tangential cells in Drosophila: γ‐Aminobutyric acid receptors and chemical release sites. The Journal of ….

Raghu, S., Joesch, M., Sigrist, S.J., Borst, A., and Reiff, D.F. (2009). Synaptic organization of lobula plate tangential cells in Drosophila: Dalpha7 cholinergic receptors. J Neurogenet *23*, 200-209.

Rancz, E.A., Franks, K.M., Schwarz, M.K., Pichler, B., Schaefer, A.T., and Margrie, T.W. (2011). Transfection via whole-cell recording in vivo: bridging single-cell physiology, genetics and connectomics. Nat Neurosci *14*, 527-532.

Reiff, D.F., Plett, J., Mank, M., Griesbeck, O., and Borst, A. (2010). Visualizing retinotopic half-wave rectified input to the motion detection circuitry of Drosophila. Nature neuroscience *13*, 973-978.

Renn, S.C., Park, J.H., Rosbash, M., Hall, J.C., and Taghert, P.H. (1999). A pdf neuropeptide gene mutation and ablation of PDF neurons each cause severe abnormalities of behavioral circadian rhythms in Drosophila. Cell *99*, 791-802.

Rideout, E.J., Billeter, J.C., and Goodwin, S.F. (2007). The sex-determination genes fruitless and doublesex specify a neural substrate required for courtship song. Curr Biol *17*, 1473-1478.

Rieger, D., Stanewsky, R., and Helfrich-Forster, C. (2003). Cryptochrome, compound eyes, Hofbauer-Buchner eyelets, and ocelli play different roles in the entrainment and masking pathway of the locomotor activity rhythm in the fruit fly Drosophila melanogaster. Journal of biological rhythms *18*, 377-391.

Rister, J., Pauls, D., Schnell, B., Ting, C.Y., Lee, C.H., Sinakevitch, I., Morante, J., Strausfeld, N.J., Ito, K., and Heisenberg, M. (2007). Dissection of the peripheral motion channel in the visual system of Drosophila melanogaster. Neuron *56*, 155-170.

Ritzenthaler, S., Suzuki, E., and Chiba, A. (2000). Postsynaptic filopodia in muscle cells interact with innervating motoneuron axons. Nat Neurosci *3*, 1012-1017.

Rivera-Alba, M., Vitaladevuni, S.N., Mischenko, Y., Lu, Z., Takemura, S.Y., Scheffer, L., Meinertzhagen, I.A., Chklovskii, D.B., and de Polavieja, G.G. (2011a). Wiring economy and volume exclusion determine neuronal placement in the Drosophila brain. Curr Biol *21*, 2000-2005.

Rivera-Alba, M., Vitaladevuni, S.N., Mishchenko, Y., Lu, Z., Takemura, S.Y., Scheffer, L., Meinertzhagen, I.A., Chklovskii, D.B., and de Polavieja, G.G. (2011b). Wiring economy and volume exclusion determine neuronal placement in the Drosophila brain. Curr Biol *21*, 2000-2005.

Rodieck, R.W. (1979). Visual pathways. Annu Rev Neurosci *2*, 193-225.

Roeder, T. (2003). Metabotropic histamine receptors--nothing for invertebrates? Eur J Pharmacol *466*, 85-90.

Rolls, M.M., Satoh, D., Clyne, P.J., Henner, A.L., Uemura, T., and Doe, C.Q. (2007). Polarity and intracellular compartmentalization of Drosophila neurons. Neural Dev *2*, 7.

Root, C.M., Ko, K.I., Jafari, A., and Wang, J.W. (2011). Presynaptic facilitation by neuropeptide signaling mediates odor-driven food search. Cell *145*, 133-144.

Roper, S.D. (2007). Signal transduction and information processing in mammalian taste buds. Pflugers Archiv : European journal of physiology *454*, 759-776.

Rosenzweig, M., Brennan, K.M., Tayler, T.D., Phelps, P.O., Patapoutian, A., and Garrity, P.A. (2005). The Drosophila ortholog of vertebrate TRPA1 regulates thermotaxis. Genes Dev *19*, 419-424.

Rosenzweig, M., Kang, K., and Garrity, P.A. (2008). Distinct TRP channels are required for warm and cool avoidance in Drosophila melanogaster. Proc Natl Acad Sci U S A *105*, 14668-14673.

Rothermel, M., Brunert, D., Klupp, B.G., Luebbert, M., Mettenleiter, T.C., and Hatt, H. (2009). Advanced tracing tools: functional neuronal expression of virally encoded fluorescent calcium indicator proteins. Journal of neurovirology *15*, 458-464.

Ruggero, M.A. (1992). Responses to sound of the basilar membrane of the mammalian cochlea. Curr Opin Neurobiol *2*, 449-456.

Ruta, V., Datta, S.R., Vasconcelos, M.L., Freeland, J., Looger, L.L., and Axel, R. (2010). A dimorphic pheromone circuit in Drosophila from sensory input to descending output. Nature *468*, 686-690.

Ryner, L.C., Goodwin, S.F., Castrillon, D.H., Anand, A., Villella, A., Baker, B.S., Hall, J.C., Taylor, B.J., and Wasserman, S.A. (1996). Control of male sexual behavior and sexual orientation in Drosophila by the fruitless gene. Cell *87*, 1079-1089.

Sakai, T., and Kitamoto, T. (2006). J Neurobiol *66*, 821.

Salcedo, E., Zheng, L., Phistry, M., Bagg, E.E., and Britt, S.G. (2003). Molecular basis for ultraviolet vision in invertebrates. J Neurosci *23*, 10873-10878.

Samuel, A.D., Silva, R.A., and Murthy, V.N. (2003). Synaptic activity of the AFD neuron in Caenorhabditis elegans correlates with thermotactic memory. J Neurosci *23*, 373-376.

Sanchez-Soriano, N., and Prokop, A. (2005). The influence of pioneer neurons on a growing motor nerve in Drosophila requires the neural cell adhesion molecule homolog FasciclinII. J Neurosci *25*, 78-87.

Sanes, J.R., and Zipursky, S.L. (2010). Design principles of insect and vertebrate visual systems. Neuron *66*, 15-36.

Sarthy, P.V. (1991). Histamine: a neurotransmitter candidate for Drosophila photoreceptors. J Neurochem *57*, 1757-1768.

Satterlie, R.A. (1985). Reciprocal inhibition and postinhibitory rebound produce reverberation in a locomotor pattern generator. Science *229*, 402-404.

Sayeed, O., and Benzer, S. (1996). Behavioral genetics of thermosensation and hygrosensation in Drosophila. Proc Natl Acad Sci U S A *93*, 6079-6084.

Schlief, M.L., and Wilson, R.I. (2007). Olfactory processing and behavior downstream from highly selective receptor neurons. Nature neuroscience *10*, 623-630.

Schmitt, S., Evers, J.F., Duch, C., Scholz, M., and Obermayer, K. (2004). New methods for the computer-assisted 3-D reconstruction of neurons from confocal image stacks. Neuroimage *23*, 1283-1298.

Schnell, B., Raghu, S.V., Nern, A., and Borst, A. (2012). Columnar cells necessary for motion responses of wide-field visual interneurons in Drosophila. J Comp Physiol A, 1-7.

Schubert, P., and Kreutzberg, G.W. (1974). Axonal transport of adenosine and uridine derivatives and transfer to postsynaptic neurons. Brain Res *76*, 526-530.

Schwab, M.E., and Thoenen, H. (1976). Electron microscopic evidence for a transsynaptic migration of tetanus toxin in spinal cord motoneurons: an autoradiographic and morphometric study. Brain Res *105*, 213-227.

Scott, E.K., Raabe, T., and Luo, L. (2002). Structure of the vertical and horizontal system neurons of the lobula plate in Drosophila. J Comp Neurol *454*, 470-481.

Scott, K., Brady, R., Cravchik, A., Morozov, P., and Rzhetsky, A. (2001). Cell *104*, 661.

Seelig, J.D., Chiappe, M.E., Lott, G.K., Dutta, A., Osborne, J.E., Reiser, M.B., and Jayaraman, V. (2010). Two-photon calcium imaging from head-fixed Drosophila during optomotor walking behavior. Nat Methods *7*, 535-540.

Sengupta, P., Chou, J.H., and Bargmann, C.I. (1996). Cell *84*, 899.

Seung, H.S. (2009). Reading the book of memory: sparse sampling versus dense mapping of connectomes. Neuron *62*, 17-29.

Shang, Y., Haynes, P., Pirez, N., Harrington, K.I., Guo, F., Pollack, J., Hong, P., Griffith, L.C., and Rosbash, M. (2011). Imaging analysis of clock neurons reveals light buffers the wake-promoting effect of dopamine. Nat Neurosci *14*, 889-895.

Shaw, S.R., Frohlich, A., and Meinertzhagen, I.A. (1989). Direct connections between the R7/8 and R1-6 photoreceptor subsystems in the dipteran visual system. Cell Tissue Res *257*, 295-302.

Sheeba, V., Gu, H., Sharma, V.K., O'Dowd, D.K., and Holmes, T.C. (2008). Circadian- and light-dependent regulation of resting membrane potential and spontaneous action potential firing of Drosophila circadian pacemaker neurons. J Neurophysiol *99*, 976-988.

Shenoy, S.K., and Lefkowitz, R.J. (2005). Receptor-specific ubiquitination of beta-arrestin directs assembly and targeting of seven-transmembrane receptor signalosomes. J Biol Chem *280*, 15315-15324.

Shorey, H.H. (1962). Nature of the Sound Produced by Drosophila melanogaster during Courtship. Science *137*, 677-678.

Shreve, S.M., Kelty, J.D., and Lee, R.E., Jr. (2004). Preservation of reproductive behaviors during modest cooling: rapid cold-hardening fine-tunes organismal response. J Exp Biol *207*, 1797-1802.

Sincich, L.C., and Horton, J.C. (2004). The circuitry of V1 and V2: integration of color, form, and motion. Annu Rev Neurosci *28*, 303-326.

Single, S., and Borst, A. (1998). Science *281*, 1848.

Song, W., Onishi, M., Jan, L.Y., and Jan, Y.N. (2007). Peripheral multidendritic sensory neurons are necessary for rhythmic locomotion behavior in Drosophila larvae. Proc Natl Acad Sci U S A *104*, 5199-5204.

Sporns, O., Tononi, G., and Kotter, R. (2005). The human connectome: A structural description of the human brain. PLoS Comput Biol *1*, e42.

Stagljar, I., Korostensky, C., Johnsson, N., and te Heesen, S. (1998). A genetic system based on split-ubiquitin for the analysis of interactions between membrane proteins in vivo. Proc Natl Acad Sci U S A *95*, 5187-5192.

Stanewsky, R. (2003). Genetic analysis of the circadian system in Drosophila melanogaster and mammals. J Neurobiol *54*, 111-147.

Stark, H. (2003). [News on the old histamine. II. Ion channels in Drosophila]. Pharm Unserer Zeit *32*, 93.

Stockinger, P., Kvitsiani, D., Rotkopf, S., Tirian, L., and Dickson, B.J. (2005). Neural circuitry that governs Drosophila male courtship behavior. Cell *121*, 795-807.

Strausfeld, N.J., and Hildebrand, J.G. (1999). Curr Opin Neurobiol *9*, 634.

Strausfeld, N.J., and Lee, J.K. (1991). Neuronal basis for parallel visual processing in the fly. Vis Neurosci *7*, 13-33.

Strausfeld, N.J., Sinakevitch, I., and Vilinsky, I. (2003). Microsc Res Tech *62*, 151.

Struhl, G., and Basler, K. (1993). Organizing activity of wingless protein in Drosophila. Cell *72*, 527-540.

Suh, G.S., Wong, A.M., Hergarden, A.C., Wang, J.W., and Simon, A.F. (2004). Nature *431*, 854.

Sun, Y., Liu, L., Ben-Shahar, Y., Jacobs, J.S., Eberl, D.F., and Welsh, M.J. (2009). TRPA channels distinguish gravity sensing from hearing in Johnston's organ. Proc Natl Acad Sci U S A *106*, 13606-13611.

Swanson, L.W., and Bota, M. (2010). Foundational model of structural connectivity in the nervous system with a schema for wiring diagrams, connectome, and basic plan architecture. Proc Natl Acad Sci U S A *107*, 20610-20617.

Sweeney, S.T., Broadie, K., Keane, J., Niemann, H., and O'Kane, C.J. (1995). Targeted expression of tetanus toxin light chain in Drosophila specifically eliminates synaptic transmission and causes behavioral defects. Neuron *14*, 341-351.

Taghert, P.H. (2001). How does the circadian clock send timing information to the brain? Seminars in cell & developmental biology *12*, 329-341.

Taghert, P.H., Hewes, R.S., Park, J.H., O'Brien, M.A., Han, M., and Peck, M.E. (2001). Multiple amidated neuropeptides are required for normal circadian locomotor rhythms in Drosophila. J Neurosci *21*, 6673-6686.

Takemura, S.-Y., Karuppudurai, T., Ting, C.-Y., Lu, Z., Lee, C.-H., and Meinertzhagen, Ian A. (2011). Cholinergic Circuits Integrate Neighboring Visual Signals in a Drosophila Motion Detection Pathway. Curr Biol *21*, 2077-2084.

Takemura, S.Y., Lu, Z., and Meinertzhagen, I.A. (2008). Synaptic circuits of the Drosophila optic lobe: the input terminals to the medulla. J Comp Neurol *509*, 493-513.

Tanaka, N.K., Awasaki, T., Shimada, T., and Ito, K. (2004). Curr Biol *14*, 449.

Tang, Y., Rampin, O., Giuliano, F., and Ugolini, G. (1999). Spinal and brain circuits to motoneurons of the bulbospongiosus muscle: retrograde transneuronal tracing with rabies virus. J Comp Neurol *414*, 167-192.

Tanouye, M.A., and Wyman, R.J. (1980). Motor outputs of giant nerve fiber in Drosophila. J Neurophysiol *44*, 405-421.

Tauber, E., and Eberl, D.F. (2001). Song production in auditory mutants of Drosophila: the role of sensory feedback. J Comp Physiol A *187*, 341-348.

Thaminy, S., Miller, J., and Stagljar, I. (2004). The split-ubiquitin membrane-based yeast two-hybrid system. Methods Mol Biol *261*, 297-312.

Thanos, S., and Bonhoeffer, F. (1983). Investigations on the development and topographic order of retinotectal axons: anterograde and retrograde staining of axons and perikarya with rhodamine in vivo. J Comp Neurol *219*, 420-430.

Thanos, S., and Bonhoeffer, F. (1987). Axonal arborization in the developing chick retinotectal system. J Comp Neurol *261*, 155-164.

Thorne, N., Chromey, C., Bray, S., and Amrein, H. (2004). Curr Biol *14*, 1065.

Thum, A.S., Knapek, S., Rister, J., Dierichs-Schmitt, E., Heisenberg, M., and Tanimoto, H. (2006). Differential potencies of effector genes in adult Drosophila. J Comp Neurol *498*, 194-203.

Thyagarajan, A., and Ting, A.Y. (2010). Imaging activity-dependent regulation of neurexin-neuroligin interactions using trans-synaptic enzymatic biotinylation. Cell *143*, 456-469.

Todi, S.V., Sharma, Y., and Eberl, D.F. (2004). Anatomical and molecular design of the Drosophila antenna as a flagellar auditory organ. Microsc Res Tech *63*, 388-399.

Tovee, M.J. (1995). Ultra-violet photoreceptors in the animal kingdom: their distribution and function. Trends in ecology & evolution *10*, 455-460.

Tracey, W.D., Jr., Wilson, R.I., Laurent, G., and Benzer, S. (2003). painless, a Drosophila gene essential for nociception. Cell *113*, 261-273.

Ugolini, G., Kuypers, H.G., and Strick, P.L. (1989). Transneuronal transfer of herpes virus from peripheral nerves to cortex and brainstem. Science *243*, 89-91.

Ungerleider, L.G., and Mishkin, M. (1982). The Analysis of Visual Behavior (Nature Publishing Group), pp. 549-586.

van der Goes van Naters, W., and Carlson, J.R. (2007). Receptors and neurons for fly odors in Drosophila. Curr Biol *17*, 606-612.

Varadan, R., Assfalg, M., Haririnia, A., Raasi, S., Pickart, C., and Fushman, D. (2004). Solution conformation of Lys63-linked di-ubiquitin chain provides clues to functional diversity of polyubiquitin signaling. J Biol Chem *279*, 7055-7063.

Varshney, L.R., Chen, B.L., Paniagua, E., Hall, D.H., and Chklovskii, D.B. (2011). Structural properties of the Caenorhabditis elegans neuronal network. PLoS Comput Biol *7*, e1001066.

Venken, Koen J.T., Simpson, Julie H., and Bellen, Hugo J. (2011). Genetic Manipulation of Genes and Cells in the Nervous System of the Fruit Fly. Neuron *72*, 202-230.

Villella, A., and Hall, J.C. (1996). Courtship anomalies caused by doublesex mutations in Drosophila melanogaster. Genetics *143*, 331-344.

Villella, A., and Hall, J.C. (2008). Neurogenetics of courtship and mating in Drosophila. Advances in genetics *62*, 67-184.

Viney, T.J., Balint, K., Hillier, D., Siegert, S., Boldogkoi, Z., Enquist, L.W., Meister, M., Cepko, C.L., and Roska, B. (2007). Local retinal circuits of melanopsin-containing ganglion cells identified by transsynaptic viral tracing. Curr Biol *17*, 981-988.

Vishnivetskiy, S.A., Paz, C.L., Schubert, C., Hirsch, J.A., Sigler, P.B., and Gurevich, V.V. (1999). How does arrestin respond to the phosphorylated state of rhodopsin? J Biol Chem *274*, 11451-11454.

von Philipsborn, A.C., Liu, T., Yu, J.Y., Masser, C., Bidaye, S.S., and Dickson, B.J. (2011). Neuronal control of Drosophila courtship song. Neuron *69*, 509-522.

Vosshall, L.B., Amrein, H., Morozov, P.S., Rzhetsky, A., and Axel, R. (1999). A spatial map of olfactory receptor expression in the Drosophila antenna. Cell *96*, 725-736.

Vosshall, L.B., and Stocker, R.F. (2007). Molecular architecture of smell and taste in Drosophila. Annu Rev Neurosci *30*, 505-533.

Vosshall, L.B., Wong, A.M., and Axel, R. (2000). Cell *102*, 147.

Wagh, D.A., Rasse, T.M., Asan, E., Hofbauer, A., Schwenkert, I., Durrbeck, H., Buchner, S., Dabauvalle, M.C., Schmidt, M., Qin, G.*, et al.* (2006). Bruchpilot, a protein with homology to ELKS/CAST, is required for structural integrity and function of synaptic active zones in Drosophila. Neuron *49*, 833-844.

Waldron, I. (1964). Courtship Sound Production in Two Sympatric Sibling Drosophila Species. Science *144*, 191-193.

Waldvogel, F.-M., and Fischbach, K.-F. - Plasticity of the landing response of <i>Drosophila melanogaster</i>. - *169*.

Wang, J., Ma, X., Yang, J.S., Zheng, X., Zugates, C.T., Lee, C.H., and Lee, T. (2004a). Transmembrane/juxtamembrane domain-dependent Dscam distribution and function during mushroom body neuronal morphogenesis. Neuron *43*, 663-672.

Wang, J.W., Wong, A.M., Flores, J., Vosshall, L.B., and Axel, R. (2003). Cell *112*, 271.

Wang, Z., Singhvi, A., Kong, P., and Scott, K. (2004b). Cell *117*, 981.

Wang, Z., Singhvi, A., Kong, P., and Scott, K. (2004c). Taste representations in the Drosophila brain. Cell *117*, 981-991.

Wanner, K.W., Nichols, A.S., Walden, K.K., Brockmann, A., Luetje, C.W., and Robertson, H.M. (2007). A honey bee odorant receptor for the queen substance 9-oxo-2-decenoic acid. Proc Natl Acad Sci U S A *104*, 14383-14388.

Wardill, T.J., List, O., Li, X., Dongre, S., McCulloch, M., Ting, C.Y., O'Kane, C.J., Tang, S., Lee, C.H., Hardie, R.C*., et al.* (2012). Multiple spectral inputs improve motion discrimination in the Drosophila visual system. Science *336*, 925-931.

Wassle, H. (2004). Parallel processing in the mammalian retina. Nat Rev Neurosci *5*, 747-757.

Watts, R.J., Schuldiner, O., Perrino, J., Larsen, C., and Luo, L. (2004). Glia engulf degenerating axons during developmental axon pruning. Curr Biol *14*, 678-684.

White, J.G., Southgate, E., Thomson, J.N., and Brenner, S. (1986). The structure of the nervous system of the nematode Caenorhabditis elegans. Philosophical transactions of the Royal Society of London Series B, Biological sciences *314*, 1-340.

Wickersham, I.R., Finke, S., Conzelmann, K.K., and Callaway, E.M. (2007a). Retrograde neuronal tracing with a deletion-mutant rabies virus. Nat Methods *4*, 47-49.

Wickersham, I.R., Lyon, D.C., Barnard, R.J., Mori, T., Finke, S., Conzelmann, K.K., Young, J.A., and Callaway, E.M. (2007b). Monosynaptic restriction of transsynaptic tracing from single, genetically targeted neurons. Neuron *53*, 639-647.

Wickersham, I.R., Lyon, D.C., Barnard, R.J.O., Mori, T., Finke, S., Conzelmann, K.-K., Young, J.A.T., and Callaway, E.M. (2007c). Monosynaptic restriction of transsynaptic tracing from single, genetically targeted neurons. Neuron *53*, 639-647.

Williams, J.A., and Sehgal, A. (2001). Molecular components of the circadian system in Drosophila. Annual review of physiology *63*, 729-755.

Witte, I., Kreienkamp, H.-J., Gewecke, M., and Roeder, T. (2002). Putative histamine-gated chloride channel subunits of the insect visual system and thoracic ganglion. J Neurochem *83*, 504-514.

Wong, A.M., Wang, J.W., and Axel, R. (2002). Spatial representation of the glomerular map in the Drosophila protocerebrum. Cell *109*, 229-241.

Woodard, C., Huang, T., Sun, H., Helfand, S.L., and Carlson, J. (1989). Genetics *123*, 315.

Xiao, K., Shenoy, S.K., Nobles, K., and Lefkowitz, R.J. (2004). Activation-dependent conformational changes in {beta}-arrestin 2. J Biol Chem *279*, 55744-55753.

Xu, P., Atkinson, R., Jones, D.N., and Smith, D.P. (2005). Drosophila OBP LUSH is required for activity of pheromone-sensitive neurons. Neuron *45*, 193-200.

Yabuta, N.H., and Callaway, E.M. (1998). Functional streams and local connections of layer 4C neurons in primary visual cortex of the macaque monkey. J Neurosci *18*, 9489-9499.

Yagi, R., Mayer, F., and Basler, K. (2010). Refined LexA transactivators and their use in combination with the Drosophila Gal4 system. Proc Natl Acad Sci U S A *107*, 16166-16171.

Yamaguchi, S., Wolf, R., Desplan, C., and Heisenberg, M. (2008a). Motion vision is independent of color in Drosophila. Proc Natl Acad Sci U S A *105*, 4910-4915.

Yamaguchi, S., Wolf, R., Desplan, C., and Heisenberg, M. (2008b). Motion vision is independent of color in Drosophila. Proc Natl Acad Sci USA *105*, 4910-4915.

Yang, E.-C., Lin, H.-C., and Hung, Y.-S. (2004). Patterns of chromatic information processing in the lobula of the honeybee, Apis mellifera L. J Insect Physiol *50*, 913-925.

Yarmolinsky, D.A., Zuker, C.S., and Ryba, N.J. (2009). Common sense about taste: from mammals to insects. Cell *139*, 234-244.

Yasuyama, K., Meinertzhagen, I.A., and Schürmann, F.W. (2002). J Comp Neurol *445*, 211.

Yeh, E., Gustafson, K., and Boulianne, G.L. (1995). Green fluorescent protein as a vital marker and reporter of gene expression in Drosophila. Proc Natl Acad Sci U S A *92*, 7036-7040.

Yorozu, S., Wong, A., Fischer, B.J., Dankert, H., Kernan, M.J., Kamikouchi, A., Ito, K., and Anderson, D.J. (2009). Distinct sensory representations of wind and near-field sound in the Drosophila brain. Nature *458*, 201-205.

Yoshioka, T., Levitt, J.B., and Lund, J.S. (1994). Independence and merger of thalamocortical channels within macaque monkey primary visual cortex: anatomy of interlaminar projections. Vis Neurosci *11*, 467-489.

Yu, D., Baird, G.S., Tsien, R.Y., and Davis, R.L. (2003). Detection of calcium transients in Drosophila mushroom body neurons with camgaroo reporters. J Neurosci *23*, 64-72.

Zars, T. (2001). Two thermosensors in Drosophila have different behavioral functions. J Comp Physiol A *187*, 235-242.

Zhang, M., Chung, S.H., Fang-Yen, C., Craig, C., Kerr, R.A., Suzuki, H., Samuel, A.D., Mazur, E., and Schafer, W.R. (2008). A self-regulating feed-forward circuit controlling C. elegans egg-laying behavior. Curr Biol *18*, 1445-1455.

Zhang, Y.Q., Rodesch, C.K., and Broadie, K. (2002). Living synaptic vesicle marker: synaptotagmin-GFP. Genesis *34*, 142-145.

Zheng, Y., Hirschberg, B., Yuan, J., Wang, A.P., Hunt, D.C., Ludmerer, S.W., Schmatz, D.M., and Cully, D.F. (2002). Identification of two novel Drosophila melanogaster histamine-gated chloride channel subunits expressed in the eye. J Biol Chem *277*, 2000-2005.

Zhu, Y., Nern, A., Zipursky, S.L., and Frye, M.A. (2009). Peripheral visual circuits functionally segregate motion and phototaxis behaviors in the fly. Curr Biol *19*, 613-619.

Zuker, C.S., Cowman, A.F., and Rubin, G.M. (1985). Isolation and structure of a rhodopsin gene from D. melanogaster. Cell *40*, 851-858.

Zuker, C.S., Montell, C., Jones, K., Laverty, T., and Rubin, G.M. (1987). A rhodopsin gene expressed in photoreceptor cell R7 of the Drosophila eye: homologies with other signal-transducing molecules. J Neurosci *7*, 1550-1557.

Chapter 3

GENERAL DISCUSSION

3.1 Summary and conclusions

The numerically simple fly brain offers several advantages as a model system to study the mechanisms that translate neural circuits to meaningful behavioral responses. In addition to the ability to allow genetic manipulations of specific neuronal populations, fruit flies exhibit a rich repertoire of simple and complex behaviors. This allows designing new approaches that permit delineation of behaviorally meaningful neural circuits. We have developed a novel methodology, Tango-trace to identify functional synaptic connections in the *Drosophila* brain. This strategy can be extended to any neural circuit in the brain with a known neurotransmitter in both flies and mice. The photoreceptors in *Drosophila* depolarize to light and release histamine. The visual system of *Drosophila* is comprised of an enormous diversity of cell types. The modular arrangement of these cell types in the optic lobe and the robust visual behaviors exhibited by fruit flies makes the *Drosophila* visual system a great model system for tracing neural circuits. We used histamine Tango-trace to identify the postsynaptic targets that receive histamine from the inner photoreceptors p/y R7s and p/y R8s among this pool of diverse cell types and tested the Tango-trace trans-synaptic tracer as a proof-of-principle. p/yR7s and p/y R8s that are stochastically distributed in the retina make precise connections with four unique connectors that relay information to the lobula complex. The synaptic connections we have identified with this method have helped us understand how visual information collected by the four photoreceptor subtypes is represented in the optic lobe.

Anatomical and physiological characterization of behaviorally relevant neural circuits requires the access to genetically labeled cells in specific neuronal populations. The transcriptional readout of the Tango-trace method allows expression of ion channels, calcium indicators and other proteins to manipulate the activity of the tango labeled neurons. Enhancer trap and promoter fusion lines permit the labeling of neurons without *a priori* knowledge of their functional implications. Delineation of neural circuits using these methods poses a challenge of establishing the functional relationship of the partners of a circuit by physiological or behavioral studies. Elucidation of neural circuits and the mechanisms involved in translating the circuitry into a meaningful behavioral response with a method like Tango-trace allows labeling of neurons in an activity-dependent manner based on the release of an endogenous neurotransmitter at a synapse. Thus, this approach ensures that the labeled neurons are functionally related, synaptically connected and reduces the steps involved in further characterization of circuits. Therefore, approaches like Tango-trace brings us one step closer to the final goal of understanding how the brain works.

In insects, although the nervous system is numerically simple, it is involved in complex computations that result in diverse behaviors. For instance, in the olfactory system, the sensory cues guide innate behaviors such as attraction or aversion as well as associative learned behaviors. The underlying circuitry and the mechanisms for these very diverse behaviors is initiated by the recognition of an odorant molecule by the olfactory receptors. Neurons expressing the same receptors project precisely to one or two spatially invariant glomeruli within the antennal lobe (Gao et al., 2000; Vosshall et al., 2000; Scott et al., 2001). A topographic map of receptor activity in the periphery is therefore represented in the antennal lobe. The next step of olfactory transformation is exhibited in the representation of

PNs in the higher centers, the MB and the lateral horn. Innate olfactory-driven behaviors are likely to derive from stereotyped, determined neural circuits in the lateral horn whereas learned behaviors may be mediated by the random convergent input in the mushroom body (Marin et al., 2002b; Murthy et al., 2008; Wong et al., 2002). How is this information integrated in the higher olfactory centers to drive these behaviors? Where in the higher brain is an odor percept formed? Moreover, chemotaxis is not a purely olfactory behavior. An odor may be encountered far downwind from its source, and hence navigation may also depend on information about wind direction and the visual environment. Thus, chemotaxis involves integrating information across sensory modalities. How are these sensory modalities integrated in the higher brain centers? What are the computations involved in this integration that generate such diverse behaviors? Future advances in understanding these questions will require a systematic analysis and characterization of these circuits. The studies described in this thesis provide approaches to analyze circuits and understand their functional implications.

The delineation of the neural circuitry using these novel approaches in the fly visual system, as described in chapter 2, has provided an understanding of the mechanisms of these circuits that drive diverse visual behaviors. In the fly visual system, the visual pathways can be broadly classified as chromatic and achromatic pathways. R1-6 is thought to be involved in achromatic motion vision, whereas, R7 and R8 are believed to be involved in chromatic and spectral vision. A behavioral study showed that flies exhibited barely any optomotor response to alternating blue and green moving bars of high color contrast at a point of equiluminance (Yamaguchi et al., 2008b). In addition, they saw no optomotor responses in flies lacking functional R1-6 and suggesting that motion vision is independent of color

vision in flies. EM reconstructions using an *ort-Gal4* line implied synaptic connections of R7/R8 with Tm5 and Tm9. This study implied synaptic connections of L3, a postsynaptic partner of R1-6 with Tm5 and Tm9. Although these connections were not tested functionally or behaviorally, these authors concluded that the chromatic and achromatic pathways are not strictly segregated in flies (Gao et al., 2008a). We used a fly on the ball behavioral set-up and presented motion stimuli under bright light conditions. When we selectively rescue norpA mutants in R8 cells, we see optomotor responses that differ from the responses we see with R1-6 rescue flies and wild-type flies. These data show that R8s influence motion-evoked behavioral responses under bright light conditions. This is analogous to the rod and cone vision in vertebrates where rods respond under dim light conditions and cones respond under bright light conditions. Consistent with our results, recent behavioral and electrophysiological studies reveal that spectral information from the inner photoreceptors contributes to the motion pathway (Wardill et al., 2012). Therefore, these pathways are not strictly segregated.

Motion vision is processed in the lobula plate before it reaches the motor output. The LPTCs of the lobula plate show direction selective responses to motion stimuli. While the inputs from R1-6 to the lobula plate are still unknown, the four subtypes of TmY cells we identified as the postsynaptic partners of R7s and R8s with HA-Tango-trace are likely to provide inputs from the inner photoreceptors to the lobula plate. These cells project to all four layers of the lobula plate implying contribution of spectral information to the motion pathway. The anatomy of these cells provides a neural substrate for behavioral experiments showing responses of inner photoreceptors to motion stimuli. Gap junctions between the inner and outer photoreceptors (Shaw et al., 1989; Wardill et al., 2012) could afford an

explanation for the convergence of the two pathways. This by itself is sufficient for visual discrimination or, alternatively, the postsynaptic partners of R7 and R8 may additionally provide inputs to the motion pathway. Thus, spectral and motion pathways may converge repetitively at each stage of the circuit.

However, it still remains to be seen if the TmY cells we have identified directly contribute to motion vision. By silencing the TmY cells and examining the behavioral responses and physiological responses to motion stimuli, we can confirm the direct contribution of TmY cells to motion vision. Furthermore, p/yR7s and p/y R8s that are stochastically distributed in the retina make precise connections with four unique connectors that relay information to the lobula complex. An investigation of the induction mechanisms for these precise connections will provide insights into the developmental program of these neural circuits.

Interestingly, immunohistochemical studies in the blow fly lobula plate tangential cells and *Gal4* lines in *Drosophila* have revealed that excitatory nicotinic acetylcholine receptors (nAChRs) as well as inhibitory γ-aminobutyric acid receptors (GABARs) are expressed on LPTCs (Brotz et al., 2001; Raghu et al., 2007; Raghu et al., 2009). In *Drosophila*, the excitatory and inhibitory transmitter receptors were found to be located on the fine dendritic branches of the LPTCs (Raghu et al., 2007; Raghu et al., 2009). Thus, the variability in the fine dendritic branches is likely to result in a change in the distribution of these receptors. Furthermore, in blowflies, although LPTCs spatially integrate and represent the summated output of local motion detectors, signals of individual motion detectors can also be observed in the fine dendritic branches (Egelhaaf et al., 1989; Haag et al., 2004; Single and Borst, 1998). Moreover, recent studies in *Drosophila* show that compared to stationary flies,

LPTCs in walking and flying flies show enhanced responses to motion stimuli (Chiappe et al., 2010; Maimon et al., 2010) implying a state-dependent gain modulation of these responses. Further investigation of the responses of these fine axonal branches of TmY cells and the fine dendritic branches of the LPTCs to motion vision will provide an understanding of their contribution to motion vision. A similar wiring specificity was shown to achieve direction selectivity in the vertebrate direction-selective ganglion cells (DSGCs) (Briggman et al., 2011). Starbust amacrine cells (SACs) have been known to provide input to DSGCs in a direction selective manner and release both acetylcholine and GABA. An asymmetry in the number of inhibitory synaptic contacts from the dendrites of SACs in the null direction of the ganglion cells coupled with the orientation of an individual SAC dendrite determines the inhibition of null direction in DSGCs.

The TmY cells also send their projections to the innermost layer of the lobula with a stereotyped projection pattern that appear conserved across the retinal coordinates, TmY subtypes and individuals. This layer of the lobula could be involved in comparison of different spectral inputs. Imaging or physiology experiments in this layer of the lobula might provide more insights into mechanisms of color vision in *Drosophila*.

3.2 Histamine neuromodulation in the central brain

Studies in *Drosophila* have provided insights into behavioral states, neuronal activity, and the role of neuromodulation in circuit function. Recent studies have demonstrated the role of neuromodulation in gustatory and olfactory circuits in flies. A starved fly shows enhanced responses to cider vinegar, which is mediated by the neuromodulation of the OR42b sensory neurons by neuropeptide-F (NPF) (Root et al., 2011). Similarly, a wet-

starved fly shows enhanced sugar sensitivity, which is mediated by neuromodulation of GR5a sensory neurons by dopamine (Inagaki et al., 2012), (Appendix 1). Histaminergic neurons have been implicated in temperature preference and circadian rhythms (Hamasaka and Nässel, 2006; Hong et al., 2006). Immunohistochemistry reveals long-range projections of these histaminergic neurons in the central brain. Modulatory neurons often exhibit widespread projections throughout the brain (Mao and Davis, 2009; Monastirioti, 1999). Therefore, these behaviors are likely to result from neuromodulation of central brain circuits mediated by histamine.

Histamine in temperature preference

Insects are able to track suitable temperatures for survival and thus maintain their body temperature. The large surface area-to-volume ratio of fruit flies causes the body temperature to be easily affected by the surrounding environment (Sayeed and Benzer, 1996; Zars, 2001). To counter harmful effects of environmental temperature fluctuations, molecular and behavioral mechanisms are coordinated to select optimal temperatures for survival. Many studies on thermotaxis and temperature preference in model organisms (Mori et al., 1999; Sayeed and Benzer, 1996; Zars, 2001) have elucidated how organisms prefer certain temperatures for optimal survival. However, the molecular mechanisms mediating temperature preference are poorly understood. *Caenorhabditis elegans* is the most studied model system for temperature preference. Cell ablation studies and calcium imaging techniques demonstrated that the neuronal circuitry is involved in thermotactic behavior, and genetic screens have further identified several thermotactic genes (Kimura et al., 2004; Mori et al., 1999; Samuel et al., 2003). In vertebrates, the preoptic area (POA) was discovered as

a temperature-regulating center (Boulant, 2000). In *Drosophila*, many temperature-sensing genes including *dTRPA1*, *Painless*, *Hsp70*, and *Pyrexia* have been investigated (Goto and Kimura, 1998; Lee et al., 2005; Overgaard et al., 2005; Rosenzweig et al., 2005; Tracey et al., 2003). Recently, a study identified *histidine decarboxylase (hdc)* and two histamine receptors*, ora transientless (ort)* and *histamine-gated chloride channel subunit 1 (hisCl1)* to be involved in temperature-preference regulation. *Drosophila* strains with mutations in these genes showed abnormal temperature preferences (Hong et al., 2006). Furthermore, these genes are essential in determining critical temperature limits, leading to a state of coma when they go beyond this temperature limit (Shreve et al., 2004). Moreover, expression of these genes was detected in various regions of the brain, further supporting their critical roles. These results imply that the histaminergic system participates in regulating physiological responses to hot and cold temperatures determining a thermal threshold to low and high temperature for survival and thus modulating temperature preference in *Drosophila*.

Histamine in circadian rhythms

Animals adapt to environmental daily cycles with the help of endogenous circadian clocks. These clocks drive daily rhythms in behavior, physiology, and metabolism and can be synchronized with the environmental cycles by means of multiple cues, mediated by sensory systems. *Drosophila* has been one of the major model organisms in the analysis of components of the circadian clock (Helfrich-Forster, 2003, 2005; Stanewsky, 2003), (Hall, 2003; Taghert et al., 2001; Williams and Sehgal, 2001). The central circadian clock of *Drosophila* is composed of several sets of pacemaker neurons that generate daily rhythms,

sensory pathways mediating entrainment and output pathways responsible for the execution of the daily activities (Hall, 2003; Helfrich-Forster, 2003; Stanewsky, 2003; Taghert, 2001). Neurons in the *Drosophila* brain have been shown to express specific sets of clock genes and have been implicated to be pacemakers of the circadian clock (Helfrich-Forster, 2003, 2005; Kaneko, 1998; Kaneko and Hall, 2000; Kaneko et al., 1997). In the adult brain, the clock gene expressing neurons are three sets of lateral neurons, s-LNv, l-LNv, and LNd, and three sets of dorsal neurons, DN1–3. Four of the s-LNvs and all the l-LNvs express the neuropeptide, pigment-dispersing factor (PDF), and these neurons are critical for circadian activity rhythms (Helfrich-Forster, 1995; Park et al., 2000; Renn et al., 1999). Moreover, there is evidence that PDF is the main factor of the LNv clock neurons, necessary for maintaining the circadian locomotor activity and eclosion rhythm under constant dark conditions (Blau and Young, 1999; Park et al., 2000; Renn et al., 1999)as well as for synchronizing pacemaker activity (Lin et al., 2004). However, the cellular targets of the PDF containing clock neurons have not been explicitly identified, and neuronal pathways for synchronization of the clock with the environment and other clock-related circuits are poorly known.

A recent study used Gal4 lines driving green fluorescent protein (GFP) expression in clock neurons expressing genes for PDF (*pdf*) and timeless (*tim*). In these studies, histaminergic neurons photoreceptor axon terminals derived from the extraretinal eyelet may contact the LNv dendrites in the adult brain (Hamasaka and Nässel, 2006). These axons of the eyelet terminate among the dendritic branches of the LNvs, suggesting histaminergic inputs to these neurons from the extraretinal photoreceptors. It would be of interest to localize functional HA receptors to the adult LNvs. Light entrainment is known to be

mediated by photoreceptor inputs both from the compound eyes and the extraocular eyelet photoreceptors as well as by the photopigment cryptochome located in some of the clock neurons (Helfrich-Forster, 2002; Helfrich-Forster et al., 2001; Rieger et al., 2003). Thus histamine may mediate light entrainment signals in the adult *Drosophila*. The functional role of HA in central neuronal circuits of insects is poorly understood. Characterization of these circuits requires approaches that can detect neurons that can drive these behaviors.

In the HA Tango assay, we observed projections of histamine receptive neurons that were visualized with *UAS mCD8-GFP* (Figure S3, chapter 2, n=4; Figure 3.1, chapter 3) in several areas of the central brain like the ellipsoid body (EB), fan shaped body (FSB), suboesophageal ganglion (SOG), antennal mechanosensory and motor center (AMMC), protocerebral regions, mushroom bodies (MB) and antennal lobes (AL). These projections are in accord with the immunohistochemistry of histaminergic neurons in the brain (Figure S2, chapter 2). We further analyzed these projections in the central brain by quantitative analysis of the reporter expression. We observed variable reporter expression in various neural structures suggesting that these brain areas receive variable amounts of histamine (Figure 1). Tango assay can be used to study this other important aspect of neural circuits by measuring the intensity of signal before and after neuromodulation. This approach was successfully used to map neuromodulation of dopamine mediated sugar sensitivity in flies using dopamine tango-map (Appendix 1), (Inagaki et al., 2012). Further studies will shed light on the mechanisms involved in these circuits that result in behaviors like temperature preference and circadian rhythms in flies. Neuromodulatory neurons usually have long-range projections and the mode of action of these neurons over such long distances is by volume transmission. The lack of fast and tight reuptake mechanisms and the diffused

release of neuromodulators makes it challenging to achieve a high signal to noise ratio. However with new technologies in image analysis, a change in fluorescence can be easily measured to map the areas of neuromodulation in the brain with tango (Inagaki et al., 2012).

3.3 Histaminergic connections in the mechanosensory and auditory system

Histamine has been detected in mechanosensory neurons (Buchner et al., 1993; Melzig et al., 1996). Auditory systems are critical to the behavior of many insects. In *Drosophila melanogaster*, acoustic communication is essential for making decisions related to mate selection (Dickson, 2008; Manoli et al., 2006). During courtship, male flies flap one wing to produce a complex pattern of airborne vibrations comprising sine song and pulse song (Ejima and Griffith, 2008; Villella and Hall, 2008). The pulse song enables the female to determine whether her suitor is of the same species (Eberl et al., 1997). Courting males also monitor their own sounds to fine tune the courtship song (Tauber and Eberl, 2001). The fly's antennae are designed to detect odor molecules as well as respond to mechanical stimulation using the feathery arista that protrudes from the third segment. Near-field sound vibrates the arista, which twists segment a3 relative to a2, thus activating the collection of stretch receptors connected to the joint between these two segments (Gopfert and Robert, 2001). Although the fly ear acts mechanical stimulation and the human ear responds to sound pressure, studies of the antenna and associated arista using laser vibrometry have revealed striking similarities between the biomechanics of the fly antenna and human hair cells (Ruggero, 1992). This similarity at the level of the auditory receptors presents *Drosophila* audition as an excellent model system to study the neural circuitry and the mechanisms of hearing. The courtship song is detected by auditory sensory neurons linking the Johnston

organ (JO) at the second antennal segment to the antennal mechanosensory and motor center (AMMC) zones AB in the brain (Krashes et al., 2009; Shorey, 1962; Waldron, 1964).

The Johnston's Organ (JO) comprises of ~480 mechanosensory neurons housed in segment a2 of the antenna (Kamikouchi et al., 2006; Todi et al., 2004). The JO neurons project along the antennal nerve to largely innervate the antennal mechanosensory and motor center (AMMC) of the brain. This neuropil receives mechanosensory input from the JO as well as from other mechanosensory cells of the antenna and head. The detailed projections of most of the JO neurons have been elucidated using a combination of JO-expressing GAL4 lines and single-cell labeling (Kamikouchi et al., 2006). JO neurons, dependent on where their somata are located in the antenna, project to one of roughly five zones in the AMMC. It remains to be determined if this map corresponds to tonotopy based on the frequency tuning of individual JO neurons. However, computational models predict that JO neurons do roughly map static and vibratory mechanical stimuli in the AMMC. Two recent studies examined the calcium responses of subsets of JO neurons to sound and other mechanical stimuli, such as gravity (Kamikouchi et al., 2009) or wind (Yorozu et al., 2009). When the antenna was deflected statically, JO neurons that innervate zones C and E of the AMMC showed measurable calcium responses that lasted as long as antennal deflection was maintained. In contrast, JO neurons innervating zones A and B, responded phasically to stimuli such as fly song and sinusoids, and showed, as a population, frequency and intensity dependent tuning. Genetic manipulations by selectively silencing JO subsets demonstrated that JO neurons in zone B are required for sound detection during courtship whereas zone C/E neurons are required for gravity or wind detection. This study identified the expression of a TRPN (transient receptor potential) N ion channel, NompC, specifically in the sound-

sensitive A/B JO neurons (Sun et al., 2009). Other ion channels expressed in JO neurons include the TRPV channels, nanchung and inactive as well as the TRPA channel, painless (Sun et al., 2009). Mutations in these channels disrupt sound responses (Gong et al., 2004) although how these channels are gated by the mechanical inputs to the antenna remains unknown.

Four different projection neurons (PNs) innervating the AMMC zones AB have been characterized based on Gal4 expression patterns (Kamikouchi et al., 2009). The giant fiber neuron involved in the visually guided escape jump response links AMMC zone A to the inferior ventrolateral protocerebrum (IVLP) and thoracic ganglia. AMMC-A1 neuron connects AMMC zone A and the IVLP, AMMC-B1 neuron links AMMC zone B to the IVLP, and AMMC-B2 neurons are commissural neurons connecting AMMC zone B in both hemispheres. These innervations of the IVLP suggest that the IVLP functions as a second-level auditory processing center (Kamikouchi et al., 2009). More recently, stochastic labeling of 16,000 single neurons in the entire fly brain revealed that many AMMC PNs terminate at a second brain region, the caudoventrolateral protocerebrum (CVLP) (Chiang et al., 2011), suggesting that the IVLP/CVLP region may be involved in higher order auditory processing (Lai et al., 2012).

The projections of histamine receptive neurons that we visualized with HA-Tango assay in AMMC, protocerebral regions and SOG (Figures 3.2, 3.3 and 3.4) are likely to contribute to the mechanosensory circuits in *Drosophila*. In the SOG and AMMC, the projections of these neurons overlap with projections of neurons labeled by *SN-Gal4* (Song et al., 2007) and *NompC-Gal4* (Cheng et al., 2010) lines that label mechanosensory neurons in the *Drosophila* brain (Figure 3.2) and VNC (Figure 3.3). In addition, the projections of the HA-

Tango labeled neurons overlap with the proposed higher order neurons in the protocerebral areas (Figure 3.4A). Is the auditory information represented as a tonotopic map in the higher auditory centers of the *Drosophila* brain? What is the nature of this map? Is this map further transformed into a representation that translates into a behavioral output? Further characterization of these circuits with HA-Tango-trace will provide insights into the representation of mechanosensory and auditory information that drive diverse behaviors in *Drosophila*.

3.4 Tracing connections with ACh-Tango

Acetylcholine is a major neurotransmitter of the olfactory and gustatory systems in *Drosophila*. The olfactory sensory neurons, PNs and the gustatory sensory neurons release acetylcholine (ACh) as a neurotransmitter (Jefferis et al., 2007; Vosshall and Stocker, 2007). The higher order olfactory neurons in the lateral horn and mushroom body and the second order neurons in the gustatory circuits in flies are still not identified. ACh-Tango was designed to trace functional connections in the olfactory and gustatory systems. The *Drosophila* muscarinic AChR was fused to Gal4 through a linker with TEV protease cleavage site and was expressed under the control of heat shock promoter. Human arrestin was fused to TEV protease and expressed under the control of tubulin promoter. *UAS CD8-GFP* was used as a reporter for tango readout. We co-expressed *hs-dmAChR-TCS-Gal4*, *tubp-Arr-TEV* and *UAS mCD8-GFP* in *Drosophila* S2 cells. Treatment of these cells with acetylcholine resulted in a dose-dependent increase in reporter expression (Figure 3.5). We next introduced the histamine tango system into flies and generated animals expressing *hs-dmAChR-TCS-Gal4* and *tubp-Arr-TEV*, as well as *UAS mCD8-GFP*. We refer to these flies as “ACh-Tango” flies. After inducing the expression of AChR in adults by heatshock for

1hour, ACh-Tango flies were exposed to odors to label ACh-receptive neurons in the olfactory system (Figure 3.6).

Fly ORNs release acetylcholine as a major neurotransmitter. In ACh-Tango flies that are exposed to odors that activate specific ORNs, ACh-Tango should label cells that receive ACh from these sensory neurons. As expected, stimulation with a general odor like isoamylacetate (IAA) labeled 80% of the PN cell bodies (Figure 3.6B), whereas, a private odor like geranyl acetate (GA) (Figure 3.6C) labeled 2-3 specific PNs. These results demonstrate that ACh-Tango labels specific neurons in an activity-dependent manner. In control flies that were not stimulated with any odors, ACh-Tango labeling was not observed (Figure 3.6A). The odors were spotted on a filter paper dipped in sucrose solution to attract the flies to the odor source. Thus, this experimental method also labeled sugar responsive neurons in the SOG. The low signal of ACh-Tango was inefficient in labeling the axons of the projection neurons. However, future improvements in the assay should enable better signal to noise ratio and provide insights into how olfactory information is integrated in the higher olfactory centers to drive various behaviors. Characterization of circuits in higher brain areas may help us understand how odor and taste percepts are formed and how these sensory modalities are processed in the higher brain centers to generate diverse olfactory and gustatory behaviors.

3.5 Future of Tango-trace

Tango-trace can be used as a general tracer to trace functional synaptic connections in neural circuits with any known neurotransmitter in an unbiased manner. Tango-trace is a protein-protein interaction (PPI) assay that detects the interaction between GPCRs and arrestin. The modular design of the Tango system allows further optimization of the assay to

achieve a high signal-to-noise ratio (SNR). The two components of the assay, the GPCR-Gal4 fusion and the Arrestin-TEV fusion can be individually further optimized.

GPCR-Gal4

The GPCR-Gal4 fusion can be manipulated by adding serine-glycine linkers, and minimize the steric hindrance. Optimizing the linker length between the components can render the cleavage site more accessible to its protease resulting in an efficient cleavage of Gal4 and an increased SNR. Upon receptor stimulation and subsequent β-arrestin recruitment to the cytoplasmic membrane, two patterns emerge. For some receptors, there is transient, low-affinity binding characterized by a rapid concentration of β-arrestin at the activated receptor. β-Arrestin is subsequently released after targeting the receptor to clathrin-coated pits. This pattern, termed Class A, is typified by the β2 adrenergic receptors. Class A receptors typically undergo rapid recycling to the plasma membrane after their internalization. In contrast, Class B receptors, such as the AT1AR, show a much stronger and more prolonged binding to β-arrestin, such that following recruitment to clathrin-coated pits, the receptor and β-arrestin remain bound together on the surface of endocytic vesicles (Oakley et al., 2000). Due to their prolonged interaction with β-arrestins, Class B receptors recycle to the cell surface much more slowly than Class A receptors. Replacing the C-terminal tail of class A GPCRs with the tail from class B receptors will prolong the GPCR-arrestin interaction and result in efficient cleavage of Gal4 from the GPCR.

Arrestin-TEV

β-arrestins undergo their own activation-dependent conformational changes to facilitate downstream signaling. The X-ray structures of bovine visual arrestin and β-arrestin1 in the basal inactive state indicate that arrestin is an elongated molecule with two domains (N- and C-domain), connected through a 12-residue linker region (Granzin et al., 1998; Han et al., 2001; Hirsch et al., 1999; Milano et al., 2002). A notable feature is a hydrogen-bonded network of buried, charged side chains embedded between the N- and C-domains at the fulcrum of the β-arrestin molecule (Vishnivetskiy et al., 1999). It was recently demonstrated that addition of the carboxyl tail of V2R to β-arrestin2 in vitro led to the exposure of a buried tryptic cleavage site (arginine 394) as well as the release of residues 371 to 379 in the C terminus of β-arrestin, which contain the sites for clathrin interaction (Xiao et al., 2004). Thus, changes occurring in β-arrestin conformation results in a rearrangement of the two ends of β-arrestin.

A lysine doublet in the N terminus (residues 11, 12) of β-arrestin2 functions as a crucial site for stable ubiquitination and is required for endosomal trafficking as well as for scaffolding in these compartments (Shenoy and Lefkowitz, 2005). These ubiquitination patterns may correspond to particular β-arrestin conformations induced upon receptor binding that expose specific lysine residues for ubiquitination, thus allowing for receptor-specific signaling pathways mediated by β-arrestin. Unlike in phosphorylation, the attachment of ubiquitin adds tertiary structure to the substrate protein, allowing larger conformational changes. Polyubiquitin chains (Varadan et al., 2004), such as those formed on β-arrestin, may specify further conformational complexities and present a foundation for the binding of the many downstream endocytic and signaling partners of β-arrestin. Thus, the each of these interactions of N- and C- domains of β-arrestin appears to be

nonoverlapping, enabling β-arrestin to scaffold receptor, downstream kinases, and components of the endocytic machinery within a membrane microdomain. Addition of linkers between β-arrestin and TEV can stabilize the GPCR-arrestin interaction and enhance the SNR in Tango assay.

Replacing TEV protease in Arrestin-TEV

TEV protease is a 27 kDa protein and could be replaced with a much smaller protease in the arrestin-TEV fusion such that the arrestin-GPCR interaction is not sterically hindered. TEV protease is maximally active at 34 °C and lower temperatures require longer incubation times. A neurotransmitter induced interaction of a GPCR and arrestin at a synapse occurs at short time scales and is likely to require a more efficient protease than TEV protease. Protein-fragment complementation assays (PCAs) are based on the fusion of the two interacting proteins to two rationally designed fragments of a reporter protein (Michnick et al., 2000). The interaction between bait and prey proteins brings the split reporter fragments close enough to enable their non-covalent and specific reassembly followed by the recovery of its native structure and activity. Ubiquitin is an 8.5 kDa small protein present in all cells. In the split ubiquitin technique (Johnsson and Varshavsky, 1994), ubiquitin is split into two inactive fragments (Nub and Cub), which are fused to the bait and the prey proteins, respectively. Upon interaction between bait and prey proteins, the function of ubiquitin is restored by complementation of its fragments, leading to the cleavage of a reporter protein by ubiquitin-dependent proteases at very fast time-scales. Refined split ubiquitin techniques were particularly successfully applied to identifying interactions between membrane proteins using different reporter proteins (Stagljar et al., 1998; Thaminy

et al., 2004) and have recently been employed in systematically screening membrane protein interactomes (Obrdlik et al., 2004). Replacing TEV with the split ubiquitin technique could be another way of improving the signal in Tango assay.

Furthermore, genetic manipulations allowing overexpression of transporters that are involved in reuptake of neurotransmitters from synapses like monoamine transporters can reduce the background of Tango assay. Optimal engineering of the components of Tango can reduce the background and increase the signal of the assay. The studies described in this thesis provide approaches to analyze neural circuits and understand their functional implications in both flies and mice. Our understanding of the nervous system can benefit greatly from improved versions of these tools. In future, a Tango-trace tool kit to trace functional synaptic connections and Tango-map tool kit to map neuromodulation can be a great addition to the *Drosophila* genetic tool kits for neurobiology.

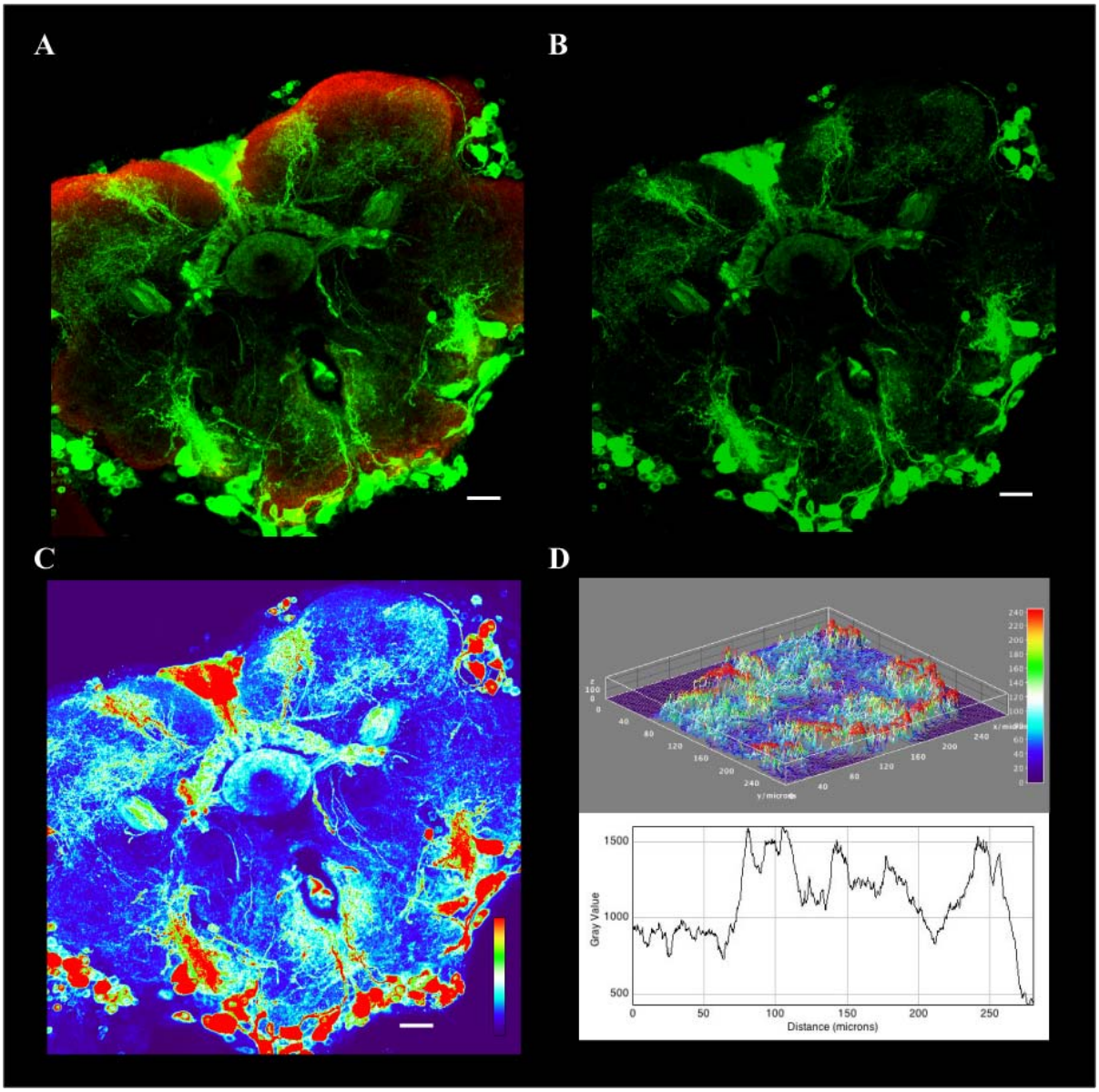
A
B
C
D
Gray Value
1500
1000
500
0
50
100
150
200
250
Distance (microns)

Figure 3.1. Histamine-Tango labeling in the central brain

Histamine tango labeling with mCD8-GFP as a reporter to visualize the projections of tango labeled neurons in the central brain. The brains were immunostained for GFP (green) and nc82 (red). (A) A counterstained brain with nc82 showing labeling in the central complex and other protocerebral areas. (B) Projections of these neurons in the green channel. (C) A heat map of GFP intensity in the central brain shows variable Tango reporter expression suggesting variable amounts of histamine released in these areas. (D) Surface plot and a 2D plot profile of quantitative analysis of GFP intensity in the different brain areas. A quantitative analysis of reporter expression before and after temperature changes or circadian clocks will provide insights into behavioral effects due to histamine neuromodulation in the *Drosophila* brain. Scale bar is 20μ.

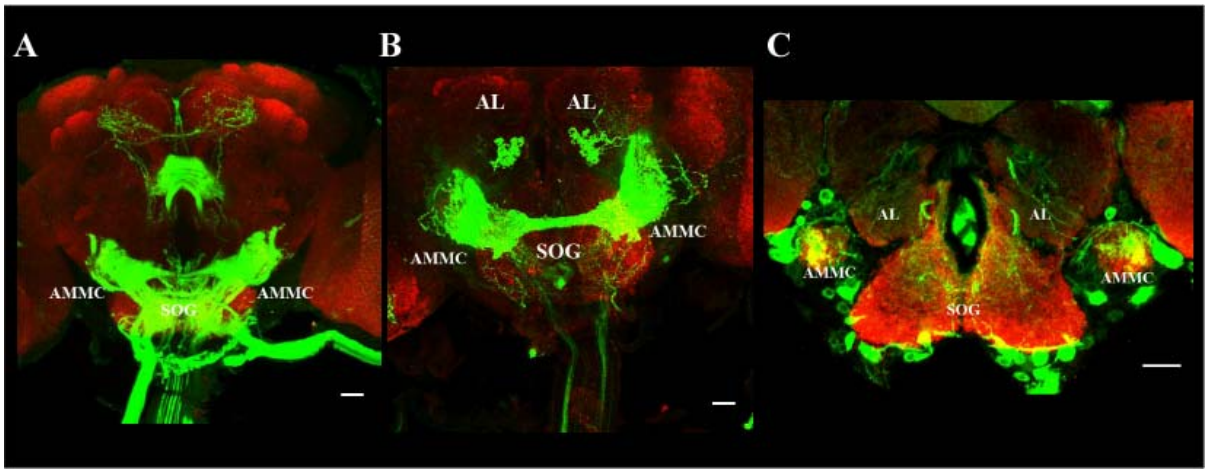
A
AMMC
SOG
AMMC
B
AL
AL
AMMC
SOG
AMMC
C
AL
AL
AMMC
SOG
AMMC

Figure 3.2. Projections of mechanosensory neurons in the central brain.

(A) *SN-Gal4* expressing CD8-GFP in all the sensory neurons exhibits projections of mechanosensory neurons in the AMMC and SOG. (B) *NompC-Gal4* expressing CD8-GFP in mechanosensory neurons in AMMC, SOG and AL. (C) HA-Tango labeled brain expresses mCD8-GFP in AMMC and SOG suggesting histamine receptive projecting into these areas. The brains were immunostained for GFP (green) and nc82 (red). Scale bar is 20μ.

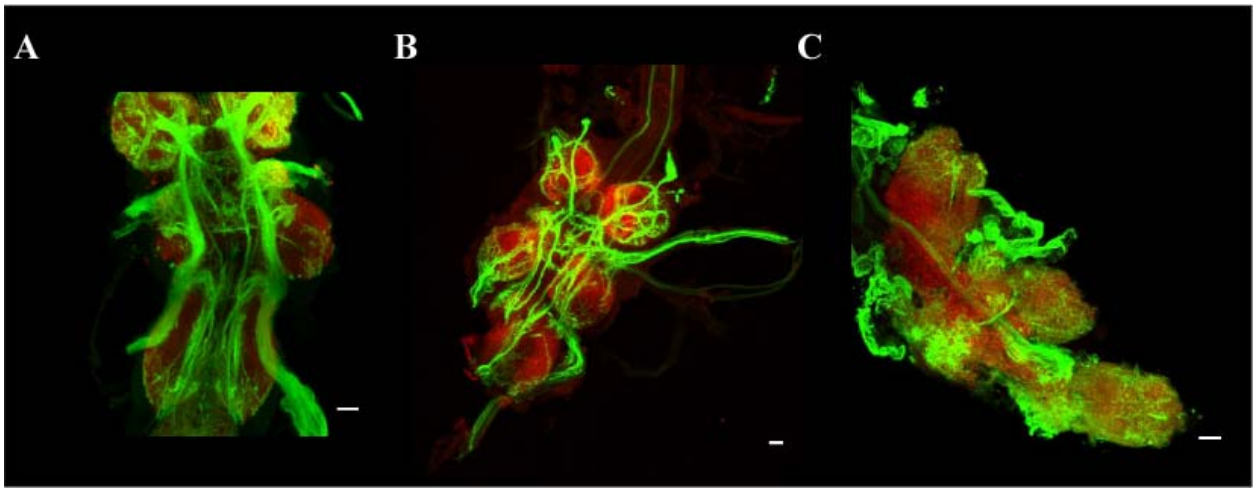
A
B
C

Figure 3.3 Projections of mechanosensory neurons in the VNC.

(A) *SN-Gal4* expressing CD8-GFP in all the sensory neurons exhibits projections of mechanosensory neurons in the VNC. (B) *NompC-Gal4* expressing CD8-GFP in mechanosensory neurons in the VNC that project to the AMMC, AL and SOG. (C) HA-Tango labeled brain expresses mCD8-GFP in the VNC and project to AMMC and SOG suggesting histamine receptive projecting into these areas. The brains were immunostained for GFP (green) and nc82 (red). Scale bar is 20μ.

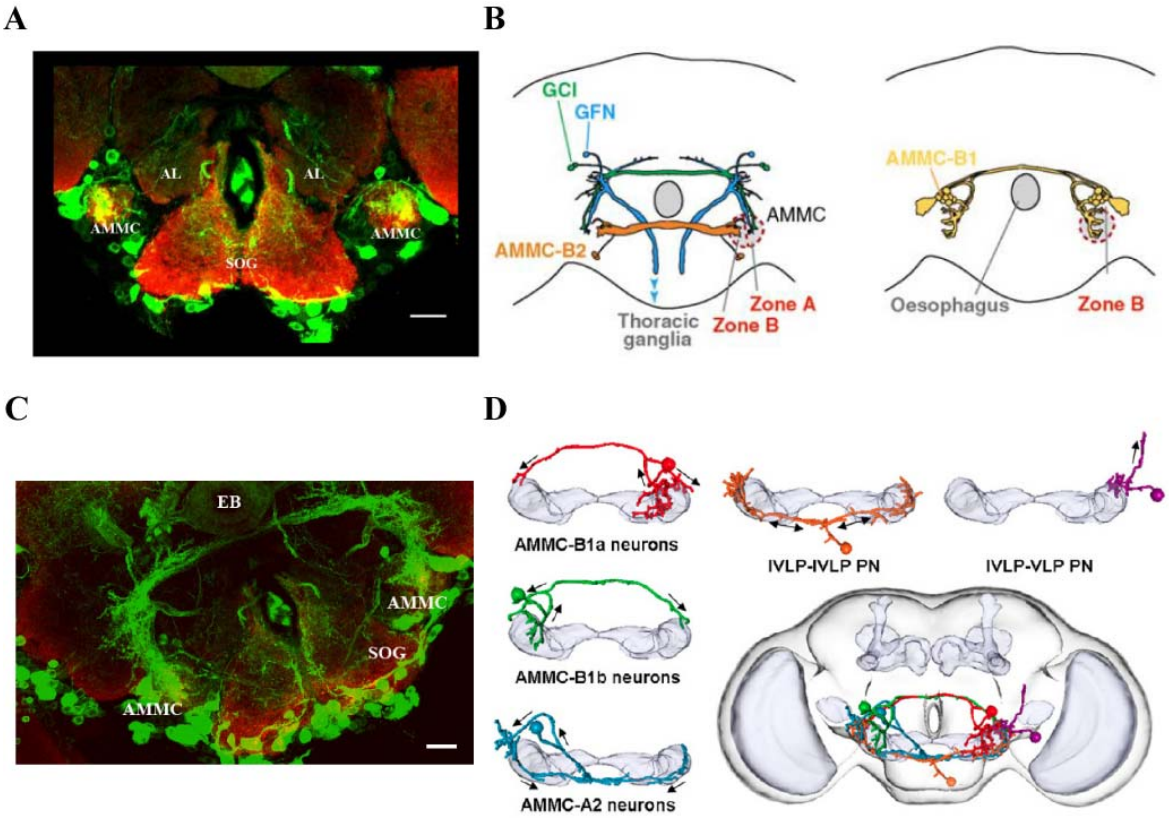
A
AL
AL
AMMC
AMMC
SOG
B
GCI
GFN
AMMC
AMMC-B2
Zone A
Zone B
Thoracic ganglia
AMMC-B1
Oesophagus
Zone B
C
EB
AMMC
SOG
AMMC
D
AMMC-B1a neurons
IVLP-IVLP PN
IVLP-VLP PN
AMMC-B1b neurons
AMMC-A2 neurons

Figure 3.4. The auditory circuit in *Drosophila*

(A) HA-Tango labeled neurons innervating the AMMC and SOG. These neurons project from the VNC and antennal nerve and labial nerves.

(B) A circuit of identified central neurons that innervate zones A and B of the AMMC: the giant commissural interneuron (GCI), the giant fiber neuron (GFN), and AMMC-B2 (left), and AMMC-B1 (right). Adapted from (Murthy, 2010)

(C) HA-Tango labeled neurons that project from the AMMC to higher protocerebral brain areas.

(D) The neurons project from AMMC zones AB into the IVLP via AMMC-B1 and AMMC-A2 neurons. AMMC-B1a, AMMC-B1b, and AMMC-A2 neurons respond to 100 Hz, 100–300 Hz, and 100–700 Hz, respectively. Ventrolateral protocerebrum (VLP) is composed of glomerular structures that receive visual inputs from the lobula. A pheromone-sensing circuit that expresses Gr32a also targets the VLP. Furthermore, some JO neurons bypass AMMC to directly terminate at the ventrolateral brain, a neuropil region equivalent to CVLP plusVLP. Thus, VLP may act as a center to integrate visual, gustatory, and auditory information. This auditory map suggests that narrowly and broadly tuned auditory reception by specific JO neurons are further represented in AMMC-B1a, AMMC-B1b, and AMMC-A2 neurons. Subsequent IVLP-VLP PNs then serve as generalists relaying all frequencies of auditory information to the VLP. Adapted from (Lai et al., 2012). The brains were immunostained for GFP (green) and nc82 (red). Scale bar is 20μ.

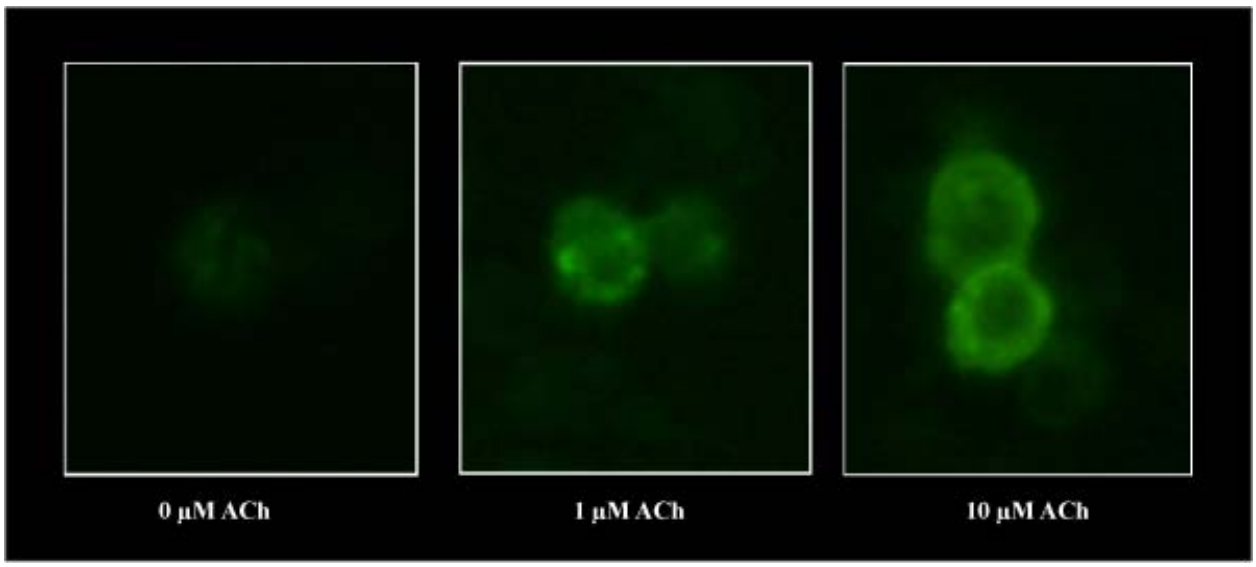
0 µM ACh
1 µM ACh
10 µM ACh

Figure 3.5. Dose-dependent ACh-Tango labeling in S2 cells

S2 cells were transfected with *hs-dmAChR-TCS-Gal4*, *tubp-Arr-TEV* and *UAS mCD8-GFP* in *Drosophila* S2 cells. Treatment of these cells with acetylcholine resulted in a dose-dependent increase in reporter expression.

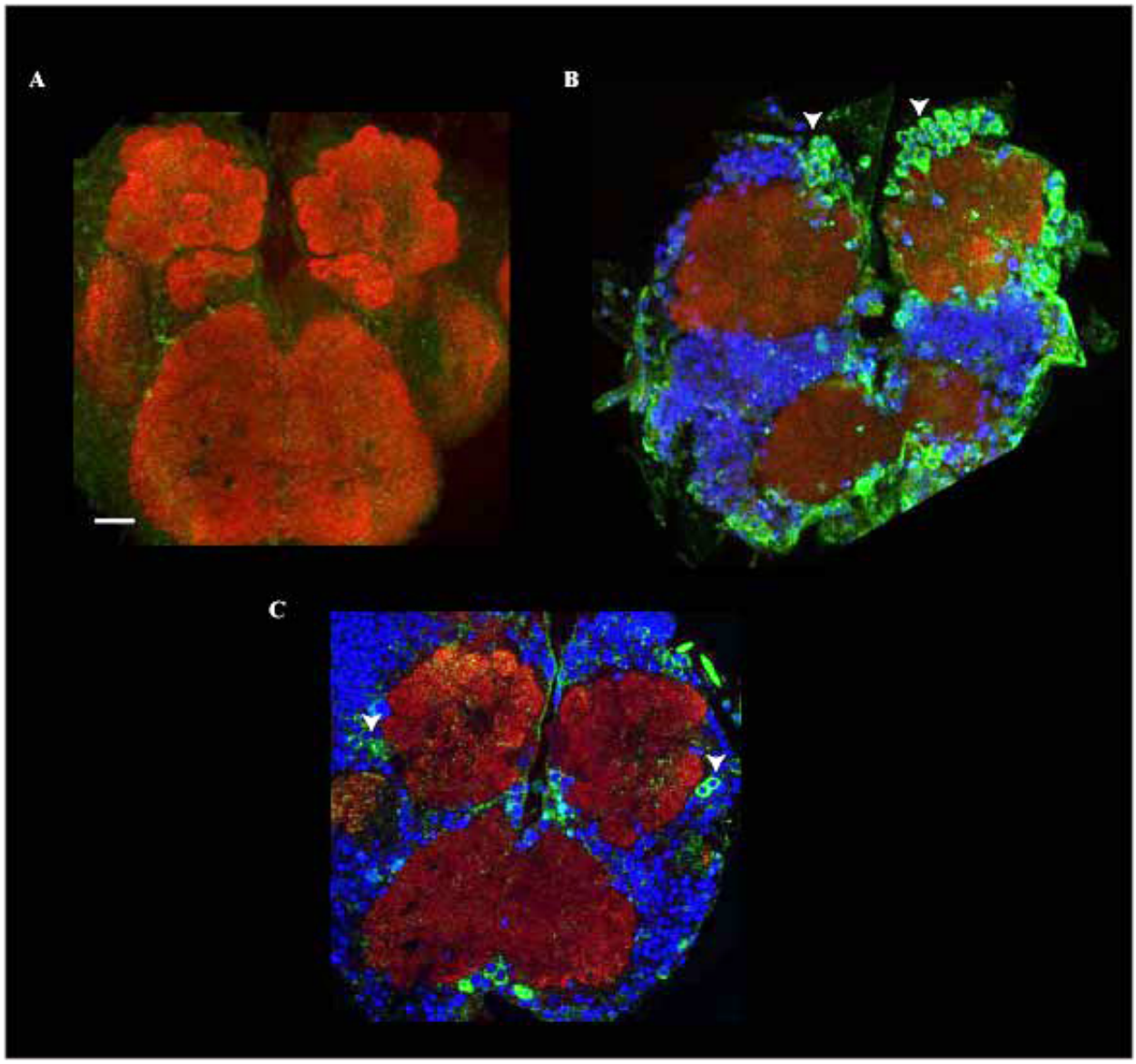
A
B
C

Figure 3.6. Activity-dependent ACh-Tango labeling in the *Drosophila* brain

Odor and sugar dependent ACh-Tango labeling in the antennal lobe and SOG visualized with mCD8-GFP. Ach-Tango (genotype: *w; UAS CD8-GFP/ hs DmAChR-TCS-Gal4; tubP Arr-TEV/Tm6B*) adult flies were heat shocked for 1.5 hrs in 15 min intervals to induce receptor expression. The brains were immunostained for GFP (green) and nc82 (red). (A) Control brains with all components of ACh-Tango shows no labeling (n=5). (B) Flies were exposed to a filter paper soaked in sucrose with a drop of 100% Isoamylacetate (IAA) was blotted on it. IAA is a general odor and stimulates 80% of the PNs. There is labeling of cell bodies of dorsal, ventral and lateral PNs (arrowheads) (n=4). (C) Flies were exposed to a filter paper soaked in sucrose with a drop of 100% Geranyl acetate (GA) was blotted on it. GA is a private odor and stimulates VA6. There is labeling of cell bodies of 2-3 lateral PNs (arrowheads) (n=2). Note the labeling of cell bodies in the SOG indicating sugar sensing ACh-receptive neurons. Scale bar is 20μ

3.6 References

Blau, J., and Young, M.W. (1999). Cycling vrille expression is required for a functional Drosophila clock. Cell *99*, 661-671.

Boulant, J.A. (2000). Role of the preoptic-anterior hypothalamus in thermoregulation and fever. Clinical infectious diseases : an official publication of the Infectious Diseases Society of America *31 Suppl 5*, S157-161.

Briggman, K.L., Helmstaedter, M., and Denk, W. (2011). Wiring specificity in the direction-selectivity circuit of the retina. Nature *471*, 183-188.

Brotz, T.M., Gundelfinger, E.D., and Borst, A. (2001). Cholinergic and GABAergic pathways in fly motion vision. BMC Neurosci *2*, 1.

Buchner, E., Buchner, S., Burg, M.G., Hofbauer, A., Pak, W.L., and Pollack, I. (1993). Histamine is a major mechanosensory neurotransmitter candidate in Drosophila melanogaster. Cell Tissue Res *273*, 119-125.

Cheng, L.E., Song, W., Looger, L.L., Jan, L.Y., and Jan, Y.N. (2010). The role of the TRP channel NompC in Drosophila larval and adult locomotion. Neuron *67*, 373-380.

Chiang, A.S., Lin, C.Y., Chuang, C.C., Chang, H.M., Hsieh, C.H., Yeh, C.W., Shih, C.T., Wu, J.J., Wang, G.T., Chen, Y.C.*, et al.* (2011). Three-dimensional reconstruction of brain-wide wiring networks in Drosophila at single-cell resolution. Curr Biol *21*, 1-11.

Chiappe, M.E., Seelig, J.D., Reiser, M.B., and Jayaraman, V. (2010). Walking Modulates Speed Sensitivity in Drosophila Motion Vision. Curr Biol *20*, 1470-1475.

Dickson, B.J. (2008). Wired for sex: the neurobiology of Drosophila mating decisions. Science *322*, 904-909.

Eberl, D.F., Duyk, G.M., and Perrimon, N. (1997). A genetic screen for mutations that disrupt an auditory response in Drosophila melanogaster. Proc Natl Acad Sci U S A *94*, 14837-14842.

Egelhaaf, M., Borst, A., and Reichardt, W. (1989). Computational structure of a biological motion-detection system as revealed by local detector analysis in the fly's nervous system. J Opt Soc Am A *6*, 1070-1087.

Ejima, A., and Griffith, L.C. (2008). Courtship initiation is stimulated by acoustic signals in Drosophila melanogaster. PLoS ONE *3*, e3246.

Gao, S., Takemura, S.-Y., Ting, C.-Y., Huang, S., Lu, Z., Luan, H., Rister, J., Thum, A.S., Yang, M., Hong, S.-T.*, et al.* (2008). The neural substrate of spectral preference in Drosophila. Neuron *60*, 328-342.

Gong, Z., Son, W., Chung, Y.D., Kim, J., Shin, D.W., McClung, C.A., Lee, Y., Lee, H.W., Chang, D.J., Kaang, B.K.*, et al.* (2004). Two interdependent TRPV channel subunits, inactive and Nanchung, mediate hearing in Drosophila. J Neurosci *24*, 9059-9066.

Gopfert, M.C., and Robert, D. (2001). Biomechanics. Turning the key on Drosophila audition. Nature *411*, 908.

Goto, S.G., and Kimura, M.T. (1998). Heat- and cold-shock responses and temperature adaptations in subtropical and temperate species of Drosophila. J Insect Physiol *44*, 1233-1239.

Granzin, J., Wilden, U., Choe, H.W., Labahn, J., Krafft, B., and Buldt, G. (1998). X-ray crystal structure of arrestin from bovine rod outer segments. Nature *391*, 918-921.

Haag, J., Denk, W., and Borst, A. (2004). Fly motion vision is based on Reichardt detectors regardless of the signal-to-noise ratio. Proc Natl Acad Sci USA *101*, 16333-16338.

Hall, J.C. (2003). Genetics and molecular biology of rhythms in Drosophila and other insects. Advances in genetics *48*, 1-280.

Hamasaka, Y., and Nässel, D.R. (2006). Mapping of serotonin, dopamine, and histamine in relation to different clock neurons in the brain of Drosophila. J Comp Neurol *494*, 314-330.

Han, M., Gurevich, V.V., Vishnivetskiy, S.A., Sigler, P.B., and Schubert, C. (2001). Crystal structure of beta-arrestin at 1.9 A: possible mechanism of receptor binding and membrane Translocation. Structure *9*, 869-880.

Helfrich-Forster, C. (1995). The period clock gene is expressed in central nervous system neurons which also produce a neuropeptide that reveals the projections of circadian pacemaker cells within the brain of Drosophila melanogaster. Proc Natl Acad Sci U S A *92*, 612-616.

Helfrich-Forster, C. (2002). The circadian system of Drosophila melanogaster and its light input pathways. Zoology (Jena) *105*, 297-312.

Helfrich-Forster, C. (2003). The neuroarchitecture of the circadian clock in the brain of Drosophila melanogaster. Microsc Res Tech *62*, 94-102.

Helfrich-Forster, C. (2005). Neurobiology of the fruit fly's circadian clock. Genes, brain, and behavior *4*, 65-76.

Helfrich-Forster, C., Winter, C., Hofbauer, A., Hall, J.C., and Stanewsky, R. (2001). The circadian clock of fruit flies is blind after elimination of all known photoreceptors. Neuron *30*, 249-261.

Hirsch, J.A., Schubert, C., Gurevich, V.V., and Sigler, P.B. (1999). The 2.8 A crystal structure of visual arrestin: a model for arrestin's regulation. Cell *97*, 257-269.

Hong, S.-T., Bang, S., Paik, D., Kang, J., Hwang, S., Jeon, K., Chun, B., Hyun, S., Lee, Y., and Kim, J. (2006). Histamine and its receptors modulate temperature-preference behaviors in Drosophila. J Neurosci *26*, 7245-7256.

Inagaki, Hidehiko K., Ben-Tabou De-Leon, S., Wong, A.M., Jagadish, S., Ishimoto, H., Barnea, G., Kitamoto, T., Axel, R., and Anderson, David J. (2012). Visualizing Neuromodulation In Vivo: TANGO-Mapping of Dopamine Signaling Reveals Appetite Control of Sugar Sensing. Cell *148*, 583-595.

Jefferis, G.S.X.E., Potter, C.J., Chan, A.M., Marin, E.C., Rohlfing, T., Maurer, C.R., and Luo, L. (2007). Comprehensive maps of Drosophila higher olfactory centers: spatially segregated fruit and pheromone representation. Cell *128*, 1187-1203.

Johnsson, N., and Varshavsky, A. (1994). Split ubiquitin as a sensor of protein interactions in vivo. Proc Natl Acad Sci U S A *91*, 10340-10344.

Kamikouchi, A., Inagaki, H.K., Effertz, T., Hendrich, O., Fiala, A., Gopfert, M.C., and Ito, K. (2009). The neural basis of Drosophila gravity-sensing and hearing. Nature *458*, 165-171.

Kamikouchi, A., Shimada, T., and Ito, K. (2006). Comprehensive classification of the auditory sensory projections in the brain of the fruit fly Drosophila melanogaster. J Comp Neurol *499*, 317-356.

Kaneko, M. (1998). Neural substrates of Drosophila rhythms revealed by mutants and molecular manipulations. Curr Opin Neurobiol *8*, 652-658.

Kaneko, M., and Hall, J.C. (2000). Neuroanatomy of cells expressing clock genes in Drosophila: transgenic manipulation of the period and timeless genes to mark the perikarya of circadian pacemaker neurons and their projections. J Comp Neurol *422*, 66-94.

Kaneko, M., Helfrich-Forster, C., and Hall, J.C. (1997). Spatial and temporal expression of the period and timeless genes in the developing nervous system of Drosophila: newly identified pacemaker candidates and novel features of clock gene product cycling. J Neurosci *17*, 6745-6760.

Kimura, K.D., Miyawaki, A., Matsumoto, K., and Mori, I. (2004). The C. elegans thermosensory neuron AFD responds to warming. Curr Biol *14*, 1291-1295.

Krashes, M.J., DasGupta, S., Vreede, A., White, B., Armstrong, J.D., and Waddell, S. (2009). A neural circuit mechanism integrating motivational state with memory expression in Drosophila. Cell *139*, 416-427.

Lai, J.S., Lo, S.J., Dickson, B.J., and Chiang, A.S. (2012). Auditory circuit in the Drosophila brain. Proc Natl Acad Sci U S A *109*, 2607-2612.

Lee, Y., Lee, Y., Lee, J., Bang, S., Hyun, S., Kang, J., Hong, S.T., Bae, E., Kaang, B.K., and Kim, J. (2005). Pyrexia is a new thermal transient receptor potential channel endowing tolerance to high temperatures in Drosophila melanogaster. Nature genetics *37*, 305-310.

Lin, Y., Stormo, G.D., and Taghert, P.H. (2004). The neuropeptide pigment-dispersing factor coordinates pacemaker interactions in the Drosophila circadian system. J Neurosci *24*, 7951-7957.

Maimon, G., Straw, A.D., and Dickinson, M.H. (2010). Active flight increases the gain of visual motion processing in Drosophila. Nature neuroscience *13*, 393-399.

Manoli, D.S., Meissner, G.W., and Baker, B.S. (2006). Blueprints for behavior: genetic specification of neural circuitry for innate behaviors. Trends Neurosci *29*, 444-451.

Mao, Z., and Davis, R.L. (2009). Eight different types of dopaminergic neurons innervate the Drosophila mushroom body neuropil: anatomical and physiological heterogeneity. Front Neural Circuits *3*, 5.

Marin, E.C., Jefferis, G.S., Komiyama, T., Zhu, H., and Luo, L. (2002). Representation of the glomerular olfactory map in the Drosophila brain. Cell *109*, 243-255.

Melzig, J., Buchner, S., Wiebel, F., Wolf, R., Burg, M., Pak, W.L., and Buchner, E. (1996). Genetic depletion of histamine from the nervous system of Drosophila eliminates specific visual and mechanosensory behavior. J Comp Physiol A *179*, 763-773.

Michnick, S.W., Remy, I., Campbell-Valois, F.X., Vallee-Belisle, A., and Pelletier, J.N. (2000). Detection of protein-protein interactions by protein fragment complementation strategies. Methods in enzymology *328*, 208-230.

Milano, S.K., Pace, H.C., Kim, Y.M., Brenner, C., and Benovic, J.L. (2002). Scaffolding functions of arrestin-2 revealed by crystal structure and mutagenesis. Biochemistry *41*, 3321-3328.

Monastirioti, M. (1999). Biogenic amine systems in the fruit fly Drosophila melanogaster. Microsc Res Tech *45*, 106-121.

Mori, T., Oda, F., Umeno, D., Murata, M., and Maeda, M. (1999). Affinity separation of messenger RNA by thermo-responsive polymer carrying oligo(dT). Nucleic acids symposium series, 55-56.

Murthy, M. (2010). Unraveling the auditory system of Drosophila. Curr Opin Neurobiol *20*, 281-287.

Murthy, M., Fiete, I., and Laurent, G. (2008). Testing odor response stereotypy in the Drosophila mushroom body. Neuron *59*, 1009-1023.

Oakley, R.H., Laporte, S.A., Holt, J.A., Caron, M.G., and Barak, L.S. (2000). Differential affinities of visual arrestin, beta arrestin1, and beta arrestin2 for G protein-coupled receptors delineate two major classes of receptors. J Biol Chem *275*, 17201-17210.

Obrdlik, P., El-Bakkoury, M., Hamacher, T., Cappellaro, C., Vilarino, C., Fleischer, C., Ellerbrok, H., Kamuzinzi, R., Ledent, V., Blaudez, D.*, et al.* (2004). K+ channel interactions

detected by a genetic system optimized for systematic studies of membrane protein interactions. Proc Natl Acad Sci U S A *101*, 12242-12247.

Overgaard, J., Sorensen, J.G., Petersen, S.O., Loeschcke, V., and Holmstrup, M. (2005). Changes in membrane lipid composition following rapid cold hardening in Drosophila melanogaster. J Insect Physiol *51*, 1173-1182.

Park, J.H., Helfrich-Forster, C., Lee, G., Liu, L., Rosbash, M., and Hall, J.C. (2000). Differential regulation of circadian pacemaker output by separate clock genes in Drosophila. Proc Natl Acad Sci U S A *97*, 3608-3613.

Raghu, S., Joesch, M., and Borst…, A. (2007). Synaptic organization of lobula plate tangential cells in Drosophila: γ ‐ Aminobutyric acid receptors and chemical release sites. The Journal of ….

Raghu, S., Joesch, M., Sigrist, S.J., Borst, A., and Reiff, D.F. (2009). Synaptic organization of lobula plate tangential cells in Drosophila: Dalpha7 cholinergic receptors. J Neurogenet *23*, 200-209.

Renn, S.C., Park, J.H., Rosbash, M., Hall, J.C., and Taghert, P.H. (1999). A pdf neuropeptide gene mutation and ablation of PDF neurons each cause severe abnormalities of behavioral circadian rhythms in Drosophila. Cell *99*, 791-802.

Rieger, D., Stanewsky, R., and Helfrich-Forster, C. (2003). Cryptochrome, compound eyes, Hofbauer-Buchner eyelets, and ocelli play different roles in the entrainment and masking pathway of the locomotor activity rhythm in the fruit fly Drosophila melanogaster. Journal of biological rhythms *18*, 377-391.

Root, C.M., Ko, K.I., Jafari, A., and Wang, J.W. (2011). Presynaptic facilitation by neuropeptide signaling mediates odor-driven food search. Cell *145*, 133-144.

Rosenzweig, M., Brennan, K.M., Tayler, T.D., Phelps, P.O., Patapoutian, A., and Garrity, P.A. (2005). The Drosophila ortholog of vertebrate TRPA1 regulates thermotaxis. Genes Dev *19*, 419-424.

Ruggero, M.A. (1992). Responses to sound of the basilar membrane of the mammalian cochlea. Curr Opin Neurobiol *2*, 449-456.

Samuel, A.D., Silva, R.A., and Murthy, V.N. (2003). Synaptic activity of the AFD neuron in Caenorhabditis elegans correlates with thermotactic memory. J Neurosci *23*, 373-376.

Sayeed, O., and Benzer, S. (1996). Behavioral genetics of thermosensation and hygrosensation in Drosophila. Proc Natl Acad Sci U S A *93*, 6079-6084.

Shaw, S.R., Frohlich, A., and Meinertzhagen, I.A. (1989). Direct connections between the R7/8 and R1-6 photoreceptor subsystems in the dipteran visual system. Cell Tissue Res *257*, 295-302.

Shenoy, S.K., and Lefkowitz, R.J. (2005). Receptor-specific ubiquitination of beta-arrestin directs assembly and targeting of seven-transmembrane receptor signalosomes. J Biol Chem *280*, 15315-15324.

Shorey, H.H. (1962). Nature of the Sound Produced by Drosophila melanogaster during Courtship. Science *137*, 677-678.

Shreve, S.M., Kelty, J.D., and Lee, R.E., Jr. (2004). Preservation of reproductive behaviors during modest cooling: rapid cold-hardening fine-tunes organismal response. J Exp Biol *207*, 1797-1802.

Single, S., and Borst, A. (1998). Science *281*, 1848.

Song, W., Onishi, M., Jan, L.Y., and Jan, Y.N. (2007). Peripheral multidendritic sensory neurons are necessary for rhythmic locomotion behavior in Drosophila larvae. Proc Natl Acad Sci U S A *104*, 5199-5204.

Stagljar, I., Korostensky, C., Johnsson, N., and te Heesen, S. (1998). A genetic system based on split-ubiquitin for the analysis of interactions between membrane proteins in vivo. Proc Natl Acad Sci U S A *95*, 5187-5192.

Stanewsky, R. (2003). Genetic analysis of the circadian system in Drosophila melanogaster and mammals. J Neurobiol *54*, 111-147.

Sun, Y., Liu, L., Ben-Shahar, Y., Jacobs, J.S., Eberl, D.F., and Welsh, M.J. (2009). TRPA channels distinguish gravity sensing from hearing in Johnston's organ. Proc Natl Acad Sci U S A *106*, 13606-13611.

Taghert, P.H. (2001). How does the circadian clock send timing information to the brain? Seminars in cell & developmental biology *12*, 329-341.

Taghert, P.H., Hewes, R.S., Park, J.H., O'Brien, M.A., Han, M., and Peck, M.E. (2001). Multiple amidated neuropeptides are required for normal circadian locomotor rhythms in Drosophila. J Neurosci *21*, 6673-6686.

Tauber, E., and Eberl, D.F. (2001). Song production in auditory mutants of Drosophila: the role of sensory feedback. J Comp Physiol A *187*, 341-348.

Thaminy, S., Miller, J., and Stagljar, I. (2004). The split-ubiquitin membrane-based yeast two-hybrid system. Methods Mol Biol *261*, 297-312.

Todi, S.V., Sharma, Y., and Eberl, D.F. (2004). Anatomical and molecular design of the Drosophila antenna as a flagellar auditory organ. Microsc Res Tech *63*, 388-399.

Tracey, W.D., Jr., Wilson, R.I., Laurent, G., and Benzer, S. (2003). painless, a Drosophila gene essential for nociception. Cell *113*, 261-273.

Varadan, R., Assfalg, M., Haririnia, A., Raasi, S., Pickart, C., and Fushman, D. (2004). Solution conformation of Lys63-linked di-ubiquitin chain provides clues to functional diversity of polyubiquitin signaling. J Biol Chem *279*, 7055-7063.

Villella, A., and Hall, J.C. (2008). Neurogenetics of courtship and mating in Drosophila. Advances in genetics *62*, 67-184.

Vishnivetskiy, S.A., Paz, C.L., Schubert, C., Hirsch, J.A., Sigler, P.B., and Gurevich, V.V. (1999). How does arrestin respond to the phosphorylated state of rhodopsin? J Biol Chem *274*, 11451-11454.

Vosshall, L.B., and Stocker, R.F. (2007). Molecular architecture of smell and taste in Drosophila. Annu Rev Neurosci *30*, 505-533.

Waldron, I. (1964). Courtship Sound Production in Two Sympatric Sibling Drosophila Species. Science *144*, 191-193.

Wardill, T.J., List, O., Li, X., Dongre, S., McCulloch, M., Ting, C.Y., O'Kane, C.J., Tang, S., Lee, C.H., Hardie, R.C*., et al.* (2012). Multiple spectral inputs improve motion discrimination in the Drosophila visual system. Science *336*, 925-931.

Williams, J.A., and Sehgal, A. (2001). Molecular components of the circadian system in Drosophila. Annual review of physiology *63*, 729-755.

Wong, A.M., Wang, J.W., and Axel, R. (2002). Spatial representation of the glomerular map in the Drosophila protocerebrum. Cell *109*, 229-241.

Xiao, K., Shenoy, S.K., Nobles, K., and Lefkowitz, R.J. (2004). Activation-dependent conformational changes in {beta}-arrestin 2. J Biol Chem *279*, 55744-55753.

Yamaguchi, S., Wolf, R., Desplan, C., and Heisenberg, M. (2008). Motion vision is independent of color in Drosophila. Proc Natl Acad Sci USA *105*, 4910-4915.

Yorozu, S., Wong, A., Fischer, B.J., Dankert, H., Kernan, M.J., Kamikouchi, A., Ito, K., and Anderson, D.J. (2009). Distinct sensory representations of wind and near-field sound in the Drosophila brain. Nature *458*, 201-205.

Zars, T. (2001). Two thermosensors in Drosophila have different behavioral functions. J Comp Physiol A *187*, 235-242.

Appendix 1

Visualizing Neuromodulation In Vivo: TANGO-Mapping of Dopamine Signaling Reveals Appetite Control of Sugar Sensing

Hidehiko K. Inagaki,1,2 Shlomo Ben-Tabou de-Leon,1,2 Allan M. Wong,1,2 Smitha Jagadish,4 Hiroshi Ishimoto,3
Gilad Barnea,5 Toshihiro Kitamoto,3 Richard Axel,1,4 and David J. Anderson1,2,*
1Howard Hughes Medical Institute
2Division of Biology 156-29
California Institute of Technology, Pasadena, CA 91125, USA
3Department of Anesthesia and Interdisciplinary Programs in Genetics and Neuroscience, University of Iowa, 51 Newton Road, Iowa City, IA 52242, USA
4Columbia University College of Physicians and Surgeons, 701 West 168th Street, New York, NY 10032, USA
5Department of Neuroscience, Brown University, Providence, RI 02912, USA
*Correspondence: wuwei@caltech.edu
DOI 10.1016/j.cell.2011.12.022

Statement of relative contributions.

In this published material, all the data result from research and experiments done by DJA's group at Caltech. RA's group at Columbia University conceived the idea of In Vivo Tango.

SUMMARY

Behavior cannot be predicted from a ‘‘connectome’’ because the brain contains a chemical ‘‘map’’ of neuromodulation superimposed upon its synaptic connectivity map. Neuromodulation changes how neural circuits process information in different states, such as hunger or arousal. Here we describe a genetically based method to map, in an unbiased and brain-wide manner, sites of neuromodulation under different conditions in the *Drosophila* brain. This method, and genetic perturbations, reveal that the well- known effect of hunger to enhance behavioral sensi- tivity to sugar is mediated, at least in part, by the release of dopamine onto primary gustatory sensory neurons, which enhances sugar-evoked calcium influx. These data reinforce the concept that sensory neurons constitute an important locus for state-dependent gain control of behavior and introduce a methodology that can be extended to other neuro- modulators and model organisms.

INTRODUCTION

The physiological responses of an animal’s nervous system to sensory stimuli can differ, depending on internal states such as hunger or arousal (Chiappe et al., 2010; Dubner, 1988; Maimon et al., 2010; Niell and Stryker, 2010; Shea and Margoliash, 2010; Tsuno and Mori, 2009). Such state-dependent influences enable animals to adjust their behavioral responses to metabolic, emotional, attentional, or other demands. Neuromodulators, such as biogenic amines and acetylcholine, as well as neuropeptides play a major role in encoding or

mediating internal states (Harris-Warrick and Marder, 1991; Pfaff et al.,2008), by altering the input-output properties of specific neural circuits (Birmingham and Tauck, 2003; Marder and

Bucher, 2007). Hunger and satiety represent a prototypic model for an internal state(s) that influences behavior. In the vinegar fly *Drosophila* melanogaster, for example, food deprivation is known to affect olfactory sensitivity (Root et al., 2011), formation, and expression of food-associated memory (Krashes et al., 2009), the extent of feeding (Riemensperger et al., 2011), and locomotor activity (Lee and Park, 2004; Meunier et al., 2007) . In addition, in *Drosophila* (Scheiner et al., 2004) as well as in other species (Berridge, 1991; Dethier, 1976; Gillette et al., 2000; Moskowitz et al., 1976; Moss and Dethier, 1983; Page et al., 1998), starvation changes the consummatory response to tastants, typically by enhancing the acceptance of energy resources such as sugar, with an associated increased tolerance for bitter-tasting contaminants. This dramatic starvation-dependent shift in sensitivity to sweet versus unpalatable and potentially toxic energy resources illustrates how state-dependent control of behavior is critical for survival.

Despite the importance of hunger for regulating animal behavior, we know relatively little about the circuit-level mecha- nisms underlying such regulation. Studies in blowflies and honey- bees have demonstrated that biogenic amines can modulate feeding-related behaviors (Brookhart et al., 1987; Long et al.,1986; Scheiner et al., 2002). Whether such modulators actually mediate the effect of hunger on these behaviors, however, has been more difficult to establish in these systems due to the lack of genetic tools. It has also been challenging to identify the circuitry through which such modulators mediate behavioral responses to starvation. Modulatory neurons often exhibit wide- spread projections throughout the brain

(Mao and Davis, 2009; Monastirioti, 1999) and act via multiple receptors. Identifying the behaviorally relevant circuitry on which a given modulator acts, and demonstrating that such modulation is required for a specific state-dependent influence on a specific behavior in vivo, has been achieved in only a few cases (Crocker et al., 2010; Kong et al., 2010; Krashes et al., 2009; Lebestky et al., 2009; Root et al., 2011). *Drosophila* provides an attractive system to address the circuit-level mechanisms underlying neuromodulation of feeding behavior because of the availability of powerful genetic tools and our growing understanding of the gustatory receptors and neural circuitry that control feeding in this species (Dahanukar et al., 2007; Gordon and Scott, 2009; Marella et al., 2006; Mon- tell, 2009; Scott et al., 2001; Thorne et al., 2004; Wang et al., 2004; Weiss et al., 2011). Although several neuropeptides, as well as biogenic amines, have been implicated in mediating the influence of food deprivation on feeding behavior in *Drosophila* (Na¨ ssel and Winther, 2010), with few exceptions (Root et al., 2011; Wu et al., 2005) the circuit-level mechanisms underlying their influences remain poorly understood.

Here we have developed and applied a method, called TANGO-map, to detect the release of endogenous neuromodulators in vivo and identify the circuits on which they act. We have used this method to examine the mechanisms that underlie a starvation-induced change in a feeding behavior in *Drosophila*. Our results identify a hunger-dependent, dopamine (DA)-mediated gain control of behavior at the level of primary gustatory sensory neurons. They also provide proof-of- principle for a methodology that may have general applicability in the genetic dissection of circuit-level neuromodulatory mechanisms.

RESULTS

Design and Validation of a *Drosophila* DA Receptor-Tango System In Vitro

We sought to develop a genetically based tool that reports endogenous neuromodulator release and sites of action in vivo with anatomic specificity. To do this, we adapted to *Drosophila* the Tango system (Barnea et al., 2008), which transforms a tran- sient ligand/receptor interaction into a stable, anatomical readout of reporter gene expression. The reporter gene is acti- vated by a ‘‘private,’’ synthetic signal transduction pathway, using a bacterial transcription factor (lexA) that is covalently coupled (via a specific tobacco etch virus [TEV] protease-sensi- tive cleavage site) to the exogenous DA receptor expressed in the cells of interest (Figure 1B). The transcription factor is cleaved from the DA receptor following ligand binding, by recruitment of an arrestin-TEV protease fusion protein, and translocates to the nucleus where it activates a lexAop-driven reporter. This system was originally developed to detect receptor activation in cultured mammalian cell lines (Barnea et al., 2008), but whether it could also be used to detect receptor activation in vivo was not clear.

To adapt this system to identify circuit-level sites of endoge- nous neuromodulator action in Drosophila in vivo, we generated a Tango system for DA (DopR-Tango), using the *Drosophila* DA receptor DopR1 (Gotzes et al., 1994; Sugamori et al., 1995) and *Drosophila* Arrestin1 (Figure 1A). Here, LexA is used as the tethered transcription factor. Stoichiometric coexpression of the Arrestin-TEV protease fusion was achieved using a 2A peptide (Szymczak and Vignali, 2005), which we have shown to permit bicistronic expression in *Drosophila* (Figures S1A– S1C available online). To test whether DopR-Tango specifically reports cellular acti- vation by DA, we coexpressed DopR-Tango in

human embry- onic kidney (HEK) 293 cells with a lexAop-b-galactosidase (b-gal) reporter. Treatment of these cells with DA or a DopR1 agonist (6,7-ADTN) resulted in a dose-dependent increase in reporter gene expression (Figure 1C). The EC50 of DopR1-Tango to DA and the D1 agonist are c.a. 1 mM in this experiment, similar to values previously reported in insect cell lines (Sugamori et al., 1995). In contrast, neuromodulators that are not ligands for DopR1, such as 5-HT or octopamine (OA), did not induce reporter gene expression (Figure 1C). Together, these results indicate that (1) a *Drosophila* DA receptor and arrestin can be successfully used to generate a functional Tango system; (2) *Drosophila* DopR-Tango can activate reporter expression in response to DA receptor ligands, in a dose-dependent manner; and (3) DopR-Tango maintains the ligand specificity of the orig- inal DA receptor. Analogous results in HEK293 cells were ob- tained with a Tango system constructed using a *Drosophila* OA receptor (OctR-Tango) (data not shown).

DopR-Tango Induces Reporter Expression in a Ligand-Specific Manner in *Drosophila* In Vivo

We chose *Drosophila* as a model to test whether the Tango system can report ligand activity in vivo. To do this, we generated transgenic flies that express DopR-Tango components under the control of elav-GeneSwitch (elav-GS), a pan-neuronally ex- pressed, hormone (RU486) inducible form of GAL4 (GAL4-PR) (Osterwalder et al., 2001). This transgenic line (referred to sub- sequently as ‘‘DopR-Tango flies’’) also contains a lexAop-mCD2::GFP transgene that encodes a membrane-tethered form of green fluorescent protein (GFP), as the Tango reporter. The use of an inducible GAL4 was based on the

assumption that background signal would be minimized by restricting expression of the DopR-Tango system to a 24 hr period just prior to the experimental manipulation, thereby avoiding develop- mental accumulation of the reporter.

After feeding with RU486 for 12–24 hr, widespread expression of DopR-Tango was detected throughout the brain by immuno- staining with an antibody to an HA epitope-tag present on LexA (Figure 1D2). Importantly, widespread brain expression of the GFP Tango reporter was also observed (Figure 1D1), beginning at 12 hr and peaking at 36 hr after the onset of Tango expression (Figure S1E). The pattern of reporter expression was not identical to that of the HA-tag, due to the different subcellular localization of the two markers (membrane versus nuclear; Figure 1D3). Expression of the GFP reporter was not detected in control flies that expressed DopR fused to LexA without the Arrestin-TEV protease fusion protein (Figure S1D). These data indicate that GFP expression in DopR-Tango flies is Arrestin-TEV protease dependent and not due to basal transcription of the lexAop-mCD2::GFP reporter transgene or TEV-protease-independent cleavage of TEVcs-LexA.

To investigate whether Tango reporter expression in flies can report changes in levels of endogenous DA signaling, we examined expression of the reporter after drug treatments. Feeding DopR-Tango flies with L-dopa, a precursor of DA that is known to increase DA levels in the fly brain (Bainton et al., 2000), for 2 days after RU486 treatment caused a statis- tically significant increase in reporter expression in various neural structures including the antennal lobe (AL), the subeso- phageal ganglion (SOG), and b and g lobes of the mushroom body (MB) ((Figures 2A2–2A3, 2B1–4, and S2E; see Figures S2A–S2C for details of GFP reporter quantification). This increase, moreover, was reduced by SCH23390 (Sugamori et al., 1995), a D1 receptor antagonist, to a statistically signifi- cant extent in the

AL (Figure 2B1) and MB b lobe (Figure 2B3), and exhibited a trend to reduction that did not reach signifi- cance in the SOG (Figure 2B2) and MB g lobe (Figure 2B4). The dynamic range of this reporter (2- to 150fold; Figures 2B1–2B4) is similar to that of the best currently available genet- ically encoded calcium indicators (GECIs) (Tian et al., 2009), although the signal-to-noise ratio (SNR; c.a. 4) is lower (see Extended Experimental Procedures). These data confirm that DopR-Tango can read out a statistically significant increase in reporter gene expression in response to an experimentally induced increase in DA levels in vivo.

We also investigated the source of the baseline expression of the Tango reporter observed in unmanipulated flies (Figure 2A2). Genetic elimination of DA in DopR-Tango flies was not feasible, as null mutations in Tyrosine hydroxylase (Th) are embryonic lethal (Riemensperger et al., 2011). Instead, we fed flies with SCH23390 or the DA synthesis inhibitor 3-iodotyrosine (3IY) (Bainton et al., 2000). SCH23390 feeding significantly decreased, but did not abolish, Tango reporter expression in both the AL and SOG (Figures 2C1 and 3C1). 3IY feeding also decreased reporter expression in the AL (Figure 2C2) in a statisti- cally significant manner, but the decrease in the SOG did not reach significance (Figure 3C2). The incomplete effects of the antagonist to inhibit basal (as well as L-dopa-induced; Figures2B1–2B4) expression of the reporter may reflect limits on the effective levels of the drug that can be achieved in vivo, due to instability, nonspecific absorption, or toxicity. Alternatively, it may reflect some level of DA-independent expression of the Tango reporter, for example due to ligand-independent binding of Arrestin-TEVp to DopR-Tango. Whatever the explanation, these results indicate that the level of baseline GFP reporter expression in DopR-Tango flies is, at least in part, a reflection of endogenous DA signaling

in the brain. DopR-Tango reporter expression also exhibited ligand speci- ficity in vivo. When DopR-Tango flies were fed with either L-dopa or chlordimeform (CDM), an OA receptor agonist, only L-dopa feeding increased expression of the reporter in the SOG (Figure 2D2). L-dopa feeding also yielded an increase in DopR- Tango reporter signal in the AL (Figure 2D1), but in this case a smaller but still significant induction was observed using CDM. This difference may reflect an indirect effect of CDM to increase dopaminergic signaling in the AL, given that OA did not activate DopR-Tango in vitro (Figure 1C). In OctR-Tango flies fed with L-dopa or CDM, only CDM increased expression of the GFP reporter in the AL (Figure S2D). These data suggest that in vivo, as well as in HEK293 cells, DopR-Tango can specifically report an artificially induced increase in DA signaling.

DopR-Tango Reveals Increased DA Release onto Primary Gustatory Neurons during Starvation

To investigate whether DopR-Tango can identify neural circuits that are targets of modulation by endogenous DA, we exposed DopR-Tango flies to various treatments and looked for increases in reporter expression. Wet starvation of DopR-Tango flies for 2 days produced a statistically significant increase in GFP expression in the SOG, the primary gustatory center (Figures
3A and 3C1–3C2), but not in the MB b and g lobes or the AL (Figures 3D1–3D3). Inclusion of the DopR antagonist SCH23390 or the DA synthesis inhibitor 3IY abolished the starvation-induced increase in GFP expression in the SOG (Figures 3C1 and 3C2). Based on the time course of Tango reporter expression, we esti- mate that the enhanced GFP

expression likely reflects cumula- tive DopR-Tango activation integrated over the first 24 hr of food deprivation (Figure S1E). Two lines of evidence suggest that the starvation-induced increase in GFP expression in the SOG occurs, at least in part, in the terminals of primary gustatory receptor neurons (GRNs). First, the pattern of Tango reporter expression in the SOG resem- bled that of the projections of sugar-sensing GRNs, as visualized

To pin down the physiological mechanism underlying starva- tion-dependent enhancement of PER behavior, we tested whether starvation and DA augment presynaptic Ca2+ influx in sugar-sensing GRNs. For this purpose, we performed calcium imaging, using two-photon microscopy, of sugar-sensing GRNs in flies expressing a genetically encoded calcium sensor (GCaMP3.0; Tian et al., 2009) under the control of Gr5a-GAL4. Delivery of increasing concentrations of sucrose (from 0 mM to 400 mM) to the labellum yielded increasing GCaMP 3.0 fluores- cence signal in Gr5a-expressing nerve fibers in the SOG (Figures 6B–6D), consistent with a previous report (Marella et al., 2006). Strikingly, both wet-starved and L-dopa-fed flies showed a statistically significant enhancement of sucrose-evoked GCaMP fluorescence, compared to nonstarved control flies, at 100 mM sucrose and a nonsignificant trend to enhancement at 400 mM sucrose (Nusbaum and Beenhakker, 2002) (Figure 6D). A scatterplot of integrated GCaMP fluorescence signal inten- sity versus the fraction of flies showing a PER response at each sucrose concentration revealed a strong positive correla- tion between the two measures ($R2 = 0.969$) (Figure 6E). The simplest interpretation of this correlation is that the starvation- induced enhancement of calcium influx in sugar-sensing GRNs underlies the parallel enhancement of PER behavior.

Finally, to examine more directly whether DA acts on Gr5a GRNs to modulate Ca2+ influx, we compared the sugar responses of these GRNs before versus after exposure to

1 mM DA in the bath. Following 5 min of such exposure, there was an rv1.2-fold increase in basal Ca2+ influx and an rv1.3- to 1.4-fold increase in Ca2+ influx caused by 400 mM sucrose; the fold increase at 400 mM sucrose was significantly higher than at 0 mM sucrose ($p < 0.05$, Wilcoxon matched pairs test) (Figures 6F1 and 6G). Importantly, RNAi-mediated knockdown of DopEcR expression in sugar-sensing GRNs attenuated this increase in Ca2+ influx (Figures 6F2 and 6G). These data indicate that DA acts directly on Gr5a GRNs via DopEcR to enhance both baseline and sucrose-induced increases in intracellular free Ca2+.

DISCUSSION

Drosophila is a potentially powerful model system for under- standing how neuromodulators control state-dependent changes in behavior. However, establishing the behaviorally relevant, circuit-level mechanisms of action of neuromodulators remains challenging. This is partially because standard methods used to measure the release of endogenous neuromodulators in vertebrates, such as fast-scan cyclic voltammetry (Phillips et al., 2003) or microdialysis (Benveniste and Hu¨ ttemeier, 1990), are of limited applicability in *Drosophila*. Moreover, such methods cannot identify the neurons on which released neuromodulators act. The data presented here provide proof-of-principle for the utility of a new method, called TANGO-map, to identify, in a brain-wide and relatively unbiased manner, circuit-level sub- strates of neuromodulation relevant to a particular state-depen- dent influence on behavior.

Starvation Regulates Gustatory Sensitivity in *Drosophila* and Causes DA Release onto Sugar-Sensing GRNs

We show here that sweet taste sensitivity in the labellum is enhanced with increasing duration of food deprivation in *Drosophila*. This observation confirms and extends previous reports in *Drosophila* (Meunier et al., 2007; Scheiner et al., 2004) and is consistent with observations in many other animal species (Dethier, 1976; Moskowitz et al., 1976; Page et al., 1998). We have used this phenomenon as a prototypic case of a state-dependent change in behavior to investigate the ability of TANGO-map to identify underlying neuromodulatory mechanisms.

Our results indicate that starvation enhances endogenous DA release onto primary GRNs, as detected by increased expres- sion of the DopR-Tango reporter in vivo. In contrast, starvation did not increase the DopR-Tango reporter in the MB or AL, although L-dopa feeding did so. These data indicate that DopR-Tango is capable of revealing selective sites of endoge- nous DA release in a brain-wide manner, under specific behav- ioral conditions.

DA Release onto Sugar-Sensing GRNs Is Required for the Behavioral Effect of Starvation to Enhance PER Sensitivity

Our results indicate that a mutation in the DA receptor DopEcR, as well as specific knockdown of this receptor in sugar-sensing GRNs, eliminates the effect of starvation to enhance the sucrose sensitivity of the PER. However, this phenotype was only observed at 6 hr of starvation; after 24 hr of food deprivation, these genetic manipulations no longer had

an effect. This is not because these manipulations themselves became ineffec- tive at later times, as the same manipulations did attenuate the increased PER sensitivity caused by L-dopa feeding for 24 hr. This suggests that at an early stage of starvation, DA is neces- sary to enhance the sugar sensitivity of the PER, whereas at later stages additional factors come into play (Figure 6H).

The slow kinetics of Tango reporter accumulation (Figure S1E) preclude the detection of statistically significant increases in signal as early as 6 hr following an experimental manipulation. However, the level of reporter expression detected in animals examined after 48 hr of treatment likely reflects the integration of increases in dopaminergic signaling occurring throughout the first 12–24 hr of the treatment period (Figure S1E). Thus, although we detected an increase in DopR-Tango signal at a starvation time point when genetic reduction of DopEcR levels no longer impaired the behavioral effect of starvation and observed a behavioral phenotype at a time point too early to be evaluated directly by the TANGO-map method, this should not be taken to imply that no DA release occurred after 6 hr of starvation. Importantly, given the kinetics of the system, the DopR-Tango signals we detect in vivo are likely to reflect primarily changes in tonic levels of DA signaling, rather than brief episodes of phasic DA release. Further improvements of the TANGO-map method are required to increase its temporal reso- lution. Nevertheless, the present methodology provides a power- ful method to identify sites where dopaminergic modulation of a given behavior may occur, even if it cannot reveal precisely how quickly such regulation is exerted.

Mechanism of Dopaminergic Regulation of GRN Sensitivity

Several lines of evidence suggest that the dopaminergic modulation of sugar-sensing GRNs revealed here may involve an enhancement of Ca2+ influx at the nerve terminal. Both starvation and L-dopa feeding increased sucrose-evoked Ca2+ influx, without changing the frequency of action potentials measured extracellularly at GRN somata (Figure S5), despite a previous report to the contrary (Meunier et al., 2007). Furthermore, we found that direct exposure of the brain to DA increased Ca2+ influx at the presynaptic terminals of sugar-sensing GRNs in a DopEcR-dependent manner. A model consistent with these data is that starvation leads to increased DA release, which increases calcium influx into sugar-sensing GRNs via DopEcR, leading to increased neurotransmitter release. The fact that DopEcR signals via the cAMP/PKA pathway (Srivastava et al., 2005), and that this pathway has been reported to increase Ca2+ channel currents in *Drosophila* (Bhattacharya et al., 1999), is also consistent with this scenario. Nevertheless, our genetic data suggest that there are additional pathways through which starvation modulates feeding behavior in this system.

Our finding that DA modulates primary GRNs to control starvation-dependent changes in behavioral sensitivity to sugar echoes the observation of a similar influence of food deprivation on odorant sensitivity in *Drosophila* (Root et al., 2011). Such neuromodulatory gain control at the level of primary sensory neurons has also been reported in a variety of other invertebrate as well as vertebrate species (Bicker and Menzel, 1989; Hurley et al., 2004). Although we cannot exclude the possibility that hunger also influences PER behavior at higher-order synapses in the circuit (Gordon and Scott, 2009), our data add to a growing body of information indicating that modulation of primary sensory neurons is a general

mechanism for implementing state-dependent changes in behavioral responses to the stimuli detected by these neurons.

TANGO-Map as a Tool to Monitor Neuromodulation at the Circuit Level

TANGO-map affords a number of unique advantages to study neuronal modulation in the brain (see Table S1 for comparison to other methods). First, and most importantly, it permits the detection of increases in endogenous neuromodulator release in vivo, in an organism in which the application of conventional methods is not feasible. Second, it provides an anatomical readout of neuromodulation at the neural circuit level. The use of a pan-neuronal GAL4 driver to express the sensor permits, in principle, an unbiased survey of potential sites of neuromodu- latory activity throughout the brain. Third, the sensor has ligand specificity. The modular design of the Tango system (Barnea et al., 2008) affords the ability to develop in vivo Tango reporters for other biogenic amines and neuropeptides that work via G protein-coupled receptors (GPCRs). Importantly, because the method employs a synthetic, ‘‘private’’ signal transduction pathway (Barnea et al., 2008), the readout of the reporter should be relatively insensitive to interference from conventional signal transduction pathways activated by other endogenous receptors. Systematic and comprehensive application of this approach could, in principle, provide an overview of anatomic patterns of neuromodulation in the brain in a given behavioral setting. Finally, because the Tango system is transcriptionally based, in principle it permits the expression not only of neutral reporters but also of effectors such as RNAi’s or ion channels in the neurons receiving neuromodulatory input. Although the TANGO-map system can certainly benefit from

improvements in its kinetics and SNR, it affords a means of identifying points-of-entry for studying circuit-level mechanisms of behaviorally relevant neuromodulation that are currently difficult to access in any other way. The extension of this methodology to other neuromodulators and model organisms should further our under- standing of state-dependent control of neural activity and behavior.

EXPERIMENTAL PROCEDURES

Fly Strains

Adult female *Drosophila* melanogaster were used for all experiments. All control genotypes were tested in the same genetic background as the experimental genotype. Construction of recombinant DNA and descriptions of transgenic fly strains are described in the Extended Experimental Procedures.

TANGO-Map

DopR-Tango flies or OctR-Tango flies were first dry-starved for 4 hr to make sure they consumed any drugs provided. Then, flies were moved into a vial containing 0.5 mM RU486 mixed in 89 mM sucrose and allowed to feed for 12 or 24 hr (for subsequent drug feeding or starvation experiments, respec- tively). After this RU486 feeding, flies were moved to either food vials (fed condition), vials containing a wet filter paper (wet-starved condition), or vials containing a drug dissolved in 89 mM sucrose (drug-fed condition). Two days later, fly brains were dissected and immunostained.

PER Assays

For standard PER assays, 3- to 7-day-old female flies were wet starved or fed in vials and tested as described previously (Shiraiwa and Carlson, 2007). In brief, 10–20 experimental flies were mounted into pipetman tips. After excluding flies that keep responding to water, fly response to stepwise increasing concentration of sucrose was tested. The same sets of flies were tested with all concentrations of sucrose. For ChR2 experiments, flies were fed with 200 mM all trans-Retinal and tested for the response to blue light (emitted by a standard mercury lamp and filtered by GFP filter: 470/40 nm [center wavelength/ bandwidth]) under a fluorescent microscope. For details, see Extended Experimental Procedures.

Calcium Imaging

Two-photon imaging was performed on an Ultima two-photon laser scanning microscope (Prairie Technology) with an imaging wavelength at 925 nm. After a brief anesthesia on ice, flies were mounted on a thin plastic plate with wax as shown in Figure 6B. The top side of the plate contained a well made with wax, and the fly head was immersed in saline. In this saline bath, the antennae and cuticle at the anterior side of the fly head capsule were surgically removed with sharp forceps, so that the SOG could be imaged. At the bottom side of the plate, a glass tube was mounted with the opening facing the proboscis of the mounted fly. A piece of twisted Kimwipe was placed just behind the fly. During imaging, a sucrose solution was delivered from the glass tubing to stimulate gustatory neurons in the proboscis and was removed by the Kimwipe. Details of the preparation and data processing are described in Extended Experimental Procedures.

SUPPLEMENTAL INFORMATION

Supplemental Information includes Extended Experimental Procedures, five figures, and one table and can be found with this article online at doi:10.1016/j.cell.2011.12.022.

ACKNOWLEDGMENTS

We thank Dr. K.J. Lee for sharing Tango DNA constructs prior to publication. We also thank Drs. T. Lee, K. Deisseroth, A. Stathopoulos, and B. Pfeiffer for plasmids. Fly stocks were generously provided by the Bloomington Stock Center, the VDRC stock center, the *Drosophila* RNAi Screening Center, and Drs. G.M. Rubin, J. Simpson, L.L Looger, H.

Keshishian, K. Scott, T. Lee, S. Birman, P.A. Garrity, C.Q. Doe, and K. Ito. We also thank Drs. H. Otsuna and Y. Wan for Fluorender and members of the Anderson lab for helpful discussion and sharing of flies. H.K.I. is supported by the Nakajima Founda- tion. G.B. is a Pew scholar and is supported in part by NIH grant 5R01MH086920. D.J.A. is an investigator of the Howard Hughes Medical Institute. This work was supported in part by NIH grant 1RO1 DA031389 to D.J.A.

Received: July 14, 2011

Revised: October 7, 2011

Accepted: December 23, 2011

Published: February 2, 2012

REFERENCES

Bainton, R.J., Tsai, L.T., Singh, C.M., Moore, M.S., Neckameyer, W.S., and Heberlein, U. (2000). Dopamine modulates acute responses to cocaine, nico- tine and ethanol in *Drosophila*. Curr. Biol. 10, 187–194.

Barnea, G., Strapps, W., Herrada, G., Berman, Y., Ong, J., Kloss, B., Axel, R., and Lee, K.J. (2008). The genetic design of signaling cascades to record receptor activation. Proc. Natl. Acad. Sci. USA 105, 64–69.

Benveniste, H., and Hu¨ ttemeier, P.C. (1990). Microdialysis—theory and appli- cation. Prog. Neurobiol. 35, 195–215.

Berridge, K.C. (1991). Modulation of taste affect by hunger, caloric satiety, and sensory-specific satiety in the rat. Appetite 16, 103–120.

Bhattacharya, A., Gu, G.G., and Singh, S. (1999). Modulation of dihydropyri- dine-sensitive calcium channels in *Drosophila* by a cAMP-mediated pathway. J. Neurobiol. 39, 491–500.

Bicker, G., and Menzel, R. (1989). Chemical codes for the control of behaviour in arthropods. Nature 337, 33–39.

Birmingham, J.T., and Tauck, D.L. (2003). Neuromodulation in invertebrate sensory systems: from biophysics to behavior. J. Exp. Biol. 206, 3541–3546.

Brookhart, G.L., Edgecomb, R.S., and Murdock, L.L. (1987). Amphetamine and reserpine deplete brain biogenic amines and alter blow fly feeding behavior. J. Neurochem. 48, 1307–1315.

Chiappe, M.E., Seelig, J.D., Reiser, M.B., and Jayaraman, V. (2010). Walking modulates speed sensitivity in *Drosophila* motion vision. Curr. Biol. 20, 1470–1475.

Crocker, A., Shahidullah, M., Levitan, I.B., and Sehgal, A. (2010). Identification of a neural circuit that underlies the effects of octopamine on sleep:wake behavior. Neuron 65, 670–681.

Dahanukar, A., Lei, Y.T., Kwon, J.Y., and Carlson, J.R. (2007). Two Gr genes underlie sugar reception in *Drosophila*. Neuron 56, 503–516.

Dethier, V.G. (1976). The Hungry Fly: A Physiological Study of the Behavior Associated with Feeding (Cambridge, MA: Harvard University Press).

Dubner, R. (1988). The effect of behavioral state on the sensory processing of nociceptive and non-nociceptive information. Prog. Brain Res. 77, 213–228.

Friggi-Grelin, F., Coulom, H., Meller, M., Gomez, D., Hirsh, J., and Birman, S. (2003). Targeted gene expression in *Drosophila* dopaminergic cells using regulatory sequences from tyrosine hydroxylase. J. Neurobiol. 54, 618–627.

Gillette, R., Huang, R.C., Hatcher, N., and Moroz, L.L. (2000). Cost-benefit analysis potential in feeding behavior of a predatory snail by integration of hunger, taste, and pain. Proc. Natl. Acad. Sci. USA 97, 3585–3590.

Gordon, M.D., and Scott, K. (2009). Motor control in a *Drosophila* taste circuit. Neuron 61, 373–384.

Gotzes, F., Balfanz, S., and Baumann, A. (1994). Primary structure and func- tional characterization of a *Drosophila* dopamine receptor with high homology to human D1/5 receptors. Receptors Channels 2, 131–141.

Hamada, F.N., Rosenzweig, M., Kang, K., Pulver, S.R., Ghezzi, A., Jegla, T.J., and Garrity, P.A. (2008). An internal thermal sensor controlling temperature preference in *Drosophila*. Nature 454, 217–220.

Han, K.A., Millar, N.S., Grotewiel, M.S., and Davis, R.L. (1996). DAMB, a novel dopamine receptor expressed specifically in *Drosophila* mushroom bodies. Neuron 16, 1127–1135.

Harris-Warrick, R.M., and Marder, E. (1991). Modulation of neural networks for behavior. Annu. Rev. Neurosci. 14, 39–57.

Hearn, M.G., Ren, Y., McBride, E.W., Reveillaud, I., Beinborn, M., and Kopin, A.S. (2002). A *Drosophila* dopamine 2-like receptor: Molecular characteriza- tion and identification of multiple alternatively spliced variants. Proc. Natl. Acad. Sci. USA 99, 14554–14559.

Hurley, L.M., Devilbiss, D.M., and Waterhouse, B.D. (2004). A matter of focus: monoaminergic modulation of stimulus coding in mammalian sensory networks. Curr. Opin. Neurobiol. 14, 488–495.

Kong, E.C., Woo, K., Li, H., Lebestky, T., Mayer, N., Sniffen, M.R., Heberlein, U., Bainton, R.J., Hirsh, J., and Wolf, F.W. (2010). A pair of dopamine neurons target the D1-like dopamine receptor DopR in the central complex to promote ethanol-stimulated locomotion in *Drosophila*. PLoS ONE 5, e9954.

Krashes, M.J., DasGupta, S., Vreede, A., White, B., Armstrong, J.D., and Wad- dell, S. (2009). A neural circuit mechanism integrating motivational state with memory expression in *Drosophila*. Cell 139, 416–427.

Lebestky, T., Chang, J.S., Dankert, H., Zelnik, L., Kim, Y.C., Han, K.A., Wolf, F.W., Perona, P., and Anderson, D.J. (2009). Two different forms of arousal in *Drosophila* are oppositely regulated by the dopamine D1 receptor ortholog DopR via distinct neural circuits. Neuron 64, 522–536.

Lee, G., and Park, J.H. (2004). Hemolymph sugar homeostasis and starvation- induced hyperactivity affected by genetic manipulations of the adipokinetic hormone-encoding gene in *Drosophila* melanogaster. Genetics 167, 311–323.

Long, T.F., Edgecomb, R.S., and Murdock, L.L. (1986). Effects of substituted phenylethylamines on blowfly feeding behavior. Comp. Biochem. Physiol. C. Comp. Pharmacol. Toxicol. 83, 201–209.

Maimon, G., Straw, A.D., and Dickinson, M.H. (2010). Active flight increases the gain of visual motion processing in *Drosophila*. Nat. Neurosci. 13, 393–399.

Mao, Z., and Davis, R.L. (2009). Eight different types of dopaminergic neurons innervate the *Drosophila* mushroom body neuropil: anatomical and physiolog- ical heterogeneity. Front Neural Circuits 3, 5.

Marder, E., and Bucher, D. (2007). Understanding circuit dynamics using the stomatogastric nervous system of lobsters and crabs. Annu. Rev. Physiol. 69, 291–316.

Marella, S., Fischler, W., Kong, P., Asgarian, S., Rueckert, E., and Scott, K. (2006). Imaging taste responses in the fly brain reveals a functional map of taste category and behavior. Neuron 49, 285–295.

Meunier, N., Belgacem, Y.H., and Martin, J.R. (2007). Regulation of feeding behaviour and locomotor activity by takeout in *Drosophila*. J. Exp. Biol. 210,1424–1434.

Miller, M.R., Robinson, K.J., Cleary, M.D., and Doe, C.Q. (2009). TU-tagging: cell type-specific RNA isolation from intact complex tissues. Nat. Methods 6, 439–441.

Monastirioti, M. (1999). Biogenic amine systems in the fruit fly *Drosophila* mel- anogaster. Microsc. Res. Tech. 45, 106–121.

Montell, C. (2009). A taste of the *Drosophila* gustatory receptors. Curr. Opin. Neurobiol. 19, 345–353.

Moskowitz, H.R., Kumraiah, V., Sharma, K.N., Jacobs, H.L., and Sharma, S.D. (1976). Effects of hunger, satiety and glucose load upon taste intensity and taste hedonics. Physiol. Behav. 16, 471–475.

Moss, C.F., and Dethier, V.G. (1983). Central nervous system regulation of finicky feeding by the blowfly. Behav. Neurosci. 97, 541–548.

Na¨ ssel, D.R., and Winther, A.M. (2010). *Drosophila* neuropeptides in regulation of physiology and behavior. Prog. Neurobiol. 92, 42–104.

Niell, C.M., and Stryker, M.P. (2010). Modulation of visual responses by behav- ioral state in mouse visual cortex. Neuron 65, 472–479.

Nusbaum, M.P., and Beenhakker, M.P. (2002). A small-systems approach to motor pattern generation. Nature 417, 343–350.

Osterwalder, T., Yoon, K.S., White, B.H., and Keshishian, H. (2001). A condi- tional tissue-specific transgene expression system using inducible GAL4. Proc. Natl. Acad. Sci. USA 98, 12596–12601.

Page, R.E., Jr., Erber, J., and Fondrk, M.K. (1998). The effect of genotype on response thresholds to sucrose and foraging behavior of honey bees (Apis mellifera L.). J. Comp. Physiol. A Neuroethol. Sens. Neural Behav. Physiol.182, 489–500.

Pauli, A., Althoff, F., Oliveira, R.A., Heidmann, S., Schuldiner, O., Lehner, C.F., Dickson, B.J., and Nasmyth, K. (2008). Cell-type-specific TEV protease cleavage reveals cohesin functions in *Drosophila* neurons. Dev. Cell 14 239–251.

Pfaff, D.W., Kieffer, B.L., and Swanson, L.W. (2008). Mechanisms for the regu- lation of state changes in the central nervous system: an introduction. Ann. N Y Acad. Sci. 1129, 1–7.

Phillips, P.E., Robinson, D.L., Stuber, G.D., Carelli, R.M., and Wightman, R.M. (2003). Real-time measurements of phasic changes in extracellular dopamine concentration in freely moving rats by fast-scan cyclic voltammetry. Methods Mol. Med. 79, 443–464.

Riemensperger, T., Isabel, G., Coulom, H., Neuser, K., Seugnet, L., Kume, K., Iche´ - Torres, M., Cassar, M., Strauss, R., Preat, T., et al. (2011). Behavioral consequences of dopamine deficiency in the *Drosophila* central nervous system. Proc. Natl. Acad. Sci. USA 108, 834–839.

Root, C.M., Ko, K.I., Jafari, A., and Wang, J.W. (2011). Presynaptic facilitation by neuropeptide signaling mediates odor-driven food search. Cell 145, 133–144.

Scheiner, R., Plu¨ ckhahn, S., Oney, B., Blenau, W., and Erber, J. (2002). Behavioural pharmacology of octopamine, tyramine and dopamine in honey bees. Behav. Brain Res. 136, 545–553.

Scheiner, R., Sokolowski, M.B., and Erber, J. (2004). Activity of cGMP-depen- dent protein kinase (PKG) affects sucrose responsiveness and habituation in *Drosophila* melanogaster. Learn. Mem. 11, 303–311.

Scott, K., Brady, R., Jr., Cravchik, A., Morozov, P., Rzhetsky, A., Zuker, C., and Axel, R. (2001). A chemosensory gene family encoding candidate gustatory and olfactory receptors in *Drosophila*. Cell 104, 661–673.

Shea, S.D., and Margoliash, D. (2010). Behavioral state-dependent reconfigu- ration of song-related network activity and cholinergic systems. J. Chem. Neuroanat. 39, 132–140.
Shiraiwa, T., and Carlson, J.R. (2007). Proboscis extension response (PER) assay in *Drosophila*. J. Vis. Exp. 3, 193.

Srivastava, D.P., Yu, E.J., Kennedy, K., Chatwin, H., Reale, V., Hamon, M., Smith, T., and Evans, P.D. (2005). Rapid, nongenomic responses to ecdyste- roids and catecholamines mediated by a novel *Drosophila* G-protein-coupled receptor. J. Neurosci. 25, 6145–6155.

Sugamori, K.S., Demchyshyn, L.L., McConkey, F., Forte, M.A., and Niznik, H.B. (1995). A primordial dopamine D1-like adenylyl cyclase-linked receptor from *Drosophila* melanogaster displaying poor affinity for benzazepines. FEBS Lett. 362, 131–138.

Szymczak, A.L., and Vignali, D.A. (2005). Development of 2A peptide-based strategies in the design of multicistronic vectors. Expert Opin. Biol. Ther. 5, 627–638.

Thibault, S.T., Singer, M.A., Miyazaki, W.Y., Milash, B., Dompe, N.A., Singh, C.M., Buchholz, R., Demsky, M., Fawcett, R., Francis-Lang, H.L., et al. (2004). A complementary transposon tool kit for *Drosophila* melanogaster using P and piggyBac. Nat. Genet. 36, 283–287.

Thorne, N., Chromey, C., Bray, S., and Amrein, H. (2004). Taste perception and coding in *Drosophila*. Curr. Biol. 14, 1065–1079.

Tian, L., Hires, S.A., Mao, T., Huber, D., Chiappe, M.E., Chalasani, S.H., Petreanu, L., Akerboom, J., McKinney, S.A., Schreiter, E.R., et al. (2009). Imaging neural activity in worms, flies and mice with improved GCaMP calcium indicators. Nat. Methods 6, 875–881.

Tsuno, Y., and Mori, K. (2009). Behavioral state-dependent changes in the information processing mode in the olfactory system. Commun. Integr. Biol. 2, 362–364.

Wang, Z., Singhvi, A., Kong, P., and Scott, K. (2004). Taste representations in the *Drosophila* brain. Cell 117, 981–991.

Weiss, L.A., Dahanukar, A., Kwon, J.Y., Banerjee, D., and Carlson, J.R. (2011). The molecular and cellular basis of bitter taste in *Drosophila*. Neuron 69, 258–272.

Wu, Q., Zhao, Z., and Shen, P. (2005). Regulation of aversion to noxious food by *Drosophila* neuropeptide Y- and insulin-like systems. Nat. Neurosci. 8, 1350–1355.

Zhang, F., Wang, L.P., Boyden, E.S., and Deisseroth, K. (2006). Channelrho- dopsin-2 and optical control of excitable cells. Nat. Methods 3, 785–792.

Zhang, W., Ge, W., and Wang, Z. (2007). A toolbox for light control of *Drosophila* behaviors through Channelrhodopsin 2-mediated photoactivation of targeted neurons. Eur. J. Neurosci. 26, 2405–2416.

Supplemental Information

EXTENDED EXPERIMENTAL PROCEDURES Recombinant DNA Construction

Plasmids were constructed by standard DNA cloning and PCR methods. All PCR reactions were performed using PrimeStar HS DNA polymerase (Takara). PCR-amplified DNA fragments were inserted into the pCRII Vector (Invitrogen). After amplification all sequences were verified by DNA sequencing. Completed vectors for expression in *Drosophila* (UAS-DopR-Tango, UAS-OctR-Tango, UAS-DopEcR, and UAS-ChR2(C128T)) were inserted into either the attP2 site or attP40 site (Pfeiffer et al., 2010) using attB/attP and C31-mediated recombination (Genetic Services, Inc.) (Groth et al., 2004;

Markstein et al., 2008). Plasmids containing UAS-DopR-Tango and UAS-OctR-Tango were created in several steps as shown below. The ‘‘Valium’’ vector was used as the backbone for all constructions (Ni et al., 2008).

pCRII-2A

A DNA fragment encoding the F2A peptide (Donnelly et al., 2001) was amplified by PCR using primers 2A-f (CCTAGGGAGCAGA AGGGCCCCGGGCTAAGAGATCAGGTTC) and 2A-r (GCTAGCGAGCAGGGCCGGCCTGGCCCTGGGTTGGACTCC), and a plasmid generously provided by Dr. Pin Wang. The pCRII vector containing this DNA fragment was named pCRII-2A.

Valium-2A-TEVp

The DNA fragment encoding TEV protease (TEVp) was amplified by PCR using primers TEVp-f (GAATTC CCTAGGGAGCAG GCTAGCTTGTTTAAGGGACCACG) and TEVp-r (GTCTAGATCAAGCGTAATCTGGAACATCA), and a vector generously provided by Dr. Kevin J. Lee (Barnea et al., 2008). This fragment was subcloned into the C-terminal side of 2A in pCRII-2A using AvrII and NheI. Subsequently, the DNA fragment containing both 2A and TEV protease was subcloned into a Valium vector (Ni et al., 2008), a vector containing both UAS and attB sequence, using EcoRI and XbaI.

Valium-TEVcs-LexA-HAtag-2A-TEVp

A DNA fragment encoding the TEV cleavage site (TEVcs) and a hemagglutinin (HA) epitope tag sequence was created by PCR and inserted into the pCRII vector. For the initial

version of DopR Tango (used only in Figures 2D, S2D, and S2E), GGSGGENLY FQLGGSGG was used as a cleavage sequence, where GGSGG at both ends are linkers. Subsequent experiments showed that the S/N in vitro was better using a different cleavage sequence with shorter linkers, GENLYFQLG. Therefore, a modified DopR-Tango containing this TEVcs sequence was used for the remainder of the study. The constructed sequence is shown below (the TEVcs is GENLYFQLG):

GCCTAGGACGAGTCCGCGGCCGCGGAGAAAATCTCTATTTCCAGCTAGGACCCG
GGTTGGTTCCCATATGATGGACCTGCACC
GTGGTGGCGGTCGTATCTTTTATCCGTATGACGTGCCGGACTATGCCGGCTATCC
ATACGATGTCCCCGACTACGCTGGATCCTA
CCCCTACGACGTCCCAGATTATGCCGCTCATGGCGGAGGGCCCG.

A DNA fragment encoding LexA::VP16 (LexA) (Lai and Lee, 2006) was amplified by PCR using primers LexA-f (GCCCGGGA AAGCGTTAACGGCCAGG) and LexA-r (GCATATGCCCACCGTACTCGTCAATT), and a plasmid generously provided by Dr. Tzumin Lee. This DNA fragment was subcloned in between the TEVcs and the HA tag by using XmaI and NdeI, to create a fusion sequence, TEVcs-LexA-HAtag. This DNA fragment was in turn subcloned 50 to the 2A sequence in Valium-2A-TEVp using AvrII and ApaI. This vector was named Valium-TEVcs-LexA-HAtag-2A-TEVp.

Valium-TEVcs-LexA-HAtag-2A-Arrestin-TEVp

A *Drosophila* Arrestin1 coding sequence was amplified by PCR using primers Arrestin-f (GGGCCGGCCCATGGTGGTCAATTT CAAGGTG) and Arrestin-r (GCTAGCGCCTCCGCTGCCACCGTAGGCCTCAATGGAGCCC), and a cDNA

template synthesized from the heads of wild-type (Canton-S) flies. This DNA fragment was subcloned into Valium-TEVcs-LexA-HAtag-2A-TEVp between the 2A and TEVp sequences using FseI and NheI.

UAS-DopR-Tango (Valium-DopR1-TEVcs-LexA-HAtag-2A-Arrestin-TEVp)

A *Drosophila* DopR1 coding sequence was amplified by PCR using primers DopR1-f (GCCTAGGCAAAATGTACACACCACACC CATTTG) and DopR1-r (GGCGGCCGCCGCAAATCGCAGACACCTGCTC), and a cDNA template synthesized from the heads of Canton-S flies. This DNA fragment was subcloned into Valium-TEVcs-LexA-HAtag-2A-Arrestin-TEVp using AvrII and NotI, to produce the final product Valium-DopR1-TEVcs-LexA-HAtag-2A-Arrestin-TEVp. For simplicity this vector was re-named UAS- DopR-Tango.

UAS-OctR-Tango (Valium-OctR1-TEVcs-LexA-HAtag-2A-Arrestin-TEVp)

A *Drosophila* OctR1 coding sequence was amplified by PCR using primers OctR-f (CCTAGGCAAAATGAATGAAACAGAGTGC GAGG) and OctR-r (GCGGCCGCCCCTGGGGTCGTTGCTCAT), and a cDNA template synthesized from the heads of Canton-S flies. This DNA fragment was subcloned into Valium-TEVcs-LexA-HAtag-2A-Arrestin-TEVp using AvrII and NotI, to produce Valium- OctR1-TEVcs-LexA-HAtag-2A-Arrestin-TEVp. For simplicity this vector was named UAS-OctR-Tango.

UAS-DopEcR

A *Drosophila* DopEcR coding sequence was amplified by PCR using primers DopEcR-f (GGCGGCCGCCAAAATGCAGGAAAT GAGCTACCTAC) and DopEcR-r

(GTCTAGACTAGTCATCTGGGTCCAACC), and a cDNA template synthesized from the heads of Canton-S flies. This DNA fragment was subcloned into pJFRC-MUH (Pfeiffer et al., 2010) using NotI and XbaI.

UAS-ChR2(C128T)

DNA fragment of ChR2(C128T)::eYFP (Berndt et al., 2009) was amplified by PCR using primers chr2-f (AGAGAACTCTGAATAGATCT CACCatggactatggcggcgctttg) and chr2-r (TTCCTTCACAAAGATCCTCTAGAttacttgtacagctcgtcca), and a plasmid generously provided by Dr. Karl Deisseroth. The amplified PCR products were subcloned into pJFRC-MUH using SLIC cloning (Li and Elledge, 2007).

Fly Strains

Th-GAL4 (Friggi-Grelin et al., 2003), Gr5a-GAL4 (Scott et al., 2001), elav-GenesSwitch (Osterwalder et al., 2001), empty promoter- GAL4 (a GAL4 line with a *Drosophila* synthetic core promoter but no enhancer 50 to this promoter, which has been shown to have no detectable expression in the adult CNS (Pfeiffer et al., 2008)), and n-synaptobrevin-GAL4 (nsyb-GAL4) (Pauli et al., 2008) were obtained from Dr. Serge Birman, Dr. Kristin Scott, Dr. Haig Keshishian, Barret Pfeiffer, Dr. Gerald M. Rubin, and Dr. Julie Simpson, respectively. UAS-mCD8::GFP (pJFRC2 described in Pfeiffer et al., 2010), UAS-DsRed (Verkhusha et al., 2001), UAS-GCaMP3.0 (Tian et al., 2009), UAS-dTRPA1 (Hamada et al., 2008), UAS-UPRT (Miller et al., 2009), and LexAop-mCD2::GFP (Lai and Lee, 2006) were generously provided by Dr. Gerald M. Rubin, Dr. Kei Ito, Dr. Loren L Looger, Dr. Paul A. Garrity, Dr. Chris Q. Doe, and Dr. Tzumin Lee, respectively. RNAi lines (Dietzl et

al., 2007) were generously provided by Dr. Barry J. Dickson via the VDRC stock center (UAS-DopEcR RNAi [KK 103494], UAS-DopR2 RNAi [KK 105324], UAS-GFP, and UAS-Dicer2 [on X chromosome]), or the *Drosophila* RNAi Screening Center (UAS-D2R RNAi [JF02025] and UAS-luciferase) (Dietzl et al., 2007). UAS-Dicer2 on X chromo- some are combined with nsyb-GAL4 and called nsyb-GAL4 in this paper. UAS-dTRPA1 on second chromosome and third chromo- some are combined to make a fly strain with two copies of UAS-dTRPA1, which are described as UAS-dTRPA1 in this paper. For DopEcR rescue in Gr5a GRNs in DopEcR mutant (Figure 5D3), Gr5a-GAL4(II); DopEcRc02142(III) and UAS-DopEcR(II); DopEcRc02142(III) were crossed (Loss of DopEcR expression was checked with qRT-PCR).

Cell Culture

HEK293 cells were maintained in Dulbecco's modified Eagle medium (DMEM) (Invitrogen) supplemented with 4 mM L-glutamate (Invitrogen), 10% fetal bovine serum (Invitrogen), and 100 units/ml penicillin and streptomycin. Cells were grown at 37o C with 5% CO2. Cells in 24-well plates were transfected with 0.8 mg each of three plasmids (CMV-Gal4, UAS-DopR-Tango, and LexAop- bgal) by using Lipofectamin2000 (Invitrogen). Twelve hours after the transfection, the medium was changed into medium containing one of the following drugs: dopamine hydrochloride (Sigma); 6,7-ADTN (Sigma); serotonin hydrochloride (Sigma); or octopamine hydrochloride (Sigma), and cultured for 24 hr. Cells were harvested and the activity of b-galactosidase was measured using

‘‘b-Galactosidase Enzyme Assay System with Reporter Lysis Buffer’’ kit (Promega) . Schneider cells (S2 cells) were maintained in fresh complete Schneider’s *Drosophila* Medium (Invitrogen). Effecrene transfection reagenet (QIAGEN) was used for transfection.

TU-Tagging and qPCR

Five hundred transgenic flies carrying Gr5a-GAL4 and UAS-UPRT were fed with 1 mM 4-TU solved in sucrose solution for 8 hr. The proboscis of each fly was excised and collected, and TU-tagged RNA was purified from this tissue as described previously (Miller et al., 2009). cDNA was synthesized using Super Script VILO cDNA Synthesis kit (Invitrogen). Real-time PCR was performed using EXPRESS SYBR GreenER (Invitrogen) and a 7300 Real Time PCR system (Applied biosystems). Cyclophilin1 (Cyp1), a housekeeping gene, was used as a standard (TATA binding protein [tbp] was also used as a standard to give similar results; data not shown). Using melting temperature analysis, each primer pair was confirmed to produce a single PCR product. Primers listed below were used:

Cyp1-f: AGTCTGGCAAGACCTCCAAG Cyp1-r: TTGCATCGCACCTTCTTAAA

DopR1-f: GAAGTCCATCAAGGCGGTAA DopR1-r: AGCCAGGTGAGGATCTTGAA

DopR2-f: GAGGATCTCTGAGCCACTCG DopR2-r: GCAGGCGTAAATCACAGGAT

D2R-f: CACAAGGCCTCGAAAAAGAA D2R-r: GCGAAACTCGGGATTGAATA

DopEcR-f: TTTGACCGGAGAATGGATGT DopEcR-r: ATGCAAATGTGCGTCATGTT

Gr5a-f: CCTTCGTGCTGCTGGTAGTT Gr5a-r: CTTCTTCGTGGGCAGAAGTC

Gr66a-f: ATCTGGTTCGCTGTTTCGTT Gr66a-r: TTATGCTTCTCGTGCGTGTC

qRT-PCR of mutant or RNAi was performed by synthesizing cDNA from the heads of >10 flies and performing Real-time PCR using the same sets of primers described above.

TANGO-Map and Confocal Imaging

DopR-Tango flies or OctR-Tango flies (UAS-DsRed [X]; LexAop-mCD2::GFP [II]; elva-GeneSwitch/ UAS-DopR-Tango [III; or UAS- OctR-Tango]) were collected using CO2 anesthesia and allowed to recover for 2 days. Flies were first dry-starved for 4 hr to make sure they consumed any drugs provided. Then, flies were moved into a vial containing 0.5 mM RU486 mixed in 89 mM sucrose and allowed to feed for 12 or 24 hr (for subsequent drug feeding or starvation experiments, respectively). After this RU486 feeding, flies were moved to either food vials (fed condition), vials containing a wet filter paper (wet-starved condition), or a drug dissolved in 89 mM sucrose (drug-fed condition). Two days later, fly brains were dissected and immunostained. Drugs used for feeding were L-dopa precursor (Sigma, 3 mg/ml), Chlordimeform (CDM) (Sigma, 0.5 mg/ml), SCH23390 (Sigma, 5 mg/ml), and 3-Iodo-L-tyrosine (3IY) (Sigma, 10 mg/ml). In the case of 3IY and SCH23390, feeding was started 5 days before RU486 feeding, or on the day of RU486 feeding, respectively, to achieve effective levels of the drugs. All food vials containing drugs were freshly prepared and drug-fed flies were transferred to fresh drug vials daily for the duration of any feeding period.

Dissected brains were fixed in 4% formaldehyde in PEM (0.1M PIPES, pH 6.95, 2 mM EGTA, 1 mM MgSO4) for 2 hr at 4o C. After three 15 min rinses with PBS, brains were incubated with primary antibodies overnight. Following three 15 min rinses with PBS,

brains were incubated with secondary antibody overnight. Following three rinses, brains were incubated in 50% glycerol in PBS for 2 hr and cleared with VECTASHIELD (VECTA). All procedures were performed in 4o C. For observation of native fluorescence, incubation with primary and secondary antibodies was omitted. An LSM 510 confocal microscope (Carl Zeiss) was used to obtain confocal serial optic sections.

The antibodies used were as follows: Rat anti-HA High Affinity monoclonal antibody (Roche Applied Science), Mouse Tyrosine Hydroxylase Antibody (ImmunoStar), Cy5-conjugated AffiniPure Goat Anti-Mouse IgG (H+L) (Jackson ImmunoResearch), and DyLight549-conjugated AffiniPure Donkey Anti-Rat IgG (H+L) (Jackson ImmunoResearch). Image processing methos are described in Figure S2. Fluorender software (Wan et al., 2009) was used to make 3D reconstructed images of these processed images. Regions of interest (ROIs) were identified based on the signal of the coexpressed UAS-DsRed; in this way, the expression level of the GFP reporter does not affect the size or identification of the ROI. ROIs were measured in single optical sections in the Z plane and not in the projection images.

For labellum ablation experiments, the labellum (not including other parts of the proboscis) was surgically ablated using sharp forceps 24 hr after RU486 feeding. The brains were dissected 2 days after this manipulation.

SNR of DopR-Tango

The SNR is defined as SNR = m/s, where m is the mean signal (signal in a given experimental condition) and s is the standard deviation of the noise (deviation in signal level of control flies). In case of L-dopa feeding (Figures 2B1–2B4) the measured SNR was 4.1,

4.0, 3.9, and 1.5 in the AL, SOG, MB b lobe, and MB g lobe, respectively. The SNR in the g lobe is low due to one outlier point in the control sample, which increased s. The relatively low SNR may due to variability among flies in endogenous factors (e.g., differences in levels of endogeneous baseline DA release) and/or exogenous factors (e.g., differences in the expression level of DopR-Tango, or the extent of DA-independent cleavage).

PER Assays

All PER tests were performed by an experimenter blind to genotype or experimental condition. All experimental flies were maintained on a 12 hr day-night cycle. Newborn female flies were CO2 anesthetized and allowed to recover for more than 3–7 days prior to the assay at 25o C (or 10–14 days at 27o C in the case of RNAi flies, to boost the effect of RNAi). For standard PER assays, 10–20 flies were pre-incubated for the indicated times in a vial containing a piece of filter paper soaked with 1 ml of water, in the case of wet-starved flies, or with 1 ml of 89 mM sucrose solution in the case of sucrose-fed flies. For L-dopa feeding experiments, L-dopa precursor (Sigma) was dissolved in the sucrose solution, and flies maintained with this solution for 2 days (in all experiments with L-dopa feeding, a concentration of 3 mg/ml was used unless otherwise indicated; higher concentrations of L-dopa was not used because of side effects such as changes in body coloration or death). Prepared 10–20 experimental flies were mounted into 200 ml pipetman tips as described previously (Shiraiwa and Carlson, 2007). After mounting, the backs of flies were glued to the pipetman tip to avoid their escape. Flies were allowed 3 min for acclimation prior to testing. A 10 ml pipetman (Gilson) was used to present 0.5 ml drops of water or sucrose solutions to the labellum of the flies. All flies were initially checked for responses to water.

If flies showed a PER to water, they were allowed to drink until they stopped. This procedure was repeated twice, and flies still responding to water were excluded from subsequent testing. Next we tested the responses to stepwise increasing concentrations of sucrose, ranging from 6.25 mM to 400 mM (or 800 mM). The same sets of flies were tested with all concentrations of sucrose. We presented the same concentration of sucrose twice to each fly, and if they extended their proboscis to either of the two presentations, we scored a positive response. Only full extensions of the proboscis, but not partial extensions, were scored as positive. We withdrew the drop as soon as possible after touching it to the labellum, so that flies could not drink the sucrose solution. The fractions of flies showing a PER response as a function of sucrose concentration was calculated. For each experimental condition, an experimental trial using 10–20 flies was repeated independently at least five times to perform statistics (the number of repetitions is the n shown in legends, e.g., n = 5 means the curve represents data from 5 such independent exper- iments. Thus the total number of flies used for the curve is 50–100). The standard PER assay was performed at room temperature (23o C ± 2o C). Mean acceptance thresholds (MATs) (Long et al., 1986) were calculated as described below in the section ‘‘Calculation of Mat.’’

For TrpA1 experiments, flies were raised at 21o C. Flies were mounted at 23o C, and PER assays performed at either 23o C or 30o C. The PER test was performed immediately after transferring the flies to different temperature and finished within 10 min. Th-GAL4;UAS-dTRPA1 flies showed partial proboscis extensions without sugar stimulation at 30o C but rarely showed full extensions without the stimulation. Only full extensions were scored as positive responses.

Calculation of MAT

In order to calculate MAT, sugar concentration where 50% of flies show PER, sigmoid interpolation was performed (PER response curves were fitted into sigmoid curves). The sigmoid curve can be described as a logistic function:

Ss: fraction of flies showing PER on different sugar concentration. Scon: sugar concentration (mM).

MAT: sugar concentration where 50% of flies show PER.

as: slope of the sigmoid curve.

For all experimental data, polynomial curve fitting, which finds the coefficients that fit the data by the least-squares method, was done with Matlab (MathWorks). Goodness-of-fit was tested by two-way ANOVA between the actual PER response curves, and the sigmoid curve with the calculated coefficients (Figure S3B). All wild-type sucrose response data were well-fit by a sigmoid curve (two-way ANOVA). The value of MAT decreased with starvation time, while as shows a statistical significant decrease after
2 days of starvation or L-dopa feeding ($p < 0.05$ by one-way ANOVA followed by a post-hoc t test with Bonferroni correction; Fig- ure S3C). Decrease in MAT indicates the increase in behavioral sugar sensitivity, and decrease in as implies (1) increase in distin- guishability between two sugar concentration, (2) increase in sugar sensitivity at lower sugar concentration, or (3) increase in vari- ation in sugar sensitivity among flies. Because we are interested in the changes in behavioral sugar sensitivity, MAT was used for data analysis. It should be noted that the use of MAT as a metric for comparison does not require that the

PER response be titrated to saturation for each experimental or control condition, because MAT is a probabilistic measure (i.e., it measures the sucrose concen- tration at which 50% of the flies in a population are likely to show a PER response), whose value by definition therefore ranges between 0 and 1 (Long et al., 1986). The values of MAT are normally distributed among the data obtained from wild-type flies under the same condition of food deprivation (Lillifors test and Jarque-BARA test, and also checked by linearity in a probability plot). Thus parametric statistical tests were used for analysis of MAT data. With the exception of the data from the TH-Gal4;UAS-TrpA1 exper- iment at 30o C (Figure 4C1), and the DopEcR mutant fed with L-dopa (Figure 5A2), all of the experimental curves were well-fit by sigmoid curves (two-way ANOVA). Therefore, the value of MAT (50% probability of a PER response) was interpolated from the experimental data based on the sigmoidal curve-fitting. In case of the DopEcR mutant fed with L-dopa (Figures 5A2 and 5A3), the MAT was estimated by linear interpolation between the two nearest data points above and below a 50% response. In addition, to the comparison of MAT values, these experiments were also analyzed using two-way ANOVA of experimental versus control curves.

ChR2 Assay

All trans-Retinal powder (Sigma) was stored in -20o C as 20 mM solution dissolved in ethanol. After overnight wet starvation, Gr5a- GAL4;UAS-ChR2(C128T) flies were transferred into a vial with 200 mM all trans-Retinal diluted in 89 mM sucrose, and allowed to feed for 24 hr. These vials were maintained in the dark to avoid photoisomerization of all

trans-Retinal. After retinal feeding, flies were either fed or wet starved for 1 day,or fed with L-dopa precursor (3 mg/ml) for 2 days.

Flies were mounted into pipet tips, as in the standard PER assay, and placed under a fluorescent microscope (Lecia MZ FLIII Fluo- rescence Stereomicroscope). Light emitted by a standard mercury lamp (HBO 100w/2, OSRAM) equipped with a GFP filter (Leica, 470/40 nm: center wavelength/bandwidth) was used to stimulate ChR2-expressing flies. The light was switched on by moving the filter manually. The fraction of flies showing a full proboscis extension in response to light in the first 5 s was scored. The intensity of the light was controlled by changing the magnification of the microscope. The light power density at 488 nm was measured with Power meter (Model 1931, New port). Each fly was tested only at a single intensity of light because repeated exposure to light decreased the behavioral response.

Calcium Imaging

The protocol for calcium imaging was modified from that described in Marella et al. (2006). After a brief anesthesia on ice, flies were mounted on a thin plastic plate with wax as shown in Figure 6B. The top side of the plate contained a well made with wax, and the fly head was immersed in ice-cold Ca2+ free saline (108 mM NaCl, 5 mM KCl, 8.2 mM MgCl2, 4 mM NaHCO3, 1 mM NaH2PO4, 15 mM Ribose, 5 mM HEPES, pH 7.5; note that Ribose, which does not stimulate *Drosophila* sugar-sensing neurons, is used instead of other sugars). In this saline bath, the antennae and cuticle at the anterior side of the fly head capsule were surgically removed with sharp forceps, so that the SOG could be imaged. The fat body, air sacs, and esophagus were gently removed to give a clear view of the brain and to minimize

its movement. At the bottom side of the plate, a glass tube was mounted with the opening facing the proboscis of the mounted fly. A piece of twisted Kimwipe was placed just behind the fly. During imaging, a sucrose solution was delivered from the glass tubing to stimulate gustatory neurons in the proboscis and was removed by the Kimwipe.

Following dissection, the ice-cold Ca2+ free saline was removed and the fly brain was immersed in 1 ml of room-temperature imaging

saline (108 mM NaCl, 5 mM KCl, 2 mM CaCl2, 8.2 mM MgCl2, 4 mM NaHCO3, 1 mM NaH2PO4, 15 mM Ribose, 5 mM HEPES, pH 7.5). This setup was moved under an Ultima two-photon laser scanning microscope (Prarie Instruments, Inc) with a 40 3 0.8 N.A. objective (Olympus, Inc). The glass tubing was connected to four silicon tubes with a plastic manifold (MP-4, Warner Instruments). Each silicon tube was connected to 50 ml syringes filled with either 15 ml of 0 mM, 25 mM, 100 mM, or 400 mM sucrose dissolved in the imaging saline solution. The flow of sucrose solution was controlled using electrically triggered pinch valves (ALA-VM8, ALA Scientific Instru- ments) that compressed the silicon tubes between the syringes and the manifold. The timing of valve opening was controlled by the two-photon acquisition system and its software (Prairie view and Trigger Sync, Prairie) so that the timing was linked with the image acquisition. ! DF/F dt, the integral of DF/F during the period of exposure to each stimulus, was calculated using MatLab (MathWorks). Because the behavioral effect of L-dopa feeding was smaller in Gr5a-GAL4; UAS-GCaMP3.0 flies compared to other flies with different genetic backgrounds, we fed these flies with 5 mg/ml of L-dopa precursor (rather than the standard 3 mg/ml) for both imaging and the PER. PER assays of Gr5a-GAL4; UAS-GCaMP3.0 flies were performed as described in the PER assay.

For direct DA exposure during imaging (Figures 6F1–6F3), first the GCaMP response to sugar was measured as described above. Then 10 ml of 100 mM dopamine chloride (dissolved in the imaging saline) was added to 1 ml of imaging saline in which the fly brain was immersed using a pipetman, so that the final concentration of DA became 1 mM. The 100 3 DA stock solution was prepared freshly just before each experiment to avoid oxidation. After 5 min of incubation, the same brain was scanned before and during stim- ulation with different concentrations of sucrose. These responses were imaged in the same presynaptic terminals that were imaged prior to DA addition, and a comparison of the calcium signal in each condition (0 mM, 25 mM, 100 mM, and 400 mM sucrose) was made pre- versus post-DA addition.. To do this, the average fluorescence signal in the absence of sucrose (0 mM), prior to DA addi- tion, was used as F to calculate DF/F both before and after DA addition (DF/Fbefore DA = (Ft_before-F0_before)/F0_before and DF/Fafter DA = (Ft_after-F0_before)/F0_before, where Ft is F at time t). From these values, we calculated the fold increase in F as the ratio of the integrated signals post/pre DA addition (Figure 6G). This analysis could be performed because the signals both before and after addition of DA were scanned from the same neurons in the same fly. To eliminate the contribution of motion artifacts, we ensured that scans were performed on the same focal plane for each measurement. To further control for nonspecific changes in fluorescence due to move- ment during addition of the concentrated DA solution to the imaging bath, we imaged a series of flies in which we added 10 ml of imaging saline (without DA) to the bath.

Electrophysiology

The tip recording method was used for the recording of the electrophysiological responses of labellar taste neurons (Hodgson et al., 1955; Weiss et al., 2011). Briefly, the fly was mounted and immobilized for recording by inserting a pulled glass capillary (BF150-86- 10, Sutter instruments) from the dorsal surface of the thorax to the tip of the labellum, passing through the cervical connective and the head. The mounting glass capillary was filled with recording solution (7.5 g/l NaCl, 0.35 g/l KCl, 0.279 g/l CaCl2$2H2O and 11.915 g/l HEPES [Sigma-Aldrich]) and served as indifferent electrode. Another glass capillary, pulled to a tip diameter of 10 to 20 mm and filled with tastant solution, was used for both introducing the taste molecules to the tip of the relevant sensillum and for the recording of the electrophysiological responses of the gustatory neurons innervating this sensillum. Sucrose was dissolved in water solution contain- ing 30 mM tri-choline chloride (TCC; Sigma-Aldrich), as an electrolyte. TCC solution was used as a control to monitor the sponta- neous activity of the sugar neurons in the absence of sucrose.

In each recording, the relevant sensillum was exposed to the tastant solution or to the control solution for 7 s. The recordings were made by using MultiClamp 700B amplifier and Digidata 1440A A/D converter (Molecular Devices). The recorded data were sampled at a rate of 10 KHz, filtered (band pass filter between 100 Hz and 3 KHz) and stored on a PC hard drive with Clampex 10 software (Molecular Devices). The data were analyzed by sorting the action potentials and measuring their frequency in the indicated time windows along the trace with Clampfit software (Molecular Devices). Only the first exposure of sensilla that responded to high concentrations of sucrose (100 mM) were included in the analysis. In every experiment, several sensilla from the same fly were tested.

SUPPLEMENTAL REFERENCES

Berndt, A., Yizhar, O., Gunaydin, L.A., Hegemann, P., and Deisseroth, K. (2009). Bi-stable neural state switches. Nat. Neurosci. 12, 229–234.

Dietzl, G., Chen, D., Schnorrer, F., Su, K.C., Barinova, Y., Fellner, M., Gasser, B., Kinsey, K., Oppel, S., Scheiblauer, S., et al. (2007). A genome-wide transgenic RNAi library for conditional gene inactivation in *Drosophila*. Nature 448, 151–156.

Donnelly, M.L., Hughes, L.E., Luke, G., Mendoza, H., ten Dam, E., Gani, D., and Ryan, M.D. (2001). The 'cleavage' activities of foot-and-mouth disease virus 2A site-directed mutants and naturally occurring '2A-like' sequences. J. Gen. Virol. 82, 1027–1041.

Friggi-Grelin, F., Coulom, H., Meller, M., Gomez, D., Hirsh, J., and Birman, S. (2003). Targeted gene expression in *Drosophila* dopaminergic cells using regulatory sequences from tyrosine hydroxylase. J. Neurobiol. 54, 618–627.

Groth, A.C., Fish, M., Nusse, R., and Calos, M.P. (2004). Construction of transgenic *Drosophila* by using the site-specific integrase from phage phiC31. Genetics 166, 1775–1782.

Hodgson, E.S., Lettvin, J.Y., and Roeder, K.D. (1955). Physiology of a primary chemoreceptor unit. Science 122, 417–418.

Lai, S.L., and Lee, T. (2006). Genetic mosaic with dual binary transcriptional systems in *Drosophila*. Nat. Neurosci. 9, 703–709.

Li, M.Z., and Elledge, S.J. (2007). Harnessing homologous recombination in vitro to generate recombinant DNA via SLIC. Nat. Methods 4, 251–256. Lim, J.S. (1990). Two-Dimensional Signal and Image Processing (Englewood Cliffs, NJ: Prentice Hall).

Mank, M., Santos, A.F., Direnberger, S., Mrsic-Flogel, T.D., Hofer, S.B., Stein, V., Hendel, T., Reiff, D.F., Levelt, C., Borst, A., et al. (2008). A genetically encoded calcium indicator for chronic in vivo two-photon imaging. Nat. Methods 5, 805–811.

Markstein, M., Pitsouli, C., Villalta, C., Celniker, S.E., and Perrimon, N. (2008). Exploiting position effects and the gypsy retrovirus insulator to engineer precisely expressed transgenes. Nat. Genet. 40, 476–483.

Ni, J.Q., Markstein, M., Binari, R., Pfeiffer, B., Liu, L.P., Villalta, C., Booker, M., Perkins, L., and Perrimon, N. (2008). Vector and parameters for targeted transgenic RNA interference in *Drosophila* melanogaster. Nat. Methods 5, 49–51.

Pfeiffer, B.D., Jenett, A., Hammonds, A.S., Ngo, T.T., Misra, S., Murphy, C., Scully, A., Carlson, J.W., Wan, K.H., Laverty, T.R., et al. (2008). Tools for neuro- anatomy and neurogenetics in *Drosophila*. Proc. Natl. Acad. Sci. USA 105, 9715–9720.

Pfeiffer, B.D., Ngo, T.T., Hibbard, K.L., Murphy, C., Jenett, A., Truman, J.W., and Rubin, G.M. (2010). Refinement of tools for targeted gene expression in *Drosophila*. Genetics 186, 735–755.

Shafer, O.T., Kim, D.J., Dunbar-Yaffe, R., Nikolaev, V.O., Lohse, M.J., and Taghert, P.H. (2008). Widespread receptivity to neuropeptide PDF throughout the neuronal circadian clock network of *Drosophila* revealed by real-time cyclic AMP imaging. Neuron 58, 223–237.

Verkhusha, V.V., Otsuna, H., Awasaki, T., Oda, H., Tsukita, S., and Ito, K. (2001). An enhanced mutant of red fluorescent protein DsRed for double labeling and developmental timer of neural fiber bundle formation. J. Biol. Chem. 276, 29621–29624.

Wan, Y., Otsuna, H., Chien, C.B., and Hansen, C. (2009). An interactive visualization tool for multi-channel confocal microscopy data in neurobiology research. IEEE Trans. Vis. Comput. Graph. 15, 1489–1496.

Wilson, R.I., Turner, G.C., and Laurent, G. (2004). Transformation of olfactory representations in the *Drosophila* antennal lobe. Science 303, 366–370.

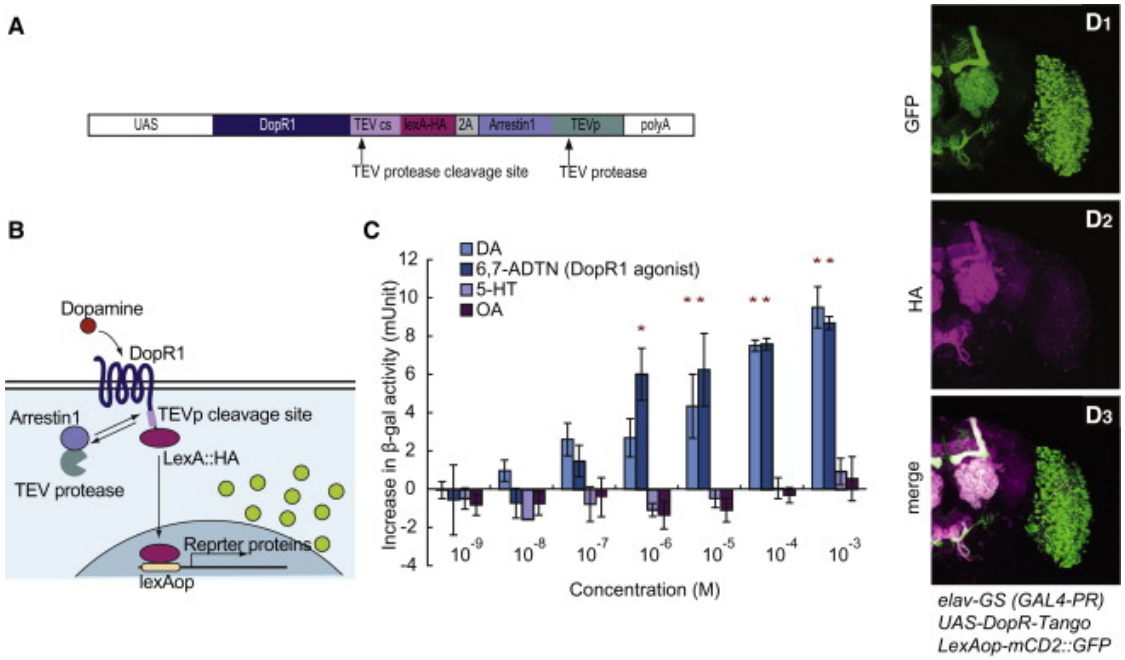
A
UAS
DopR1
TEV cs
lexA-HA
2A
Arrestin1
TEVp
polyA
TEV protease cleavage site
TEV protease
B
Dopamine
DopR1
Arrestin1
TEVp cleavage site
LexA::HA
TEV protease
Reprter proteins
lexAop
C
DA
6,7-ADTN (DopR1 agonist)
5-HT
OA
Increase in β-gal activity (mUnit)
Concentration (M)
D1
D2
D3
GFP
HA
merge
elav-GS (GAL4-PR)
UAS-DopR-Tango
LexAop-mCD2::GFP

Figure 1. Characterization of DopR-Tango In Vitro and in Drosophila

(A) Design of the DopR-Tango transgene; note HA epitope tag on LexA. (B) Schematic illustrating DopR-Tango mechanism.

(C) DopR-Tango reporter (b-gal) activity in response to indicated ligands in HEK293 cells cotransfected with CMV-GAL4, UAS-DopR-Tango, and LexAop-b-gal. Increases in b-gal activity relative to background are shown. Error bars represent the standard error of mean (SEM). Asterisks represent statistically significant increases ($p < 0.05$, t test with Bonferroni correction, $n = 3$).

(D) Representative confocal projections of whole-mount brains from DopR-Tango flies visualized with GFP native fluorescence (green) and anti-HA immuno- staining (magenta). See also Figure S1 and Table S1.

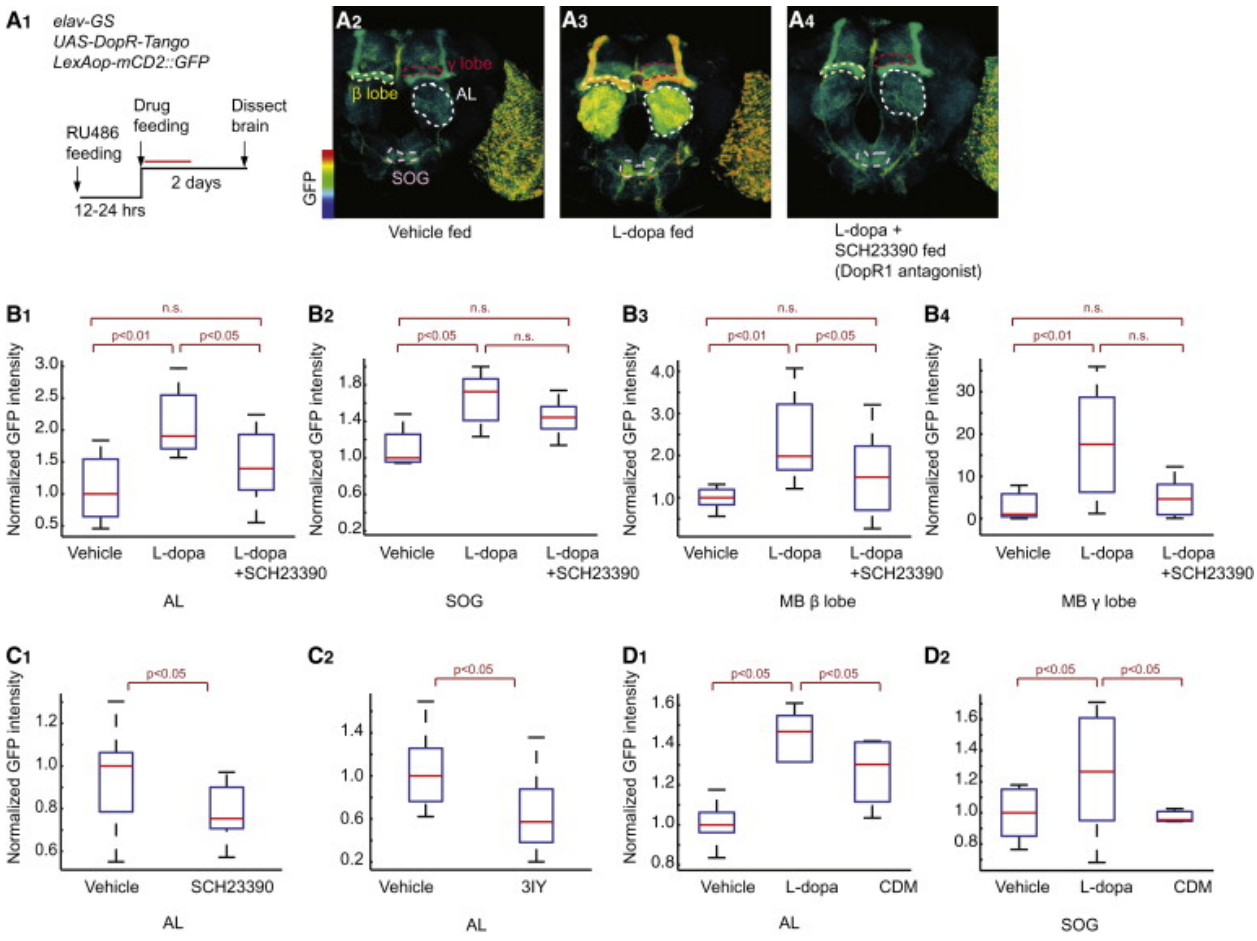
A1
elav-GS
UAS-DopR-Tango
LexAop-mCD2::GFP
RU486 feeding
Drug feeding
Dissect brain
2 days
12-24 hrs
A2
γ lobe
β lobe
AL
SOG
GFP
Vehicle fed
A3
L-dopa fed
A4
L-dopa + SCH23390 fed (DopR1 antagonist)
B1
B2
B3
B4
Normalized GFP intensity
n.s.
p<0.01
p<0.05
Vehicle
L-dopa
L-dopa +SCH23390
AL
SOG
MB β lobe
MB γ lobe
C1
C2
D1
D2
SCH23390
3IY
CDM

Figure 2. Characterization of DopR-Tango in Transgenic Flies

(A) Specific activation of DopR-Tango by L-dopa in vivo. (A1) Experimental design. Red line represents 24 hr detection window for Tango reporter (see Fig- ure S1E). (A2–4) Pseudocolor images of DopR-Tango reporter (GFP) expression; color scale to left. See Figure S2 for image processing details. Neuropils indicated by dashed outlines are as follows: AL, antennal lobe (white); SOG, subesophageal ganglion (pink); mushroom body (MB) b and g lobes (yellow and red, respectively).

(B–D) Quantification of reporter expression in the indicated neuropils. SCH23390, D1 receptor antagonist; 3IY (3-iodotyrosine, DA synthesis inhibitor). Unless otherwise indicated, p values in this and subsequent figures represent Kruskal-Wallis one-way ANOVA followed by Mann-Whitney U tests with Bonferroni correction. $n > 5$ for each experimental group. Boxplots: lower and upper whiskers represent 1.5 interquartile-range (IQR) of the lower and upper quartiles, respectively; boxes indicate lower quartile, median, and upper quartile, from bottom to top.

See also Figure S2.

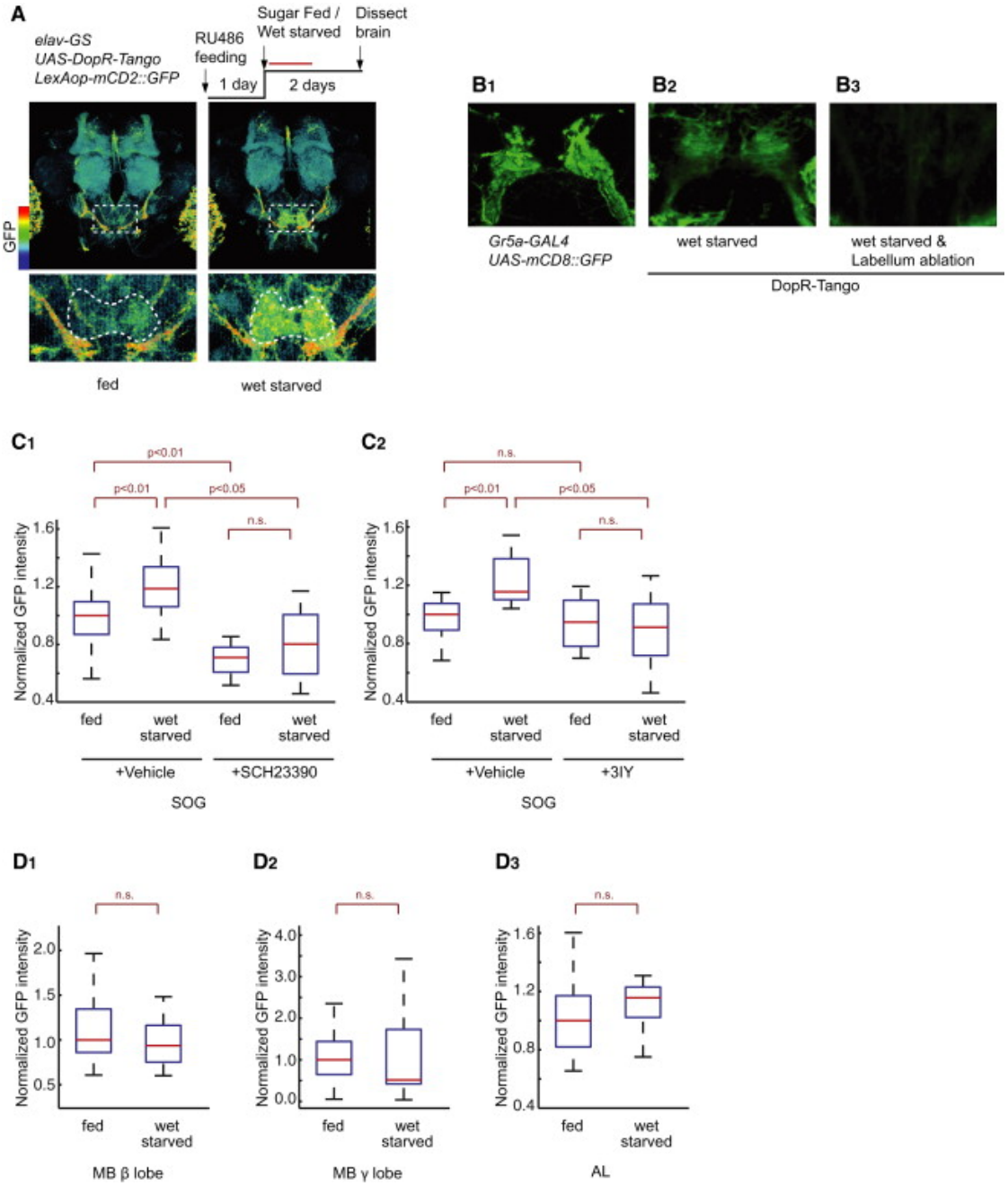
A
elav-GS
UAS-DopR-Tango
LexAop-mCD2::GFP
RU486 feeding
1 day
Sugar Fed / Wet starved
2 days
Dissect brain
GFP
fed
wet starved
B1
B2
B3
Gr5a-GAL4
UAS-mCD8::GFP
wet starved
wet starved & Labellum ablation
DopR-Tango
C1
C2
p<0.01
p<0.01
p<0.05
n.s.
Normalized GFP intensity
fed
wet starved
+Vehicle
+SCH23390
+3IY
SOG
D1
D2
D3
MB β lobe
MB γ lobe
AL

Figure 3. DA Release onto GRNs Increases during Starvation

(A) Experimental design and normalized Tango reporter (GFP) expression in brains of fed versus 48 hr wet-starved flies; color scale to left. Laser scanning was performed at a higher gain setting to increase sensitivity. Dashed boxes delineate SOG (enlarged in lower panels). White dashed line in lower panels show ROIs used for quantification, based on UAS-DsRed expression in SOG neuropil.

(B) Representative confocal projections of sugar-sensing GRNs (B1) and Tango reporter expression (B2 and B3) in the SOG of normal (B1 and B2) or labellum- ablated (B3) flies.

(C and D) Normalized GFP expression in DopR-Tango flies quantified in the SOG (C1–2), MB b lobe (D1), MB g lobe (D2), and AL (D3). $n > 6$ for each experimental group.

See also Figure S3.

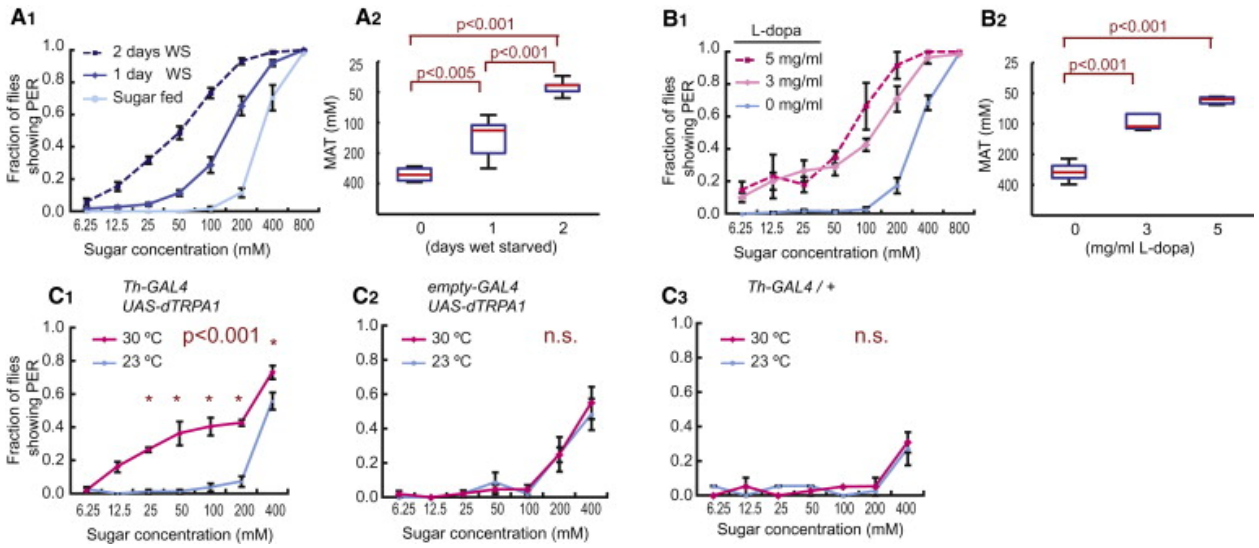
A1
2 days WS
1 day WS
Sugar fed
Fraction of flies showing PER
Sugar concentration (mM)
A2
p<0.001
p<0.001
p<0.005
MAT (mM)
(days wet starved)
B1
L-dopa
5 mg/ml
3 mg/ml
0 mg/ml
Fraction of flies showing PER
Sugar concentration (mM)
B2
p<0.001
p<0.001
MAT (mM)
(mg/ml L-dopa)
C1
Th-GAL4
UAS-dTRPA1
30 °C
23 °C
p<0.001
Fraction of flies showing PER
Sugar concentration (mM)
C2
empty-GAL4
UAS-dTRPA1
30 °C
23 °C
n.s.
Sugar concentration (mM)
C3
Th-GAL4 / +
30 °C
23 °C
n.s.
Sugar concentration (mM)

Figure 4. Hunger and DA Increase the Sugar Sensitivity of the PER

(A) Fraction of fed versus wet-starved (WS) flies showing a PER at different concentrations of sucrose. (A1) Average responses. Error bars represent SEM. (A2) MAT (mean acceptance threshold; the sugar concentration where 50% of the flies show PER), plotted as a function of starvation time. One-way ANOVA followed by t test with Bonferroni correction ($n > 4$ for each experimental group).

(B) PER responses in nonstarved flies fed with the indicated concentrations of L-dopa ($n > 4$ for each experimental group).

(C) Genetic activation of DA neurons increases sugar sensitivity. PER versus sugar concentration curves are shown for experimental Th-GAL4;UAS-dTRPA1 (C1) and genetic control flies (C2 and C3) at the permissive (red) and nonpermissive (blue) temperatures for dTRPA1. Within-genotype differences between temperatures were analyzed using a two-way ANOVA with replication followed by post-hoc t tests with the Bonferroni correction at each sugar concentration.

*$p < 0.05$; n.s., not significant ($n > 4$ for each experimental group). See also Figure S3.

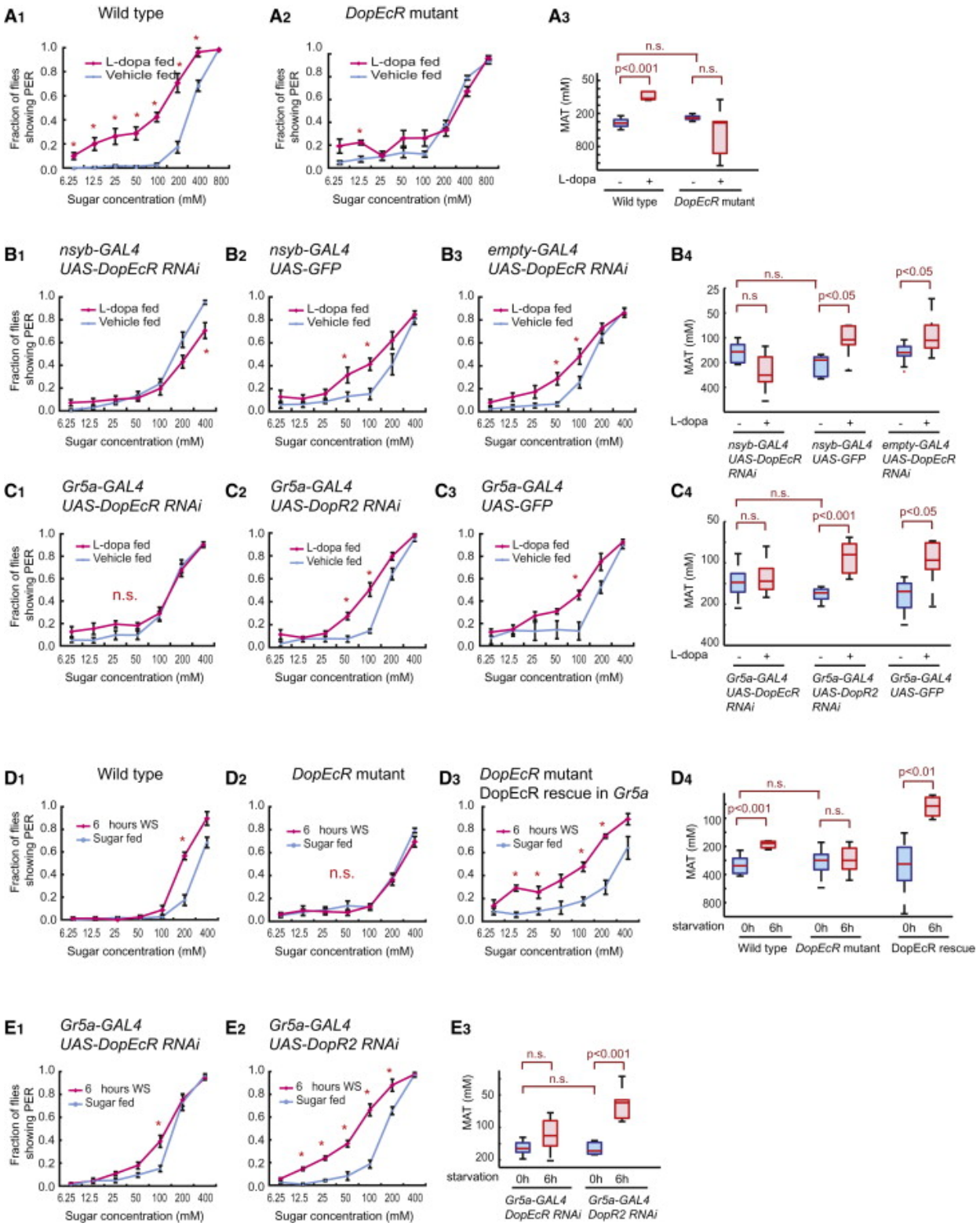
A1
Wild type
L-dopa fed
Vehicle fed
Fraction of flies showing PER
Sugar concentration (mM)
A2
DopEcR mutant
A3
n.s.
p<0.001
MAT (mM)
L-dopa
Wild type
DopEcR mutant
B1
nsyb-GAL4
UAS-DopEcR RNAi
B2
nsyb-GAL4
UAS-GFP
B3
empty-GAL4
UAS-DopEcR RNAi
B4
p<0.05
C1
Gr5a-GAL4
UAS-DopEcR RNAi
C2
Gr5a-GAL4
UAS-DopR2 RNAi
C3
Gr5a-GAL4
UAS-GFP
C4
p<0.001
D1
Wild type
6 hours WS
Sugar fed
D2
DopEcR mutant
D3
DopEcR mutant
DopEcR rescue in Gr5a
D4
p<0.01
starvation
0h
6h
DopEcR rescue
E1
Gr5a-GAL4
UAS-DopEcR RNAi
E2
Gr5a-GAL4
UAS-DopR2 RNAi
E3

Figure 5. DopEcR Expression in Gr5a GRNs Is Necessary and Sufficient for L-dopa Feeding- and Starvation-Induced Increases in PER Sugar Sensitivity

(A) Sugar sensitivity of wild-type and DopEcR mutant flies after L-dopa (3 mg/ml) feeding. The wild-type data are identical to Figure 4B1 and are reproduced here for ease of comparison.

(B–E) Sugar sensitivity of RNAi flies or mutant flies after L-dopa feeding (B and C) or 6 hr wet starvation (WS; D and E). UAS-DopEcR RNAi and UAS-DopR2 RNAi are in the same genetic background. Note that DopR2 is not expressed at a detectable level in sugar-sensing GRNs (Figure S4A).

In PER curves, error bars represent SEM. Boxplots: lower and upper whiskers represent 1.5 IQR of the lower and upper quartiles, respectively; boxes indicate lower quartile, median, and upper quartile, from bottom to top. The statistical significance of within-genotype differences between PER curves, or MAT values, for L-dopa versus vehicle treatment or feeding versus wet starvation was analyzed using two-way ANOVA with replication followed by post-hoc t tests with Bonferroni correction. *$p < 0.05$; n.s., not significant ($n > 4$ for each experimental group). A significant interaction between genotype and feeding manipulation was revealed by a two-way ANOVA in (A3) $p < 0.0001$, (B4) $p < 0.005$, (C4) $p < 0.01$, (D4) $p < 0.05$, and (E3) $p < 0.005$, indicating that the genetic manipulations interfered with the effect of wet starvation or L-dopa feeding.

See also Figure S4.

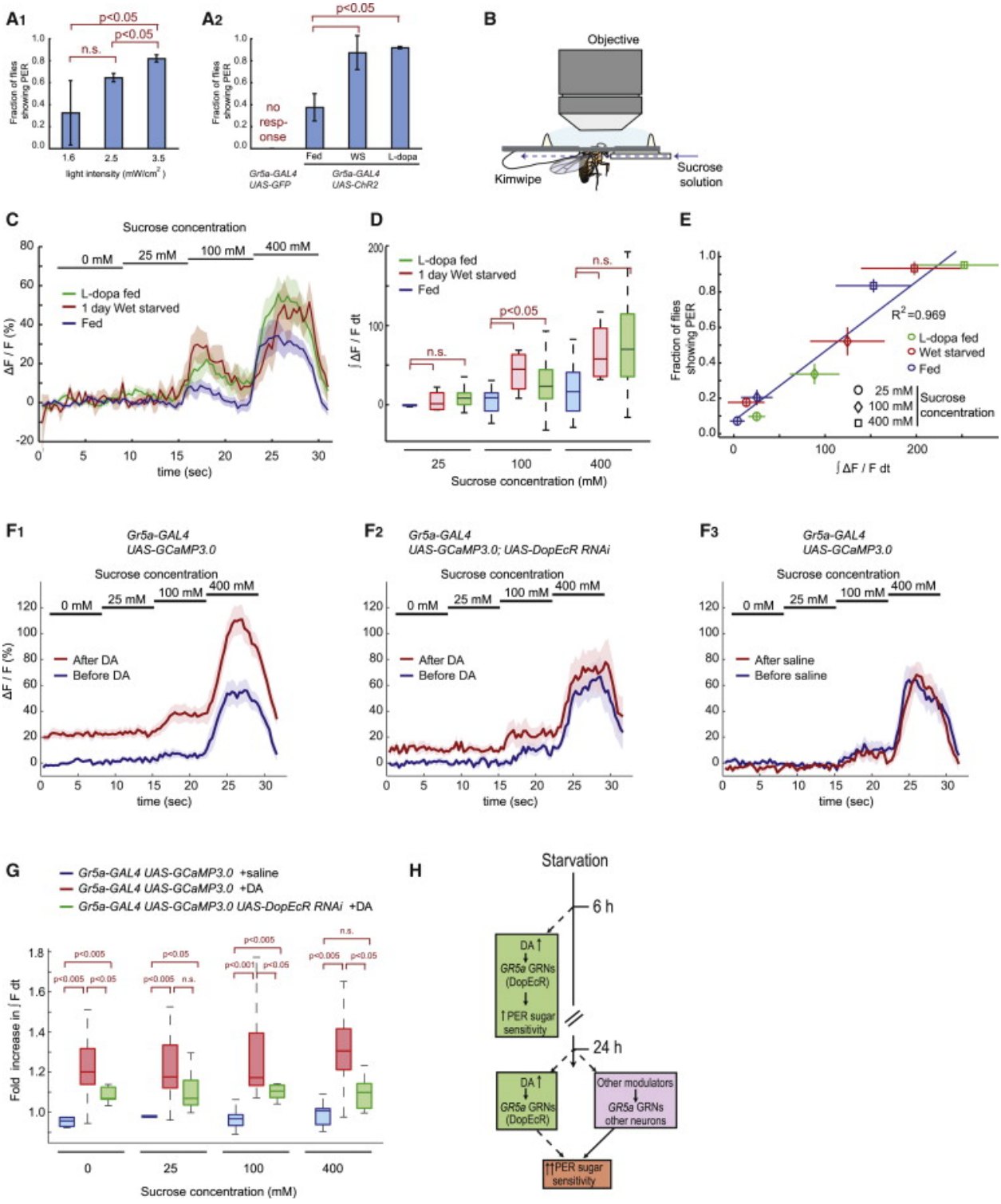
A1
p<0.05
p<0.05
n.s.
Fraction of flies showing PER
light intensity (mW/cm2)
A2
p<0.05
no resp-onse
Fed
WS
L-dopa
Gr5a-GAL4 UAS-GFP
Gr5a-GAL4 UAS-ChR2
B
Objective
Kimwipe
Sucrose solution
C
Sucrose concentration
0 mM
25 mM
100 mM
400 mM
L-dopa fed
1 day Wet starved
Fed
ΔF / F (%)
time (sec)
D
L-dopa fed
1 day Wet starved
Fed
n.s.
p<0.05
n.s.
∫ ΔF / F dt
Sucrose concentration (mM)
E
Fraction of flies showing PER
R2=0.969
L-dopa fed
Wet starved
Fed
25 mM
100 mM
400 mM
Sucrose concentration
∫ ΔF / F dt
F1
Gr5a-GAL4
UAS-GCaMP3.0
Sucrose concentration
0 mM
25 mM
100 mM
400 mM
After DA
Before DA
ΔF / F (%)
time (sec)
F2
Gr5a-GAL4
UAS-GCaMP3.0; UAS-DopEcR RNAi
Sucrose concentration
0 mM
25 mM
100 mM
400 mM
After DA
Before DA
time (sec)
F3
Gr5a-GAL4
UAS-GCaMP3.0
Sucrose concentration
0 mM
25 mM
100 mM
400 mM
After saline
Before saline
time (sec)
G
Gr5a-GAL4 UAS-GCaMP3.0 +saline
Gr5a-GAL4 UAS-GCaMP3.0 +DA
Gr5a-GAL4 UAS-GCaMP3.0 UAS-DopEcR RNAi +DA
Fold increase in ∫ F dt
Sucrose concentration (mM)
H
Starvation
6 h
DA↑
GR5a GRNs (DopEcR)
↑PER sugar sensitivity
24 h
DA↑
GR5a GRNs (DopEcR)
Other modulators
GR5a GRNs other neurons
↑↑PER sugar sensitivity

Figure 6. Starvation or L-dopa Feeding Enhance Calcium Transients in Sugar-Sensing GRNs

(A) Channelrhodopsin 2-evoked PER. Gr5a-GAL4;UAS-ChR2 or Gr5a-GAL4;UAS-GFP control flies were stimulated with blue (470/40 nm: center wavelength/ bandwidth) light at the indicated intensities (A1) or at 1.6 mW/cm2 under the indicated conditions (A2). Error bars represent SEM. (B) The setup for calcium imaging of sugar-sensing GRNs. Blue dashed arrow indicates direction of flow of sugar solution.

(C) Responses (DF/F) to different concentrations of sucrose in the central projections of sugar-sensing GRNs in Gr5a-GAL4;UAS-GCaMP3.0 flies. The solid lines represent average trace, and envelopes indicate SEM (n > 7 for each condition).

(D) Quantification of fluorescent changes. ! DF/F dt, integrated DF/F during stimulus period. Data analyzed from (C); Mann-Whitney U tests with Bonferroni correction.

(E) Correlation between GCaMP signals (analyzed in B and C) and behavioral responses (PER) of Gr5a-GAL4;UAS-GCaMP3.0 flies (n > 4). Error bars represent SEM.

(F) Responses (DF/F) to different concentrations of sucrose in the central projections of sugar-sensing GRNs before and after 5 min exposure of the brain to saline with or without 1 mM DA. The solid lines represent average trace, and envelopes indicate SEM (n > 7 for each condition).

(G) Fold increase in !F dt (!F dt[After DA]/!F dt[Before DA]) during each stimulus period, calculated from the data in (F). Mann-Whitney U tests with Bonferroni correction.

(H) Schematic illustrating mechanisms controlling starvation-induced increases in the sugar sensitivity of PER behavior. See also Figure S5.

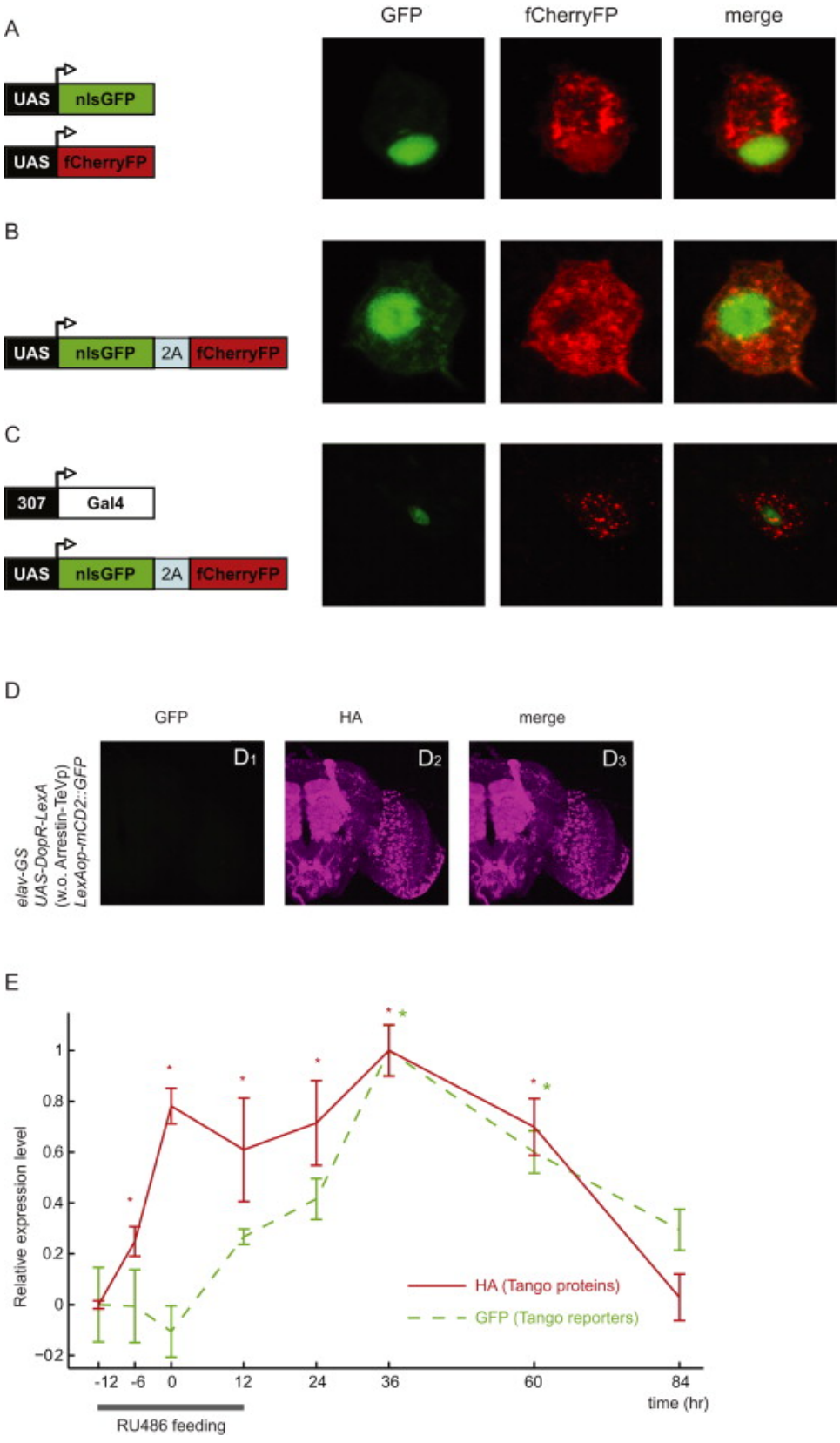
A
GFP
fCherryFP
merge
UAS
nlsGFP
UAS
fCherryFP
B
UAS
nlsGFP
2A
fCherryFP
C
307
Gal4
UAS
nlsGFP
2A
fCherryFP
D
GFP
HA
merge
D1
D2
D3
elav-GS
UAS-DopR-LexA
(w.o. Arrestin-TeVp)
LexAop-mCD2::GFP
E
Relative expression level
1
0.8
0.6
0.4
0.2
0
-02
-12
-6
0
12
24
36
60
84
time (hr)
HA (Tango proteins)
GFP (Tango reporters)
RU486 feeding

Figure S1. Bicistronic Expression using a 2A Peptide in Drosophila and Kinetics of DopR-Tango Activation In Vivo, Related to Figure 1

(A and B) Characterization of 2A peptide in Drosophila Schneider 2 (S2) cells. nls::GFP (GFP tagged with nuclear localization signal; green) and fCherryFP (mCherry tagged with farnesylation signal; red) were expressed from two separate cotransfected vectors (UAS-nls::GFP and UAS-fCherryFP; A), or from a single vector with a 2A peptide (UAS-nlsGFP-2A-fCherryFP; B). Actin promoter-Gal4 driver was used to induce the expression. The nuclear-cytoplasmic segregation of GFP and fCherry expression, respectively, in (B) indicates that the 2A peptide is functional in S2 cells.

(C) The 2A peptide is functional in the Drosophila brain in vivo. UAS-nlsGFP-2A-fCherryFP was expressed in a giant fiber neuron using the 307-GAL4 driver. The nuclear-cytoplasmic segregation of GFP and fCherry signals implies cleavage of the 2A sequence in vivo.

(D) DopR Tango reporter expression is dependent on coexpression of Arrestin-TEVp. Representative confocal projections of a whole-mount brain from DopR- Tango flies expressing UAS-DopR-TEVcs-LexA without Arrestin1-TEVp coexpression, visualized using GFP native fluorescence (green; D1) and anti-HA immunostaining (magenta; D2). Note absence of GFP reporter expression.

(E) Time course of DopR-Tango and GFP reporter expression in DopR-Tango flies coexpressing elav-GeneSwitch after RU486 feeding. x axis/abcissa (time)

represents the time after DopR-Tango expression (determined by anti-HA antibody staining) reached steady-state levels (RU486 was fed for 24 hr between -12 to 12 hr). Fluorescent pixel intensities were quantified in the antennal lobe, and are expressed relative to baseline values determined at t = -12 hr. One-way ANOVA was followed by t test with Bonferroni correction (*: signal is significantly different from that of time point 0). Error bars represent standard deviation, n = 2–

4 for each experimental group.

A time course of DopR-Tango and GFP reporter expression (panel E) indicated that the expression of the former starts within 6–12 hr after the initiation of RU486 feeding, while the level of GFP reporter expression reaches a statistically significant increase 36–48 hr after that time. This implies that it takes >24 hr for the GFP reporter to accumulate to significant levels after DopR-Tango expression. This interval likely reflects the sum of the times required for (1) LexA to be cleaved after the expression of DopR-Tango, (2) LexA to be transported to the nucleus and activate GFP transcription, and (3) translation and transport of GFP to various neuropils. Therefore, in order to ensure a detectable change in GFP reporter expression following experimental manipulations of DopR-Tango flies, such as drug feeding, we chose to dissect fly brains 48 hr after the starting point of manipulation. The level of GFP reporter expression measured at this end point likely reflects the integration of DA signal over the first 24 hr of the manipulation (Figures 2A and 3A, red line). Based on our data, additional signaling in the second 24 hr period likely does not yield a sufficient additional increase in reporter expression to contribute significantly to the signal detected at the 48 hr end point.

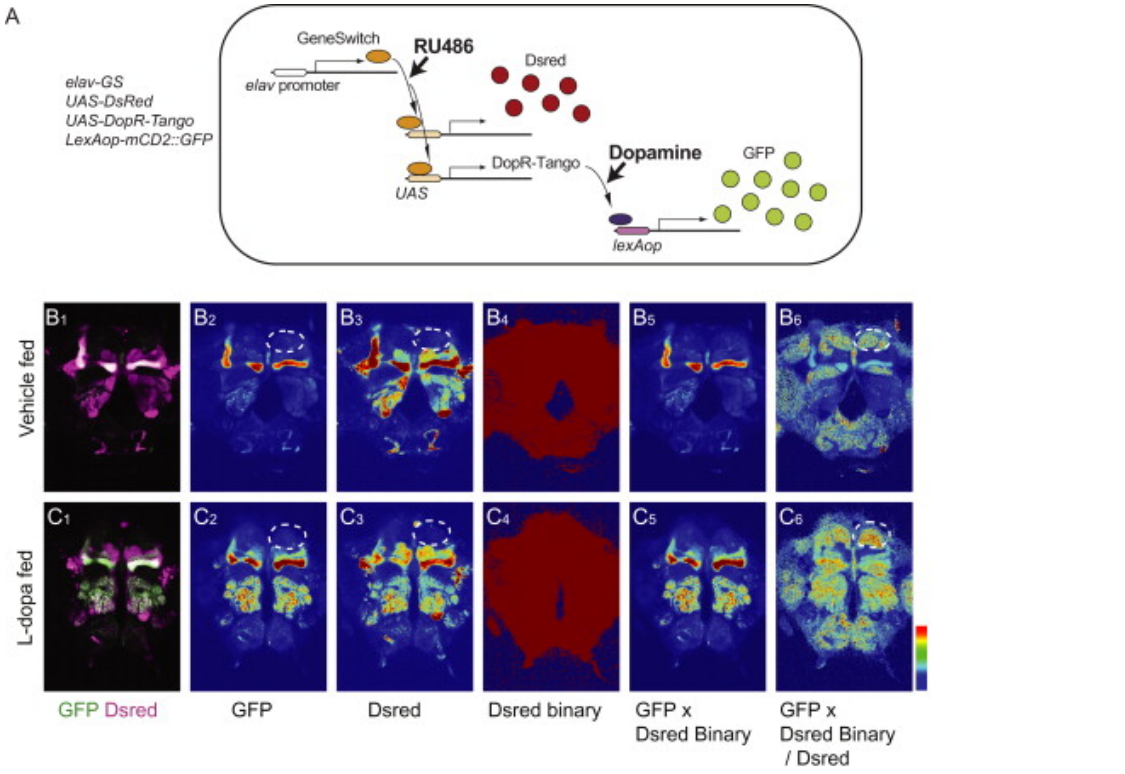
A
elav-GS
UAS-DsRed
UAS-DopR-Tango
LexAop-mCD2::GFP
GeneSwitch
elav promoter
RU486
Dsred
DopR-Tango
UAS
Dopamine
GFP
lexAop
Vehicle fed
L-dopa fed
GFP Dsred
GFP
Dsred
Dsred binary
GFP x Dsred Binary
GFP x Dsred Binary / Dsred

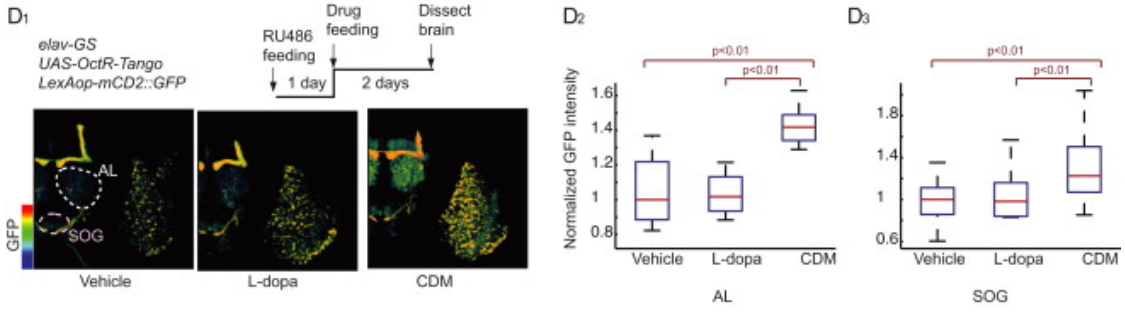
D1
elav-GS
UAS-OctR-Tango
LexAop-mCD2::GFP
RU486 feeding
1 day
Drug feeding
2 days
Dissect brain
AL
SOG
GFP
Vehicle
L-dopa
CDM
D2
Normalized GFP intensity
p<0.01
p<0.01
Vehicle
L-dopa
CDM
AL
D3
p<0.01
p<0.01
Vehicle
L-dopa
CDM
SOG

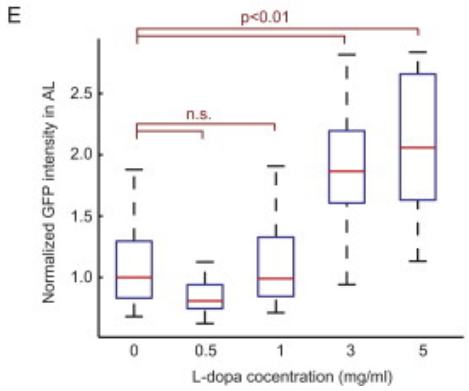
E
p<0.01
n.s.
Normalized GFP intensity in AL
L-dopa cocentration (mg/ml)

Figure S2. Normalization and Image Processing of DopR-Tango Reporter Signal In Vivo, Related to Figure 2

(A) Schematic illustrating the transgenically encoded DopR-Tango signal transduction cascade. GeneSwitch (GS)-Gal4 (orange oval) induces the expression of both DsRed and DopR-Tango. DA-dependent cleavage of DopR-Tango results in translocation of LexA (purple oval) to the nucleus, where it activates expression of the lexAop-GFP Tango reporter. The level of GFP reporter expression reflects not only the ambient level of DA, but also the expression level of the DopR-Tango cassette itself. Because both DsRed and DopR-Tango are under the control of GS, the signal intensity of DsRed should proportionately reflect the expression level of DopR-Tango, in a given region of the brain in a given specimen. Therefore, dividing the GFP signal by the DsRed signal on a pixel-to-pixel basis corrects for within- or between-specimen variations in the level of DopR-Tango expression, and provides a normalized measure of GFP reporter expression that should primarily reflect ambient levels of DA activation of the DopR-Tango cassette. Native fluorescence rather than antibody staining was used to avoid non-linear signal amplification. This method permitted quantification of the normalized GFP signal in various ROIs.

(B and C) Representative examples of image normalization process. Single optical sections from a whole-mount DopR-Tango fly brain (vehicle fed: B1–3, L-dopa fed: C1–3). Signal intensities of native GFP (B2 and C2) and DsRed (B3 and C3) are represented in pseudocolor. After noise filtering using the Wiener method (Lim,
1990), DsRed signals were converted into binary data using a threshold that cuts off noise outside the brain (B4 and C4). The GFP signal was multiplied by these binary data (B5 and C5) on a pixel-by-pixel basis. This process eliminates GFP signals in pixels lacking any

DsRed signal, thereby avoiding division by zero in the subsequent normalization step. Finally, this processed GFP signal was divided by the signal intensity of DsRed (B6 and C6) on a pixel-by-pixel basis. Note how this processing facilitates comparison of GFP signals in many brain areas, such as the dorsal protocereberum (indicated by white dashed circle), in which DsRed expression levels are low.

(D) Specific activation of OctR-Tango by CDM in vivo. Pseudocolor images of OctR-Tango reporter (GFP) expression are shown (D1). Quantification of reporter expression in the indicated neuropil structures(D2–3). p values in this figure represents the results of Kruskal-Wallis ANOVA followed by Mann-Whitney U test with Bonferroni correction for multiple comparisons. $n > 5$ for each experimental group.

(E) Dose-response profile of reporter expression in DopR-Tango flies. Reporter expression in the antennal lobe (AL) was quantified as described above after feeding with the indicated concentration of L-dopa. p values in this figure represents the results of Kruskal-Wallis ANOVA followed by a Mann-Whitney U test with the Bonferroni correction for multiple comparisons. $n > 10$ for each experimental group.

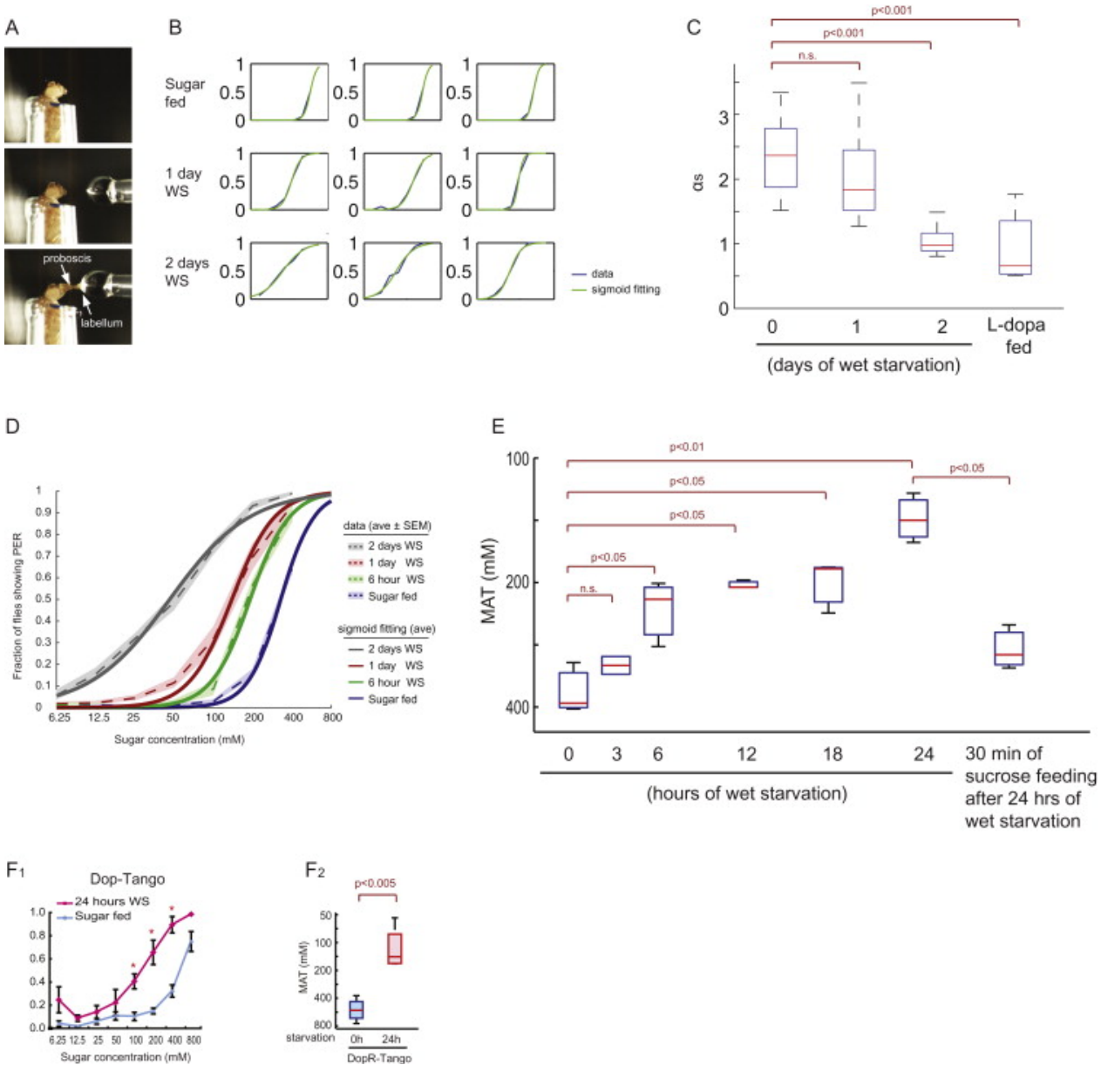
A
proboscis
labellum
B
Sugar fed
1 day WS
2 days WS
data
sigmoid fitting
C
p<0.001
p<0.001
n.s.
os
0
1
2
L-dopa fed
(days of wet starvation)
D
Fraction of flies showing PER
Sugar concentration (mM)
data (ave ± SEM)
2 days WS
1 day WS
6 hour WS
Sugar fed
sigmoid fitting (ave)
2 days WS
1 day WS
6 hour WS
Sugar fed
E
MAT (mM)
p<0.01
p<0.05
p<0.05
p<0.05
n.s.
p<0.05
0
3
6
12
18
24
(hours of wet starvation)
30 min of sucrose feeding after 24 hrs of wet starvation
F1
Dop-Tango
24 hours WS
Sugar fed
Sugar concentration (mM)
F2
p<0.005
MAT (mM)
starvation
0h
24h
DopR-Tango

Figure S3. Analysis of PER, Related to Figures 3 and 4

(A) PER assay. Presentation of sucrose solution to the tip of proboscis (labellum) causes full extension of proboscis.

(B) A response curve to the sugar (PER curve) can be fitted into a sigmoid curve. Representative examples of PER curve (3 examples each for sugar fed, 1 day wet starved, and 2 days wet-starved wild-type flies). Raw data, blue; sigmoid fitting, green. In all cases, fitting of sigmoid to the data was confirmed with two-way ANOVA. See also Extended Experimental Procedures.

(C) as decreases with two-day wet-starvation or L-dopa feeding. as is slope of the sigmoid curve (see Extended Experimental Procedures). One-way ANOVA was followed by t test with Bonferroni correction.

(D) Average curves of the fitted sigmoid curves (solid lines), fit well to the average curves of the raw data (dotted lines. Envelopes indicate SEM). Raw data are pooled from Figures 4A1 and 5D1 ($n > 4$ for each). Fitting was confirmed with two-way ANOVA.

(E) Time course of changes in MAT during starvation. MATs were measured 0, 3, 6, 12, 18, and 24 hr after wet starvation, and 30 min after sucrose feeding of 24 hr wet-starved flies ($n > 3$, each). Whereas increase in sugar sensitivity during starvation is gradual, the decrease in sugar sensitivity after feeding is abrupt, sug- gesting different mechanisms controlling sugar sensitivity under states of starvation and satiety. One-way ANOVA was followed by t test with Bonferroni correction (n.s.: $p > 0.05$).

(F) Sugar sensitivity of sugar-fed and wet-starved DopR-Tango flies tested using the PER assay. As in wild-type flies (Figure 4A1), DopR-Tango flies showed

normal PER behavior and starvation-dependent increase in sugar sensitivity. (F1) average response. See Figure S4 for the statistical method to test the difference between two PER curves. Error bars represent SEM (F2) MAT. t test ($n > 4$ for each experimental group).

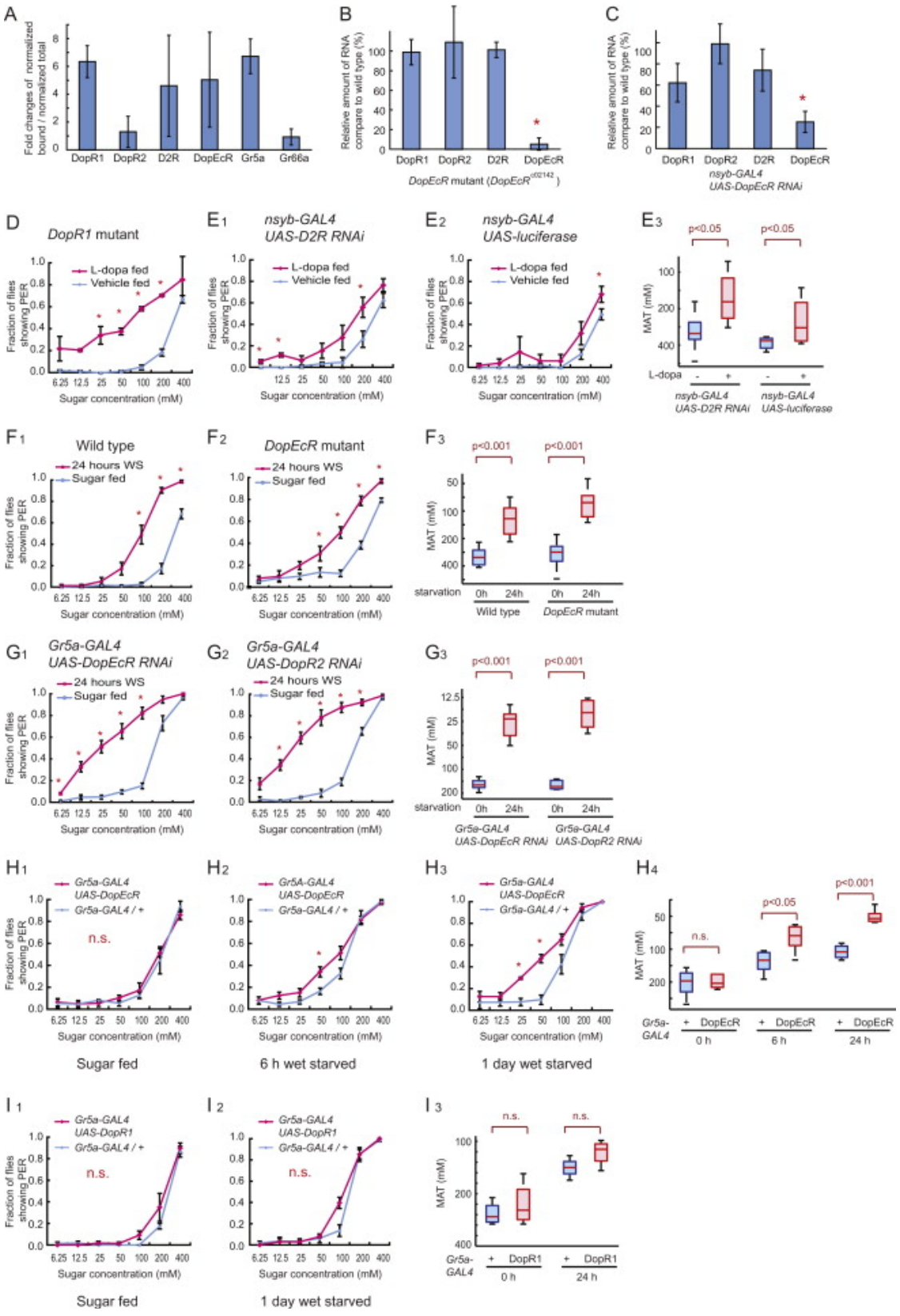
A
Fold changes of normalized bound / normalized total
DopR1 DopR2 D2R DopEcR Gr5a Gr66a
B
Relative amount of RNA compare to wild type (%)
DopR1 DopR2 D2R DopEcR
DopEcR mutant (DopEcR^d02142)
C
Relative amount of RNA compare to wild type (%)
DopR1 DopR2 D2R DopEcR
nsyb-GAL4 UAS-DopEcR RNAi
D
DopR1 mutant
L-dopa fed
Vehicle fed
Fraction of flies showing PER
Sugar concentration (mM)
E1
nsyb-GAL4 UAS-D2R RNAi
E2
nsyb-GAL4 UAS-luciferase
E3
p<0.05
p<0.05
MAT (mM)
L-dopa
nsyb-GAL4 UAS-D2R RNAi
nsyb-GAL4 UAS-luciferase
F1
Wild type
24 hours WS
Sugar fed
F2
DopEcR mutant
F3
p<0.001
p<0.001
starvation
0h 24h 0h 24h
Wild type
DopEcR mutant
G1
Gr5a-GAL4 UAS-DopEcR RNAi
G2
Gr5a-GAL4 UAS-DopR2 RNAi
G3
p<0.001
p<0.001
Gr5a-GAL4 UAS-DopEcR RNAi
Gr5a-GAL4 UAS-DopR2 RNAi
H1
Gr5a-GAL4 UAS-DopEcR
Gr5a-GAL4 / +
n.s.
Sugar fed
H2
6 h wet starved
H3
1 day wet starved
H4
n.s.
p<0.05
p<0.001
Gr5a-GAL4
+ DopEcR
0 h
6 h
24 h
I1
Gr5a-GAL4 UAS-DopR1
Gr5a-GAL4 / +
n.s.
Sugar fed
I2
1 day wet starved
I3
n.s.
n.s.
+ DopR1
0 h
24 h

Figure S4. Quantification of DA Receptor mRNA Expression and Validation of RNAi, Related to Figure 5

(A) DA receptor expression in RNA isolated from sugar-sensing GRNs by the TU-tagging method (Miller et al., 2009) and quantification by qRT-PCR. Error bars represent standard deviation (n = 2).

(B and C) The effect of the DopEcR mutation and DopEcR RNAi on the amount of DopEcR RNA was quantified using qRT-PCR. Error bars represent standard deviation (n = 3). One-way ANOVA was followed by t test with Bonferroni correction (*$p < 0.05$).

(D and E) Sugar sensitivity of DopR1 hypomorph mutant (D), pan-neuronal D2R RNAi (E1), and its genetic control flies (E2) with or without L-dopa feeding. All genotypes exhibited a significant increase in sugar sensitivity by feeding L-dopa. Data in (D) are directly comparable to wild-type data in Figures 5A1 for the same genetic background.

(F and G) Sugar sensitivity of DopEcR RNAi or mutant after 24 hr of starvation.

(H) Overexpression of DopEcR in sugar-sensing GRNs boosts the increase in sugar sensitivity caused by food deprivation. The sugar sensitivity of flies over- expressing DopEcR in sugar-sensing GRNS (Gr5a-GAL4;UAS-DopEcR; red lines) was compared to the sensitivity of its genetic control flies (Gr5a-GAL4/+; blue lines).

(I) Overexpression of DopR1 in sugar-sensing GRNs did not influence sugar sensitivity. The sugar sensitivity of flies overexpressing DopR1 in sugar GRNs (Gr5a- GAL4;UAS-DopR1; red lines) was compared to the sensitivity of its genetic control flies (Gr5a-gal4/+; blue lines). DopRf02676 was used as UAS-DopR1 (Lebestky et al., 2009).

As in Figure 5, in PER curves, error bars represent SEM. Boxplots: lower and upper whiskers represent 1.5 IQR of the lower and upper quartiles, respectively; boxes indicate lower quartile, median, and upper quartile, from bottom to top. The difference between PER curves for each pair of experimental groups (red versus blue lines in all panels) was analyzed by two-way ANOVA with replication followed by a post-hoc t test with Bonferroni correction. *$p < 0.05$, n.s.; nonsignificant ($n > 4$ for each experimental group). Differences between MATs were analyzed by two-way ANOVA with replication followed by post-hoc t test with Bonferroni correction. Interactions between genotyopes and feeding conditions (Genotypes 3 Conditions), which were calculated by the two-way ANOVA, were not significant for all cases listed below, implying that the genetic manipulations (mutation or RNAi) did not interfere the effect of feeding manipulations (wet starvation or L-dopa feeding); $p = 0.5275$ (nonsignificant) (E3), $p = 0.2876$ (F3), $p = 0.3478$ (G3).

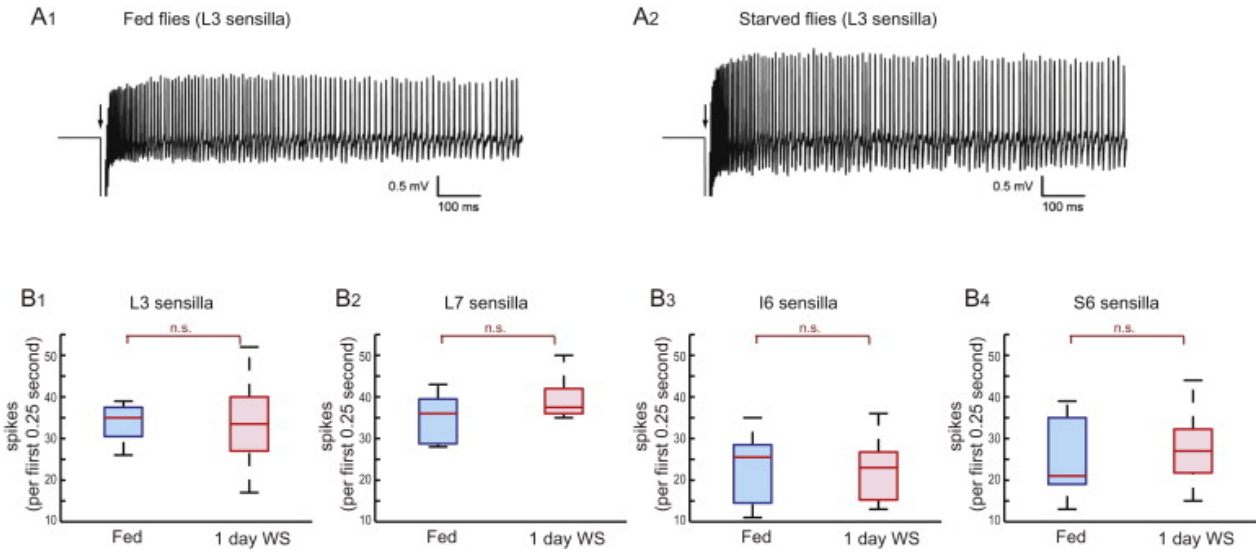
A1
Fed flies (L3 sensilla)
0.5 mV
100 ms
A2
Starved flies (L3 sensilla)
0.5 mV
100 ms
B1
L3 sensilla
B2
L7 sensilla
B3
I6 sensilla
B4
S6 sensilla
n.s.
spikes (per first 0.25 second)
Fed
1 day WS

Figure S5. Extracellular Recording of GRNs in Labellum, Related to Figure 6

(A) Sample traces of electrophysiological recordings made from L3 sensilla of fed (A1) and starved flies (A2). The electrophysiological responses of labellar sugar- sensing GRNs to 100 mM sucrose were recorded extracellularly by using the tip recording method (see Extended Experimental Procedures). Recording electrode filled with sucrose solution touched the sensilla at the time pointed by the arrow. Contact artifacts are observed at the beginning of each trace.

(B) Effect of starvation on the action potential frequency of sugar-sensing GRNs in response to 100 mM sucrose. The spike number in the first 0.25 s (B1–4) and the first 1.0 s (data not shown) of the response to sucrose was measured. No change in action potential frequency was observed between fed and starved flies in any of the sensilla tested (Mann-Whitney U test). In case of the L-type sensilla, we observed statistically significant increase in action potential amplitude in starved flies, compared to fed flies (data not shown). Because the action potential shape and amplitude, measured by extracellular recording, depend on extracellular factors, such as the distance and position of the recording electrode and the resistance of the environment around the cell, we could not conclude whether this increase in the action potential amplitude is due to a change in the sugar-sensing GRNs themselves.